2016

Development of A Multi-Electrode Array (MEA) Based on Active Recruiting of Cells and Formation of Mechanically Confined Neural Networks

Tianyi Zhou
Lehigh University

Development of A Multi-Electrode Array (MEA) Based on Active Recruiting of Cells and Formation of Mechanically Confined Neural Networks

by

Tianyi Zhou

Presented to the Graduate and Research Committee
of Lehigh University
in Candidacy for the Degree of
Doctor of Philosophy

in

Electrical Engineering

Lehigh University

May, 2016

Approved and recommended for acceptance as a dissertation in partial fulfillment of the requirements for the degree of Doctor of Philosophy.

Date

Dissertation Director

Accepted Date

Svetlana Tatic-Lucic (Committee Chair)
Electrical and Computer Engineering
Lehigh University

Yevgeny Berdichevsky
Electrical and Computer Engineering
Lehigh University

Miltiadis Hatalis
Electrical and Computer Engineering
Lehigh University

James Hwang
Electrical and Computer Engineering
Lehigh University

Daniel Ou-Yang
Physics
Lehigh University

Susan Perry
Chemical Engineering
Lehigh University

Acknowledgments

First and foremost, I would like to thank my parents, Mr. Zhi Zhou and Ms. Houjun Lan, and my other family members for their endless love and support throughout these years, no matter how difficult the situations are for me. I thank them from the bottom of my heart. It has been an extremely challenging and demanding period for me in the past year to finally come to this point. However, the end of my Ph.D. journey opens a new chapter in life, both professionally, and personally.

I would like to thank my advisor, Professor Svetlana Tatic-Lucic, who advised me with knowledge, and always supported me with passion, encouragement, candor and humor during my Ph.D. research for the past six years. I would like to thank Prof. Susan Perry for her tremendous help in biological cell/neuron culture and neuronal experiments. I greatly improved my technical writing skills with the help of Prof. Perry regarding our publications. Both Prof. Tatic-Lucic and Prof. Perry showed continuous support for my professional development throughout these years.

I would like to thank Prof. Yevgeny Berdichevsky for his guidance and discussion concerning the aspects of neuroscience research in my Ph.D. work. My committee members also provided valuable advice and support during my research: Prof. Miltiadis Hatalis, Prof. James Hwang, and Prof. Daniel Ou-Yang. I would like to thank them for reviewing my dissertation; their helpful comments and advice are much appreciated.

I would like to thank the people at the Sherman Fairchild Center of Lehigh University for their support during my Ph.D. work. Mr. Raymond Filozof, Dr. Floyd Miller, and Mr. Tony Jeffers trained and helped me a lot for the microfabrication process in the cleanroom. Ms. Linda Dreisbach just constantly made my life easier.

I would like to thank Dr. Markus Gnerlich, who helped and influenced me a lot at the beginning of my Ph.D. work, who always showed great passion and strong technical knowledge during research. Dr. Gaoshan Jing and Kanlun Li, two of my former colleagues, provided training and instruction to this research project and laid the foundation for my work. I would like to thank other former and current members of Tatic-Lucic research group: Dr. Umer Izhar, Negar Moghimi, and Yixuan Ming. I would also like to thank the students who I worked with during the summer projects for those two years. They made me a better researcher, showed me different aspects of life, and it's amazing to see them succeed, as well.

My life at Lehigh would not have been the same without all the friends: Xi Luo, Kanlun Li, Yaqing Ning, Yu Song, and Thomas Charisoulis. I thank them for all these years at Lehigh. I would like to thank Yan (Mandy) Liu for those beautiful two years, who reminded me of the most important things in life.

This work was partially supported by National Science Foundation (CAREER grant ECS-0448886 and NER grant BES-0608742), as well as National Science Foundation (NSF) grant NSF ECCS-1321356 and a grant to Lehigh University from the Howard Hughes Medical Institute (HHMI) through the Precollege and Undergraduate Science Education Program.

Table of Contents

List of Tables

List of Figures

Abstract

Multi-Electrode Array (MEA) systems have been widely used, for decades, in neuroscience research, such as the detection of neuroactive compounds and the study of neuronal electrophysiology and communication. Accurate positioning of neurons on electrodes enables the recording from and stimulation of specified individual neurons on a MEA. Various cell patterning techniques, integrated with MEAs, have been developed to ensure neuron-electrode correspondence, which is the capability that most conventional MEAs lack, because of the random distribution of neurons with respect to electrodes.

A novel multi-electrode array system has been designed and developed for active recruitment of neurons on electrodes and the formation of mechanically confined neural networks. In this system, positive dielectrophoresis (DEP) is applied to actively recruit hippocampal neurons to the electrodes of the MEA, where polymer microstructures, such as microchambers and microtrenches are created to effectively define a patterned neuronal network.

The dielectrophoresis theoretical calculation and simulation is first examined to prove the feasibility of active positioning of hippocampal neurons using positive DEP. The MEA device, referred to as DEP MEA, is designed, modeled, and fabricated on a quartz glass substrate. The fabricated DEP MEA chip (8 mm by 8 mm) is packaged, and the functionality of our MEA system is verified by active recruitment of embryonic mouse hippocampal neurons, the formation of precisely patterned hippocampal neuronal networks, as well as successful recording of spontaneous and stimulated neuronal potentials, including the propagation of evoked neuronal bursts between electrodes. The cytocompatibility of the top microstructure layer on the DEP MEA, which is a layer of thin cured SU-8 epoxy, is investigated to improve the viability of cultured primary hippocampal neurons.

We then investigate the selective trapping (separation) of mouse hippocampal neurons from glial cells using positive DEP, based on their different dielectric and physical properties. The DEP movement of neurons and glial cells in the targeted suspension medium is analyzed. By comparing the experimentally measured DEP crossover frequencies of neurons and glial cells with the simulated values, new, refined neuron and glial dielectric and physical properties are predicted that better reflect the DEP experimental results.

Finally, the design and development of the electronic circuit system and LabView control interface is introduced. We conclude with potential improvements and future work to make this MEA system a more precise, efficient, reliable and versatile BioMEMS platform for neural engineering research.

Chapter 1: Introduction

1.1 Significance

Over the past several years, there have been major breakthroughs in understanding the basic mechanics and circuitry transactions for learning, cognition and information storage in the brain. For instance, the brain slice preparation has revolutionized the study of synaptic transmission, neural integration, and long-term potentiation, the simplest synaptic analog of learning [1]. The capacity to study synaptic transmission in the slice preparation for a period as short as several hours has allowed the elucidation of many computational principles and basic molecular mechanisms. Such *in vitro* neural network, including brain slice, has become a popular research subject because of the complexity and difficulty of studying *in vivo* neural system, which usually consists of millions of neurons, and the fact that the neurons exhibit very similar electrophysiological properties as *in vivo* [1].

In reality, study of the underlying mechanism of neural network activities helps us to understand, for instance, why does seizure happen, how do drug compounds affect neural health, and how does human brain react to artificial stimulations [2]. In order to facilitate such investigations, neural signals from multiple neurons need to be measured simultaneously. As a result, a variety of multi-electrode array (MEA) systems have been developed by different research groups and commercial companies over the last three decades. These MEA systems are used in various applications including cardiac safety pharmacology investigation, drug screening, and neurotoxin detection with the capability to study spontaneous and stimulated neuronal activities, of several neurons simultaneously, across a functioning neural network. Analyzing signals acquired from multiple electrodes, researchers are able to obtain information about the formation of neural networks and intracellular features of neurons.

Extracellular multi-electrode arrays (MEAs) have been widely used for neuronal potential recording because of their non-invasive nature [3-6]. These MEAs enable the study of neuronal electrophysiology and communication through simultaneous in vitro recordings and stimulations from multiple neurons. By increasing the number of electrodes, conventional MEAs provide reliable platforms for tissue-level or high-density neural culture and recording [3,6-11]. However, most conventional MEAs lack the capability to precisely track and investigate electric signals from specific individual neurons, which is crucial to decipher the working mechanism of functioning neuronal networks. This limitation is caused by the random distribution of neurons with respect to electrodes. With normal culturing substrates such as cover slides and petri dish, neurons are randomly distributed and their dendrites and axons overlap are undefined, as can been seen in Fig. 1.1, which makes the geometrically dependent studies of functioning neural networks difficult, as well as the characteristics of individual neurons [1]. Control of the organization of neurons in defined networks in culture promises to provide a major technical innovation. With countable neurons cultured in defined networks, this allows more precise control in the manipulation of both individual neurons and microenvironment.

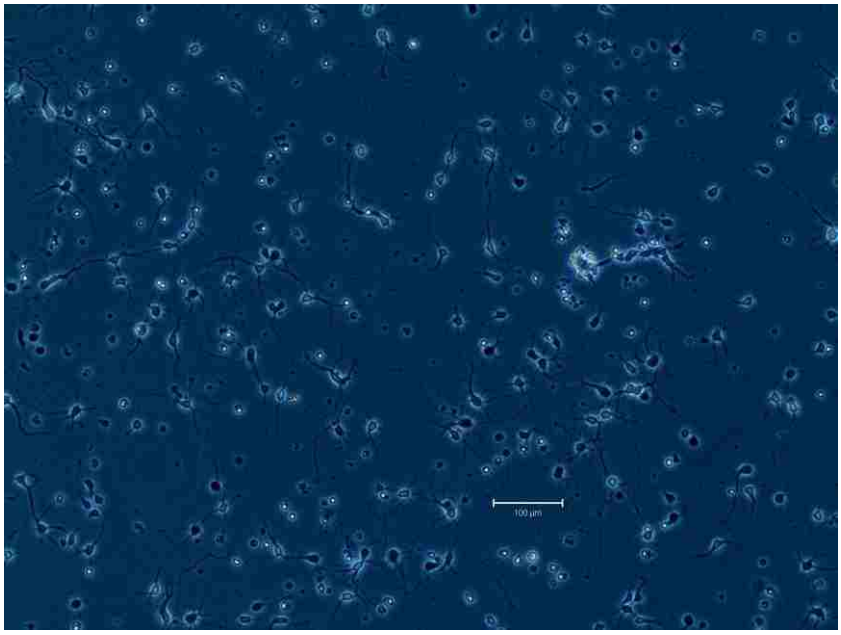

Figure 1.1 Mouse embryonic (E18) hippocampal neurons cultured on a glass cover slide on Div. 3 (days in vitro). Randomly distributed neurons and overlapped dendrites and axons make the identification and study of functioning neuronal connections difficult. (Scale bar is 100 μm)

To address this problem, various cell patterning techniques, integrated with MEAs, have been developed to ensure neuron-electrode correspondence. Microcontact printing (μCP) based on soft lithography and the use of polydimethylsiloxane (PDMS) has proved effective [12,13], where cell adhesion promoters such as poly-d-lysine or laminin are used to define cell attachment and growth at specified locations (Fig. 1.2(a)). Meanwhile, surface chemical engineering, based on self-assembled monolayers (SAMs), can accomplish patterning of immortalized cell lines by covering an MEA chip surface with cytophilic (cell-attractive) and cytophobic (cell-repulsive) coatings, alternatively [13,14], as can be seen in Fig. 1.2(b). One alternative approach is to build mechanically confining structures (Fig. 1.2(c)), such as neuronal cages [15], or posts [16]. More recently, as an alternative to cage-like microstructures to confine neurons on top of electrodes, nanopillars and nanowires (Fig. 1.2(d)), based on silicon substrate or carbon nanotubes (CNT), as well as gold mushroom-shaped microelectrodes, have been developed as neuronal interfacing platforms to facilitate cell anchoring for intracellular or extracellular recordings [17-19].

Additionally, microstructures have been fabricated for confinement of neuronal bodies and guidance of neurites using SU-8 photoresist as a structural material [20].

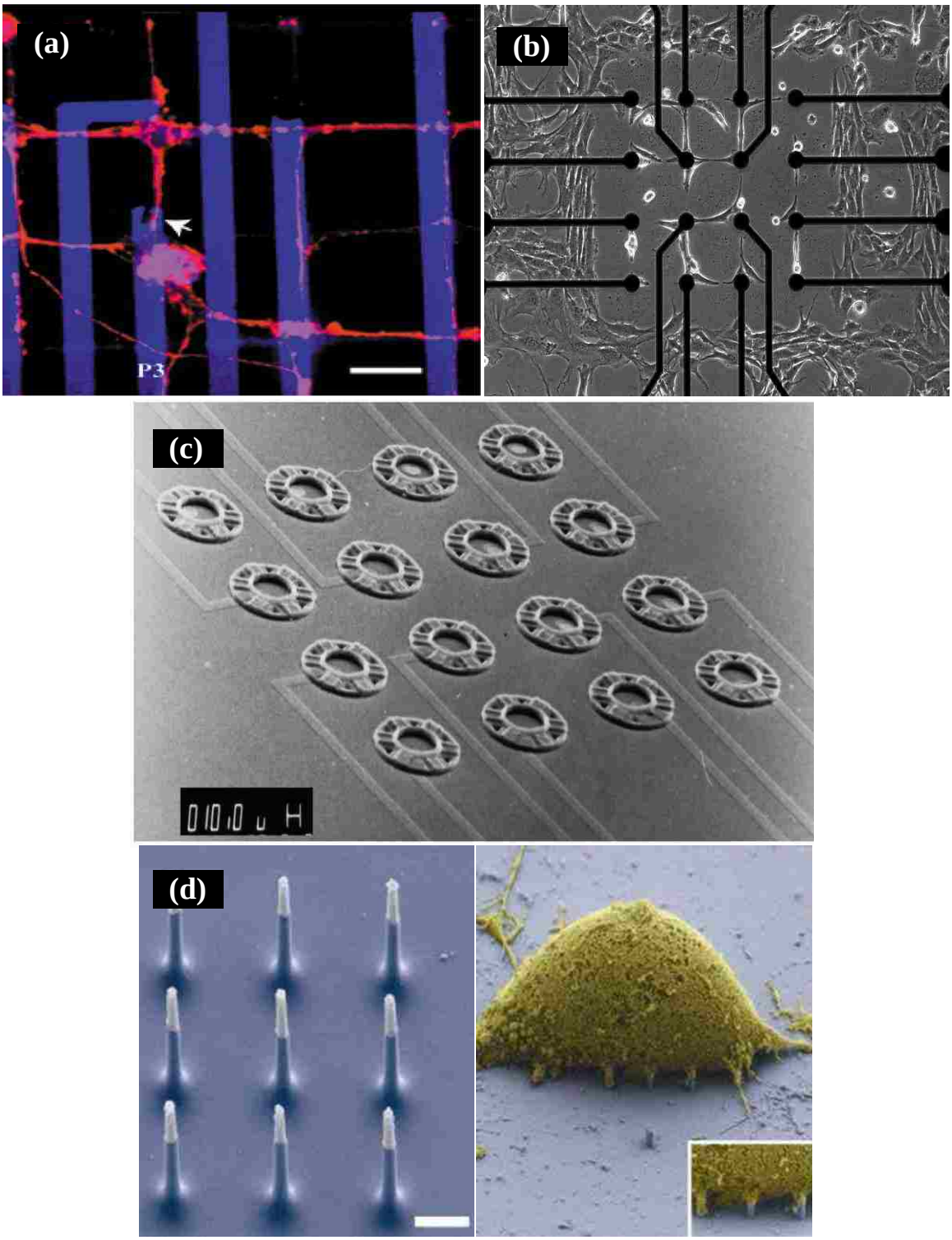

Figure 1.2 Passive cell patterning techniques integrated with MEA. (a) Fluorescence micrograph of hippocampal neurons (red) cultured on MEA (blue) surfaces that are patterned with poly-l-lysine (PLL) by μCP [12]. (b) Phase contrast micrograph of mouse hypothalamic neurons (GT1-7) cultured on a MEA surface that has been patterned with cytophilic 3-trimethoxysilylpropyl-diethylenetriamine (DETA) self-assembled monolayer (SAM). (c) SEM image of a 4x4 array of neurocages made out of parylene polymer [15]. (d) SEM image of 9 silicon nanowires that constitute a Vertical Nano Electrode Array (VNEA), and a rat cortical cell anchored on top of a VNEA [17].

Despite all these "passive" cell patterning efforts, where the positioning of cells is determined by the natural selection and anchoring of cells based on the property of the substrate, the precise positioning of primary mouse hippocampal neurons on electrodes, which are the cells normally involved in the process of thought and memory, remains challenging. Based on our experimental experience, we found that, either through cell-attractive protein patterning by microcontact printing (μCP), or cytophilic self-assembled monolayer (SAM) coating, the anchoring of somas and guidance of neurites is more affected by the placement of neighboring neurons than by predefined cell-adhesive regions [21]. Moreover, experimentally, it is preferable to pattern neurons with single-cell resolution, as multiple neurons anchored on one electrode prevent reliable tracking of the electric signals generated from one specific neuron or tracking the communication between two specific neurons. Consequently, there's a need for an active recruiting technique that can actively attract neurons onto the electrodes of a MEA with single-cell resolution, and a cell patterning approach that is capable of effectively defining the growth of neuronal processes based on predefined structures to form a patterned functioning neuronal network *in vitro*.

1.2 Objectives

In this research, we aim to measure spontaneous and stimulated neuronal potentials from specified neurons within a functioning neuronal network, as well as the propagation of neuronal potentials between connected neurons. This measurement of neuronal potentials will be realized through a multi-electrode array (MEA) system that can actively attract individual neurons to desired locations

on the MEA, which are areas on top of each electrode. Once trapped, the neurons can be cultured directly on the MEA, and the growth of the neurites will be guided, based on predefined structures, to form a patterned neuronal network. This MEA system is targeted towards the development of a new platform which can facilitate the study of neuronal electrophysiology and communication mechanism. The *in vitro* neuronal networks studied here are of particular interest because of their relative simplicity, and the ability to express similar electrophysiological properties as *in vivo*, as mentioned above. Although the *in vitro* neuronal network does not exactly represent the *in vivo* neural network, it is expected that useful information about the integration of neuronal circuits, cellular process behind the formation of neuronal networks, and neuronal responses to molecular signals, can be extracted to help decipher the human brain activity.

In order to develop such a MEA system, the following technical aspects need to be realized, which are also the objectives of this research:

(1) Individual neurons should be anchored precisely on desired regions, which are areas on top of MEA electrodes.
(2) MEA devices should be able to support *in vitro* neural networks in culture, which indicates a suitable microenvironment for primary neuron culture.
(3) Growth direction of neurites should be confined to specific regions on MEA chip surface, so that precisely patterned neuronal networks can be formed in culture.
(4) Associated integrated circuit system needs to be developed so that the proper filtration, amplification and recording of micro-volt level neuronal transmembrane potentials will be realized, as well as the generation of stimulation pulses.
(5) With the goal of single-cell resolution patterning, one-to-one recording and stimulation should be achieved for individual neurons, as well as the propagation of neuronal potentials between neurons.

(6) Neuronal signal analysis should be performed to interpret the mechanism of a functioning neuronal network.

At the same time, a number of challenges need to be overcome, to allow the functioning of the MEA system. First, the MEA device, fabricated using micro-electro-mechanical system (MEMS) technology, should be integrated in a microfluidic manner that neurons can be transported properly during the active recruiting process. Second, neuron culture on the MEA device requires a conductive liquid (neuron culture media) environment; therefore, electronic parts and their connections of the system need to be effectively isolated and protected. Third, the culture of primary neurons requires special selection and sterilization treatment for the materials used to fabricate the MEA chip.

The MEA system described below is designed to meet all of these research objectives. In addition, during the development of the system, research work has also been performed to investigate the following subjects (as will be discussed in the chapters below):

1) The pretreatment of the MEA surface material to improve the cytocompatibility for primary neuron culture, particularly as it applies to mouse hippocampal neurons.
2) The separation of embryonic mouse hippocampal neurons from glial cells using positive dielectrophoresis (DEP), as it applies to the selective attraction of neurons on the electrodes of the MEA.
3) The estimation of dielectric and physical properties for hippocampal neurons and glial cell, based on the simulation and experimental measurement of DEP crossover frequencies.

1.3 System Overview

1.3.1 Active Cell Recruiting Techniques

Active and precise neuronal recruiting techniques are needed to attract neurons onto electrodes with single-cell resolution. Active cell positioning techniques such as vacuum suction [22] and optical tweezers [23] have been developed to attract single neurons to desired positions. One disadvantage of these techniques is that they increase the complexity of the overall system. For this particular application, dielectrophoresis (DEP) is applied to actively recruit individual neurons to the electrodes of a MEA. A comprehensive comparison of the advantages and disadvantages of the active cell positioning techniques, mentioned above, is listed in Table 1.1.

Table 1.1 Comparison of different active cell positioning techniques.

Method	Advantages	Disadvantages
Vacuum Suction	1. Single cell-on-electrode trapping resolution 2. Simultaneous multi-site recording capability 3. Improved S/N ratio with the application of suction	1. Wafers need to be etched through during the fabrication (complexity). 2. Growth of neurites is not defined. 3. Effect of mechanical suction on cell health is unknown.
Optical Tweezers	1. No contact force 2. High force and displacement resolution 3. Amiability to liquid media environments	1. Only single-cell manipulation at a time 2. Separate trapping and neuronal recording systems (complexity) 3. Possible thermal or photo damage to the cell
Dielectrophoresis (DEP)	1. Simultaneous multi-cell manipulation capability 2. Same trapping and recording electrodes 3. Limited negative effect on cell health	1. Cell viability in low-conductivity positive DEP medium needs to be investigated. 2. Possible cell membrane breakdown under inappropriate electric field.

Vacuum Suction (Fig. 1.3): The cells are trapped by applying vacuum from the bottom side of the device. Cells can be trapped on electrodes with single-cell resolution. The system is capable of simultaneous multi-site recording; furthermore, the signal-to-noise ratio can be improved as the suction provides better seal between the neuron and the electrode. However, the wafers need to be

etched through to provide the suction holes for vacuum application, which increases the complexity and cost of the fabrication process. In addition, with the current systems in literature [22], the growth of neuronal processes is not defined so that patterned neuronal network is not achieved. There might also be negative effect on the cell health because of the mechanical suction force, which is unknown.

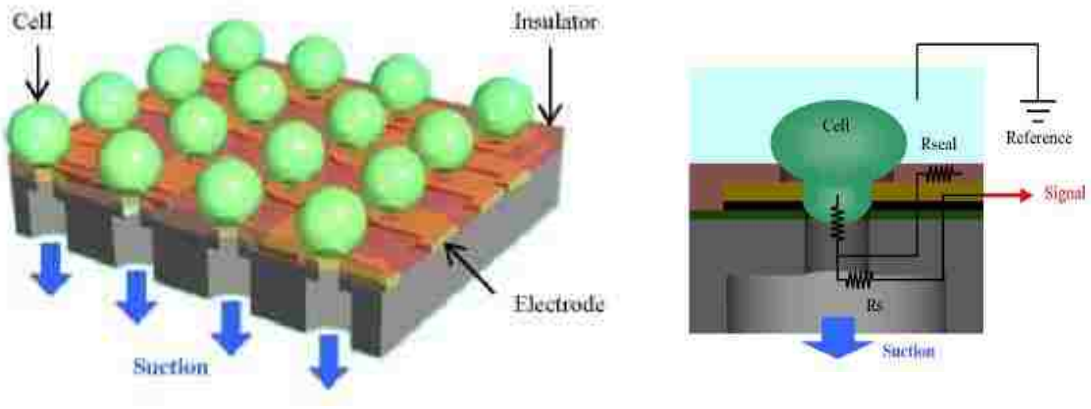

Figure 1.3 Operation and neuronal recording principle for vacuum suction active cell positioning technique [22].

Optical Tweezers (Fig. 1.4): Laser beams are focused on a cell through an objective, and the cell is manipulated by momentum transfer from the laser beams. Under this operation principle, no contact forces is applied on the cell, which protects the cell's integrity. With precise optical setup of lasers on a microscope, high force and displacement resolution can be achieved for the cell. Additionally, the cell can be manipulated in its culture media environment. Most of the current systems, however, can only move one cell at a time, which is time-consuming for multiple cell positioning purpose. It is obvious that in addition to the optical trapping system, extra neuronal recording (electrode) system needs to be integrated for the signal measurement function. Also, laser beams could bring possible photo and thermal damage to the cell [23].

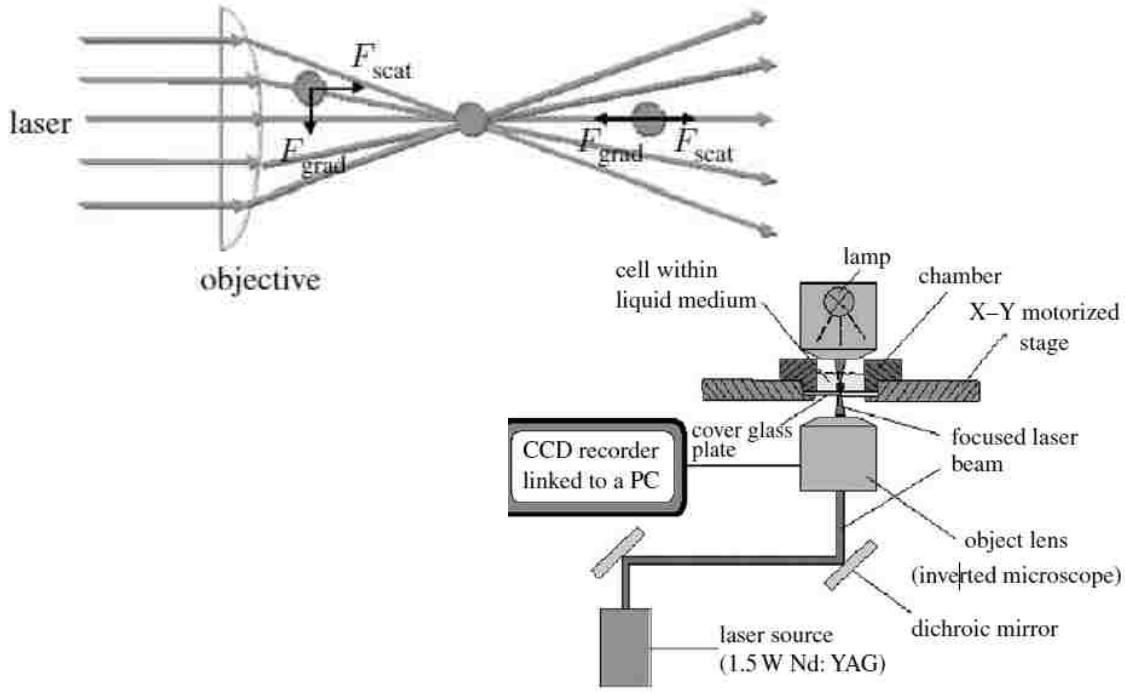

Figure 1.4 Operation principle and system overview for active cell manipulation with optical tweezer [23].

Dielectrophoresis: DEP cell manipulation takes advantage of electric field and the polarization of the biological particles (e.g. cells) to move the cells to predefined positions. Normally, the electric field is created by applying AC electric signals to electrodes, which can be the positions where cells are trapped; furthermore, these electrodes can also function as the recording electrodes, simplifying the system design. With electrode arrays, DEP systems bring the capability of simultaneous multi-cell manipulation. Additionally, previous study has reported that the negative effect of DEP on cell health is limited [24]. At the same time, concerns for the cell health because of the DEP medium and electric field call for more investigations to ensure the viability and health of the cells.

1.3.2 DEP MEA Design Overview

Combining the considerations above, and the fact that DEP has been studied in our research group for the manipulation of biological particles, we have chosen positive dielectrophoresis (pDEP) as

an active cell trapping technique to actively recruit neurons to the electrodes of our MEA system, referred to as DEP MEA, with the goal of achieving single-cell resolution. Dielectrophoresis is a process in which a force is acting on a dielectric particle (e.g. a biological cell) when a non-uniform electric field is applied [25]. Depending on the relative dielectric and conductive properties of the cells and the suspension medium, cells can be driven towards the maximum of electric field under positive dielectrophoresis (pDEP) or to the minimum of electric field under negative dielectrophoresis (nDEP). In this work, an electric field maximum is created above each electrode of a MEA to actively trap hippocampal neurons on top of them, by positive dielectrophoresis (Fig. 1.5). Compared with other DEP systems, our DEP MEA is also designed to realize the following unique features:

1) Single-cell-to-electrode positioning resolution.
2) Patterned neuronal network based on predefined structures.
3) Long-term optical and electrical monitoring with transparent quartz substrate.
4) Simultaneous neuronal signal recording and stimulation with the same DEP electrode configuration.

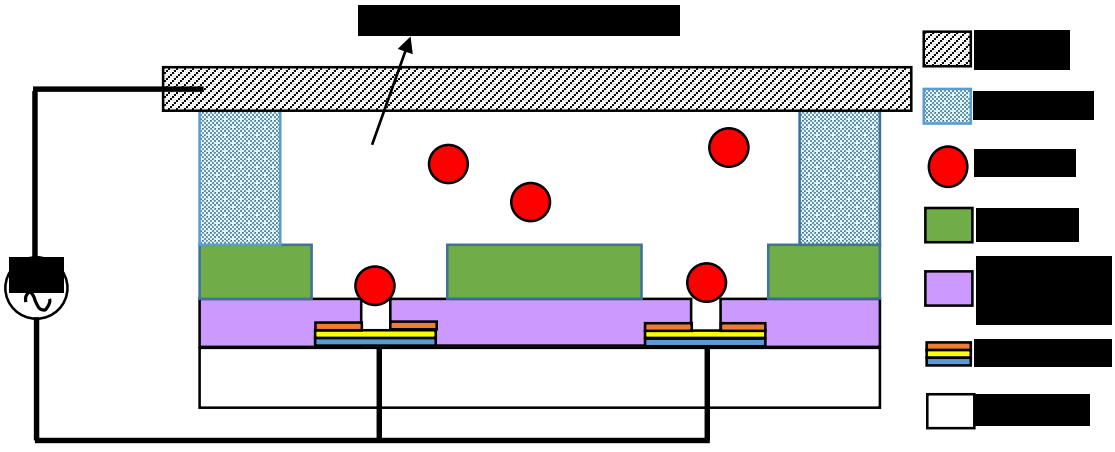

Figure 1.5 Positive DEP cell recruiting principle for our DEP MEA system.

Once recruited, the growth of neuronal processes is mechanically confined to predefined microstructures based on SU-8 photosensitive epoxy, resulting in the formation of patterned neuronal networks. The SU-8 microstructures consist of microchambers, which are created on top of each electrode, to confine the placement of the soma (cell body) of the neurons; and microtrenches connecting those microchambers, which are designed to guide the growth of neurites, so that a patterned neuronal network can be formed *in vitro*. From previously reported work [15-16, 20], mechanical confinement of neuronal growth has proven effective with predefined microstructures. With this MEA system, spontaneous and stimulated neuronal signals are detected from specific neurons growing on top of electrodes, as well as the propagation of evoked neuronal potential spikes.

Chapter 2: DEP MEA System Design and Fabrication

2.1 Dielectrophoresis

2.1.1 Theoretical Background

Dielectrophoresis (DEP) is a phenomenon in which a force is exerted on a dielectric particle (e.g. a biological cell) when it is subjected to a non-uniform electric field [25]. This force does not require the particle to be charged. All particles exhibit dielectrophoretic activity in the presence of electric fields. DEP is a process that relies on electrical polarization of neutral cells present in a solution (Fig. 2.1). The process depends on dielectric and conductive properties of both the cells and solution and is controlled by the electric field amplitude and frequency [27]. Particles can migrate to the maximum of electric field in positive dielectrophoresis (pDEP) or to the minimum of electric field in negative dielectrophoresis (nDEP).

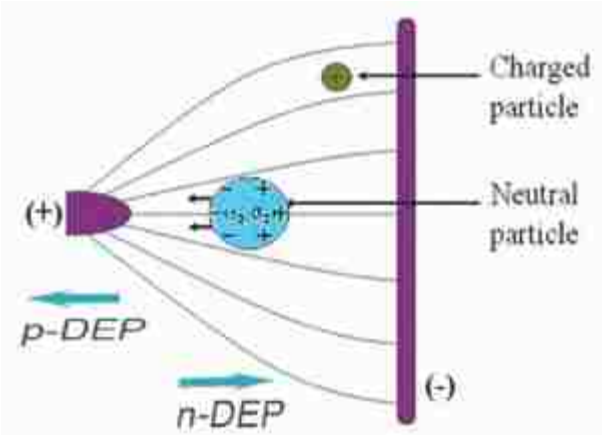

Figure 2.1 Dielectrophoresis results in the polarization of a neutral particle (formation of a dipole). As a result, such a particle will move in an electric field either toward an electric field maximum area or an electric field minimum area, depending on permittivity and conductivity parameters of the whole system [26].

Recently, dielectrophoresis has been revived due to its potential in the manipulation of microparticles, nanoparticles and biological cells [28, 29]. Dielectrophoresis can be used to

manipulate, transport, separate and sort different types of particles. Since biological cells have different dielectric properties [27], dielectrophoresis has many medical applications.

The governing equation for dielectrophoretic force exerted on a dielectric particle in a non-uniform electric field is expressed as [28]:

$$F = 2\pi r^3 \varepsilon_m Re[K] \nabla E^2 \tag{2.1}$$

where r is the radius of dielectric particle, ε_m is the electric permittivity of suspension medium, E is the non-uniform electric field and Re[K] is the real part of Clausius-Mossotti (C-M) factor K where [27]:

$$K = \frac{\varepsilon_p^* - \varepsilon_m^*}{\varepsilon_p^* + 2\varepsilon_m^*} \tag{2.2}$$

ε_p^* and ε_m^* are the complex dielectric permittivities of particle and medium, respectively. The complex dielectric permittivity is given by [28]:

$$\varepsilon^* = \varepsilon - i\frac{\sigma}{\omega} \tag{2.3}$$

where ε is dielectric permittivity, σ is ohmic conductivity, and ω is the electric field frequency.

If ε_p^* and ε_m^* in equation (2.2) are substituted with equation (2.3), the real part of Clausius-Mossotti factor can be calculated as:

$$Re[K] = \frac{(\varepsilon_p - \varepsilon_m)(\varepsilon_p + 2\varepsilon_m) + \frac{1}{\omega^2}(\sigma_p - \sigma_m)(\sigma_p + 2\sigma_m)}{(\varepsilon_p + 2\varepsilon_m)^2 + (\frac{\sigma_p + 2\sigma_m}{\omega})^2} \tag{2.4}$$

where ε_p, σ_p, ε_m and σ_m are the electrical permittivity and conductivity of particle and medium, respectively. The ε_p and ε_m in our research refer to the electrical permittivity of cell and suspension medium, which will be discussed in the following section, both their values are relatively close to

each other, and are orders of magnitude less than σ_p and σ_m, so the sign and magnitude of $Re[K]$ is approximately determined by σ_p and σ_m.

Therefore, from equation (2.4), we can generally distinguish between positive and negative dielectrophoretic effects:

Positive dielectrophoresis (pDEP): $Re[K]>0$ ($\sigma_p > \sigma_m$). Particles are attracted to electric field intensity maxima and repelled from minima.

Negative dielectrophoresis (nDEP): $Re[K]<0$ ($\sigma_p < \sigma_m$). Particles are attracted to electric field intensity minima and repelled from maxima.

In our DEP MEA system, positive DEP, integrated with low-conductivity medium will be applied to actively trap cells onto the top of each of the MEA electrodes.

2.1.2 Dielectrophoretical Cell Model

In order to investigate the complex frequency dependence of DEP, biological cells are often modeled as simple dielectric spherical particles with lossy shells. Walled cells are the structural building blocks of plants, but many important single-cell microorganisms also take the basically similar form [28]. Fig. 2.2(a) depicts the very simple model of a spherical walled cell, which consists of three regions: cell wall, cell membrane and cell interior (cytoplasm). The cell wall provides structural support or mechanical protection to the cell. The cell wall is usually molded as a homogeneous spherically concentric shell of finite thickness with bulk permittivity ε_w and ohmic conductivity σ_w.

The cell membrane has a selectively permeable bi-layer of liquid protein molecular; it functions as a two-way conduit for nutrients required by cell growth and waste materials from the cell [28]. The membrane serves as a low loss capacitor, and it is typically characterized by effective capacitance c_m and conductance g_m, both per unit surface area.

The cell interior contains an aqueous ionic environment where various structures are suspended, including the nucleus. Here, a homogeneous simplified model with dielectric permittivity ε_c and ohmic conductivity σ_c is used to represent the cell interior (cytoplasm).

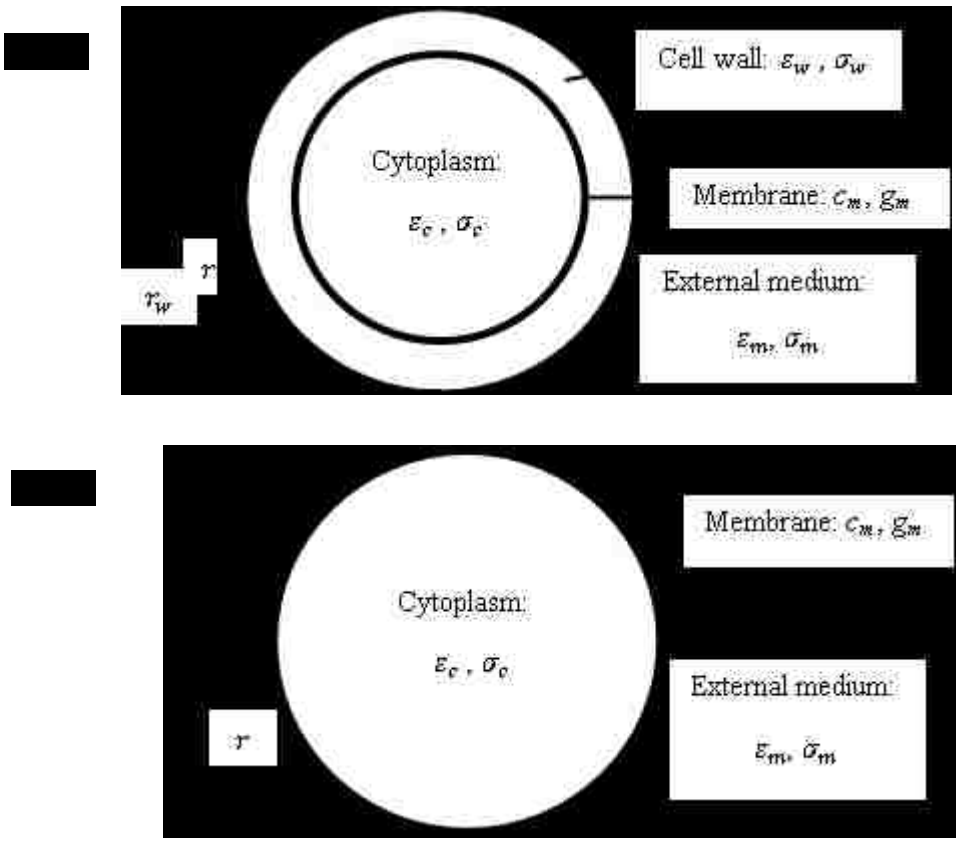

Figure 2.2 Simple dielectric model of a walled cell (a) and a mammalian cell (b).

Compared with walled cells, mammalian cells, including neurons, usually lack a cell wall. This makes the mammalian cells comparable to the protoplast model, where a conductive fluid interior is enclosed by a very thin capacitive layer (membrane), as sketched in Fig. 2.2(b). Analytical expression for cell complex permittivity ε_p^* is [28]:

$$\varepsilon_p^* = c_m r[\frac{jw\tau_c + 1}{jw(\tau_m + \tau_c) + 1}] \tag{2.5}$$

c_m is the effective cell membrane capacitance and r is the cell radius, where $\tau_m = c_m r/\sigma_c$ and $\tau_c = \varepsilon_c/\sigma_c$. Assuming the transmembrane conductance g_m is negligible, substituting equations (2.3) and (2.5) for the complex permittivity of medium and cell respectively into (2.2), the analytical expression of C-M factor for mammalian cells (neurons) in medium is:

$$K(\omega) = \left[\omega^2\left(\frac{\varepsilon_m}{\sigma_m}\frac{c_m r}{\sigma_c} - \frac{\varepsilon_c}{\sigma_c}\frac{c_m r}{\sigma_m}\right) + j\omega\left(\frac{c_m r}{\sigma_m} - \frac{\varepsilon_m}{\sigma_m} - \frac{c_m r}{\sigma_c}\right) - 1\right]\left[2 - \omega^2\left(\frac{\varepsilon_c}{\sigma_c}\frac{c_m r}{\sigma_m} + 2\frac{\varepsilon_m}{\sigma_m}\frac{c_m r}{\sigma_c}\right) + j\omega\left(\frac{c_m r}{\sigma_m} + 2\frac{\varepsilon_m}{\sigma_m} + 2\frac{c_m r}{\sigma_c}\right)\right]^{-1} \quad (2.6)$$

where r is cell radius, ε_c and ε_m are the dielectric permittivity of cell and suspension medium respectively, σ_c and σ_m are the ohmic conductivity of cell interior (cytoplasm) and medium, c_m is cell membrane effective capacitance per unit area, and ω is the angular frequency of the electric field.

2.1.3 Frequency Dependence of DEP

According to equation (2.6), the real part of Clausius-Mossotti Factor is determined by the dielectric and conductive properties of the cell and suspension medium, as well as the frequency of the electric signal used to create the electric field. Consequently, with specified biological cells and suspension medium, the frequency-dependence of DEP force exerted on mammalian cells is determined by the relationship between the real part of the C-M factor, $Re[K]$ and angular frequency ω; furthermore, a dielectrophoretic frequency spectra plot of $Re[K]$ will give the interested frequency range for expected DEP effect.

It is one of our objectives to actively attract mouse hippocampal neurons to the electrodes of the MEA, with pDEP. Therefore, the frequency spectra of $Re[K]$ has been simulated using Maple (Maplesoft, Inc.), for primary mouse hippocampal neurons in a DEP suspension medium that is a mixture of 10% sucrose (w/v in deionized water) and primary neuron culture media, NbActiv1 (BrainBits, LLC.), at different ratios (Fig. 2.3). For instance, the 30% cell media data line (magenta)

represents the mixture consisting seven parts of 10% sucrose (w/v in deionized water) and three parts of NbActiv1. These sucrose/cell media mixtures have low conductivity and appropriate physiological osmolarity for neurons to survive during pDEP trapping [30]. The simulation was based on dielectric and physical properties of neurons and suspension medium from measurement and literature, as listed in Tables 2.1 and 2.2. Medium conductivities were measured by the EC410 Conductivity/TDS/Salinity Kit (EXTECH Instruments, Inc.), and average cell radius (20 cells were measured) was determined by digital microscopy software, Motic Images Plus 2.0, on a PSM-1000 microscope (Motic Group CO., LTD.). The other properties, including suspension medium permittivity, cell interior permittivity, cytoplasm conductivity, and cell membrane effective capacitance, were obtained from the literature [31-36]. Because of the lack of the literature data on the properties of mouse hippocampal neurons, averages were taken from closely-related mouse neurons, such as mouse CA3 pyramidal neurons and interneurons [31, 34] and cortical rat neurons [33], as can be seen in Table 2.1.

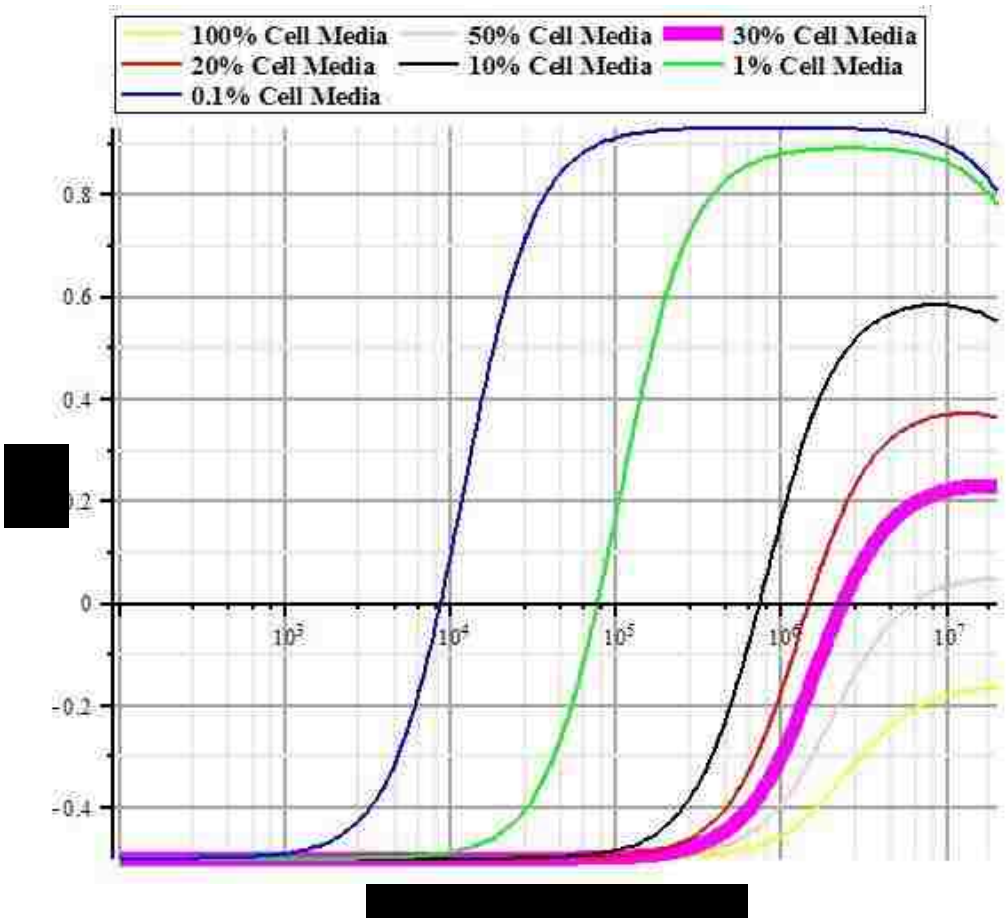

Figure 2.3 DEP spectra simulations of mouse hippocampal neurons in suspension media consisting of 10% sucrose (w/v in deionized water): cell media at different ratios.

Our modeling has shown that positive DEP (pDEP) is not possible in pure (100%) cell media (Fig. 2.3, yellow lines) within our frequency range of interest, because in that range, the real part of Clausius-Mossotti factor is negative (see Fig. 2.3). This negative DEP is caused by the high conductivity of the medium. With the addition of sucrose, however, the suspension medium conductivity is lowered, thereby enabling pDEP. The positive plateau regions in Fig. 2.3 indicate the frequency ranges for the maximum pDEP effect in different situations. The bold (magenta) data line (30% cell media) indicates the cell media concentration in suspension medium that we eventually selected to use in our neuronal trapping experiments, because this suspension medium has proved effective for pDEP hippocampal trapping (described in section 3.1 Neuronal pDEP

Active Recruiting). It contains relatively more neuron culture media than the other options, which renders it more favorable for neuronal survival.

Table 2.1 Dielectric and physical properties for hippocampal neurons simulated in Fig. 2.3.

	Cytoplasm permittivity $\varepsilon_c/\varepsilon_0$	Cytoplasm conductivity σ_c (S/m)	Cell radius r (μm)	Membrane effective capacitance c_m (F/m^2)
Hippocampal Neurons	78[a]	0.65[b]	4	0.008[c]

[a] [33, 36];
[b] Averaged from [31, 33, 34];
[c] Averaged from [31-34];

Table 2.2 Dielectric and conductive properties for DEP suspension medium.

	Medium permittivity $\varepsilon_m/\varepsilon_0$	Medium conductivity σ_m (S/m)
Cell Media (NbActiv1)	80[a]	1.104
10% Sucrose	76[b]	1.5x10^{-4}

[a] [36];
[b] [35].

2.2 Device Structure Simulation (FEA & DEP)

In order to explore the intricacies of pDEP attraction of cells on electrodes, DEP electric field simulation was performed with CoventorWare (Coventor, Inc.) finite element analysis (FEA) software. A simplified one-electrode model based on targeted device structure was built (see Fig. 2.4(a)). In this model, bottom electrode is sandwiched between glass substrate and silicon oxide passivation layer, and a via is etched through the passivation layer to open and define the electrode site. SU-8 epoxy is patterned above the passivation layer, where different microstructures, including microchambers and microtrenches, are created using using photolithography. In the electrostatic

simulation, +3V potential was applied to the electrode. The simulated electric field distribution is shown in Fig. 2.4(b). It can be seen that the electric field maximum area is located above the open via, as the central red peak extending above the surface indicates. This means the cell will be attracted to the open via on top of the electrode when pDEP is implemented [37].

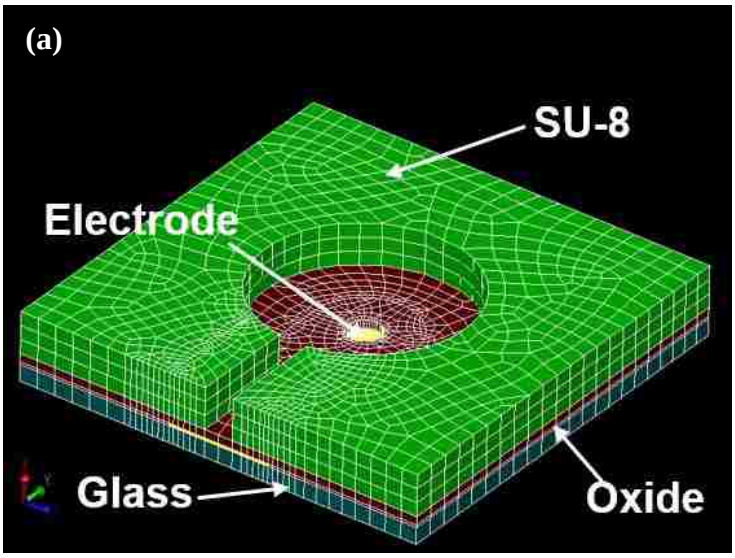

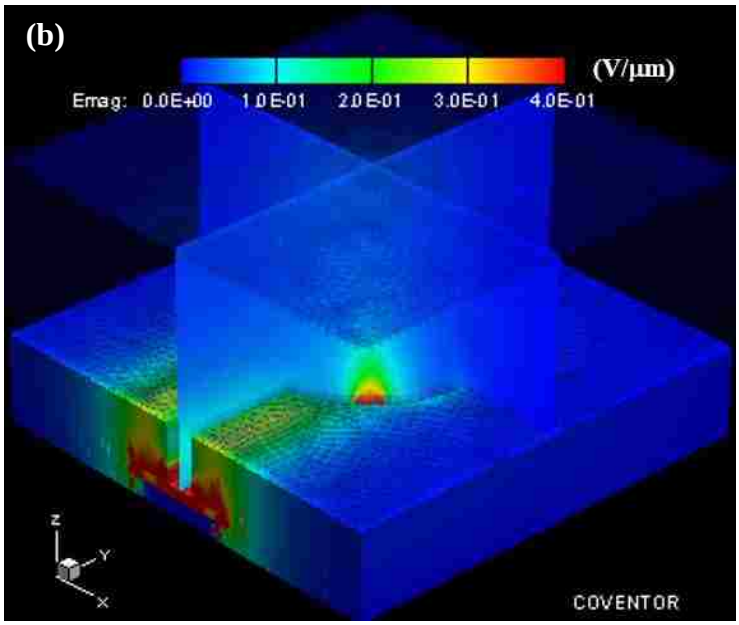

Figure 2.4 (a) FEA model of DEP MEA electrode structure where the bottom blue layer is glass, the red layer is silicon oxide, and the green layer is SU-8. The electrode (yellow) is sandwiched between the glass and silicon oxide. (b) Simulated electric field distribution using CoventorWare (Coventor, Inc.) where red area in the center that extends above the surface is attractive to cells by positive DEP because of stronger electric field intensity.

With electric potential data extracted from Coventor, 2-D electric field gradient and DEP force distribution can be calculated in MATLAB (MathWorks, Inc.) using equation (2.1). The electric field gradient and DEP force distribution at the surface above SU-8 layer, where the cells will be located before they are trapped by pDEP, are shown in Fig. 2.5. Maximum DEP force areas (shown in dark red color in Fig. 2.5 (bottom)) are also located above the open via on top of electrode.

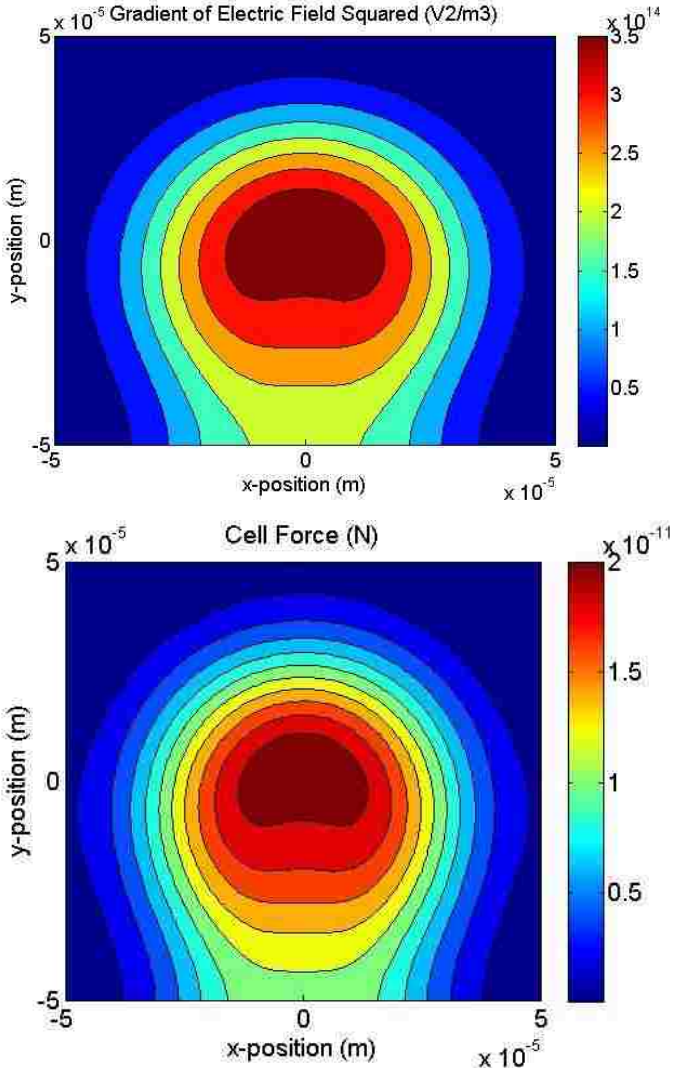

Figure 2.5 2-D MATLAB plots of gradient of electric field squared (top), and DEP force on cell (bottom). The surface of interest sits above the SU-8 epoxy layer.

2.3 Layout and Fabrication

2.3.1 Design Revision 1

Based on the electrode structure modeling, discussed above, we designed our DEP MEA device, which consists of a 16-electrode array. The fabrication process starts with a quartz glass substrate, based on a three-mask process, which is described in detail in Appendix II: DEP MEA Fabrication Process. Generally, the first metal electrode layer is created by e-beam metal evaporation and lift-off process, using the first photomask (Fig. 2.6). Then an oxide passivation layer is deposited and patterned by a second photomask (Fig. 2.7). This passivation layer forms an electrical isolation between the electrode and the ionic cell media. Finally, an epoxy layer made from a photosensitive material is patterned, using the third photomask (Fig. 2.8), to create microstructures for mechanical neuronal confinement.

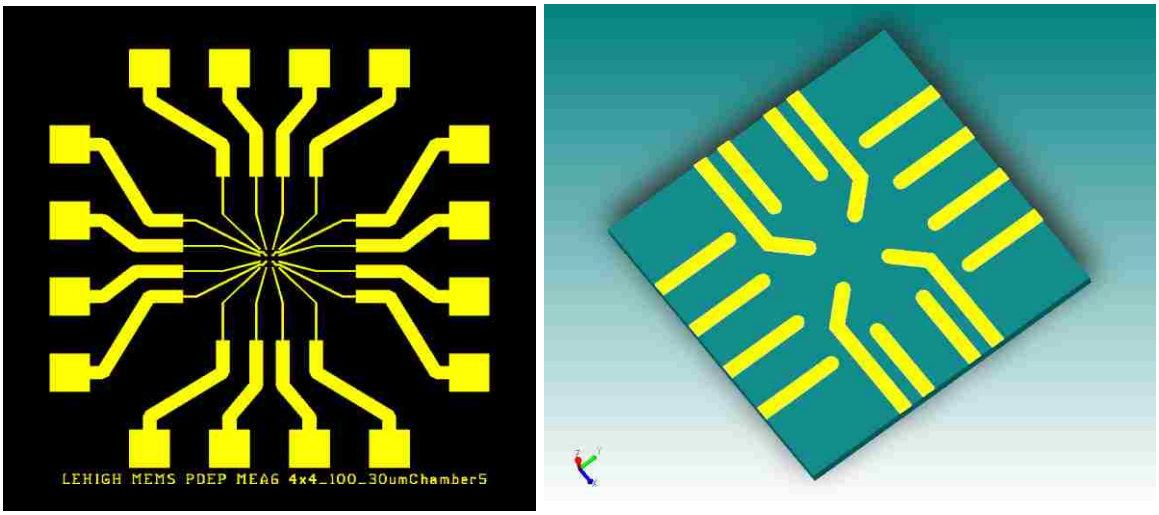

Figure 2.6 First layer mask defining the electrodes (yellow) on a quartz substrate. The entire DEP MEA die is shown on the left, a 3-D fabrication simulation focusing on the central electrode area is shown on the right.

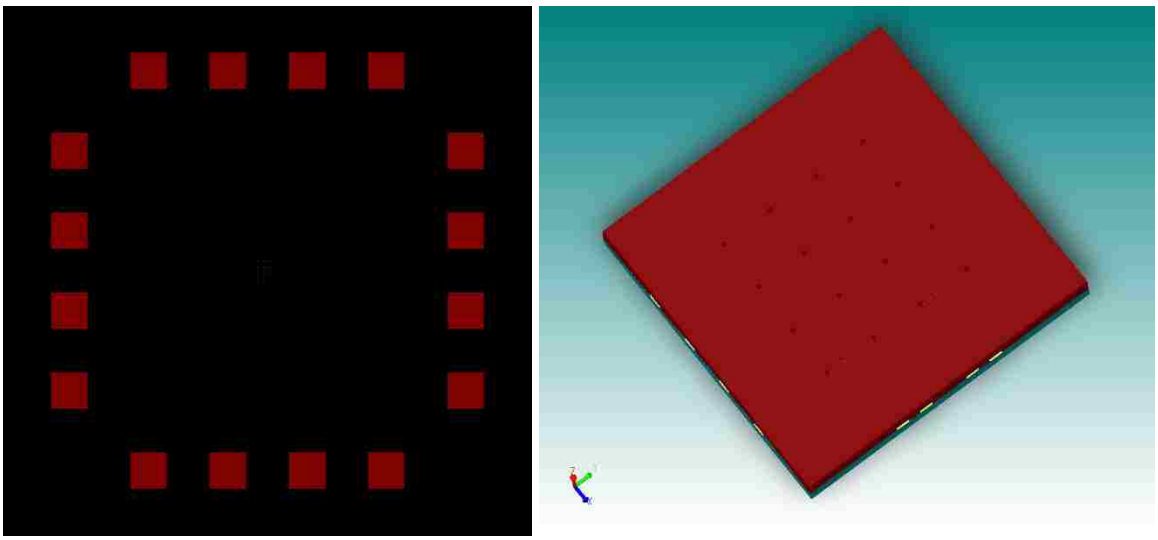

Figure 2.7 Second layer mask defining the passivation oxide (red). The entire DEP MEA die is shown on the left, a 3-D fabrication simulation focusing on the central electrode area is shown on the right.

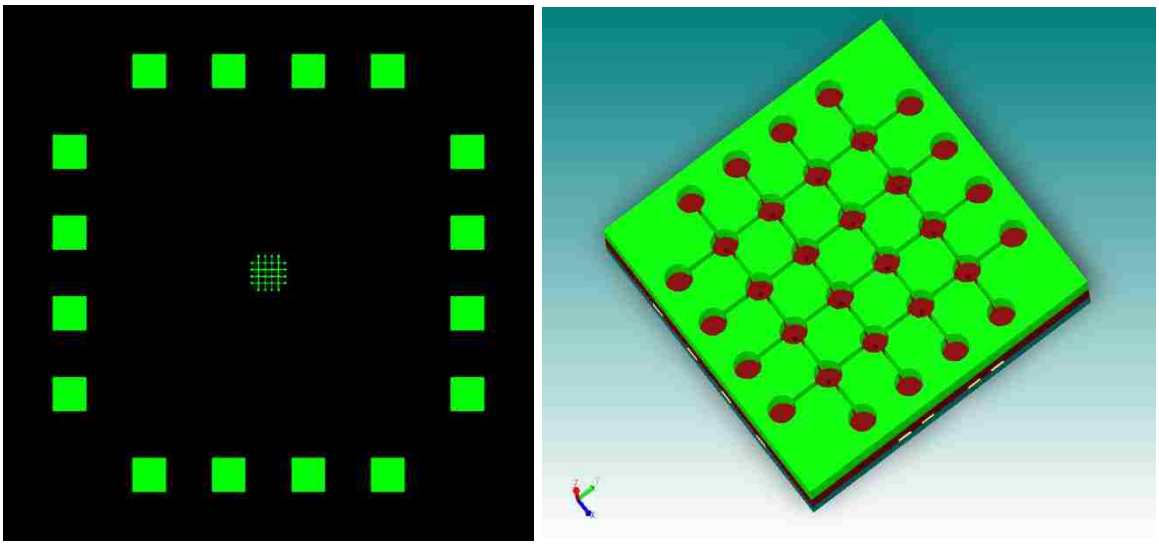

Figure 2.8 Third layer mask defining the epoxy microstructures (green). The entire DEP MEA die is shown on the left, a 3-D fabrication simulation focusing on the central electrode area is shown on the right.

The fabrication process (see Fig. 2.9) starts with a 3-inch quartz wafer (Mark Optics, Inc.). Quartz wafers are selected because of their higher purity compared to other glass wafers, and because of fewer concerns for cross-contamination issues in our microfabrication facility. First, a layer of negative photoresist for lift-off, nLOF2070 (AZ Electronic Materials Corp.), is patterned on the

wafer (a-b). Then 20 nm of titanium (Ti), 300 nm of gold (Au), and 20 nm of chromium (Cr) are deposited with an E-beam evaporator (c), followed by lift-off process (d) to define the metal electrodes and bonding pads. The Ti layer is an adhesion layer between quartz and gold; the Cr layer promotes the adhesion between gold and SU-8 epoxy, which is patterned during subsequent steps, as described below. After lift-off, 1 μm of silicon oxide is deposited using Plasma Enhanced Chemical Vapor Deposition (PECVD) (e), to be used as the passivation layer. Vias, located on top of electrodes and bonding pads, are etched by Reactive Ion Etching (RIE) using CF_4 and O_2 (f). The last layer is a photopatternable SU-8 epoxy (MicroChem Corp.), into which microstructures, including microchambers and microtrenches, are created through lithography (g). Finally, Cr etch is performed to remove the top Cr layer from the DEP electrode sites and gold bonding pads (h).

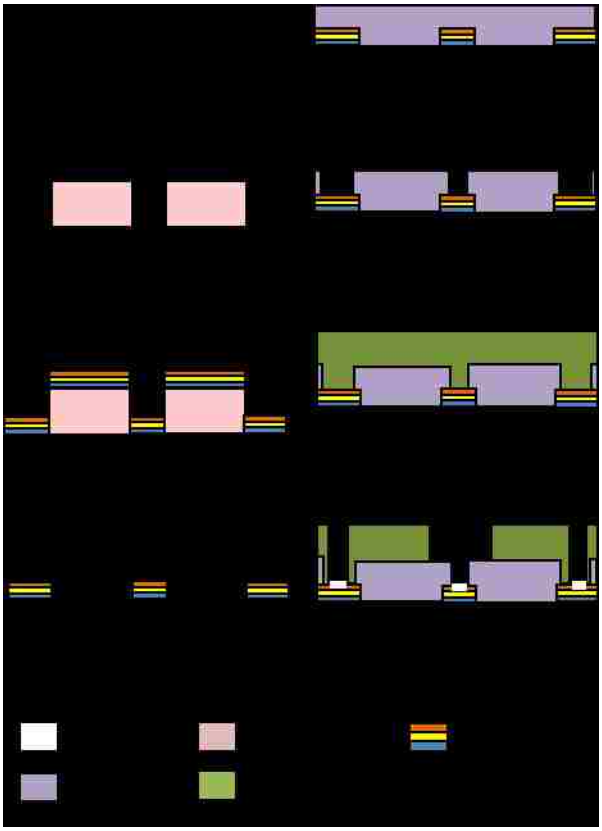

Figure 2.9 Fabrication process flow for DEP MEA.

Each DEP MEA (8 mm x 8 mm) has 16 electrodes, of 25 μm in diameter, connected to 16 wire bonding pads at the edge of the chip. The distance between adjacent electrodes is 100 μm. See Fig. 2.10 and Fig. 2.11 for an overview of the location of the major parts of the chip. Silicon oxide vias etched on top of each electrode have diameters of 6 μm, defining each electrode site, and SU-8 microchambers are patterned above each electrode, with microtrenches connecting them. These SU-8 microstructures are designed to mechanically confine the growth of neuronal processes once neurons are anchored on top of each electrode by pDEP, so that geometrically-defined neuronal networks can be formed. Different dimensions are designed, including the diameter (20μm, 30μm and 50μm) of the microchambers and the width (2 μm, 5μm and 7μm) of the microtrenches, respectively. Finally, an optical micrograph of the fabricated DEP MEA is shown in Fig. 2.12, with a close-up view of the 16-electrode array at the center of the chip and a scanning electron microscopy (SEM) image showing the detailed structure of one of the electrodes.

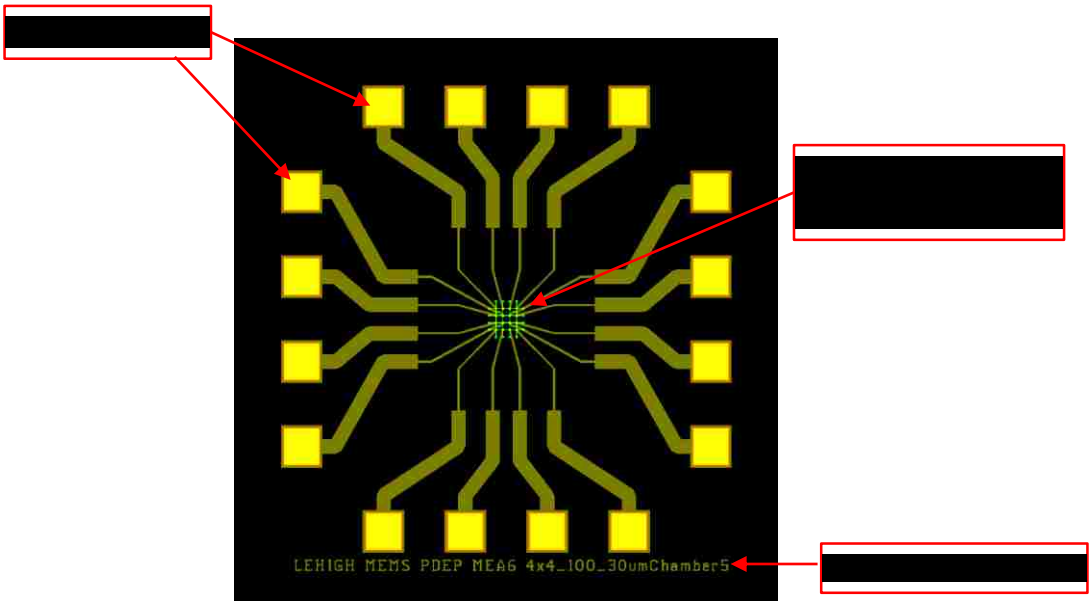

Figure 2.10 Stacked three-layer masks of a single DEP MEA die. Each device die is 8 mm by 8 mm square.

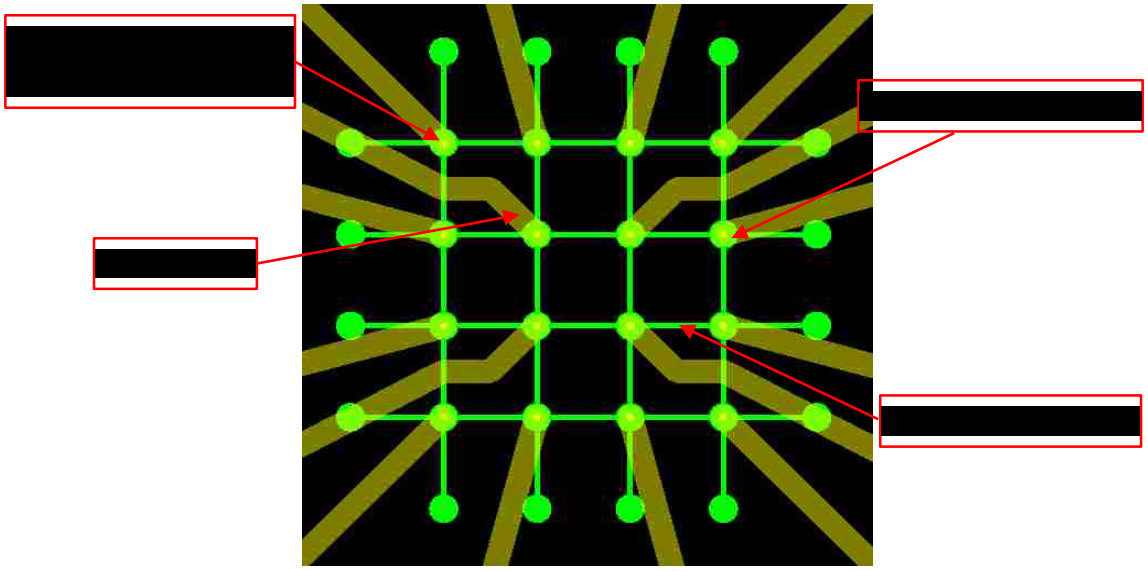

Figure 2.11 Close-up view of masks focusing the central electrode array region, with labeled features.

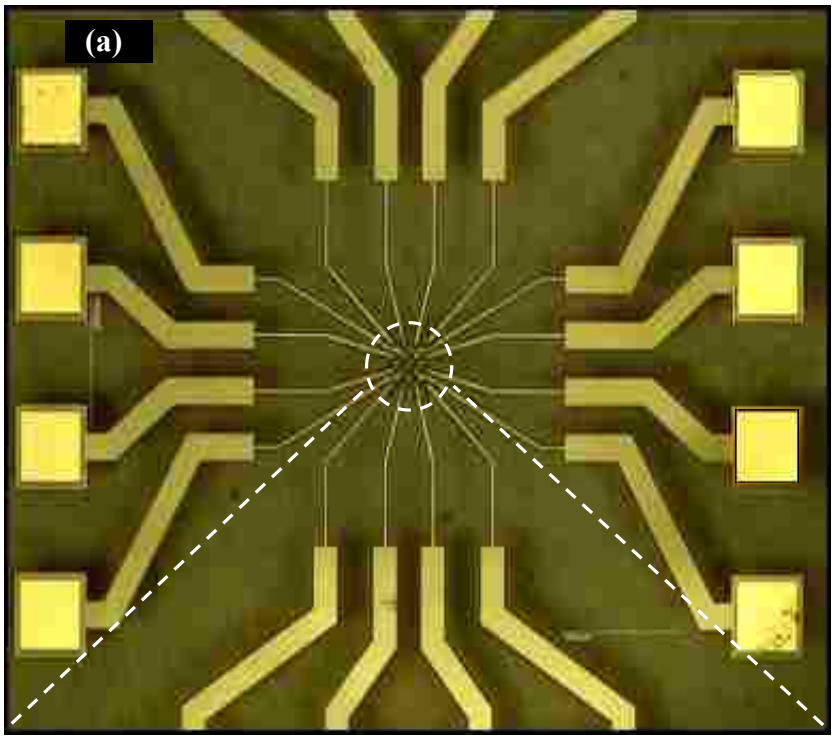

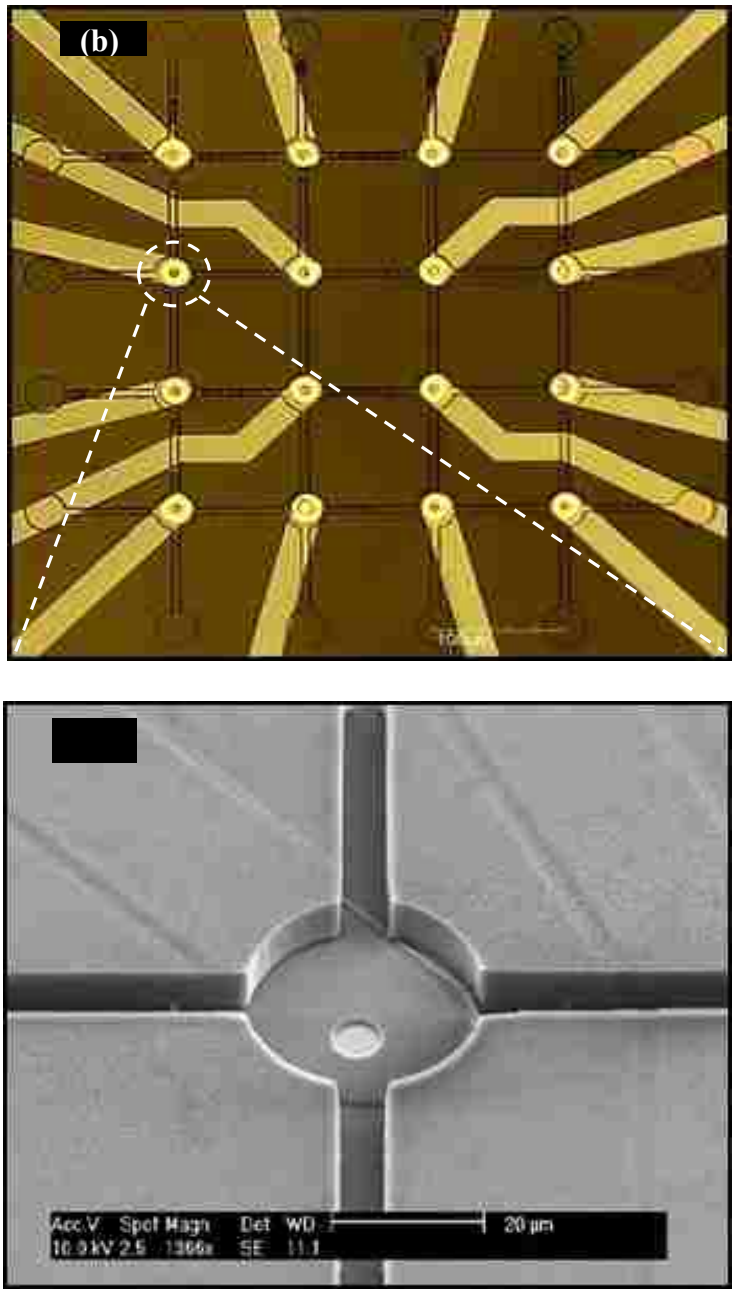

Figure 2.12 DEP MEA design and fabrication. (a) Optical micrograph of fabricated DEP MEA, another eight bonding pads on the top and bottom are not shown here. (b) A close-up view of the central 16-electrode array with SU-8 microchambers above connected by microtrenches to guide the growth of neurites. (c) An SEM image showing the structure of one electrode site. Scale bars in (a), (b) and (c) are 1000 µm, 100 µm and 20 µm respectively.

2.3.2 Design Revision 2

The DEP MEA devices were fabricated based on the first version of design, described above. Neuronal active recruiting and neural network patterning experiments were performed to verify the functions of the system, as will be discussed in detail in Chapter 3: Active Neuronal Recruiting and Patterning with DEP MEA System. A few drawbacks, about the device design, arose during the experiments, which led to potential improvements. These drawbacks are listed below.

1) With inverted microscopes (objectives sitting underneath the sample), which are usually used in biological experiments, the views of neurons trapped on the electrodes are blocked, because the 25 μm-diameter electrodes are larger than neuron bodies, and the electrodes are not transparent.

2) No reference electrode was designed on the chip, so that additional ground (reference) has to be provided during both the neuronal DEP recruiting and neuronal potential recording experiments. During the recruiting process, the DEP suspension medium has to be grounded for optimal DEP effect on the electrodes. While performing neuronal potential recording, background noise signal has to be "picked up" by the reference electrodes, so that the noise can be subtracted through differential amplification.

3) There are limited design combinations about the SU-8 microchamber diameters and microtrench width. In the first version of design, three parameter-combinations are included (microchamber diameter (μm) – microtrench width (μm)): 50-7, 30-5, and 20-3. However, it is observed in the experiments that, 20 μm chambers are best for neuronal recruiting on the electrodes with single-cell resolution, and 7 μm trenches are the most effective for the patterning of neurites. Therefore, more variable microstructure designs are needed for optimal neuronal recruiting and patterning.

4) In the first version of wafer-scale mask design, half of the wafer is arranged for DEP electrode test structures, for the purpose of pDEP cell trapping test, as described in [37].

After the cell trapping test, there is room for improving the throughput of fabrication of the DEP MEA chips.

As a result, due to these limitations, improvements are made in the second version of device design, based on the first version. The dimension of each die is kept at 8 mm by 8 mm, and the fabrication process is also the same. See Fig. 2.13 and Fig. 2.14 for an overview of the DEP MEA die in the second version of design. In the new design:

1) The diameter of the electrodes has been reduced to 10 μm, with the goal that when neurons anchored on the electrodes, partial of the neuron bodies will be viewable with inverted microscopes.

2) Four reference electrodes have been supplemented, in addition to the 16 working electrodes, to function as ground and reference in the DEP recruiting and neuronal recording processes.

3) There are more design combinations for the SU-8 microchamber diameter and microtrench width, such as (microchamber diameter (μm) – microtrench width (μm)): 20-5, 30-3, 30-7 and 50-5. In addition to 100 μm, the distances between electrodes of 150 μm and 200 μm have also been included.

4) After successful cell trapping test, in the second version of layout design, DEP MEA chips are designed throughout the whole wafer to improve the throughput of the fabrication.

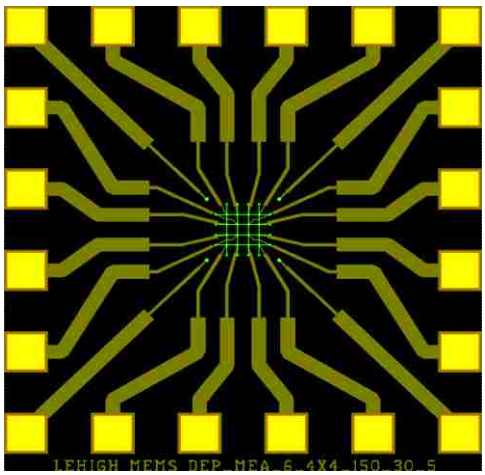

Figure 2.13 Stacked three-layer masks of a single DEP MEA die in the second version of device design. Each device die is also 8 mm by 8 mm square.

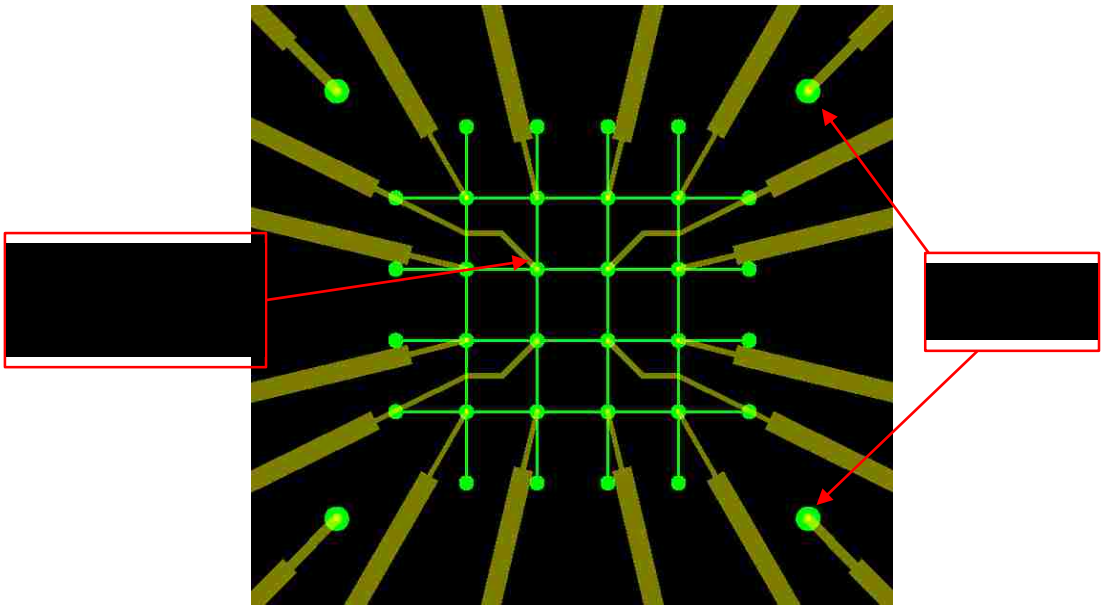

Figure 2.14 Close-up view of masks focusing the central electrode array region, with labeled new features in the second version of design.

2.4 Device Packaging

A DEP MEA chip was wire bonded (Appendix III: DEP MEA Device Packaging Process) on a Side-Brazed Dual In-Line Ceramic Package (DIP) (Spectrum Semiconductor Materials, Inc.) with a polydimethylsiloxane (PDMS) pad (0.6 mm thick) attached underneath (Fig. 2.15(a)). A three-

mm-diameter hole was drilled, by a diamond tip, at the center of the DIP to facilitate visualization with inverted microscopes. A pre-made PDMS mold was attached on the DIP package with uncured PDMS to form a five-mm-deep neuronal culture chamber, where Tygon microbore tubing (Cole-Parmer) was embedded for microfluidic transmission during the pDEP process (Fig. 2.15(a-b)). The purpose of the PDMS pad positioned underneath the MEA chip was to raise the chip's surface to the same level of the microbore tubing so that neurons driven by media were floating right on top of the MEA. The whole packaged device was autoclaved for 20 min prior to usage. In addition, a customized, printed circuit board (PCB) (Chapter 5) (Fig. 2.15(c)) was designed and fabricated to provide an electric signal interface for pDEP trapping.

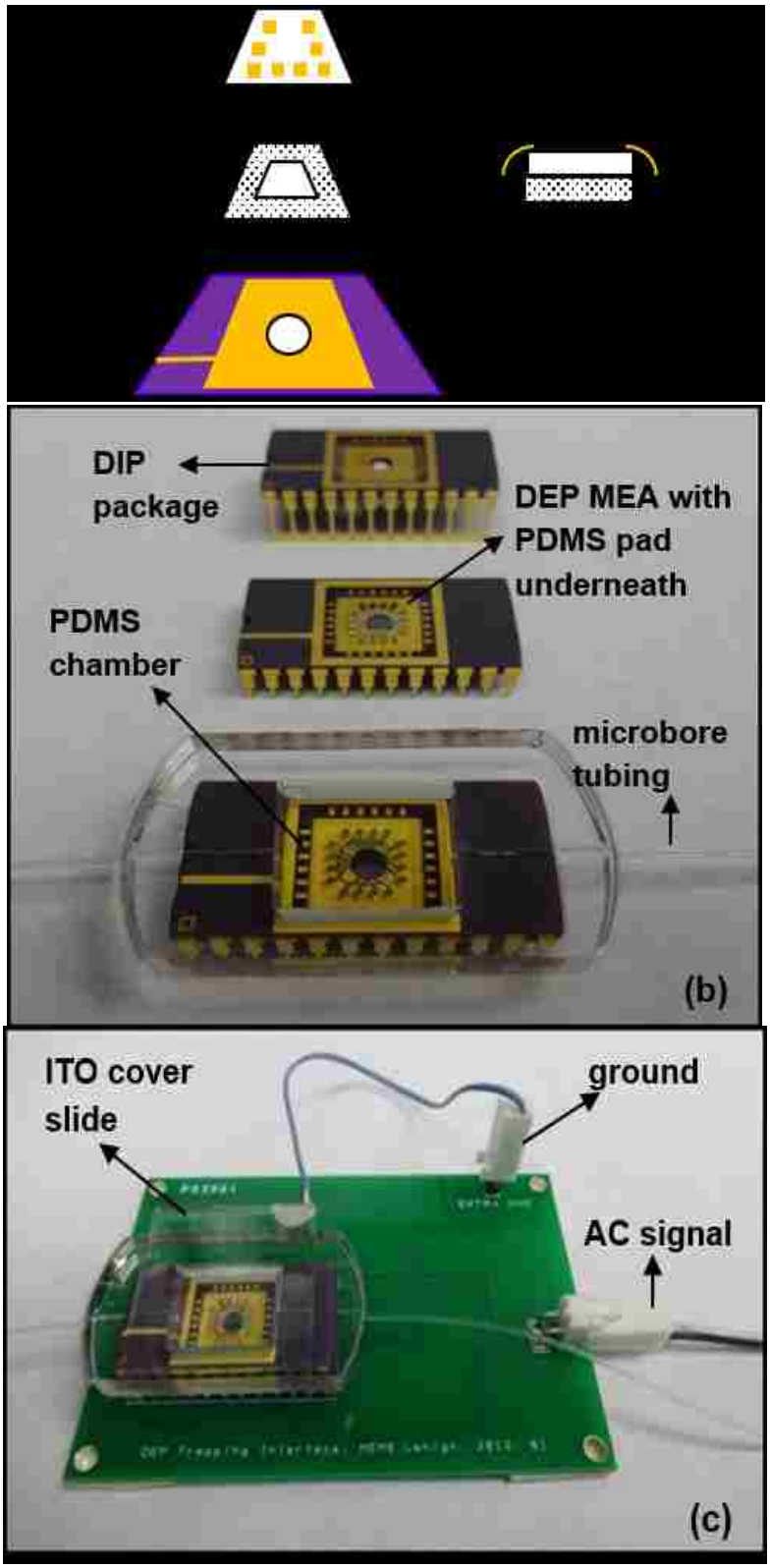

Figure 2.15 Device packaging. (a) Schematic of DEP MEA packaging process. (b) Picture showing a packaged DEP MEA device. (c) pDEP neuronal recruiting setup.

Chapter 3: Active Neuronal Recruiting and Patterning with DEP MEA System

In this chapter, positive dielectrophoresis (pDEP) is applied to actively recruit hippocampal neurons to the electrodes of our DEP MEA, whereas SU-8 microstructures such as chambers and trenches are created to effectively define a patterned neuronal network. Various pretreatment methods of SU-8 photopatternable epoxy are studied to improve the biocompatibility of thin-cured SU-8 layers implemented here as a structural material, particularly as it reflects on hippocampal neurons. The functionality of our novel MEA system is proven by the successful recording of spontaneous and stimulated neuronal potentials from primary hippocampal neurons, including the propagation of evoked neuronal bursts between electrodes. In order to pattern neurons with positive dielectrophoresis (pDEP), neurons have to survive the implementation of pDEP, which attracts them to the electrodes. In this chapter, we also systematically evaluate the long-term (up to 12 hours) viability of embryonic mouse hippocampal neurons after being actively positioned on the electrodes of a custom-made MEA using dielectrophoresis.

3.1 Neuronal pDEP Active Recruiting

3.1.1 Hippocampal Neuron Dissociation and Culture

Embryonic mouse hippocampal neurons are actively trapped to the electrodes of the DEP MEA. Hippocampal neurons are investigated in this research because of their important role in the process of thought and memory, such as the transition of short-term memory to long-term memory and special navigation. The hippocampal cells are prepared for our experiments as follows.

To isolate hippocampal cells, embryonic (day 18) mouse hippocampus tissue (BrainBits, LLC.) is treated with filtered papain (Worthington Biochem. Corp.) in Hibernate E-Ca solution (BrainBits, LLC.) in a 30°C water bath for 30 min. Then, the tissue is transferred to 2 mL Hibernate EB medium

(BrainBits, LLC.) with a sterilized 9-inch Pasteur pipette (Fisher Scientific) and triturated using a P1000 micropipette. The triturated tissue and Hibernate medium are transferred, together, into a sterile 15 mL centrifuge tube. After being centrifuged at 200g for 1 min, dissociated cells are resuspended in NbActiv1 media (BrainBits, LLC.). This neuron/glial mixed suspension, diluted with NbActiv1 media to 20 x 10^4 cells/mL, is used immediately for DEP recruiting of hippocampal neurons in cell-trapping solution, as described in the following section. To culture hippocampal neurons, directly (without DEP), cell suspensions from the dissociation process, above, are plated at 1.6 x 10^4 cells/cm^2 on DEP MEA chips in NbActiv1 neuron culture media, and maintained in a humidified incubator at 37 ^oC with 5% CO_2. Hippocampus tissue dissociation procedure is described in detail in Appendix IV: Mouse Hippocampal Neuron Dissociation and Culture Protocol.

3.1.2 Neuronal pDEP Recruiting Protocol

Positive DEP is achieved in a low-conductivity 30% cell media cell-trapping solution, with a measured conductivity of 0.331 S/m; the cell-trapping solution consisted of seven parts of 10% sucrose (w/v in deionized water) and three parts of neuron culture media NbActiv1 (BrainBits, LLC.). Detailed DEP theoretical analysis can be found elsewhere [25, 28], as discussed in Chapter 2.

While applying pDEP to position the neurons on top of electrodes, the packaged DEP MEA device is anchored on the DEP interface PCB, and an ITO (Indium tin oxide)-coated cover slide (Sigma-Aldrich Co. LLC.), connected to ground, covers the PDMS chamber as a reference electrode, as can been seen previously in Fig. 2.15. In actual experiments, instead of connecting the ITO slide to the ground pin on the PCB through a conduction wire, a (ground) probe station microcontroller is used to hold the ITO slide, through a probe tip, above the packaged DEP MEA device, as can be seen in Fig. 3.1(a). With the microcontroller, the movement of the ITO slide can be achieved with much better precision above the PDMS chamber, both on and off the device. Electrical connections

between the ITO slide and the conduction wire or the tungsten probe tip are realized by applying a conductive silver epoxy. The ITO slide is rinsed with ethanol and sterilized DI water prior to usage. An AC electric signal of 6 Vpp and 10 MHz is provided by a function generator (Agilent 33521A) and fed into the PCB. The DEP neuronal trapping setup is mounted on the stage of an upright microscope (Nikon OPTIPHOT) while performing the experiments (Fig. 3.1(b)). DEP cell-trapping solution containing sterilized 10% sucrose (w/v in deionized water) and neuron media NbActiv1 is infused through the microbore tubing and into the PDMS chamber by two syringe pumps (inlet and outlet) (Harvard Apparatus). The frequency of the electric signal is selected at 10 MHz because, as shown previously in Fig. 2.3, the frequency provides the maximum pDEP effect in DEP suspension medium containing 30% cell media; furthermore, as will be discussed in the following sections, at this particular frequency, the integrity of the cell membrane can be ensured (section 3.2.2), and only neurons, instead of glial cells will be attracted to the MEA electrodes (Chapter 4). The amplitude of the signal is chosen to be 6 Vpp, as this voltage can prevent the cell membrane from breakdown (section 3.2.2), while being pDEP-neuronal-trapping effective.

The diluted neuron/glial mixed cell suspension (in NbActiv1 media), from the procedure above, is added into the PDMS chamber directly with a micropipette, and cells are permitted to settle on the MEA surface for 5 min. 10% sucrose is then added by a micropipette to create the 30% cell media cell-trapping solution. The ITO slide is lowered by the microcontroller to cover the PDMS chamber of the MEA device after the AC electric signal is turned on. Because of the high viscosity of the sucrose solution, cells tend to float rather than settle to the surface if pumped into the chamber together with DEP suspension medium, which makes the pDEP trapping of neurons very difficult, since the DEP effect is only effective near MEA surface, as demonstrated by our previous simulation [37]. DEP suspension medium, therefore, is transmitted through the tubing alone, to move cells across the MEA chip surface. Initially, 300-400 μL/min flow rate is applied for 5 min for cells to be recruited by pDEP; afterwards, 500 μL/min flow rate is used for another 5 min to

move away extra cells that are not anchored. The electric signal is turned off after the pDEP trapping, and neuron culture media, NbActiv1, is fed into the chamber at 300 μL/min for 5 min to replace the cell-trapping medium. Finally, the ITO slide is raised up off the device and the DEP MEA device is incubated with 5% CO_2 at 37 ^oC for 15 hours, covered with a customized petri dish lid, as shown in Fig. 3.1(c).

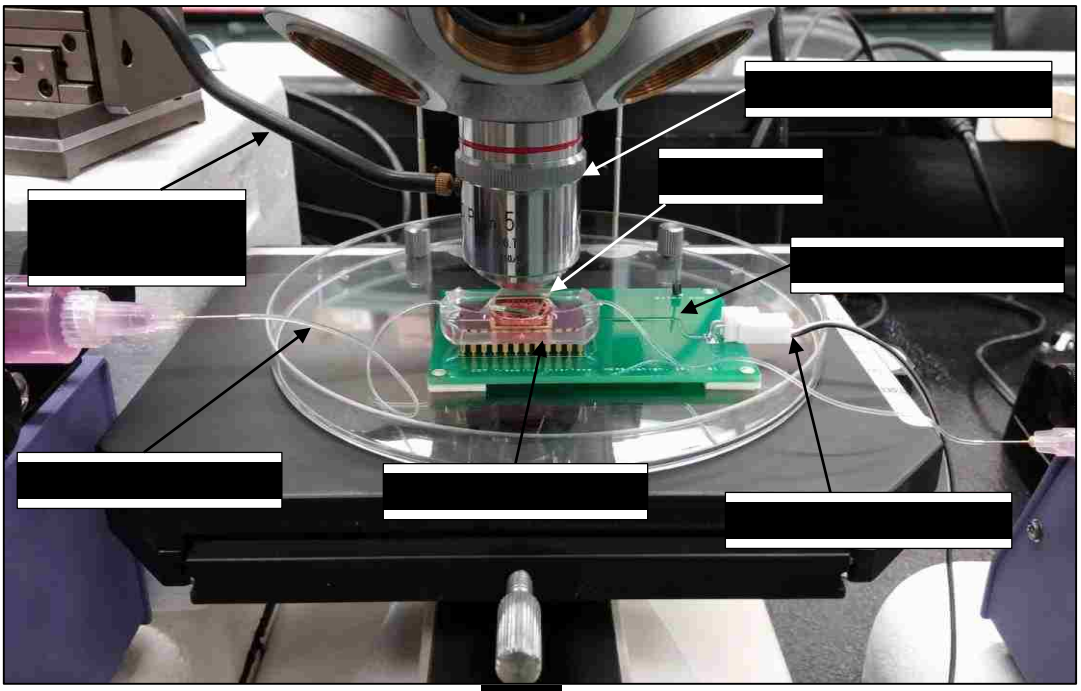

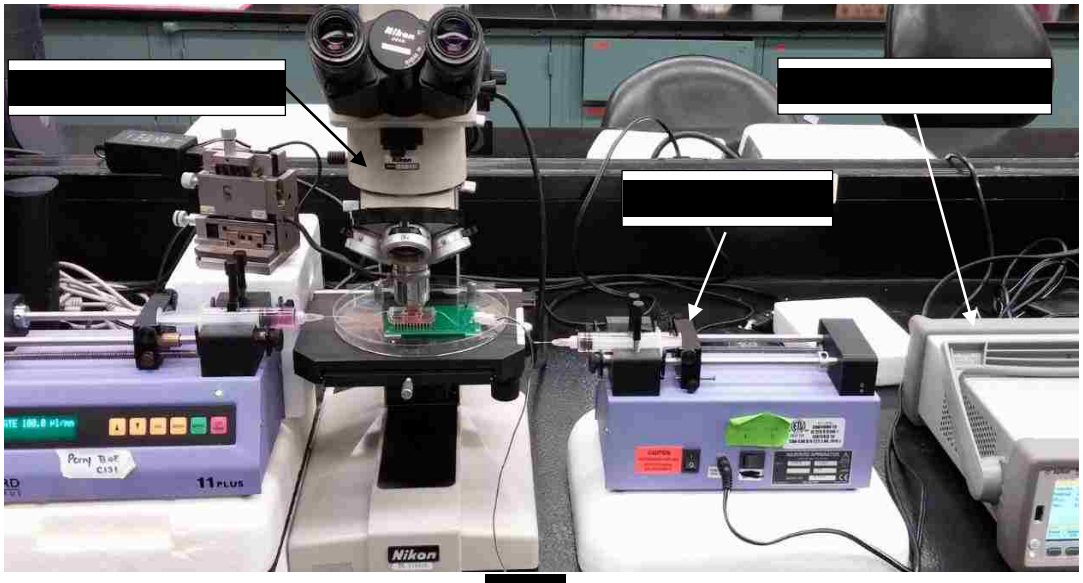

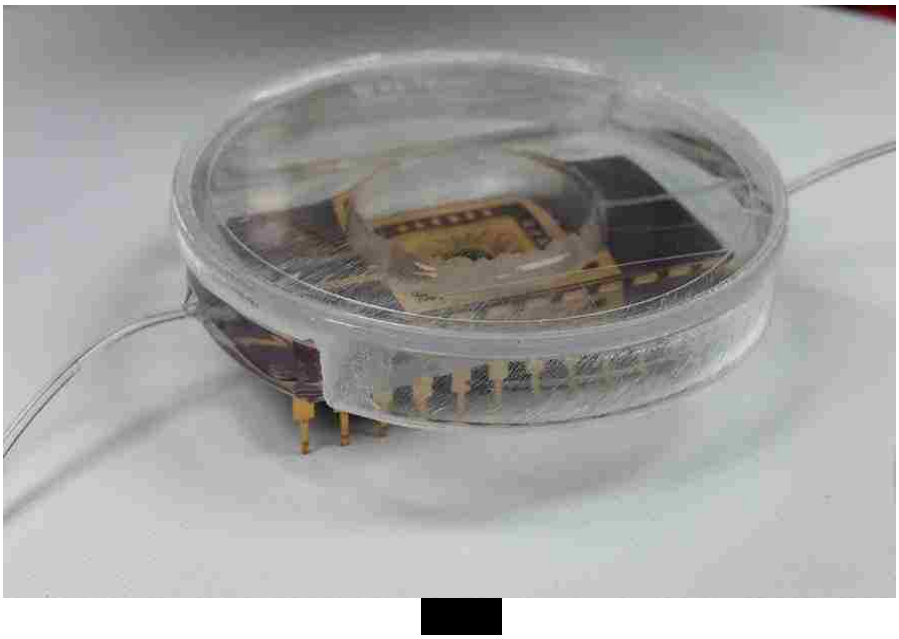

Figure 3.1 Neuronal pDEP recruiting experimental setup. (a) Close-up view of the packaged DEP MEA device during experiments, with labeled major components. A tungsten probe tip connecting the microcontroller and the ITO slide is hidden behind the microscope objective. (b) Overview of the pDEP neuronal recruiting experimental setup, with additional labeled major components. (c) A packaged DEP MEA covered with a customized petri dish lid, the lid also covers the device during the neuronal incubation.

3.1.3 Immunocytochemistry (ICC)

After DEP recruitment and 15 hours of incubation, anchored cells are fixed by 4% paraformaldehyde for 20 min at room temperature (RT), permeabilized with 0.1% Triton X-100 in phosphate buffered saline (PBS) for 15 min, and blocked with 0.01% Triton X-100 and 1% bovine serum albumin (BSA) in PBS for another 15 min. Cells are rinsed with 1X PBS, twice, between each step. Then, cells are incubated with primary antibodies, including Alexa Fluor-labeled, monoclonal neuronal class III β-Tubulin (TUJ1) (Covance; 1:500, in PBS containing 0.01% Triton X-100 and 1% BSA) and mouse monoclonal, Cy3-labeled, anti-glial fibrillary acidic protein antibody (GFAP-Cy3, 1:500, in PBS containing 0.01% Triton X-100 and 1% BSA; Sigma-Aldrich), at 4 ^{o}C for 16 hours to label neurons and glial cells, respectively. If necessary, cells are then treated with DAPI (4',6-Diamidino-2-Phenylindole) nuclear stain (Invitrogen; 1:1000, in PBS) at RT for 2

min, as a counterstain. After incubation, labeled cells are rinsed with PBS twice prior to fluorescent visualization with an Olympus 1X51 inverted microscope or a Nikon ECLIPSE E800 upright microscope. See Appendix V: Immunocytochemistry (ICC) Neuron/Glial Staining Protocol for detailed ICC operation procedure.

3.1.4 Neuronal Recruiting with Single-Cell Resolution

We have implemented active recruiting of hippocampal neurons with positive DEP according to the protocol described above. Following attachment to the MEA chip, neurons attracted to electrodes by pDEP are characterized by immunocytochemistry (ICC), as described in previous section. Labeled cells, anchored on top of electrodes are visualized using an upright fluorescence microscope Nikon ECLIPSE E800.

As shown in Fig. 3.2, the white circles indicate the SU-8 microchambers above 16 electrode sites, which in this case have diameters of 20 μm. It can be seen that all the electrodes are occupied, exclusively, by neurons (green), nine of which have single neurons anchored, four electrode sites are occupied by 2 neurons and the other three electrode sites have 3 neurons positioned. The coexistence of three glial cells is indicated by red circles. This exclusive attraction of neurons instead of glial cells will be discussed in detail in Chapter 4: Separation of Hippocampal Neurons from Glial Cells. For each of the chamber designs (20 μm, 30 μm, and 50 μm), neuronal recruiting experiments are repeated four times, and the best single-cell recruiting ratio we achieved is 57% for 20 μm chambers. This result verified that, with the implementation of pDEP at a frequency of 10 MHz, in cell-trapping solution contained 30% cell culture media, the DEP MEA system described here is capable of actively recruiting hippocampal neurons to the electrodes.

Furthermore, twelve hours after neuronal recruiting, live/dead stain shows that more than 96% (96 ±2%, n = 7) of the cells are live, as will be discussed in the following section, which indicates that hippocampal neurons are highly viable following the application of pDEP. Importantly, as also

shown in the following sections, the patterned neurons are active and functional, as we have successfully recorded both spontaneous and stimulated signals from neurons.

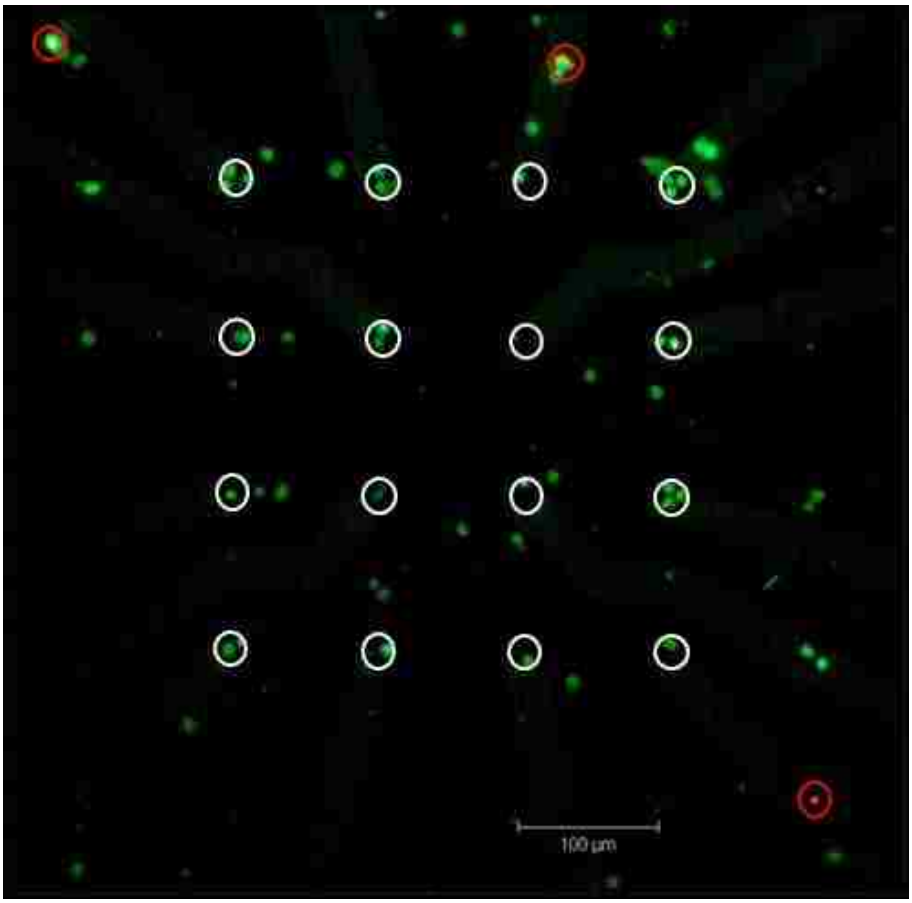

Figure 3.2 Immunofluorescence micrograph of hippocampal neurons (green) trapped by pDEP on electrodes and glial cells (red) anchored off electrodes. DEP electric signal applied: 10 MHz, 6Vpp. Cell-trapping medium contains 30% neuron culture media.

3.2 Hippocampal Neuronal Viability after DEP Positioning

Two factors influence the viability of neurons during the application of pDEP: 1) the DEP cell-trapping solution, because its low conductivity, which is desirable for trapping (pDEP is not possible in high conductivity, standard culture media), is not optimal for cell survival, and 2) electric field. The viability of a few types of neural cells, such as neural cortical cells and neural stem/progenitor cells (NSPCs), in DEP manipulation was investigated previously [24, 39], and high cell viability was achieved for short-term (1 min or less) DEP exposure. Here, we systematically

evaluate the long-term (up to 12 hours) viability of embryonic mouse hippocampal neurons after being actively positioned on the electrodes of our DEP MEA using dielectrophoresis.

3.2.1 Hippocampal Viability in Sucrose

In order for pDEP to take effect, the polarization of neurons should be stronger than that of surrounding media [28], which requires a low-conductivity environment. As a commonly used, low-conductivity buffer medium, sucrose solution is often used as the primary component of a pDEP trapping solution [39-41]. In our experiments, a 30% cell media DEP suspension medium, which is a mixture of seven parts of 10% sucrose(w/v in deionized water) and three parts of primary neuron culture media, NbActiv1 (BrainBits, LLC.), is used for neuronal pDEP recruiting on MEA. This sucrose/cell media mixture, with a measured conductivity of 0.331 S/m, has low conductivity and appropriate physiological osmolarity for neurons to survive during pDEP trapping [30].

While cell culture media does not compromise the health of neurons, the viability of embryonic mouse hippocampal neurons, in a more sever situation, 10% sucrose (only), which is the major component of the cell-trapping solution, is investigated. Dissociated hippocampal cells are resuspended in three sterile 15 mL centrifuge tubes, each containing 5 mL 10% sucrose (w/v in deionized water), and in another centrifuge tube of 5 mL cell media NbActiv1 as a control group. The three sucrose samples are placed at room temperature (RT) for 30, 60 and 90 min respectively, and the control tube is placed at RT for 90 min, as can be seen in Fig. 3.3. After each associated time period, 5 mL of phosphate buffered saline (PBS) is added to each of the sucrose tubes, and the samples are centrifuged at 200g for 5 min to harvest the cells. We find the dilution with PBS, above, necessary for pelleting the cells, because otherwise cells remain suspended in the high-viscosity sucrose solution, even after being centrifuged. The viability of harvested cells is assessed through use of Live/Dead^{TM} cell stain, (Invitrogen; Calcein, AM 2μM and Ethidium Homodimer, 1μM in cell media NbActiv1). After 15 min in dark at RT, the cell suspension is transferred to a 35 mm

petri dish using a micropipette, and five live/dead fluorescent micrographs are taken at random positions, for each sample, including the control group. Percent cell viability is calculated based on the average of five images. Typically, 30-40 cells are counted on each of the image.

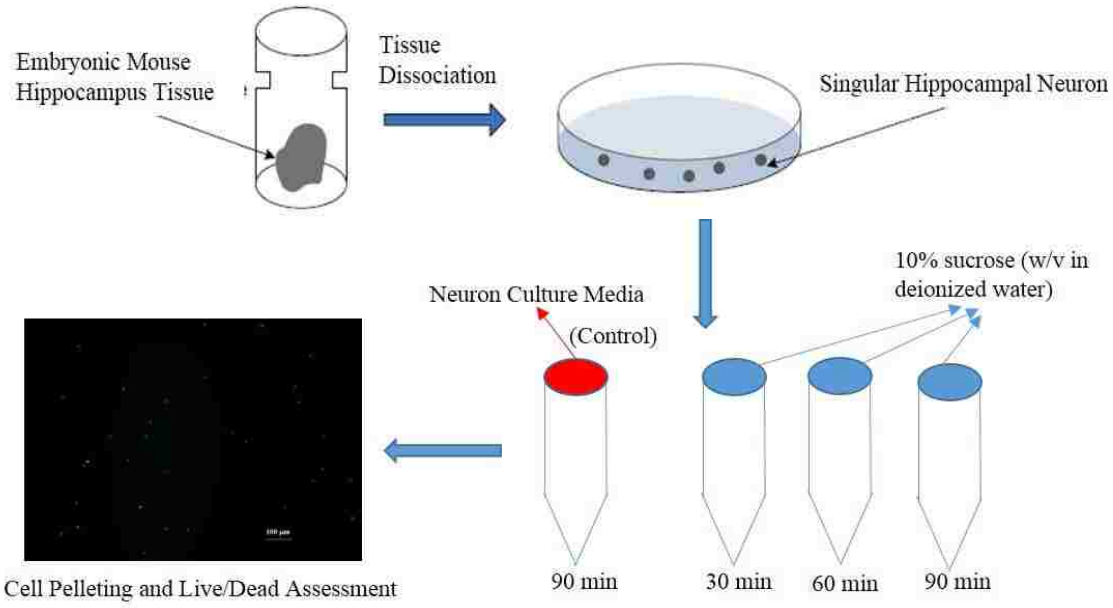

Figure 3.3 Experimental process for the study of the hippocampal viability in sucrose. Bottom left is a sample live/dead fluorescent micrograph of hippocampal cells after the sucrose treatment, scale bar is 100 μm.

The main objective of our study is to evaluate the effect of the cell-trapping solution on the viability of embryonic mouse hippocampal cells. As shown in Fig. 3.4, all three sucrose treatment samples have acceptable hippocampal viability compared to the control group (cell media); the parameter that should be kept in mind is that the entire pDEP trapping process normally lasts for less than 30 min, thus, that is the duration of exposure to cell trapping solution that has relevance for most of the experimental setups. The viability decreases slightly from 88±2% to 78±3%, as time in sucrose increases (up to 90 min), but the detrimental effect on cell survival is limited, confirming the feasibility of using 10% sucrose as the major component of the cell-trapping solution. In Fig. 3.4, the error bars represent the standard deviations of data from five randomly-taken images.

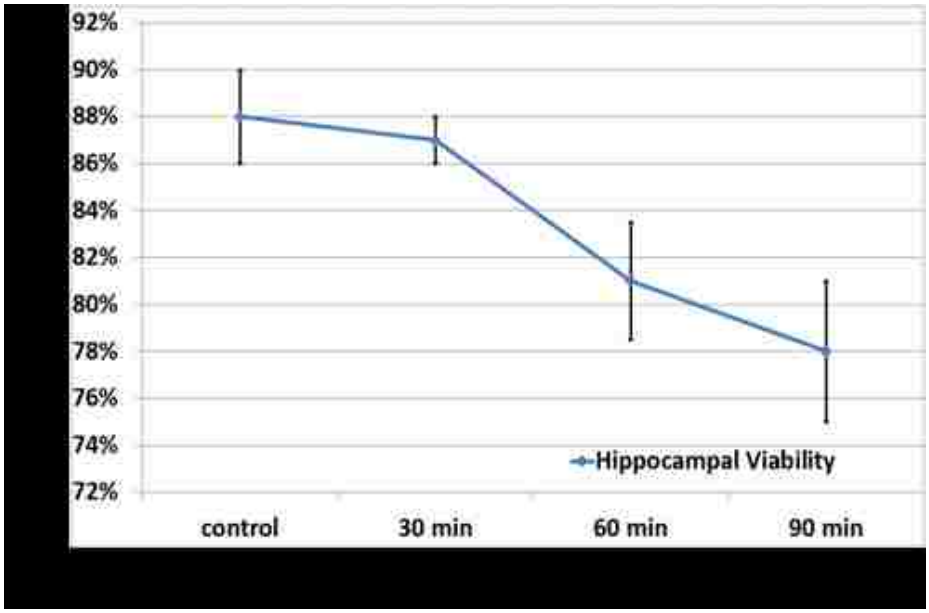

Figure 3.4 Hippocampal viability assessment after sucrose treatments for various periods of time.

3.2.2 Effect of MEA Electric Field on Hippocampal Viability

Another facet of the viability study is the investigation of the induced cell membrane potential resulting from non-uniform DEP electric field, which, if it exceeds certain threshold value, could compromise neuronal health; this threshold value is known as the breakdown potential [39, 42]. Membrane breakdown, or electroporation, is the process where a biological cell membrane is turned into a high-conductivity state because of a membrane potential induced by an external electric field [42]. This process comes with the creation of pores on the membrane. When induced membrane potential exceeds the threshold level, expansion of membrane pores or creation of more pores leads to membrane breakdown, which can be a fatal effect while trying to attract hippocampal neurons to electrodes using pDEP.

According to [43], in an AC electric field E, the generated membrane potential is given by:

$$V_m = \frac{1.5Ercos\alpha}{\sqrt{1+(2\pi f\tau)^2}} \tag{3.1}$$

with E the static electric field, r the cell radius, α the angle between the electric field line and a vector from the cell center to an associated point on the membrane, f the electric field frequency, and τ the time constant of cell membrane expressed as [42]:

$$\tau = rC_m(\frac{1}{\sigma_c}+\frac{1}{2\sigma_m}) \tag{3.2}$$

where C_m is the effective cell membrane capacitance per unit area, and σ_c and σ_m are the conductivities of cell interior (cytoplasm) and surrounding medium, respectively.

From equation (3.1), the induced membrane potential is frequency-dependent. Furthermore, the maximum potential is at the membrane point facing an electrode (assuming the cell sitting on top of a planar electrode), where the electric field line is parallel to the vector from cell center to the membrane point, giving $cos\alpha$=1 or $cos\alpha$=-1, as depicted in Fig. 3.5. The manipulation of cells using DEP requires a non-uniform global electric field, as mentioned earlier. However, if the local electric field is assumed to be uniform and static (constant E), the induced membrane potential can be calculated based on the protoplast (single-shell) model of a mammalian cell, as discussed in section 2.1.2. In this model, the mammalian cell is represented by a homogeneous cell interior (cytoplasm) with ohmic conductivity σ_c, and a thin capacitive cell membrane layer with effective capacitance C_m.

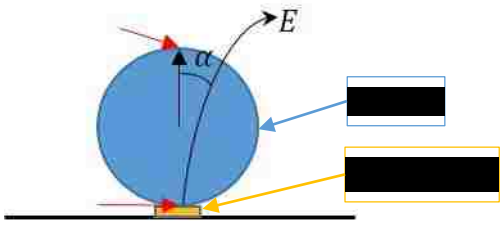

Figure 3.5 Sketch illustrates the calculation of induced cell membrane potential. Red arrows point to the positions where maximum membrane potential is created.

Detailed simulations are performed to ensure cell membrane integrity with the application of a 6 Vpp, 10 MHz AC signal. This signal is selected based on our studies on the DEP parameters that secure the attraction of neurons, only, on the electrodes, as opposed to glial cells which are also present in the cell medium [45]. In Fig. 2.4, electric field distribution is simulated on our DEP MEA electrode structure. From this electrode finite element analysis modeling, 2-D electric field data on four different planes of interest is extracted, as shown in Figure 3.6. These four planes are representative surfaces where hippocampal neurons experience induced membrane potential during pDEP anchoring. The first plane (Z1) is the surface of the silicon oxide passivation layer; the second plane (Z2) is the level of the neuron's center when the neuron lands on the silicon oxide layer; the third plane (Z3) is the surface of the SU-8 layer; and the last plane (Z4) is at the level of the center of the neuron when the neuron is positioned on top of the SU-8 layer. Z1 and Z2 are established when the cell has been trapped on an electrode; Z3 and Z4 represent the cell floating on device surface just before anchored to the electrode by DEP. The position and distance between each plane are based on dimensions obtained from a fabricated DEP MEA and from the measured radii of hippocampal neurons (r= 4 μm).

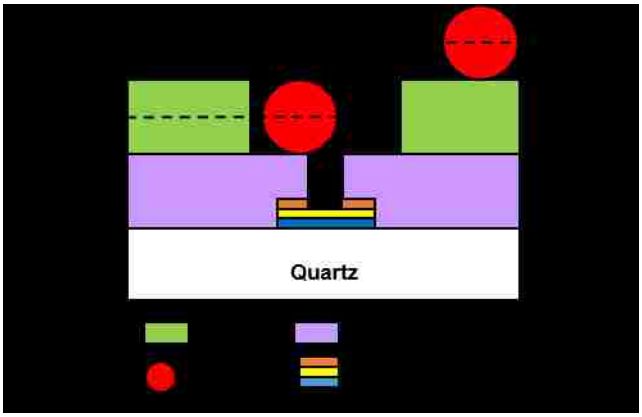

Figure 3.6 Four planes (Z1-Z4) where electric field data is extracted and induced neuron membrane potential is calculated.

As mentioned earlier (Fig. 2.4), the simulated maximum electric field is above the electrode, which is also the center point of each 2-D plane extracted. Using this electric field maxima and related

hippocampal neuronal dielectric properties [31-34], the frequency dependence of maximum ($cos\alpha$=1) induced membrane potential V_m on four planes is calculated in MATLAB (MathWorks, Inc.). In Fig. 3.7, two graphs indicate the situation where the voltages of 3 V and 4 V are applied to the electrode, respectively.

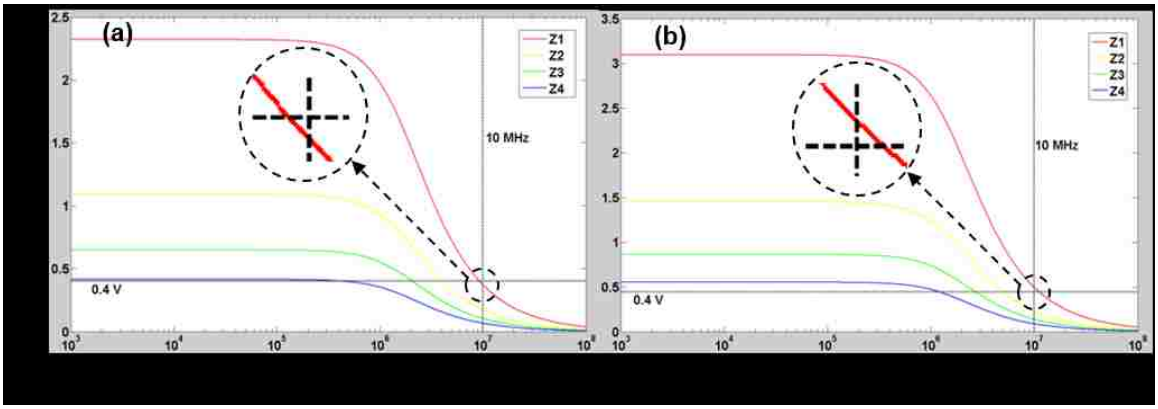

Figure 3.7 Calculated hippocampal membrane potentials induced by external electric field when (a) 3 V and (b) 4 V is applied on the electrode. Two close-up views for potentials on Z1 at 10 MHz are provided, compared with the 0.4 V threshold.

As can be seen in Fig. 3.7, the induced membrane potential is greater on lower planes (greater electric field strength); nevertheless, the potential on each plane decreases as frequency increases. With different electrode configurations and DEP conditions, Huang et al. and LaLonde et al. reported similar results [39, 45]. It was reported that an induced membrane potential below 0.4 V can probably guarantee the survival of cortical neurons, and larger membrane potentials can be tolerated by cortical cells at higher frequencies [24, 42]. Assuming 0.4 V is also the membrane breakdown threshold for hippocampal neurons, the membrane potentials are all below this level at 10 MHz when 3 V is applied, as indicated by the close-up view in Fig. 3.7(a). However, the potential is still above 0.4 V on plane Z1 if 4 V is applied at 10 MHz, which could lead to cell death when the neuron is anchored on top of the electrode. For this reason, 6 Vpp (-3 V to 3 V), 10 MHz AC signal is used for hippocampal neuronal recruiting on the MEA.

It should be mentioned, however, that this membrane potential is not the only factor impacting the viability of hippocampal neurons. For instance, some neurons may have already died during the tissue dissociation process, even before they are exposed to the electric field [24]. Therefore, approaches to simultaneously track the change of neuronal membrane potential and verify the membrane breakdown-associated cell death are in need, as such necrosis directly relates to external electric field during pDEP implementation.

3.2.3 Hippocampal Viability Verification

The next step in our work is to experimentally verify the viability of the neurons that are attracted to MEA electrodes and positioned there by pDEP. We used the DEP AC signal of 6 Vpp and 10 MHz, and implemented live/dead staining process to determine whether neurons survived the recruiting procedure. The viability of hippocampal neurons is verified using the same Live/Dead™ cell stain, as described above. Primary neuron culture media NbActiv1, which is the media neurons incubated in after the DEP positioning, is replaced carefully by the live/dead stain with a micropipette. The sample is placed in dark at RT for 15 min, and visualized immediately with a Nikon ECLIPSE E800 upright fluorescent microscope.

Live/dead staining, which requires media change and manual manipulation, is not possible immediately following the application of pDEP, because newly placed cells are easily displaced. Therefore, staining is performed 12 hours post-pDEP, for neurons to better attach on the electrode. As can be seen in Fig. 3.8, after 12 hours *in vitro*, pDEP positioned hippocampal neurons on MEA have better than 96% (96 ±2%, n = 7) viability, verifying the integrity of the cell membrane and that neurons stay alive in the cell-trapping solution during pDEP positioning.

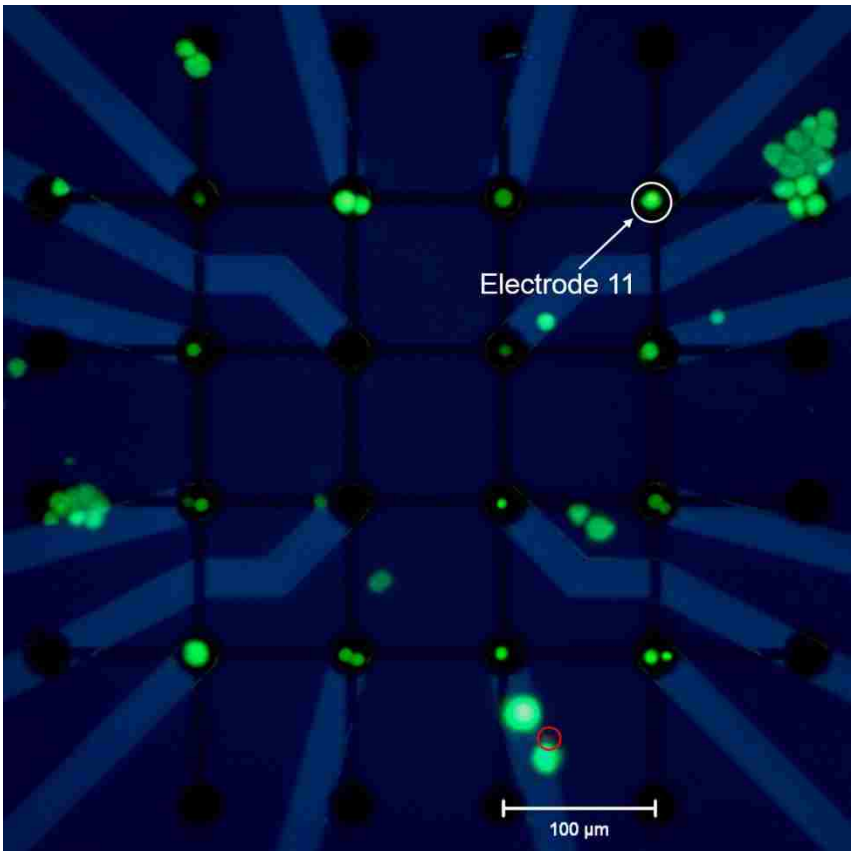

Figure 3.8 Live (green)/dead (red circle-indicated) stain of hippocampal neurons positioned on MEA at 12 h in vitro. Viability better than 96% is achieved.

At the same time (12 hours *in vitro*), spontaneous neuronal potential is successfully detected from neurons anchored on the MEA. In Fig. 3.9, a spontaneous neuronal extracellular potential spike is recorded from electrode 11, as indicated in Fig. 3.8; the spontaneous neuronal spike has an amplitude around 100 μV, which is a reasonable value according to [46]. With the recording of spontaneous neuronal potential, the electrically active properties of pDEP positioned neurons on the MEA is further verified.

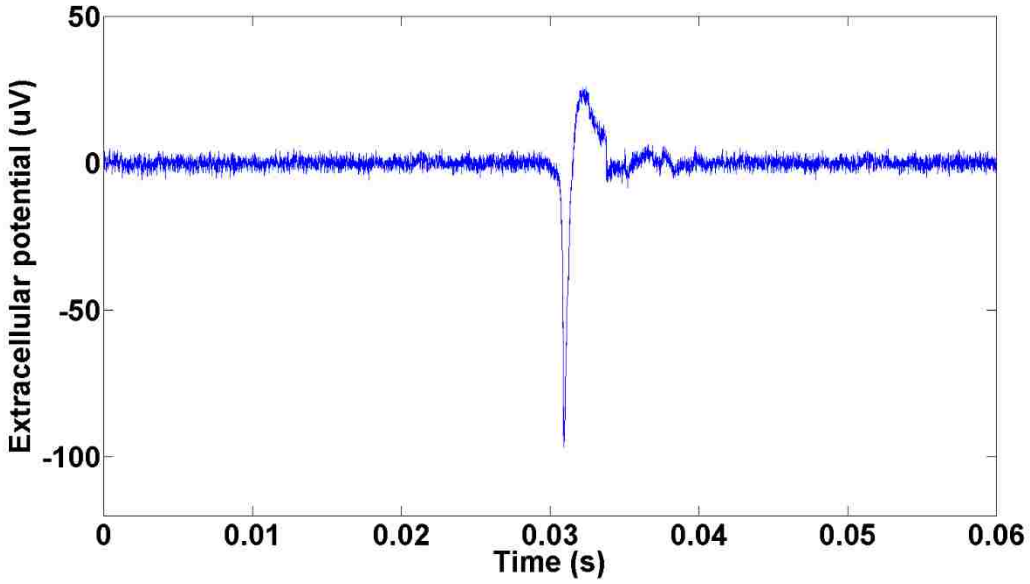

Figure 3.9 A spontaneous neuronal spike recorded from electrode 11 in Fig. 3.8, verifying the electrically active properties of pDEP positioned neurons.

Dielectrophoresis is used, with increasing frequency, in combination with microdevices, to manipulate biological cells. However, it is important to understand the impact the implementation of DEP may have on the viability of cells. Here, we have investigated the viability of mouse hippocampal neurons positioned on the electrodes of microfabricated multi-electrode arrays after the implementation of pDEP. We show that neurons maintain high viability after short-term exposure to cell-trapping solution, which contains, primarily, 10% sucrose. With electric signal of appropriate frequency and amplitude (such as 6Vpp and 10MHz), neuron membrane breakdown is prevented during the DEP process. Most importantly, we have obtained electrical signals from the neurons positioned on the MEA, 12 hours after using positive dielectrophoresis, further confirming the health and electrically active properties of neurons.

3.3 SU-8 Microstructure for Hippocampal Neuronal Patterning

3.3.1 Neuronal Patterning on SU-8 Microstructures

We designed microstructures formed of photosensitive epoxy SU-8 to mechanically confine the growth of hippocampal neurites after pDEP anchoring, as well as to confine the neuron cell body (soma). A variety of dimensions, such as the microchamber diameter and the microtrench width, are explored in order to determine the optimal values for one-to-one neuron to electrode correspondence and precise hippocampal neuronal patterning. To verify the neuronal patterning efficacy of the SU-8 microstructures, dissociated hippocampal neurons are cultured directly on DEP MEA chips, without pDEP. DEP MEA chips are sterilized by immersion in ethanol overnight and rinsed with sterilized DI water. Cell suspensions from the dissociation process, above (section 3.1.1), are plated at 1.6 x 10^4 cells/cm^2 on DEP MEA chips in NbActiv1 neuron culture media, and maintained in a humidified incubator at 37 ^oC with 5% CO_2. At 5 div, mechanical confinement and survival of the neurons is characterized by immunocytochemistry (ICC), as described in section 3.1.3.

Jaber et al. designed and fabricated similar electrode structures to position individual neurons on electrodes [20]. Although single-cell positioning was achieved, the outgrowth of neurites was not observed, nor the formation of neuronal networks, even from neurons directly plated on poly-d-lysine (PDL) coated devices, therefore not exposed to dielectrophoresis. Compared to their device structure, we use much thinner SU-8 microstructure layer (8 μm, compared to 38 μm). This thin layer of SU-8 microstructures on our device, has proved suitable and effective for hippocampal neuronal patterning and establishment of neurite-connected networks.

As can be seen in Fig. 3.10, a well-defined hippocampal neuronal network is patterned based on predefined SU-8 microstructures. This particular MEA chip has SU-8 microchambers with the diameter of 50 μm and seven-μm-wide microtrenches. We find that multiple neurons attached inside one microchamber, as indicated by blue DAPI stain, and neuron cell soma also anchored on microtrenches; ideally, however, only one neuron is expected to be anchored inside each microchamber with pDEP so that a neuronal network with single-cell resolution can be generated.

Therefore, microstructure designs with smaller features (e.g. 5 μm trenches and 20 μm chambers) are tested to ensure that microtrenches are sufficiently narrow to prevent neuronal bodies from anchoring, and to allow only single neurons to occupy each chamber. However, from the current design combinations, the structures in Fig. 3.10 (50 μm chamber, 7 μm trench) are still found to yield the most reliable neuronal networks.

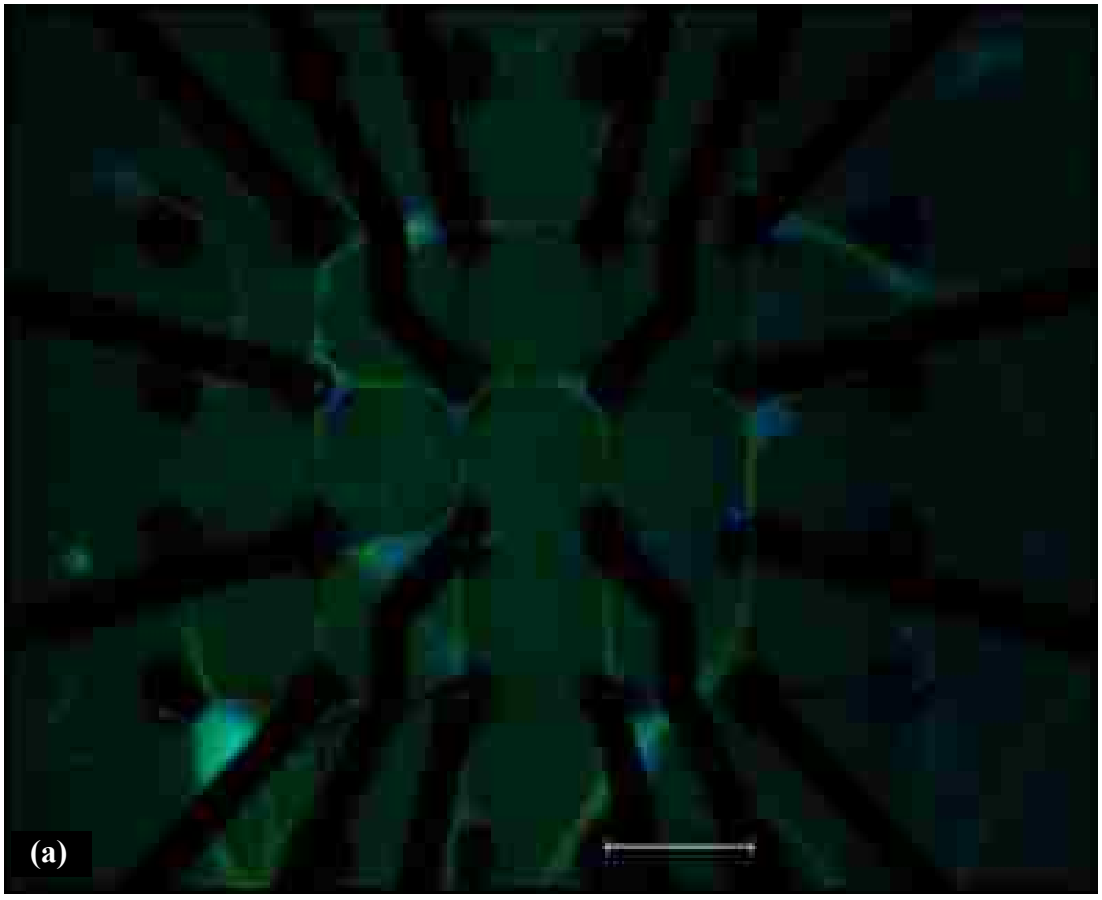

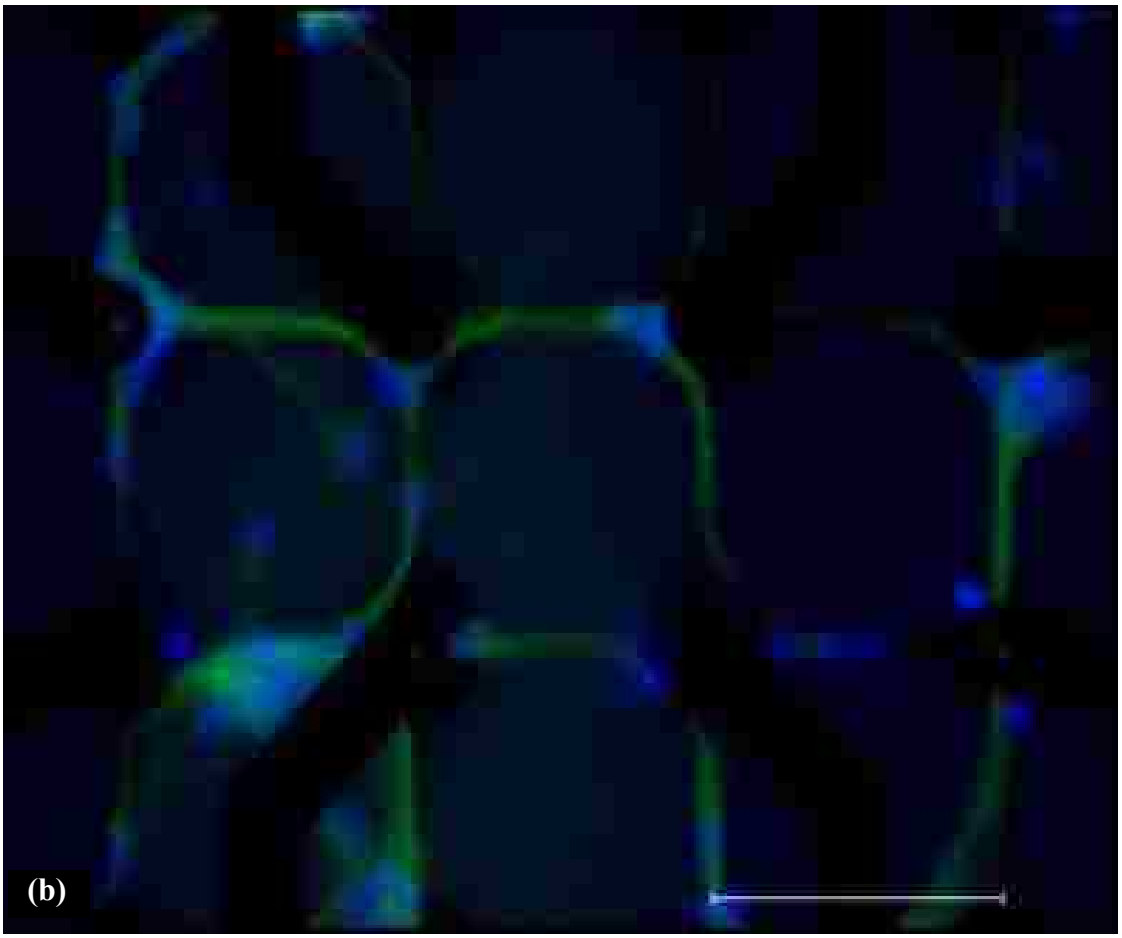

Figure 3.10 Fluorescent micrographs ((a): 10X, (b): 20X) of patterned hippocampal neurons (green) and cell nucleus (blue) at Div.5. Scalar bar is 100 μm.

MEA devices consisting seven-μm-trenches and smaller chambers (not available in current devices), are also being designed and fabricated for future single-neuron patterning work, as described in section 2.3.2 Design Revision 2. Indeed, microchannels with 10 μm width have been successfully used to guide neuronal axon growth [47, 48]. In our previous work, it was determined that the 30 μm microchamber diameter and 7 μm microtrench width were the optimal dimensions to pattern GT1-7 mouse hypothalamic neurons with single-cell resolution [37], which indicates that different types of neurons have different requirements for structural confinement. Another aspect observed, during neuronal culture experiments, is that even as a thin layer, SU-8 has poor cytocompatibility, as will be discussed in the following section.

3.3.2 Hippocampal Neuronal Viability on SU-8

Patterning hippocampal neuronal networks requires a cell-friendly microenvironment for optimal survival of primary neurons on the MEA. We have cultured the immortalized mouse hypothalamic neurons, GT1-7, and hippocampal, HT22, cell lines on our DEP MEA. SU-8 is shown to be cytocompatible for both cell lines, which verifies that SU-8 is biocompatible for cell culture. However, in the current study, it is found that the survival of primary, embryonic mouse hippocampal neurons (which are primary focus of our research, because of their role in the processes of thought and memory) on SU-8 is not as good. Other researchers have also reported poor (< 10%) viability of primary neurons when they are cultured close to or on top of untreated thick SU-8 2000 because of toxicity and poor adhesion [49]. Based on our own work, as well as prior research, it seems that the primary hippocampal neurons are more sensitive to SU-8 environment than immortalized cell lines. Various pretreatment and detoxification approaches have been investigated to improve the biocompatibility of SU-8 or SU-8 2000 for primary neuron culture, particularly. It was found that heat treatment, sonication and parylene coating could improve the viability of primary neurons, and oxygen plasma treatment rendered SU-8 surface more hydrophilic, which helped neurons to attach on SU-8 surface [49, 50].

Ultimately, hippocampal neurons are to be anchored in microchambers and extend neuritic processes along microtrenches. The floor of the microstructures is silicon oxide, which has shown to be biocompatible for primary neuron culture [7, 21]; but the cell bodies are still confined within the walls built of SU-8, and may have close contact with it. In this work, we use SU-8 3000, an improved formulation of SU-8/SU-8 2000, which utilizes the same solvent like SU-8, cyclopentenone, at approximately the same proportion. Additionally, SU-8 3000 is a permanent structural material on our DEP MEA and as noted, is relatively thin (8 μm) compared to typical (20-100 μm) SU-8 microstructure processing [20, 51]. Finally, we have executed various pretreatments to improve the cytocompatibility of cured thin SU-8 layer, as described below.

Various pretreatments on DEP MEA chips are performed to evaluate their efficacy in improving the cytocompatibility of SU-8 for primary hippocampal neurons. Prior to all pretreatments, DEP MEA chips are immersed in ethanol overnight and rinsed with sterilized DI water. As can be seen in Table 3.1, hard bake (H), sonication (S) and UV exposure (UV) are some of the selected methods applied trying to diminish neurotoxic leachants. The investigation of these specific methods is inspired by the work of Vernekar et al. (2009) [49], who applied them to detoxify thick (100 μm) uncured SU-8 layer. We have decided to slightly modify the pretreatments tested by Vernekar et al. [49], and use them here for the thin (8 μm) cured SU-8 layer on DEP MEA chips. One method we have added to this list is SAM coating (*3-trimethoxysilylpropyl-diethylenetriamine* DETA), which is typically used to improve the hydrophilic property of substrate for better cell adhesion [52]. Another method we consider here is hydroxylation (HY), which renders SU-8 hydrophilic by opening epoxy rings and providing hydroxyl groups [50]. Finally, piranha-cleaned (70% H_2SO_4 and 30% H_2O_2) cover slides (control) and reused MEA chips, which have been used for neuronal culture before, are tested for comparison. MEA chips are rinsed by sterilized DI water after each pretreatment.

Table 3.1 SU-8 pretreatment methods.

Method	Abbreviation	Process
Hard bake	H	Hard bake in a 120 ^oC convection oven for 3 hours.
Sonication	S	Sonication in IPA for 15 min.
UV exposure	UV	UV light exposure in biological fume hood for 24 hours.
SAM coating	DETA	Hydrophilic 3-trimethoxysilyl propyldiethylenetriamine (DETA) self-assembled layer (SAM) coating: immersion in 0.3% (w/w) DETA (Gelest Inc.) in methanol for 1 hour [52].
Hydroxylation	HY	Hydroxylation in 95% sulfuric acid at RT for 10 s, modified from the method of Tao et al. (2008) [50].

Dissociated mouse hippocampal neurons are plated directly on untreated and pretreated MEA chips, as well as control slides and reused chips, at $6.0x10^4$ cells/mL in cell media NbActiv1. At 7 days *in vitro* (div), cell viability is assessed through the use of Live/Dead^{TM} cell stain, (Invitrogen;

Calcein, AM 2μM and Ethdium Homodimer, 1μM in cell media NbActiv1). After 15 min in dark at RT, five live/dead fluorescent images are taken for each MEA sample. One of the images is focused on the central electrode array area, and the other four show the situation at the surrounding areas of the chip. Three independent experiments are performed, in each experiment, two samples are prepared for each treatment, including the control group. We use both % cell viability and live cell density for evaluation, of which the % viability is the ratio between live cells and total cells (live + dead), and the live cell density (cells/mm^2) represents the live cells per unit area on each micrograph.

The effects of the pretreatments on cell viability and live cell number are shown in Fig. 3.11 (six samples total for each pretreatment). As can be seen in Fig. 3.11(a) and (b), electrode array area data is extracted from one micrograph for each sample, and the data of the surrounding area on the chip (area framing the 4 x 4 electrode array) is the average of four micrographs for each sample. For the control slide, which has no electrode, surrounding area data is the average of four micrographs randomly taken across the surface of each sample.

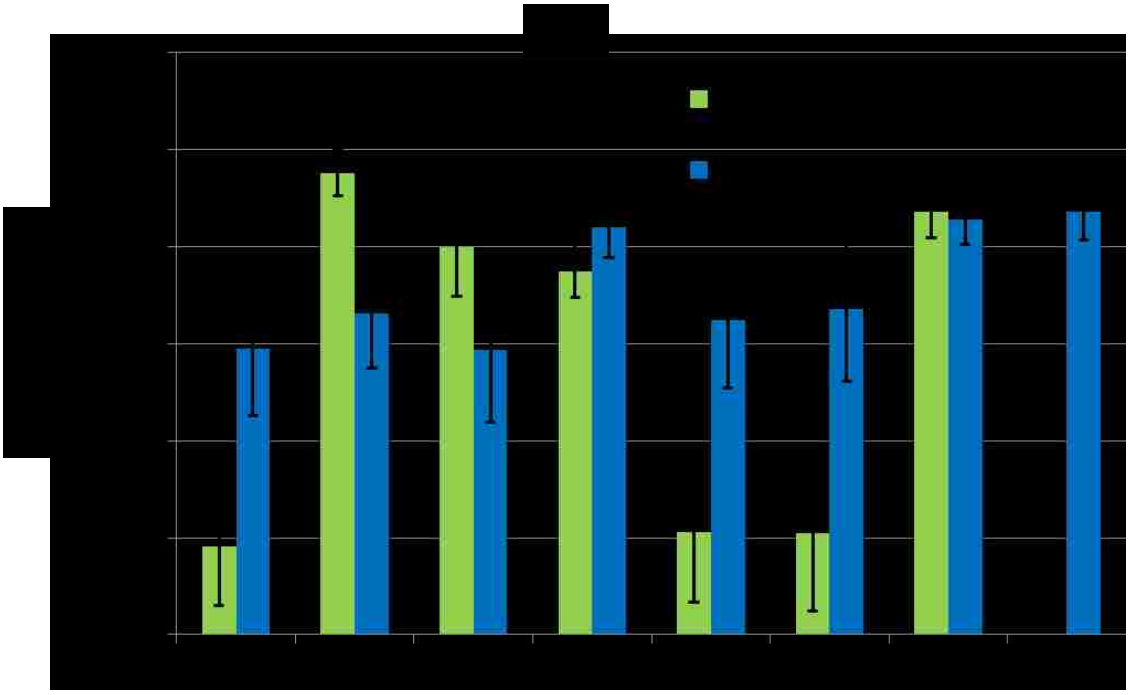

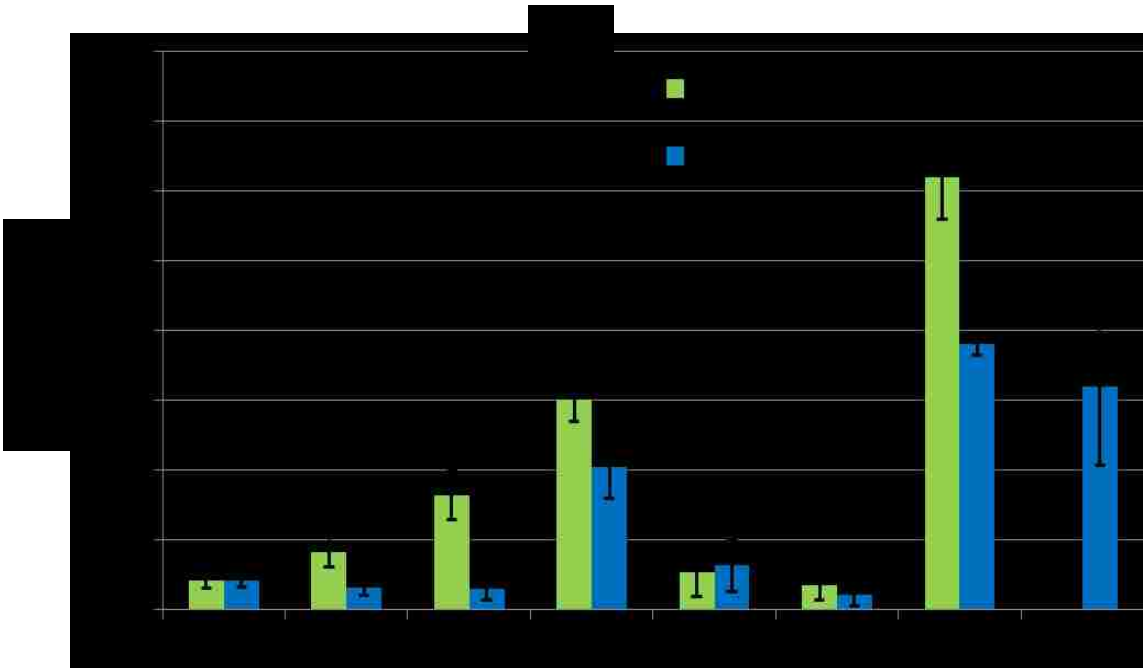

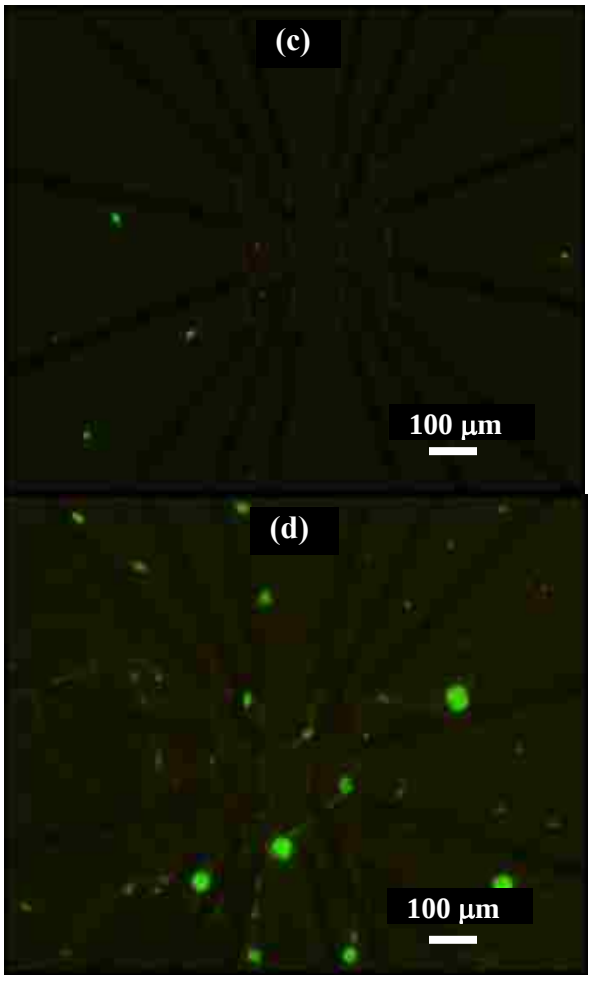
(c)
100 µm
(d)
100 µm

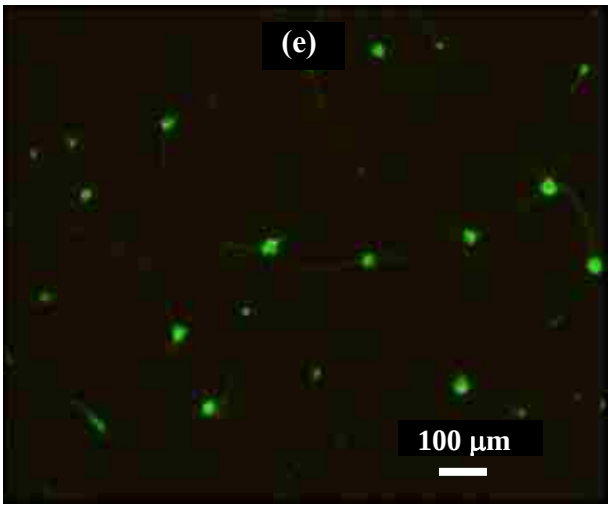

Figure 3.11 Hippocampal neuron viability assessment on different pretreated MEA. (a) % cell viability, (b) live cell density (cells/mm^2) after 7 div, (c) live/dead micrograph showing electrode array area of MEA that has been UV exposed for 24 hours, (d) electrode array area of HY treated MEA, and (e) control slide. (Live: green, dead: red)

In Fig. 3.11(a), we find that untreated, sonicated (S) and UV-irradiated (UV) samples have few live cells in the electrode array area, but they maintain a viability of approximately 60% in the surrounding area. All the other samples have >60% viability, except the surrounding area of the hard baked sample (H), which is also very close to 60%. The live cell density in Fig. 3.11(b), however, gives us more information regarding the ability of neurons to attach and grow. Compared with the initial seeding density, after 7 div, there are significant cell losses on most of the pretreated samples, except the hydroxylated sample (HY), which has a comparable live cell density in the electrode array area with the control slide. H and DETA treated samples also have improved neuron viability and live cell density in the electrode array area when compared to the untreated MEA, but less live cells attached than on the control slide. Cell loss could result from poor, initial adhesion and/or from medium change during the staining process.

At the same time, SU-8 microstructures in the electrode array area may also help anchor neurons, explaining the higher live cell density in this area than surrounding areas on some samples in Fig.

3.11(b). The reused MEA chip shows the best live cell density on both electrode array and surrounding area, indicating that neurotoxin may have already leached out during a previous culture.

It is concluded that pretreatments of UV exposure (UV) or sonication (S) do not improve the biocompatibility of cured thin SU-8 layer for primary neurons. In fact, UV exposure was shown to be detrimental and can possibly increase the amount of toxic leachants when it was previously applied on thick, uncured SU-8 layers [49]. In contrast, DETA SAM coating (DETA) and hard bake (H) do improve the cytocompatibility of SU-8 compared to untreated samples. It is observed that the adhesion ability of neurons is decreased on most of the pretreated surfaces (including untreated), compared to that observed on the control slide. However, we find that the sulfuric acid hydroxylation (HY) is the most effective pretreatment in improving SU-8 cytocompatibility, because it results in adhesion and neuron survival close to the levels observed for the control slide.

Another discovery is that the chips can be successfully reused, as long as they can be cleaned properly with ethanol (overnight) and sterilized DI water. The main problem with reusing is that sometimes it is not possible to remove all the cell debris from prior experiments; however, if they can be successfully cleaned, they can be used with confidence. For the new, unused MEAs, sulfuric acid hydroxylation is the best pretreatment. However, hydroxylation cannot be applied on the already packaged devices because of its effect on packaging materials.

3.4 Neuronal Recording and Stimulation

With a precisely patterned neuronal network cultured on a packaged DEP MEA (HY pretreated), spontaneous and stimulated extracellular potentials from neurons on specific electrodes are successfully recorded using the described signal processing system below, as is the propagation of evoked neuronal spikes. Hippocampal neurons were cultured directly in the PDMS chamber on top of the MEA (see Fig. 2.15(b)), and the patterned neuronal network was imaged with an inverted

microscope at 5 div. As can be seen in Fig. 3.12(a), the last row of four electrodes is occupied by neurons that are connected by well-defined neurites in SU-8 microtrenches (arrows). To better elaborate this phase contrast micrograph, a symbolic figure showing all the electrode sites with neuronal connections is depicted in Fig. 3.12(b). The number in each circle (electrode) is the associated channel number for signal recording, and the lines between electrodes are the patterned neurites, based on the observation from Fig. 3.12(a). There are non-terminated lines exiting electrodes (such as 3 and 5), representing the partial neuronal processes recognized.

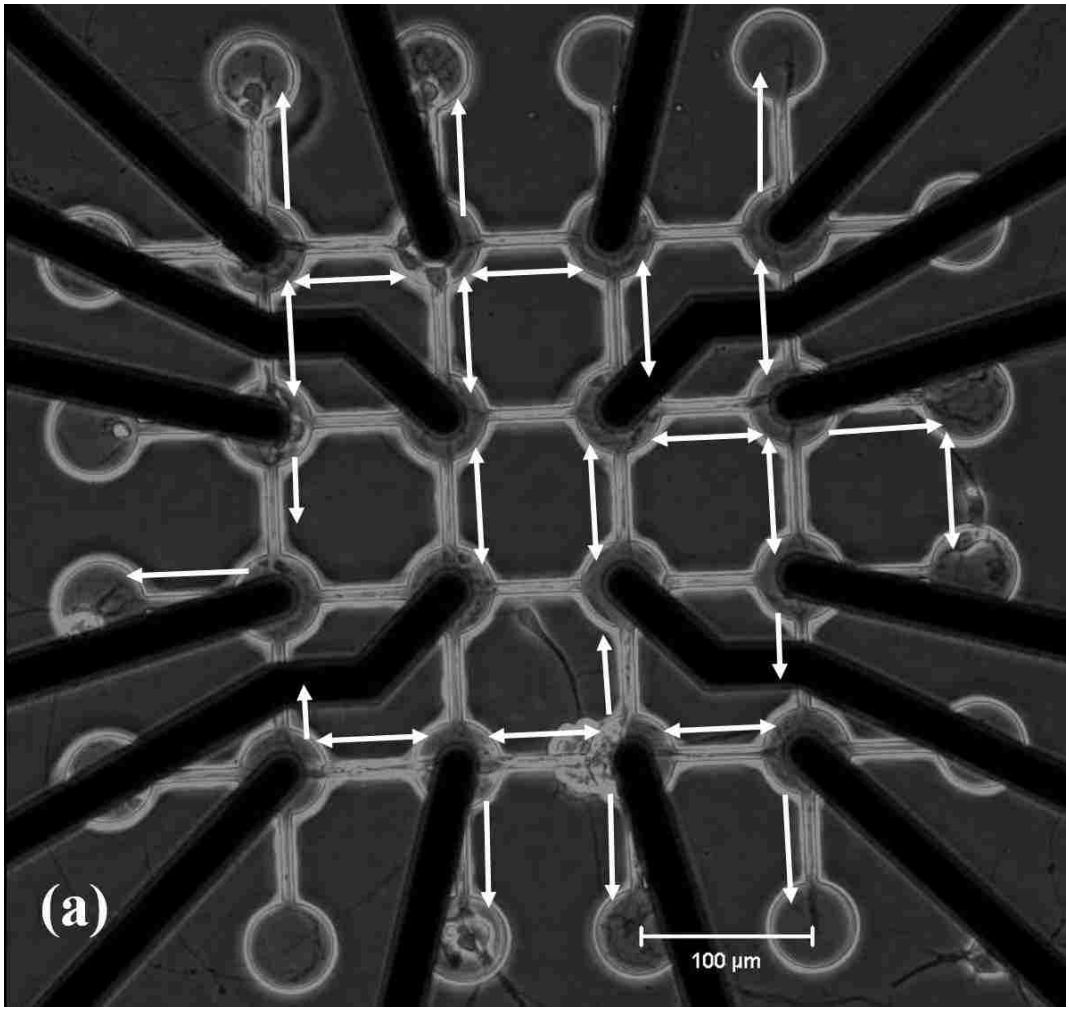

Figure 3.12 Neuronal patterning. (a) Phase contrast micrograph of patterned hippocampal neuronal network on a packaged DEP MEA (HY pretreated). (b) A symbolic depiction of the electrodes with neuronal connections. Mirochamber diameter: 50 μm, microtrench width: 7 μm.

The amplitude of neuronal extracellular potential has been shown to be within the range of 100 μV to 200 μV [53-55]. Frequency analysis of neuronal action potentials has revealed a power spectrum, primarily between 50-100 Hz and 2 KHz [55-57]. During signal recording, the packaged MEA device is fixed on a signal-processing PCB where the microvolt-level extracellular potential is filtered and magnified (Fig. 3.13). The band-pass filter, based on precision low-noise amplifiers AD624 (Analog Devices, Inc.) and low-noise, high-speed operational amplifier LT1007 (Linear Technology), has 3dB points at 12.3 Hz and 10.9 KHz, as well as a gain of 5000.

Moreover, the band-pass filter is designed to have 99% points at 76 Hz and 2.1 KHz, where the signal amplitude is 99% of its peak value in the band-pass Bode plot. While keeping the total amplifier noise less than 1.0 μV within a 2.0 KHz bandwidth, this design helps filter the neuronal potential more precisely based on the neuronal potential power spectrum described above. Filtered signals are fed into a data-acquisition (DAQ) card (NI USB-6211, National Instruments) for

recording, which is in turn controlled by a LabView Interface. On the other hand, stimulation pulses can be generated by the DAQ card, then transmitted to specific electrode of the MEA through analog multiplexers CD4051 (Texas Instruments). A switching time between stimulation and recording of less than 2 ms has proved to be suitable for detecting stimulated hippocampal neuronal signals while keeping stimulation artifact from being recorded [58]. Therefore, the switching time is set to be 2 ms in the LabView system, and low on-resistance, fast analog switch DG441 (Intersil Americas LLC) is used to realize this switch in the circuit. See Chapter 5: Supporting Electronics and LabView Control Interface for detailed discussion for the electronic circuit system design.

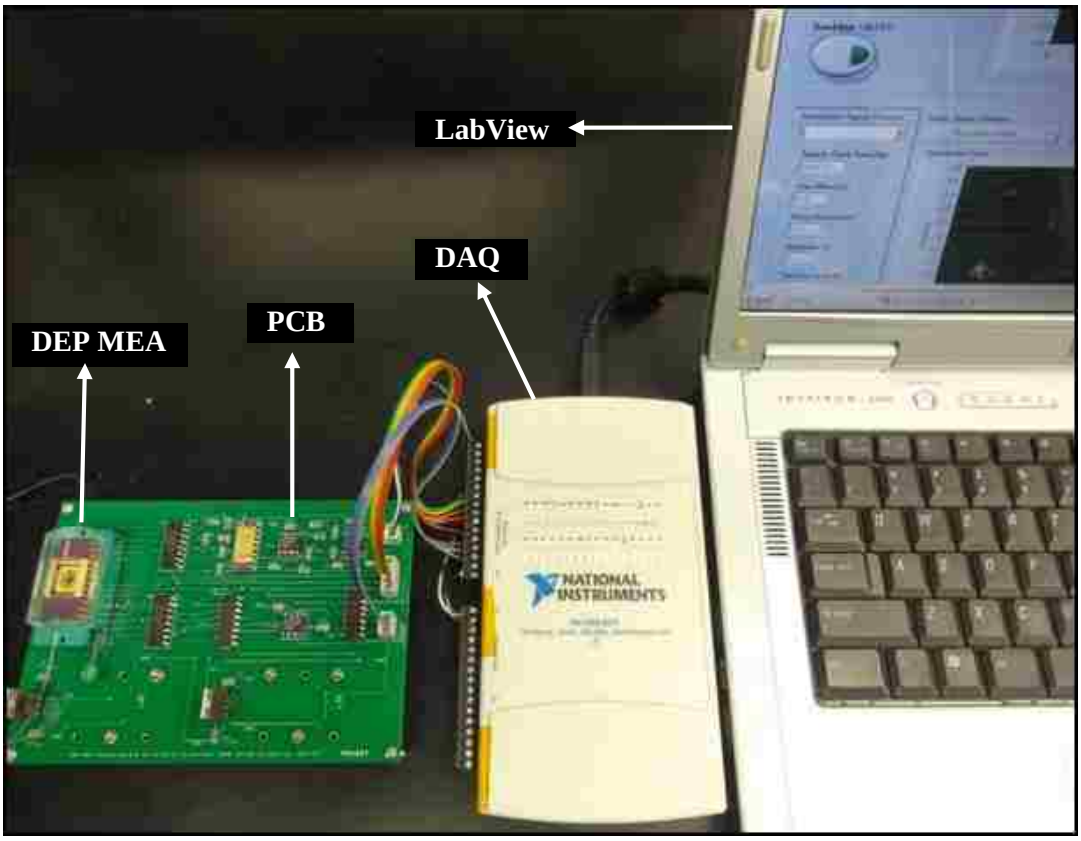

Figure 3.13 Neuronal signal recording and stimulation setup, including a signal processing PCB, NI DAQ, and LabView control program.

Spontaneous neuronal spikes were recorded from specified electrodes on multiple devices (n = 6) (Fig. 3.14), with an amplitude between 50 μV and 200 μV. Furthermore, based on the patterned

neuronal network, stimulated neuronal activities and their propagation between neurons anchoring on neighboring electrodes were recorded and analyzed (Fig. 3.15, 3.16). According to Wagenaar et al. [59], positive-then-negative voltage pulses are more effective than other pulse shapes for neuronal stimulation. In our experiments, various positive + negative biphasic pulses with an amplitude between 100 mV and 1 V, and a pulse duration between 100 μs and 1 ms were applied. The stimuli, with which repeatable responses (≥ three times) were recorded, had an amplitude of 1 V and a pulse duration of 0.1 ms (100 μs).

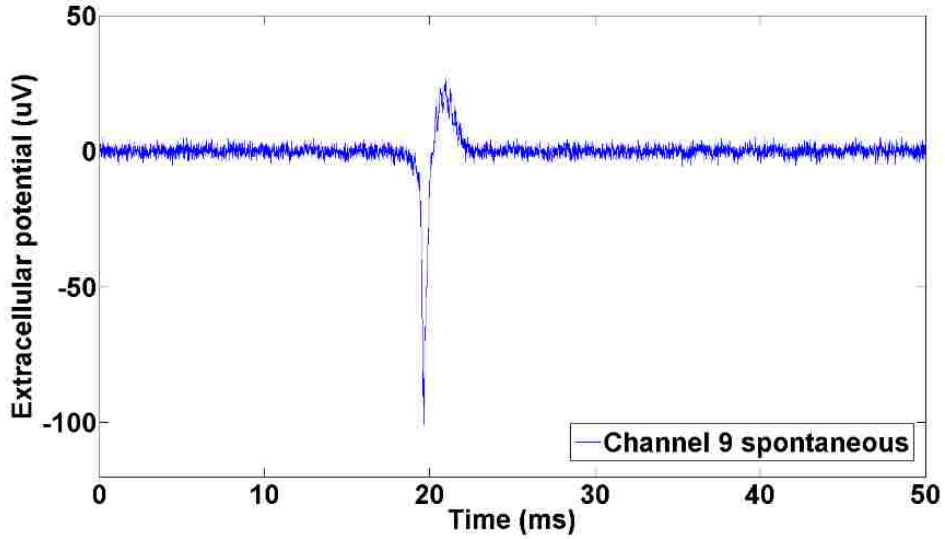

Figure 3.14 A spontaneous neuronal potential spike recorded from channel 9 in Fig. 3.12.

Fig. 3.15 represents the signals recorded from channel 9 and channel 11 of the MEA with cultured neurons depicted in Fig. 3.12. Each recording period is 0.2 s, including stimulated potential from channel 9, 2 ms after the biphasic pulse stimulation described above; and the signal from channel 11, also 2 ms after a same stimulation on channel 9. Spontaneous and evoked responses from channel 9 and 11 are summaried and analyzed in Fig. 3.16. The average delay (first peak of average evoked responses) of evoked responses from channel 9 is about 60 ms, and the average delay of evoked responses from channel 11 is about 80 ms, as can be seen in Fig. 3.16(b). In fact, all the stimulated activities we recorded have a delay between 10 ms and 100 ms, which is a reasonable

range according to similar data published [20, 59, 60]. It is noticed in Fig. 3.15, that each of the signal bursts from channel 11 appeared to be following one from channel 9, and the time lag between two respected bursts is 10-20 ms, which is consistant with the difference of response delays from two channels, as described above. Similar stimulated bursts and their propagation were also recorded between channel 13, 14 and 16. Pan et al. [47] presented same-order burst propogation delays from different electrodes that were 200 μm apart. With longer distances (400-800 μm) between connecting neurons or neuron clusters, Berdondini et al. [61] and Merz and Fromherz [60] reported neuronal signal propagation time of approximately 100 ms. These reported signal transmission speeds are similar to the value we measured, here. However, it should be noted that the propagation velocity of stimulated bursts between neurons is normally much slower than the velocity of action potential propgation along axons [62], which is of the order of 0.5 m/s [7, 47, 63]. Several variances such as neuronal population density, connection nature, and synaptic delays could affect the burst propagation speed here [47, 62].

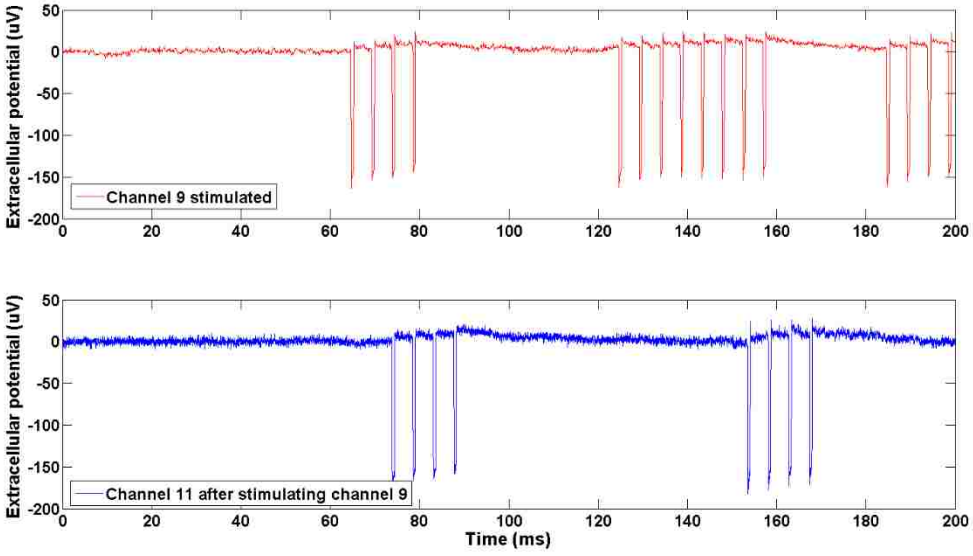

Figure 3.15 Evoked neurnonal spikes from channel 9 (top) and propagated signal from channel 11 (bottom) in Fig. 3.12; both were recorded 2ms after stimulation.

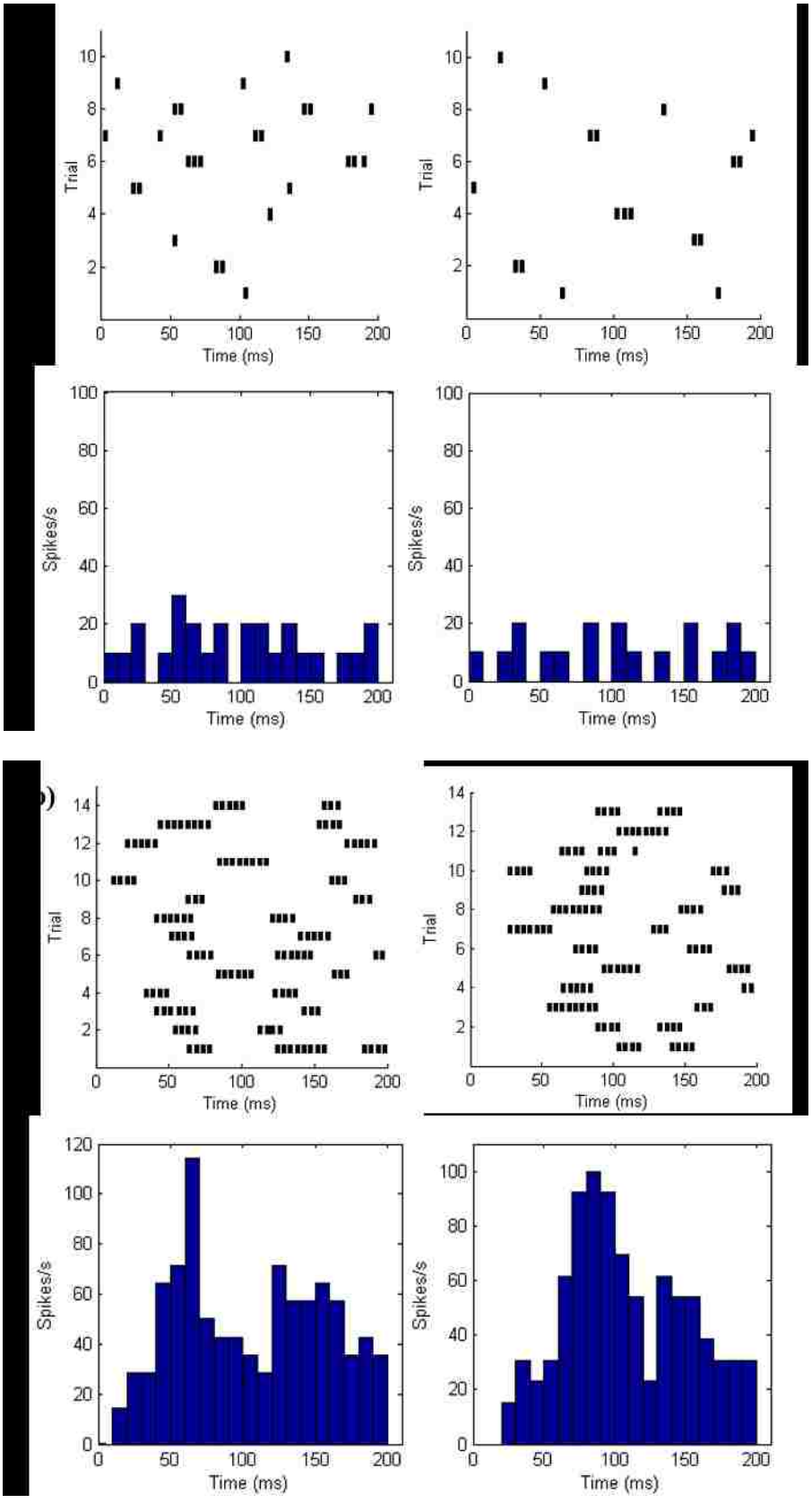
Trial
Time (ms)
Spikes/s
Time (ms)
Trial
Time (ms)
Spikes/s
Time (ms)
Trial
Time (ms)
Spikes/s
Time (ms)
Trial
Time (ms)
Spikes/s
Time (ms)

Figure 3.16 Spontaneous and evoked responses from channel 9 and 11. (a) Rasters and Post-Stimulus Time Histogram (PSTH) of spontaneous responsees from neurons on channel 9 (left) and 11 (right). Responses from 10 trials/measurements were averaged using a time bin of 10 ms. (b) Evoked responses from neurons on channel 9 (left) and 11 (right). The rasters and PSTH are aligned 2 ms after the stimulus on channel 9. Responses were also averaged using a time bin of 10 ms. Approximate delay of revoked responses (first peak on PSTH) is 60 ms and 80 ms for channel 9 and 11, respectively.

It should be mentioned that neuronal potentials were also recorded 12 hours after DEP recruiting, as disscussed in section 3.2.3, thereby confirming the survival and electrical activity of the neurons post-DEP. This result confirms experiments by Jaber at al. [20], who reported signals 24 hours after the DEP was done. In our work, we have successfully patterned hippocampal neurons with DEP and established neuronal networks by directly plating them on the device, which is an improvement compared to prior body of work [20]. It appears that DEP positioning process compromises neurons' ability to extend processes. However, DEP manipulation with high AC frequency and low amplitude has been reported to be harmless to neuronal health [24, 38], as discussed in section 3.2.2. Current work involves investigations to promote neuronal growth.

With this recording of propagated neuronal activity between neighboring electrodes, we verified the capability of this DEP MEA system to support geometrically-dependent studies of precisely-patterned, functioning neuronal networks. Neuronal recording involving more complicated signal propagation is included in future research plan.

In this chapter, we have verified the functions of our MEA system by actively anchoring mouse hippocampal neurons on top of electrodes of packaged DEP MEA, with single-cell resolution. The hippocampal viability, after the DEP process, is investigated. Neurons maintain high viability after short-term (30 min to 90 min) exposure to cell-trapping solution (10% sucrose). With appropriate frequency and amplitude of the electric signal, the integrity of the neuronal membrane and viability can be ensured. The precise patterning of neuronal networks based on predefined SU-8 microstructures is achieved. We have investigated hippocampal viability on SU-8 in the presence

of selected pretreatments of the SU-8 layer, and have identified sulfuric acid hydroxylation as the most effective pretreatment method to improve the cytocompatibility of cured thin layer of SU-8 on the DEP MEA for primary neuron culture. Finally, spontaneous and stimulated potentials are successfully recorded, and the time interval of neuronal signal propagation between neighboring electrodes is measured, from well-defined, functioning neural networks using this new MEA system. More experimental results on pDEP cell trapping and microstructure cell patterning can be found in Appendix VII: Preliminary pDEP Cell Trapping Experiments and Microstructure Cell Patterning Study.

Chapter 4: Separation of Hippocampal Neurons from Glial Cells

In the process of achieving one-to-one neuron-to-electrode correspondence on the DEP MEA, one considerable challenge to be addressed is the separation of a defined cell type from a complex cell mixture, to populate the electrode area with the desired cell type. This is particularly difficult when using primary cell cultures, such as dissociated hippocampal cell cultures. Namely, when neurons are extracted from the brain tissue (hippocampus), it is unavoidable that the initial cell culture contains glial cells, as well.

Over the past decades, various cell sorting or separation techniques have been investigated. For instance, flow cytometry methods, based on fluorescence-activated cell sorting (FACS) [64-66], or magnetic-activated cell sorting (MACS) [67, 68], have been widely used to isolate subpopulations from complex biological cell mixtures. These techniques normally require the labeling of cells with either fluorescent or magnetic markers, which recognize target features on or inside the cells. In addition, a bulk separation method of hippocampal neurons and glial cells has been reported, using ultra-centrifugations with a discontinuous density gradient of Ficoll [69], a hydrophilic polysaccharide. One of the observed limitations of this technique is the morphological damage to separated cells, such as processes being torn-off from neuron bodies. Dielectrophoresis (DEP) has also been applied to separate particles and biological cells [70-72]. For instance, polystyrene and latex beads [72], rat embryonic cortical neurons and human liver cells and endothelial cells were all successfully manipulated by DEP with planar electrode arrays [36, 71]. However, instead of individual cells, a large volume of cell populations are usually manipulated. DEP separation of neurons and glial cells in a mixed co-culture [55], as well as the isolation of neuron progenies and neural stem cells have been reported [73].

In this chapter, we describe the separation of embryonic mouse hippocampal neurons from glial cells using a positive dielectrophoresis (DEP) process. Here, we have implemented a cell trapping-

favorable, cell suspension solution with low conductivity - 30% cell media cell-trapping solution, as described in previous chapters. It enables positive dielectrophoresis for hippocampal neurons (thereby attracting them to the electrodes), while resulting in negative dielectrophoresis for glial cells (repelling them from the electrodes). We have systematically performed a mathematical simulation and analysis to anticipate the DEP frequency at which hippocampal neurons and glial cells are separated. Simulated DEP crossover frequencies have been experimentally verified, based on which new, refined neuron and glial dielectric and physical properties are suggested that better reflect the experimental results obtained. DEP movements of neurons and glial cells in targeted separation media are experimentally analyzed, under the specified electric signal. Additionally, we have confirmed our modeling results by selectively trapping neurons over electrodes on the DEP MEA, resulting in active recruitment of neurons over the stimulation and recording sites. This technique is a valuable addition to the toolbox for creating more functional and versatile multi-electrode arrays.

This part of work builds upon the previously published work in the following fashions: first, instead of large cell populations, we describe how to separate individual neurons from glial cells in a mixed suspension state, and further place neurons on pre-determined locations for neuronal patterning, using positive dielectrophoresis. Then, we should mention that whereas previously published papers addressing separating neurons and glial cells focused on postnatal rat neurons from cerebral cortical regions and hippocampi, or mouse fetal-derived cerebellar neural stem cells [20, 55, 73], we have focused our work on embryonic mouse hippocampal neurons. Additionally, we have provided, here, a systematic approach to anticipate the region of frequencies for which it is possible to separate neurons from glial cells successfully, rather than using just an experimental "trial-and-error" approach. Furthermore, based on DEP crossover frequency measurement and simulation, we have presented an approach to extract more accurate dielectric properties of neurons and glial cells than those previously available in literature.

4.1 Modeling and Simulation

In section 2.1.3, the DEP spectrum of mouse hippocampal neurons have been simulated, in suspension media consisting of 10% sucrose (w/v in deionized water): cell media at different ratios. The suspension medium containing 30% cell media has been selected, and verified for active neuronal recruiting on DEP MEA with an electric signal of 10 MHz (section 3.1), where the maximum pDEP effect exist under this particular suspension medium situation, as can be seen in Fig. 2.3. Another reason of choosing the frequency of 10 MHz is that based on the spectrum simulation, hippocampal neurons and glial cells experience the greatest DEP effect difference at this frequency, which provides a potential approach to separate hippocampal neurons and glial cells during the neuronal DEP trapping process. See below discussion for details of this DEP effect difference.

For certain applications, such as an MEA with neuron trapping capabilities, it is important to consider how to separate hippocampal neurons from the glial cells that serve important supporting roles for neuronal networks and which are always present in dissociated neural cultures, immediately following the dissociation procedures [55, 74]. The ratio of glial cells to neurons in the brain varies between animal species [75], and there are different findings about the glial to neuron ratio in human and other primate brains [75]. However, it has been confirmed that comparable amount of glial cells and neurons exist in human and mouse hippocampi [74, 76, 77]. In our specific application, the goal is to exclusively trap hippocampal neurons on electrodes. Because of the methods implemented for hippocampal neuron dissociation from hippocampus tissue (section 3.1.1 and Appendix IV: Mouse Hippocampal Neuron Dissociation and Culture Protocol), glial cells, which have an indistinguishable morphological appearance in the suspension state compared to hippocampal neurons, will also be dissociated.

Here, we investigate the separation of these two cell subpopulations, based on their different dielectric and physical properties, using positive dielectrophoresis. DEP spectra for glial cells are also simulated in the same suspension media discussed earlier in Fig. 2.3. Dielectric and conductive properties of glial cells have been researched (Table 4.1); but very limited information is available in the literature. The properties used in Maple simulation are either from previous studies, such as the glial effective membrane capacitance [32], or we have derived them from conductivity-related glial cell and tissue information [78, 79]. We have assumed the cytoplasm permittivity of glial cells to be the same as neurons. Dielectric and conductive properties of different suspension medium are listed in Table 4.2, these properties are also used in simulations in section 2.1.3. Again, medium conductivities are measured by the EC410 Conductivity/TDS/Salinity Kit (EXTECH Instruments, Inc.), and medium permittivity are obtained from the literature [35, 36]. Our modeling has shown that, instead of pDEP, glial cells will experience nDEP throughout the applied frequency range when DEP suspension media has 10% or more neuron culture media (see Fig. 4.1). This means that instead of being attracted to the electrodes, glial cells are expected to be repelled from electric field maximum area (electrode). It can also be observed that in 30% cell media condition (Fig. 4.1, bold line compared with the bold line in Fig. 2.3), hippocampal neurons and glial cells have the greatest DEP effect difference at a frequency of approximately 10 MHz. This simulation result, therefore, provides a potential method to effectively separate hippocampal neurons from glial cells in a mixed suspension.

Table 4.1 Dielectric and physical properties for glial cells simulated in Fig. 4.1 below.

	Cytoplasm permittivity $\varepsilon_c/\varepsilon_0$	Cytoplasm conductivity σ_c (S/m)	Cell radius r (μm)	Membrane effective capacitance c_m (F/m^2)
Glial Cells	80[a]	0.1[b]	4	0.0106[c]

[a] Assumed value;
[b] Derived from [78, 79];
[c] [32].

Table 4.2 Dielectric and conductive properties for DEP suspension medium.

	Cell media percentage (%) in mixture suspension							
	100% (NbActiv1)	50%	30%	20%	10%	1%	0.1%	0% (10% Sucrose)
Medium conductivity σ_m (S/m)	1.104	0.525	0.331	0.212	0.110	0.011	0.001	1.5×10^{-4}
Medium permittivity $\varepsilon_m/\varepsilon_0$	80[a]				80[b]			76[c]

[a] [36];
[b] Assumed;
[c] [35].

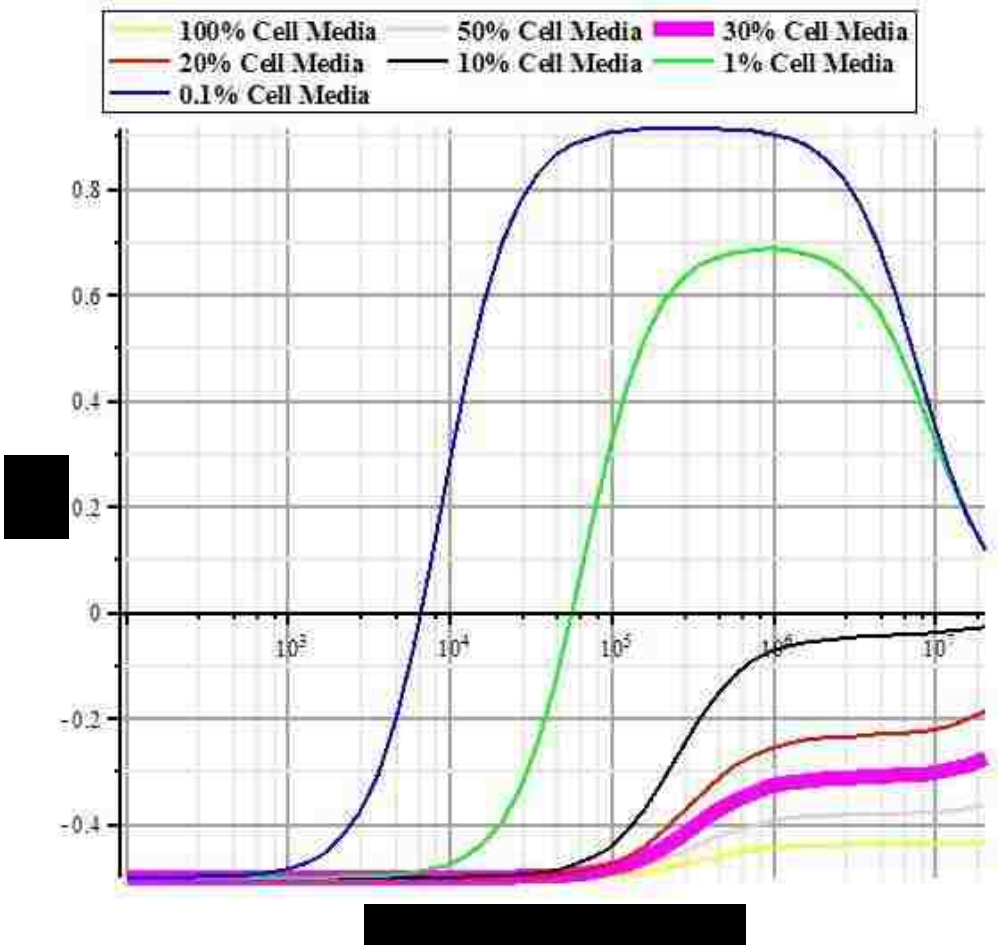

Figure 4.1 DEP spectra simulations of glial cells in suspension media consisting of 10% sucrose (w/v in deionized water): cell media at different ratios.

4.2 Neuronal and Glial DEP Crossover Frequency Verification

4.2.1 Experimental Preparation

Mouse hippocampal cells (neurons and glial cells) are dissociated from embryonic day 18 (E18) mouse hippocampus tissue (BrainBits, LLC.), as described in section 3.1.1 and Appendix IV: Mouse Hippocampal Neuron Dissociation and Culture Protocol. The dissociated neuron/glial cell mixture is resuspended in NbActiv1 media (BrainBits, LLC.). The DEP crossover frequency verification, however, requires the isolation of hippocampal neuron and glial cell population, respectively.

To enrich for neurons, the mixed cell suspension from the dissociation process, above, is plated at 1.0×10^5 /mL on a poly-d-lysine coated cover slide in NbActiv1 neuron culture media, and incubated at 37 ^{o}C with 5% CO_2. At 6 days in vitro (Div.), hippocampal neurons are harvested with 0.125% trypsin in Hibernate E-Ca (37 ^{o}C, 5 min), centrifuged at 200g for 5 min, and resuspended in NbActiv1 media. This purified neuron suspension is used for neuronal crossover frequency verification, as described in the following section.

For glial cell isolation, the cells are dissociated from hippocampus tissue by the same procedure described, above, and the cell pellet is resuspended in astroglial media, NbASTRO (BrainBits, LLC.). Cells are plated at 7500 cells /cm^2 on a poly-d-lysine coated tissue culture flask, and incubated at 37 ^{o}C with 5% CO_2. Astroglial cells are typically 90% confluent and ready to pass or harvest after 10-14 days. When confluent, glial cells are harvested with the same procedure for hippocampal neurons, described above, but resuspended in NbASTRO media instead of NbActiv1 media. Harvested glial cells are used immediately for DEP crossover verification experiments.

We try to identify the crossover frequency, which is defined as a frequency where the real part of Clausius-Mossotti factor is zero, and therefore a cell experiences no DEP effect. A quadruple

electrode array has been fabricated by depositing 20 nm of Titanium (Ti) followed by 80 nm of Platinum (Pt) based on a silicon substrate (Fig. 4.2), each electrode is connected to a metal pad (not shown in Fig. 4.2). For DEP crossover frequency experiments, the quadruple electrode array is attached on the bottom of a 35 mm petri dish with polydimethylsiloxane (PDMS) prepolymer, which is fixed on the stage of a probe station PM5 (SUSS Micro Tec.), with probe tips connected to metal pads on the chip to deliver DEP electrical signals (Fig. 4.3). AC sine-wave electric signals (6 Vpp, 1 KHz - 20 MHz) and ground signals are applied, by a function generator (Agilent 33521A), to every other metal pads, respectively, so that local electric field maxima is created at the edge of electrodes, and electric field minima is located at the central area. Initially, cells are positioned within the area indicated by the dashed square in Fig. 4.2. Cells will be attracted to the edge of electrode under positive DEP, and pushed to the center with negative DEP.

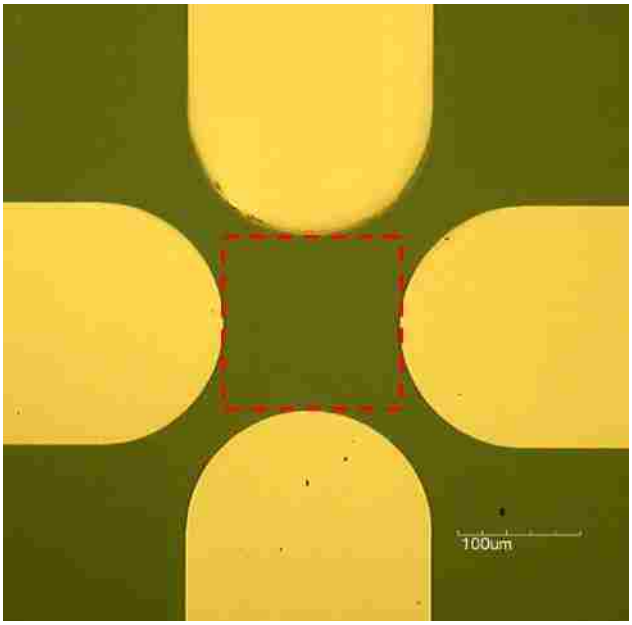

Figure 4.2 Quadruple electrode array for cell crossover frequency measurement. Cells are initially positioned in the area indicated by red dashed square.

Dielectrophoretic manipulation was performed in different mixed DEP suspension media after hippocampal neurons or glial cells settled down on the chip surface. In different compositions of suspension media, the movement of a single cell was observed at each frequency to measure the

frequencies where the cell was trapped to the edge of electrodes (pDEP in action), and repelled to the central area (nDEP in action). For each suspension media, the measurements were repeated on five cells within a time window of ten minutes. During experiments, there is a frequency range centered around the crossover frequency, where the DEP effect is too weak to observe because of the small Clausius-Mossotti factor. The start and end of this frequency range (taking into account the extremes of the frequency ranges measured on all five cells) are recorded as 'Experimental Low' and 'Experimental High' in Table 4.3, and the average of these two values is considered to be the experimental crossover frequency. The measurements on five cells were performed within 10 min (total) to minimize potential negative effect for the cell health from DEP suspension media and the electric field.

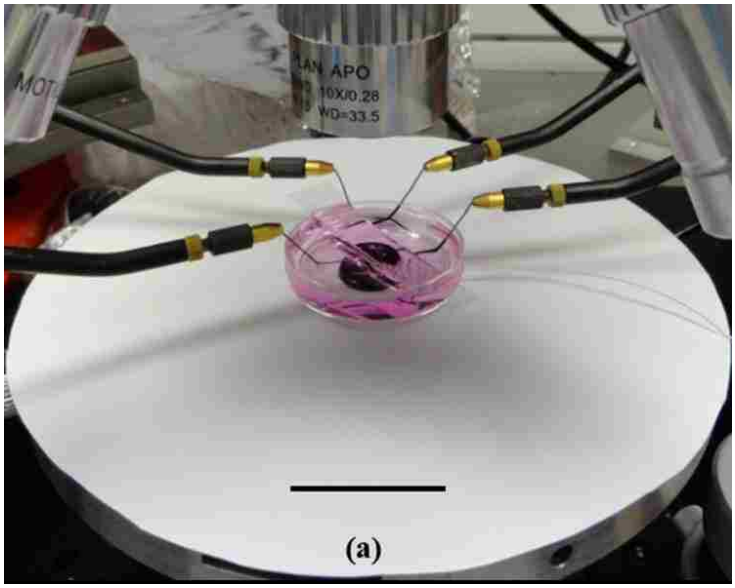

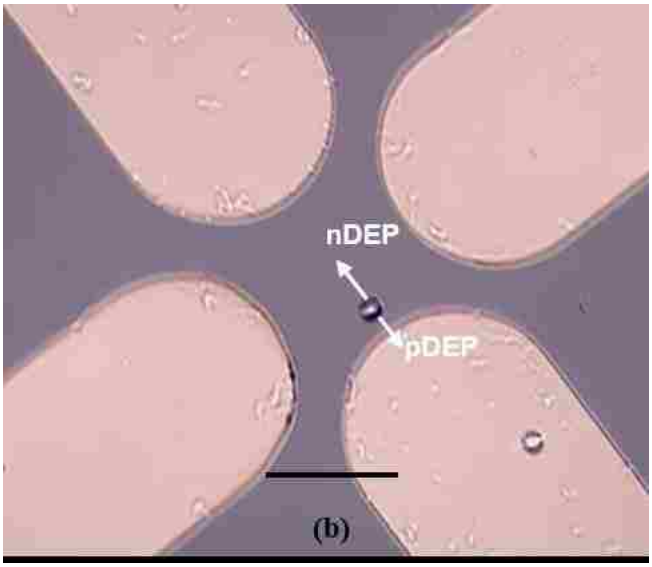

Figure 4.3 DEP crossover frequency verification experiments. (a) Experimental set up for DEP crossover measurement on a probe station. A glass cover slide above the petri dish is used to stabilize fluidic surface for better visualization under microscope. Scale bar is 30 mm. (b) A video frame showing movement of a cell subjected to pDEP or nDEP effect. Scale bar is 100 μm. The actual experiments were performed with an upright microscope (PSM-1000 microscope, Motic Group CO., LTD.), so the movement of cells could be visualized when they were on the electrodes, which were Pt non-transparent electrodes and therefore not suitable for viewing the motion on top of them using inverted microscope.

4.2.2 Experimental Results and Discussion

With the experimental setup described above, we verified the crossover frequencies of hippocampal neurons and glial cells, which had been simulated, as previously described and shown on Fig. 2.3 and 4.1. From the simulation data shown in Fig. 2.3, for neurons, the crossover between positive and negative DEP occurs at different frequencies for different suspension media, except in the 100% cell media solution, which does not have a crossover frequency. The experimental results are shown in Table 4.3 and Fig. 4.4, providing experimental evidence for the crossover frequencies obtained through Maple simulation and modeling (Fig. 2.3).

In 50% cell media solution, both the pDEP and nDEP effect are very weak around crossover frequency, and it was not possible to measure the definite frequency range. However, in the cell suspension medium containing lower ratio of cell media, comparing the simulated neuronal

crossover frequencies to the measured data in Fig. 4.4, measurement data accurately reflect the simulated crossover frequencies.

It is also noticed that notable discrepancies exist between experimentally measured and simulation values, particularly in suspension medium with higher ratio of cell media. We think the main reason for this discrepancy is that the neuronal dielectric properties used in the simulation are taken from literature averages of data of neurons closely related to those we were using but not exactly identical, rather than actual values. Additionally, crossover errors could also result from the difficulty of identifying the crossover frequency ranges, in the situations where the DEP effect is weak. Actually, when comparing the accuracy of experimentally identified crossover frequency results published by Vahey and Voldman and Gagnon et al. [80, 81], we have very similar accuracy resolution at comparable conductivity levels of the suspension medium. Most importantly, it is confirmed that in 30% cell media solution, hippocampal neurons experience positive DEP at 10 MHz, which provides the foundation for active neuronal recruiting.

Table 4.3 Simulated and experimental crossover frequencies for hippocampal neurons and glial cells.

	Cell Media Percentage (%) in Mixture Suspension				
	0.1%	1%	10%	20%	30%
Hippocampal Neurons					
Theoretical Crossover (KHz)	8.7	77.3	731.5	1466.7	2330.3
Experimental Low (KHz)	5	60	300	600	1500
Experimental High (KHz)	10	80	350	900	2000
Measured Crossover (KHz)	7.5	70	325	750	1750
Glial Cells					
Theoretical Crossover (KHz)	6.6	56.6	N/A	N/A	N/A
Experimental Low (KHz)	2	20	150	400	2000
Experimental High (KHz)	5	40	250	600	N/A
Measured Crossover (KHz)	3.5	30	200	500	N/A

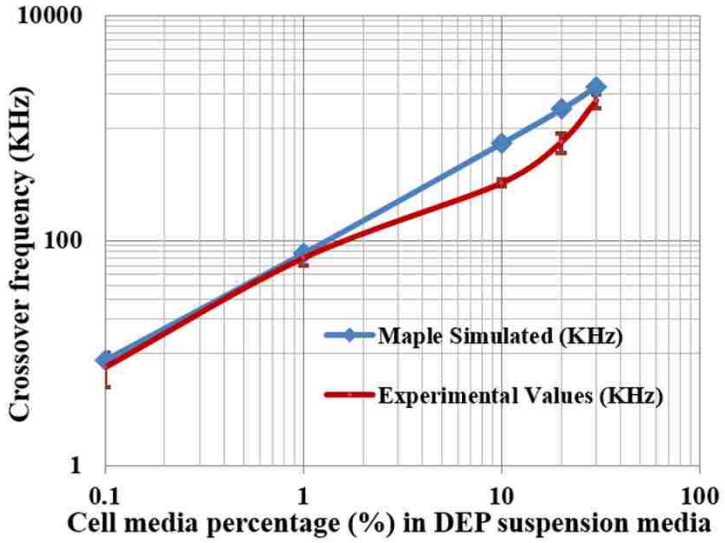

Figure 4.4 Comparison of theoretical and experimental DEP crossover frequencies for hippocampal neurons.

For glial cells, based on simulation results, crossover only happens in 0.1% and 1% cell media solution (Fig. 4.1). However, experimentally, crossover frequencies also were detected in 10% and 20% cell media solutions (Table 4.3). As for the 30% cell media solution, confirmed nDEP effect can be detected at electric signals up to 2 MHz, as recorded for 'Experimental Low' in 30% cell media solution in Table 4.3, but no DEP effect can be observed with higher frequencies. This measurement in 30% cell media solution indicates that DEP effect is very weak for glial cells at frequencies higher than 2 MHz. The reason for that is the real part of Clausius-Mossotti factor is very close to zero in that frequency range.

Despite the discrepancies between measurement and simulation in 10%, and 20% cell media solutions, the measured crossover frequencies in 0.1% and 1% cell media solutions are very close to simulated values (Table 4.3 and Fig. 4.5(a)). Again, we think the discrepancies could be attributed to the limited amount of information available in the literature on the dielectric and physical properties of glial cells, which is used as a base for our simulation work. Another possible reason for observed crossover in 10% and 20% cell media solutions, is that, in addition to astroglial

cells, other types of glial cells, such as microglial cells could also be present in our harvested glial cell pellet [82]. Various types of glial cells could have different DEP behaviors because of their distinctive dielectric or physical properties.

Furthermore, in most suspension medium, glial cells have lower crossover frequencies while transitioning from nDEP to pDEP (Table 4.3), which suggests that glial cells experience positive DEP at lower frequency than neurons. With different devices and suspension medium, Flanagan et al. and Prasad et al. reported similar results in their work [55, 83], thereby providing additional confirmation for our results. Their work, initially primarily of empirical nature, was substantially enhanced by their recent research on the characterization and separation of neural stem cells based on their biophysical membrane properties [84, 85]. Here, we have provided the theoretical and modeling framework enabling us to predict the ideal separation and trapping frequency ranges.

According to the Maple simulation, instead of the literature-derived 0.1 S/m [78, 79], if the cytoplasm conductivity of glial cells is postulated to be 0.3 S/m, then theoretical crossover frequencies will be recalculated in 10% and 20% cell media solutions (Fig. 4.5(b)), and then the simulated DEP crossover will be comparable to the experimental measurements. However, there are other discrepancies between simulation and measurements, as the simulated values for crossover frequencies are typically higher than those we measured. With further parameter refinement, we find that if the cytoplasm conductivity of glial cells is hypothesized to be between 0.3 and 0.4 S/m, the real part of Clausius-Mossotti factor (determining DEP force) is very close to zero at frequencies higher than 2 MHz in 30% cell media solution, which is now consistent with our measurement, as mentioned above.

Another interesting point is that if cell radius of 5 μm or 6 μm is utilized, instead of 4 μm, the simulated crossover frequencies are significantly closer to the experimental values (Fig. 4.5(c)). This approach could be very valuable for the extraction of more accurate parameters (dielectric

properties) from the experimentally determined crossover frequencies, compared to these that are currently available in the literature. The details of this study are discussed in section 4.6 Estimation of Neuron and Glial Dielectric Properties Using DEP Crossover Frequency.

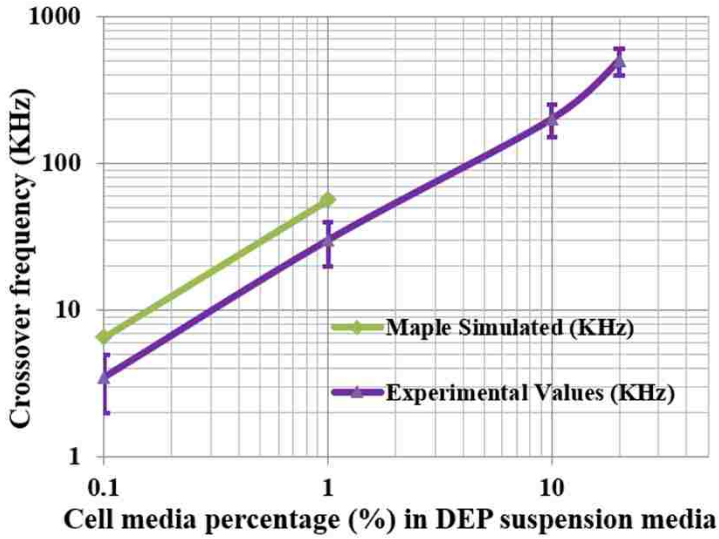

(a)

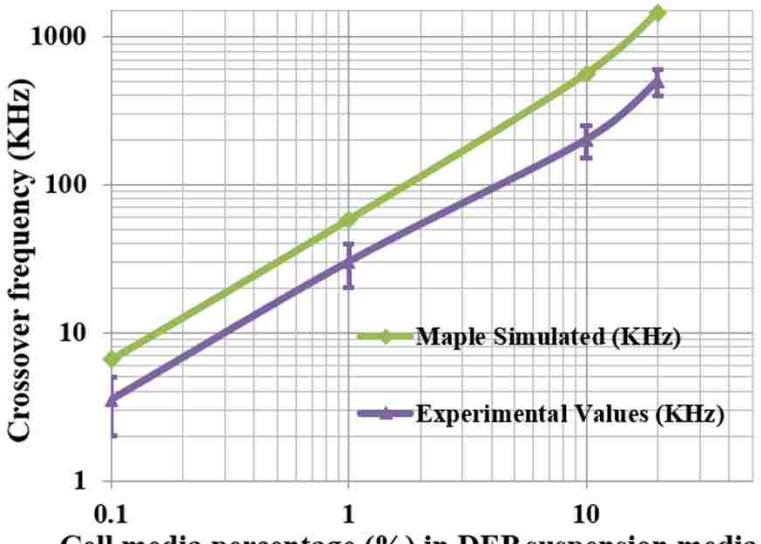

(b)

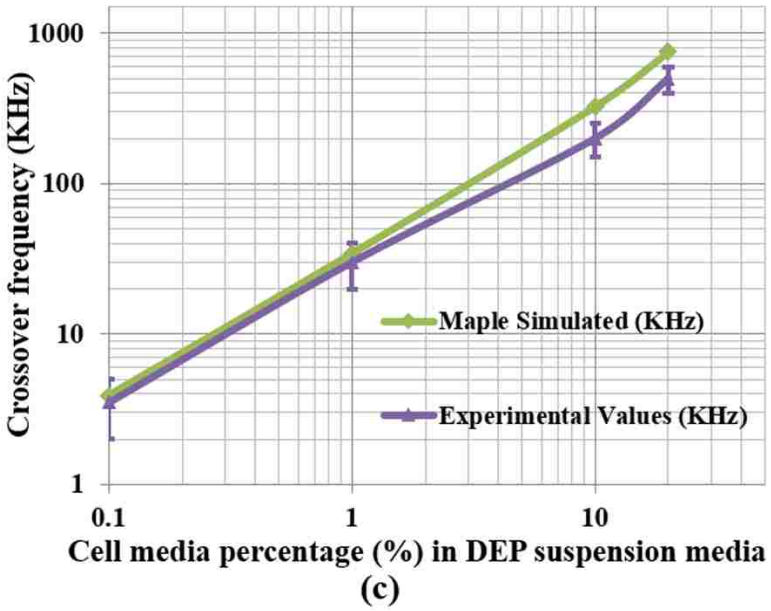

Figure 4.5 Comparison of theoretical and experimental glial DEP crossover frequencies. (a) Initially simulated values from Fig. 4.1. (b) Cytoplasm conductivity σ_c is postulated to be 0.3 S/m, theoretical crossover frequencies are generated in 10% and 20% cell media solutions. However, simulated values are larger than measured values. (c) Further parameter refinement (cytoplasm conductivity σ_c=0.35 S/m; membrane effective capacitance Cm=0.012 F/m^2; cell radius r=6 μm) generates simulated crossover frequencies much closer to the experimental values. This provides a valuable approach to extract more accurate dielectric properties from the experimentally measured crossover frequencies, as described in section 4.5.

4.3 Viability and Purity Assessment of Hippocampal Cells

The viability of hippocampal cells in different DEP suspension medium was measured, independent of DEP, to ensure the health of cells after their exposure to suspension medium for the duration of experiments determining the crossover frequencies. After the tissue dissociation process, cells were suspended in various DEP medium for 30 min at room temperature. Their viability was then assessed through the use of Live/Dead^{TM} cell stain (Invitrogen, Calcein, AM 2μM and Ethidium Homodimer, 1μM in cell media NbActiv1). The viability assessment method described here is similar to the process described in section 3.2.1, except the fact that different suspension medium (sucrose + cell media), instead of pure sucrose solution is used. As can be seen in Fig. 4.6, compared

to the control group in pure cell media, the viability of the cells suspended in various DEP medium is within the range between 80% and 90% for all suspension media with a cell media percentage ratio between 0.1% and 50%. This high cell viability indicates that the cells can remain alive in different suspension media during the DEP experiments.

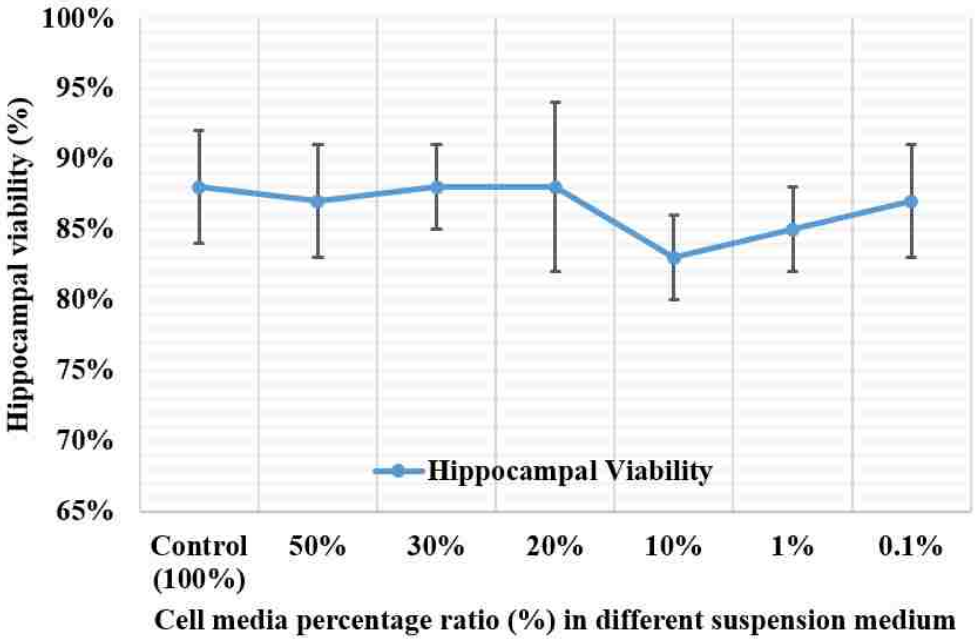

Figure 4.6 Hippocampal viability after 30 min in different DEP suspension medium without DEP. The viability data (average ± standard deviation) for each media condition was analyzed from five samples.

Additionally, the viability of cells after DEP manipulation has been verified, both immediately and 12 hours after the DEP process. The difficulty in accurately determining the viability of the cells was due to the fact that some of them potentially could be lost due to the media change in live/dead staining, so we analyzed the cells both on the device and in the exchanged media, as will be described in section 4.5.2.

It is vital, for our experiments, to have pure populations of neurons or glial cells respectively, when we are determining their crossover frequencies. In order to verify the purity of neurons and glial cells after the enrichment process described earlier, immunostaining was performed directly on

hippocampal neuronal and glial cultures, at Div. 6 and Div. 13 respectively, to quantify the percentage purity of neurons and glial cells. The staining procedure is described in Section 3.1.3. The measured percentage purity of neurons (94.1% ± 1.3%, n = 12) and glial cells (89.7% ± 4.9%, n=12), as shown in Fig. 4.7, verifies the efficacy of the enrichment process (Fig. 4.8) and the accuracy of the DEP experiments.

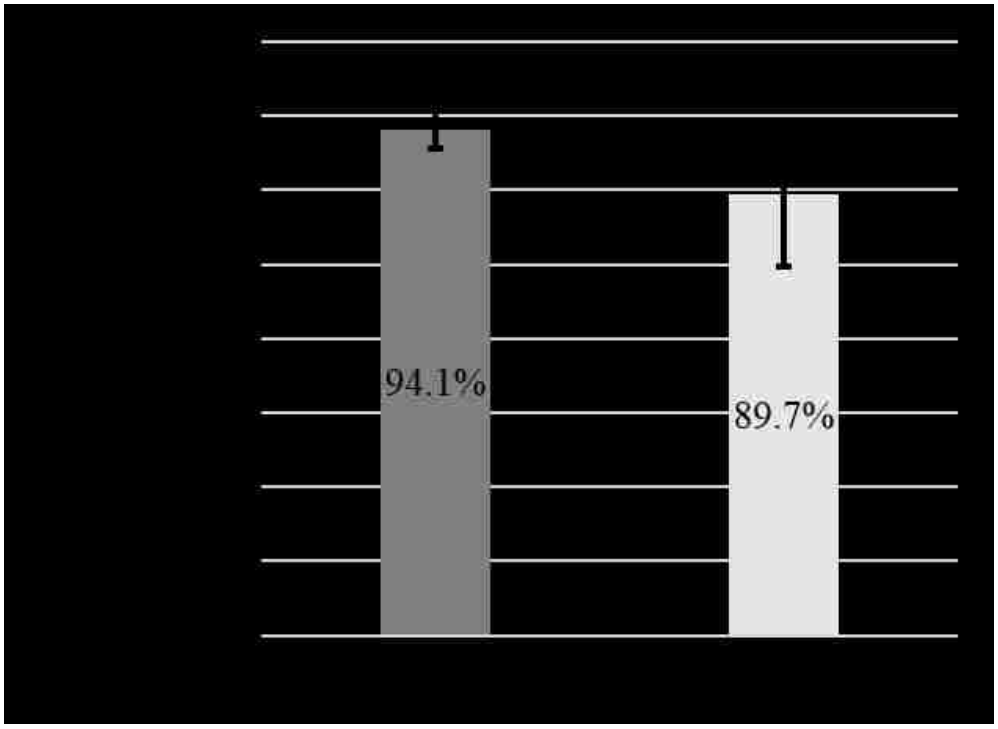

Figure 4.7 Cell percentage purity of hippocampal neurons and glial cells after enrichment culture.

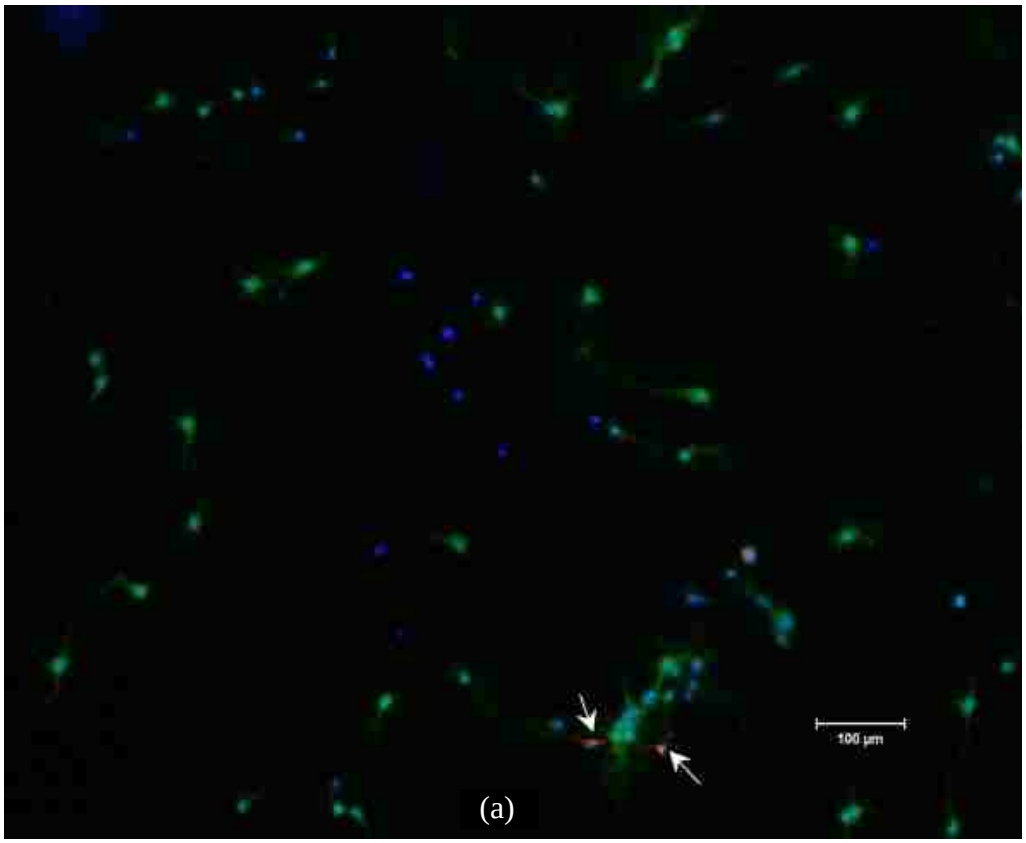

(a)

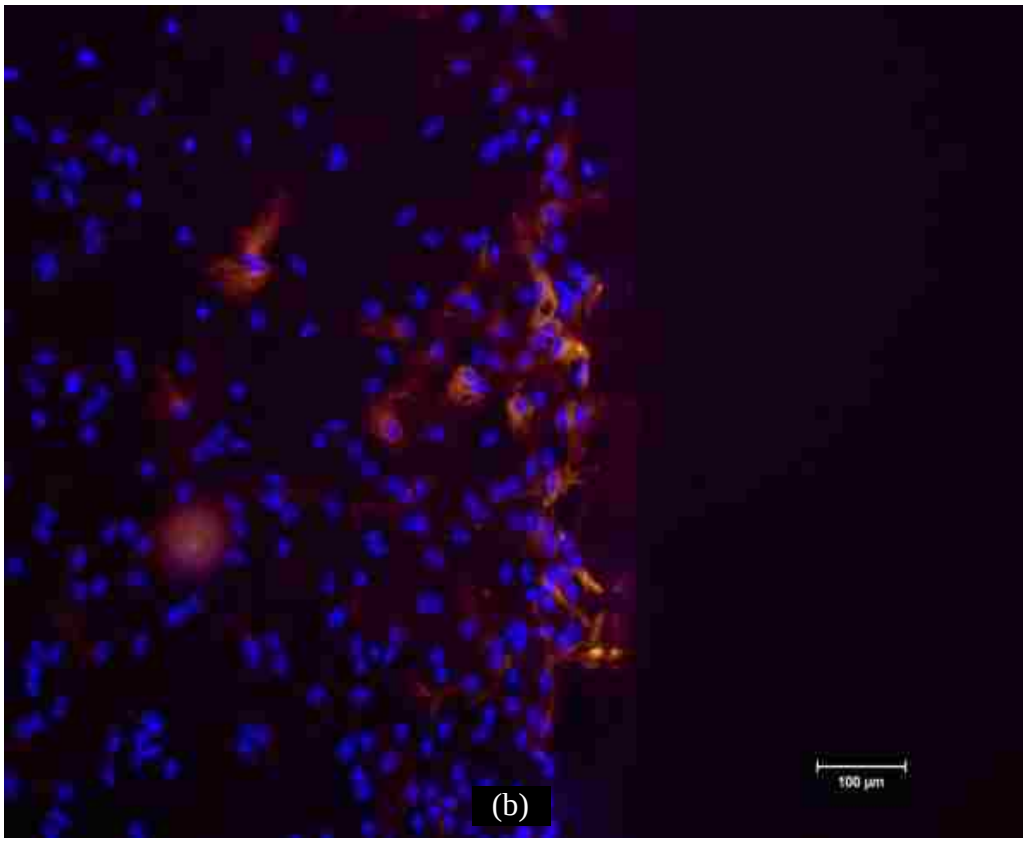

(b)

Figure 4.8 Immunostaining of hippocampal neuronal culture at Div. 6 (a) and glial cell culture at Div. 13 (b) (Green: neurons; red: glial cells). All samples were neuron and glial double stained. Blue DAPI (4',6-diamidino-2-phenylindole) nuclei staining was performed to identify individual cells. Both neurons and glial cells were cultured on poly-d-lysine coated cover slides. Two glial cells are indicated by arrows in (a). Glial cells in (b) were located at the edge of the cover slide. High neuron (94.1% ±1.3%, n = 12) and glial (89.7% ±4.9%, n=12) purity was achieved. Scale bar is 100 μm.

4.4 Neuronal and Glial DEP Movement Analysis

In this set of experiments, we have decided to fully characterize the movements of neurons and glial cells exposed to DEP. Specifically, we aimed to visually confirm the different behaviors of different type of cells when exposed to identical DEP conditions.

After DEP crossover frequency measurements, which were done separately for neurons and glial cells, equal amounts (1.0×10^4 cells) of neurons and glial cells were mixed together, and suspended in targeted separation media (containing 30% cell media, the remaining 70% of sucrose solution as explained earlier) to highlight and additionally clarify the difference of their DEP movements under the same DEP condition. Namely, we wanted to obtain verification of the frequency range where neurons exhibited positive DEP, and glial cells exhibited negative DEP, which was difficult to verify in a standard cell composition following the brain tissue dissociation, which did not have affirmative number of glial cells.

Since the polarity of DEP effect on cells does not depend on the configuration of electrodes, we used the simplified quadruple electrode array (Fig. 4.2) for better visualization and analysis of individual cells. We find in our experiments that the DEP MEA (16 electrodes) can block the view of some cells if multiple cells are monitored simultaneously. With fewer, larger electrodes, the quadruple electrode array is also easier for the experimental setup on a probe station, which is the same as in Fig. 4.3. Additionally, finite element simulation has shown that the electric field strength on this quadruple electrode array is very close to that on the DEP MEA when the same electric potential is applied. As indicated in Fig. 4.9, local maximum electric field areas, located at the edge

of each electrode, are where the cells are attracted to under positive DEP. While cells experiencing negative DEP are positioned to the local minimum electric field areas, which are the center point and inner area of each electrode. During the movement analysis experiment, 10 MHz AC and ground signals are applied to every other electrodes of the quadruple electrode array.

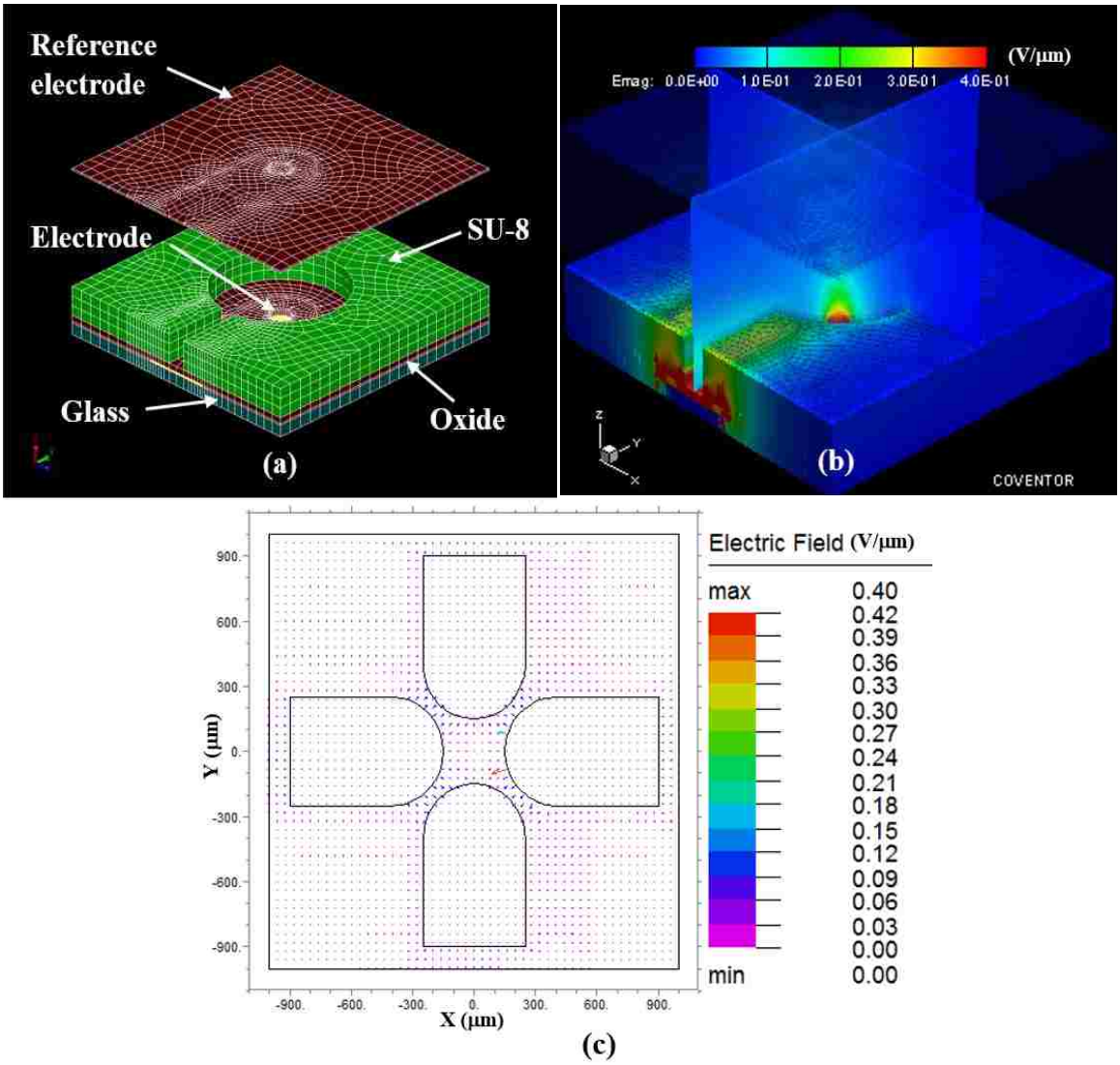

Figure 4.9 Finite element electric field simulation. (a) Finite element model of one electrode structure of the DEP MEA. (b) Simulated electric field distribution on one electrode of the DEP MEA using CoventorWare (Coventor, Inc.). Cells are attracted to the open via on top of the electrode (maximum field strength) when pDEP is implemented. (c) Simulated electric field distribution of the quadruple electrode array using FlexPDE software (PDE Solutions Inc.). Maximum filed strength areas are located at the edge of each electrode, and the electric field

strength in (c) is comparable to that in (b). Electric potential of 3V is applied to the electrodes in (b) and (c) during simulation.

After the cells were settled on the electrode surface, a 27-second video was captured using a Moticam 2300 camera (Motic Group CO., LTD.), started with the application of the electric potential. Image frames from the video were processed and retracted at 0.85 s per image through Matlab (MathWorks, Inc.). In Fig. 4.10, three images from the video are presented, timing at 5.525s (a), 14.025s (b), and 26.775s (c), respectively. Eleven cells showing relatively large movements were selected and their moving trajectories were tracked by processing the image stack, from the video, using ImageJ processing software (National Institutes of Health). Six cells (1, 3, 4, 5, 9, and 11) experienced significant positive DEP effect and were trapped or moved towards the edge of the electrodes; meanwhile, other five cells (2, 6, 7, 8, and 10) experienced negative DEP effect and moved towards the inner area of the electrodes. All the labeled cells were relatively bright and small. Based on our live/dead fluorescent staining experience, these bright and small cells represent a normal morphological appearance of live cells in suspension. The dark cells with larger diameters were excluded from the analysis, because we have experienced that these cells are dead, based on the same staining process. Considering the live/dead and neuron/glial staining techniques, available to us, would end the life cycle of the cells, no fluorescent labeling was performed here. This coexistence of cells experiencing pDEP and nDEP under the same DEP condition was observed in three independent experiments.

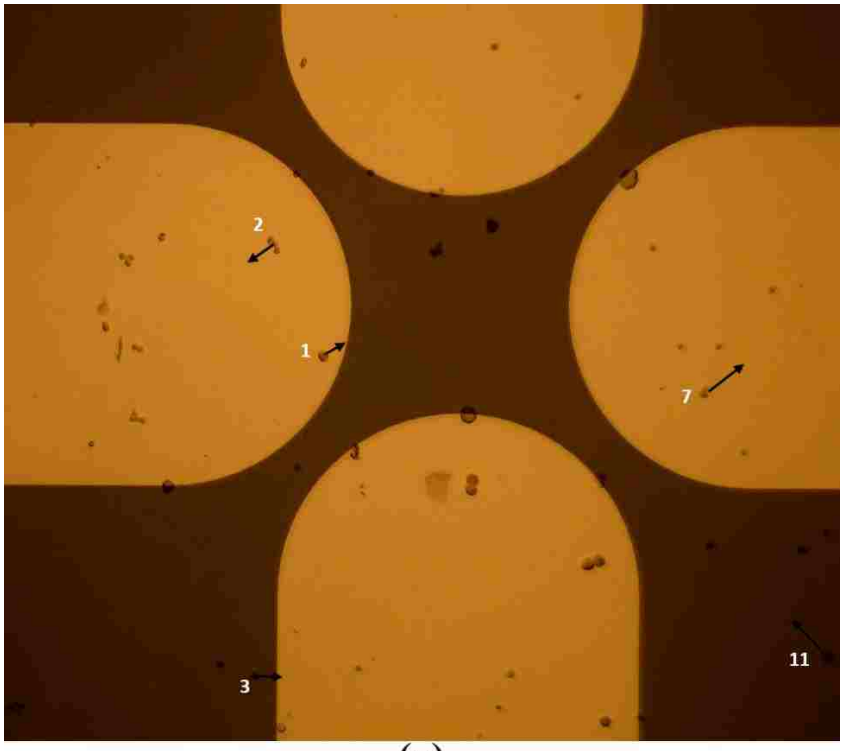

(a)

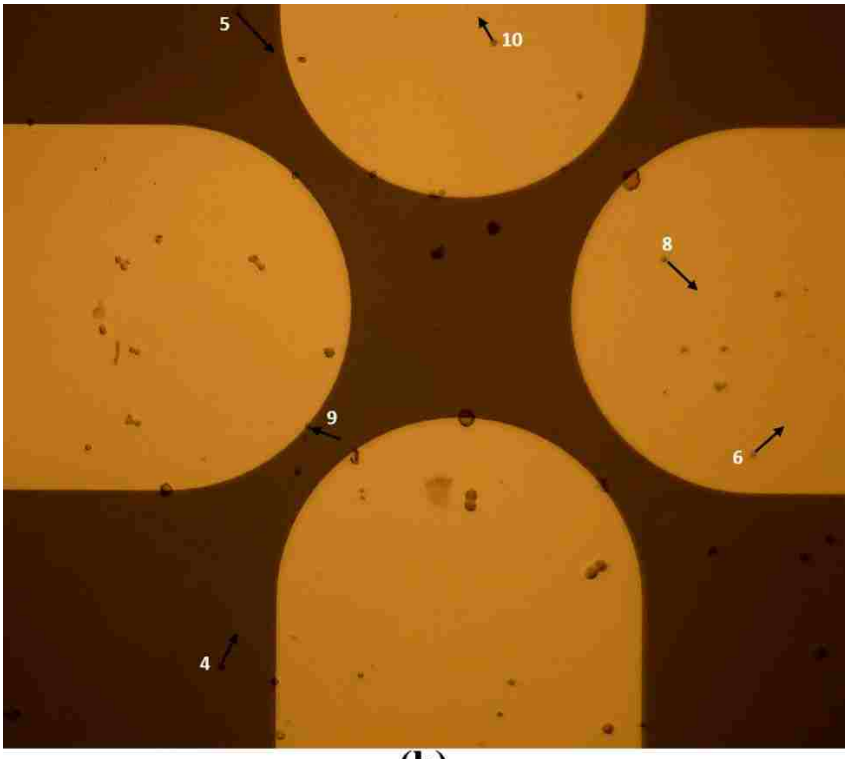

(b)

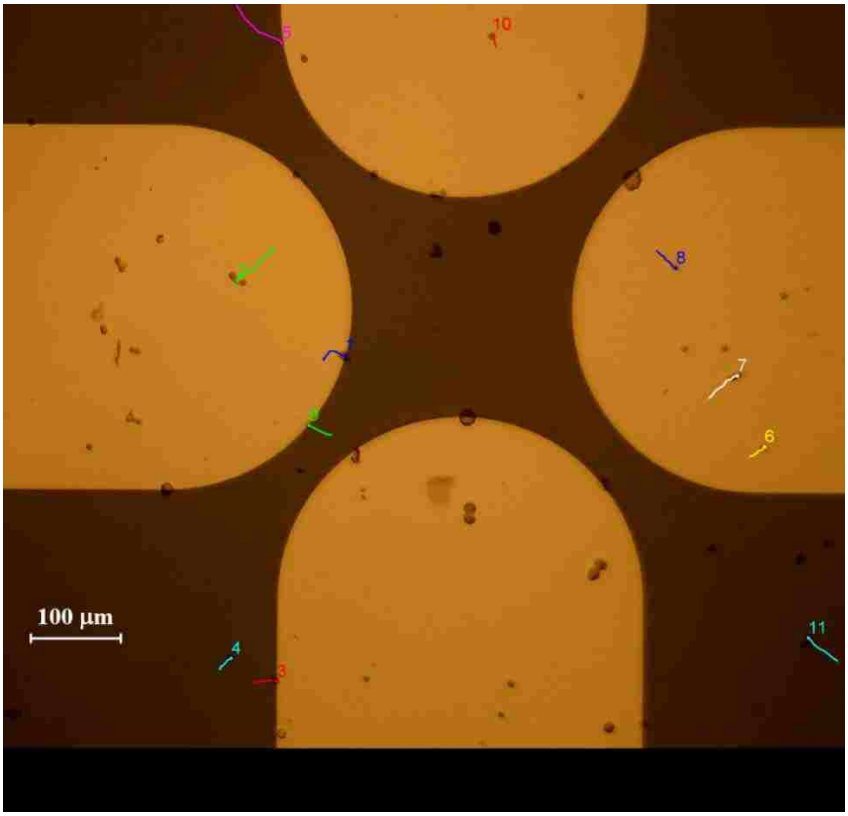

Figure 4.10 Moving directions (a) and (b) and trajectories (c) of six cells experiencing pDEP and five cells experiencing nDEP are tracked. (a), (b) and (c) are at 5.525s, 14.025s, and 26.775s, respectively, of the cell movement video (Online Resource 2). The cell numbers in (c) are the same as in (a) and (b).

As mentioned before, hippocampal neurons were confirmed to experience pDEP at 10 MHz in the targeted suspension medium, which is the same electric signal applied here. The cells used in this experiment were a mix of equal amount of neurons and glial cells, and it is apparent that some of them are experiencing positive, and some negative dielectrophoresis. Therefore, we hypothesize that the cells shown on Fig. 4.10 which moved towards the inner area of the electrodes and therefore experienced nDEP were, in fact, glial cells. Notably, however, during our previously described crossover frequency measurements (section 4.2), no obvious DEP effect was observed for glial cells exposed to the same conditions (10 MHz signal, and 30% cell media solution). We needed more information to shed light on this discrepancy.

Therefore, cell tracking data (timing and position) were obtained from ImageJ software (Fig. 4.10), to clarify the difference between DEP effects experienced by those cells. The moving speed of those cells was analyzed, so that the DEP effects they experienced were compared. As can be seen in Table 4.4, either from the average maximum velocity or the average moving velocity of the two categories of cells (pDEP and nDEP), the cells experiencing pDEP are moving much faster than cells experiencing nDEP, indicating a much stronger pDEP effect than nDEP. This could also explain why we observed very weak DEP effect for glial cells while measuring their crossover frequency. Considering the DEP spectra simulation, a weaker DEP effect for glial cells in 30% cell media solution indicates that the real part of Clausius-Mossotti factor is very close to zero at higher frequencies, resulting in less DEP force, which is consistent with our discussions above.

Table 4.4 DEP moving velocity (μm/s) of tracked cells.

	Positive DEP						Negative DEP				
Cell no.	1	3	4	5	9	11	2	6	7	8	10
[a] Maximum velocity	5.8	8.9	2.4	10.2	6.5	4.1	4.3	2.1	3.0	2.2	1.7
[b] Averaged maximum velocity	6.3 (s = 2.9)						2.7 (s = 1.0)				
[a] Averaged moving velocity	2.2	3.2	2.1	6.4	2.8	2.5	2.6	1.4	2.4	1.7	1.0
[b] Averaged moving velocity	3.2 (s = 1.6)						1.8 (s = 0.6)				

[a] Data of each cell;
[b] Averaged data of each category of cells (pDEP or nDEP);
s = standard deviation.

4.5 Hippocampal Neuronal Separation from Glial Cells

4.5.1 Experimental Verification

To experimentally verify the separation of hippocampal neurons from non-neuronal glial cells by the DEP method, equal amounts (5.0×10^4 cells) of hippocampal neurons and glial cells are mixed together, after the respective harvesting process (section 4.2.1). The separation of neurons and glial

cells in 30% cell media solution, as well as neuron recruiting onto the electrodes, are performed on a packaged DEP MEA device, following the same procedure described in section 3.1.2.

Five different neuronal separation and recruiting experiments have been performed, and each experiment was completed within 30 min. Following attachment to the MEA chip, neurons recruited to electrodes by pDEP were characterized by immunocytochemistry (ICC), as described earlier.

Instead of premixed 1:1 ratio sample, we first used the raw neuron/glial cell mixture, dissociated directly from hippocampus tissue in the experiment (Fig. 4.11(a)). It can be seen that 13 of the 16 electrodes were occupied exclusively by neurons (green). The circles (white) indicate the SU-8 microchambers above 16 electrode sites, which have diameters of 30 μm. One glial cell (red) was found close to the electrode, but not anchored on the electrode itself. As mentioned earlier, the exact ratio of glial cells in the raw embryonic neuron/glial mixture was not determined. To ensure comparable amount of glial cells existing in the sample during the separation, a premixed 1:1 ratio sample was used, in further experiments, to verify the separation of neurons and glial cells (Fig. 4.11(b)).

In Fig. 4.11(b), 15 of the 16 electrode sites were occupied exclusively by neurons. The coexistence of six glial cells was also observed and is indicated by circles (red); the glial cells were not actively trapped by pDEP on electrodes. It should be noted that because the cell culture media NbActiv1 is formulated for neuronal growth only [86], more glial cells may have died and thereby been lost during the 12 hours of incubation and staining process. Of the four MEA devices used in this experiment, 11, 14, 15, and 14 electrode sites (out of sixteen possible electrodes) were occupied by neurons respectively; and 5 to 7 glial cells were found in the central area of the device, but not anchored on the electrodes, a result which met our goal of selective neuron-to-electrode recruitment.

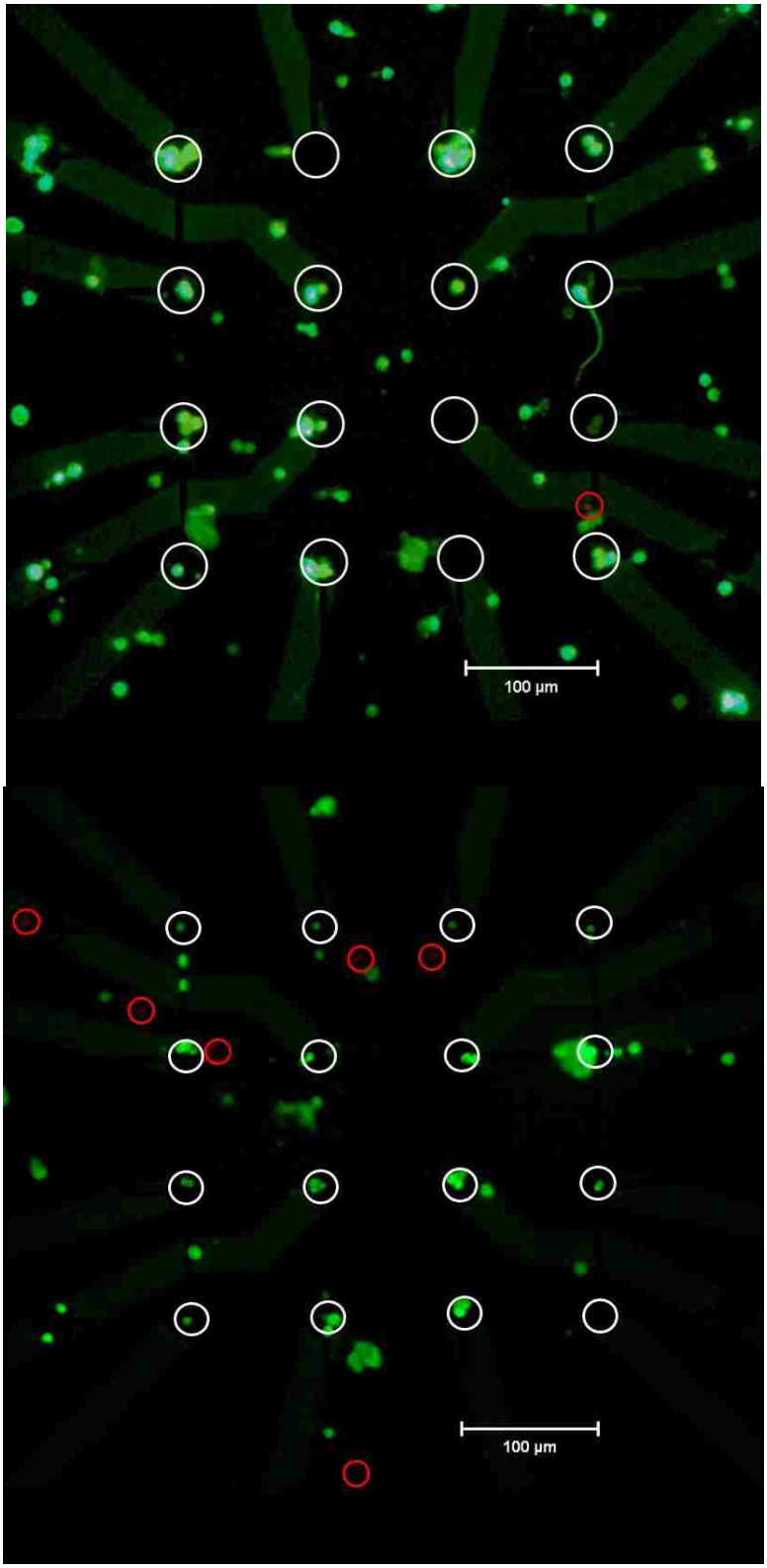

Figure 4.11 Immunofluorescence micrograph of hippocampal neurons (green) trapped by pDEP on electrodes and glial cells (red, red circle-indicated) anchored off electrodes from (a) raw dissociated tissue sample and (b) premixed 1:1 ratio sample. DEP electric signal applied: 10 MHz, 6Vpp. Suspension medium contains 30% neuron culture media.

This result successfully verified that with the implementation of pDEP, the DEP MEA system is capable of separating hippocampal neurons and glial cells from a mixed cell suspension by active neuronal recruitment on the electrodes. The DEP AC electric signal applied during experiments was at a frequency of 10 MHz, and the suspension medium contained 30% cell culture media. Hippocampal neurons, rather than glial cells, were attracted to the electrode sites at this frequency, confirming our approach for neuron/glial separation.

Another relevant conclusion is that the dielectric properties available for glial cells, derived from limited previous studies and then utilized in our simulations, might not be completely accurate. As demonstrated in Fig. 4.5, glial cell cytoplasm conductivity, in all likelihood, is greater than the value derived from the current literature. More accurate information about the dielectric properties of glial cells would further increase the accuracy of the simulation. Indeed, it has been shown by Prasad et al. that an AC DEP electric signal of 4.6 MHz and 8 Vpp (peak to peak) was appropriate to separate neurons and glial cells in a mixed co-culture [55]. In this work, these values were anticipated and then verified, via simulation as well as experimentally, and that is additional confirmation of the validity of our approach.

4.5.2 Neuronal Post-DEP Viability Verification

We have also confirmed that neurons are still alive and electrically active after their separation from glial cells and positioning using pDEP. In the related work, Prasad et al. reported immediate recording of neuronal signals after DEP positioning (there was no attempt to look at neuronal potential longer than 30 min) [55], and Jaber et al. reported spontaneous and stimulated action potentials from multiple electrodes after 24 hours in vitro, using different DEP conditions than in our work [20]. Here, we supplemented neuronal signal recording by subsequent neuron live/dead staining, which provided us with information about how many neurons survived the DEP process and whether or not they were electrically active.

In our experiments, three MEA devices were used for signal recording after neuronal separation and recruiting. Immediately after DEP positioning, we did not detect any neuronal signals from the electrodes. We also tried to live/dead stain the cells; as described previously in section 3.2.3, immediately following DEP recruiting, neurons could easily be displaced off the electrodes because of the manual operations and media disturbance. Therefore, we manually collected the cells from the device chamber using a micropipette, and live/dead stained them for viability assessment. Microscope observation revealed that no cells remained in the electrode array area of the device after this manual collection. The viability from the collected cells was 96.0% ± 7.1% (n=6). In a separate experiment, we waited 12 hours for neurons to better attach on the electrodes. After twelve hours *in vitro*, live/dead staining was performed on cells, both on the device and in the media. We found few cells in the media; however, the cells anchored in the electrode array area of the device showed that 84.2% of the cells are live (Fig. 4.12).

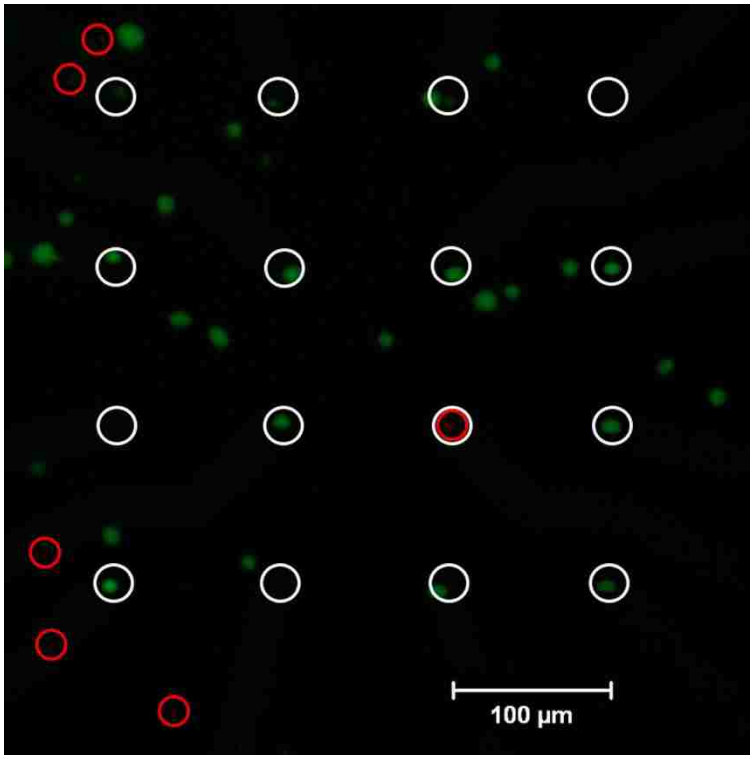

Figure 4.12 Live (green)/dead (red circle-indicated) stain of hippocampal neurons positioned on MEA at 12 h in vitro. White circles indicate the microchambers on top of each electrode. Viability

better than 84% was achieved. Neuronal separation and recruiting was performed with cells directly dissociated from hippocampus tissue, where both neurons and glial cells were present.

In section 3.2.3, Fig. 3.8 shows another fluorescent micrograph of live/dead stain of hippocampal neurons positioned on DEP MEA at 12 h in vitro, where 96% of cell viability is achieved. At the same time (12 h in vitro), spontaneous neuronal potential was detected from two electrodes on one of the three devices (MEA in Fig. 3.8), and stimulated neuronal signals were measured from two electrodes on the same device and one electrode on another device. We should mention here that we were using embryonic hippocampal neurons in our experiments, compared to postnatal neurons used by Prasad et al. and Jaber et al. [20, 55]. This might explain the scarce neuronal potentials we could measure at this stage of culture [20, 87].

Fig. 4.13 shows the spontaneous and stimulated neuronal extracellular potential we recorded from another electrode of the MEA in Fig. 3.8. Spontaneous extracellular potential has an amplitude around 100 μV, and stimulated potential has an amplitude around 150 μV. The stimulation signal we used was a biphasic positive + negative pulse with an amplitude of 1V and pulse duration of 0.1ms. The stimulated signal was recorded 1 ms after the biphasic pulse, according to the study of Jimbo et al. [58]. In addition, the stimulation artifact could cause overshooting to the signal processing system because of the 5000 signal-processing system gain, so a 1 ms switching time was set in our system before started to record. The response time between stimulation and first evoked spike was 10-50 ms, which is reasonable according to Jaber et al., Merz and Fromherz, and Wagenaar et al. [20, 59, 60].

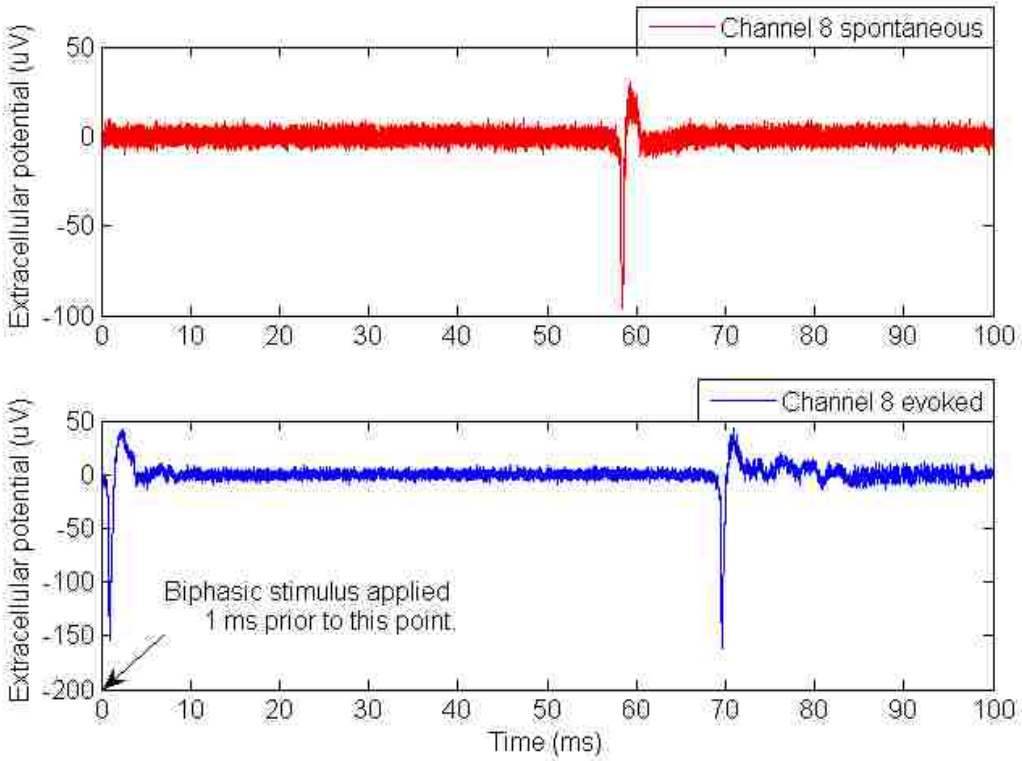

Figure 4.13 Spontaneous and evoked neuronal potential recorded from the same electrode of one MEA device. The evoked response is recorded 1ms after the stimulation pulse.

4.6 Estimation of Neuron and Glial Dielectric Properties Using DEP Crossover Frequency

As described in section 4.2.2, simulations of DEP spectra ($Re[K]$) based on averaged property values (from literature) of hippocampal neurons and glial cells have been performed, and the discrepancies between simulated and experimentally measured crossover frequencies demonstrated the need for more accurate cell property values. We have also demonstrated earlier that the refinement of glial dielectric properties can create simulated crossover frequencies better reflect the measurement values.

Various experimental approaches have been applied to measure cell interior and membrane properties. For instance, a voltage patch clamp was utilized to directly measure neuronal membrane capacitance [32], and intracellular conductivity was determined from cell membrane electric

breakdown [88]. Despite all these efforts, the dielectric properties of many mammalian cells have yet to be determined accurately because of the vast variety of cell types; the values of those that have been reported in the literature vary widely [31-34]. Specifically, the determination of the dielectric properties of neurons and glial cells, for instance, will vastly facilitate the characterization, separation, and manipulation of them and their stem cells [83, 89].

As a label-free and flexible tool, DEP has been widely used to characterize the electrical properties of not only the cell membrane, but also the cell interior [40, 90, 91]. The ability to determine cell dielectric properties with DEP has been demonstrated previously by Mahaworasilpa et al. [92], where DEP force on single cells in AC electric fields was measured to analyze cell movement. In addition, the measurement of DEP crossover frequency has been extensively applied by the groups of Pethig et al., Gascoyne et al., Voldman et al. and Gagnon et al. [40, 41, 80, 89, 90, 93-95], to characterize and separate multiple cell types. In order to ensure the validity of the approach and the accuracy of the result, detailed mathematical derivations, based on a particular dielectric model of cell, were usually given to relate the crossover frequency and the electrical properties of cells. For instance, the work reported by Pethig et al. and Gascoyne et al. determined the effective cell membrane capacitance from the slope of the plots of crossover frequency versus the medium conductivity based on a low frequency (DC) approximation [40, 89, 94, 96]. However, this DC approximation can only be applied when the measurement is performed in a medium with lower conductivity (e.g. $<10^{-3}$ S/m), where the measured crossover frequency is sufficiently lower than the dispersion frequency (~1 MHz) [97, 98], which is usually associated with the internal polarization between the cell membrane and cytoplasm. Furthermore, extended exposure to low-conductivity medium often causes ionic flux out of cell membrane, which could compromise the cytoplasmic integrity [98]. Due to the considerations above, this approach is not appropriate in some cases where DEP crossover frequency is measured to determine the dielectric properties of cells, unless more complicated models and lower level of approximations are used.

In this section of work, we will further determine the dielectric permittivity (ε_c), cytoplasm conductivity (σ_c), and specific membrane capacitance (c_m) of mouse hippocampal neuronal and glial cells using DEP crossover frequency. Instead of low-frequency approximation, this methodology is based on the simulation of crossover frequencies directly from the governing equation of the dielectric model of mammalian cells, as well as measured crossover frequencies (Table 4.3) in different suspension media with higher conductivity (with the addition of cell media). Relationships between the properties of cells and crossover frequency, as demonstrated by theory analysis, enable the simultaneous estimation of three properties by a straight forward fitting procedure. The best fit determines the estimated physical properties in question. The estimated neuronal properties significantly narrow the value ranges available from literature. Additionally, the estimated glial cell properties are a valuable addition to the scarce information currently available about this type of cell. This methodology is applicable to any type of cultured cells that can be subjected to both positive and negative DEP.

4.6.1 Theoretical Analysis

In section 2.1.2, we analyzed the dielectrophoretic model of mammalian cells. From the analytical expression of C-M factor for mammalian cells in medium (equation (2.6)), if we define A, B, C and D as follows,

$$A = \omega^2\left(\frac{\varepsilon_c}{\sigma_c}\frac{c_m r}{\sigma_m} + 2\frac{\varepsilon_m}{\sigma_m}\frac{c_m r}{\sigma_c}\right) = \omega^2(a + 2b);$$

$$B = \omega\left(\frac{c_m r}{\sigma_m} + 2\frac{\varepsilon_m}{\sigma_m} + 2\frac{c_m r}{\sigma_c}\right) = \omega(\mathrm{c} + 2\mathrm{d});$$

$$C = \omega^2\left(\frac{\varepsilon_m}{\sigma_m}\frac{c_m r}{\sigma_c} - \frac{\varepsilon_c}{\sigma_c}\frac{c_m r}{\sigma_m}\right) = \omega^2(\mathrm{b} - \mathrm{a});$$

$$D = \omega(\frac{c_m r}{\sigma_m} - \frac{\varepsilon_m}{\sigma_m} - \frac{c_m r}{\sigma_c}) = \omega(c - d);$$

where:

$$a = \frac{\varepsilon_c}{\sigma_c}\frac{c_m r}{\sigma_m}; \qquad b = \frac{\varepsilon_m}{\sigma_m}\frac{c_m r}{\sigma_c};$$

$$c = \frac{c_m r}{\sigma_m}; \qquad d = \frac{\varepsilon_m}{\sigma_m} + \frac{c_m r}{\sigma_c}.$$

then the expression of C-M factor *K*, equation (2.6) can be simplified as

$$K = \frac{C+jD-1}{2-A+jB} = \frac{[(C-1)+jD][(2-A)-jB]}{(2-A)^2+B^2} \tag{4.1}$$

The sign of the real part of C-M factor $Re[K]$ determines the type of DEP effect, a positive $Re[K]$ leads to pDEP and a negative value causes nDEP. Therefore, for cells in a suspension medium, the theoretical crossover frequency between pDEP and nDEP can be obtained by solving the equation:

$$Re(K) = \frac{(C-1)(2-A)+BD}{(2-A)^2+B^2} = 0 \tag{4.2}$$

which is further simplified as

$$2C - AC + A - 2 + BD = 0 \tag{4.3}$$

and

$$2\omega^2(b-a) - \omega^4(a+2b)(b-a) + \omega^2(a+2b) + \omega^2(c+2d)(c-d) = 2 \tag{4.4}$$

Finally, solving the quadratic equation of ω^2 will give the theoretical crossover frequency directly:

$$\omega^2 = \{[(4b-a)+(c+2d)(c-d)] \pm \{[(4b-a)+(c+2d)(c-d)]^2 - 8(a+2b)(b-a)\}^{1/2}\}[2(a+2b)(b-a)]^{-1} \quad (4.5)$$

provided $a \neq b$ ($\varepsilon_c \neq \varepsilon_m$), that is, the dielectric permittivities of cell interior and suspension medium are not exactly the same. In the expressions of $a, b, c, and\ d$, the dielectric permittivity of suspension medium ε_m is very close to the permittivity of water $80\varepsilon_o$ [36, 99], where ε_o is the permittivity of vacuum, and cell radius r and medium conductivity σ_m can be experimentally measured respectively. As a result, three cell dielectric properties cytoplasm permittivity ε_c, cytoplasm conductivity σ_c, and membrane effective capacitance c_m, can be simultaneously determined by fitting equation (4.5) to compare theoretical crossover frequencies ω with experimentally measured values.

4.6.2 Pre-fitting Analysis

Before fitting theoretical crossover frequencies to experimental data, dielectric and physical properties of hippocampal neurons and glial cells have been researched from previous studies, as shown in Table 4.5. The averages of these literature values haven been listed in Tables 2.1 and 4.1, respectively, as they are being used in DEP spectra simulations for hippocampal neurons and glial cells. For mouse hippocampal neurons, both cytoplasm conductivity σ_c and membrane effective capacitance c_m have a wide range of literature values, experimentally determined on closely-related types of mouse neurons, such as mouse CA3 pyramidal neurons and interneurons [31, 34], and cortical rat neurons [33], as can be seen in Table 4.5. Neuronal cytoplasm permittivity ε_c is set at $78\varepsilon_0$, based on literature values [33, 36], to be very close, but not equal, to that of suspension medium, as discussed in equation (4.5). However, very limited information about glial cells is available in the literature. Here, we assume the cytoplasm permittivity of glial cells ($78\varepsilon_0$) to be the same as neurons'. Glial cytoplasm conductivity was derived from conductivity-related glial cell

and tissue information [78, 79], and the membrane effective capacitance was found in only one study [32].

Here, property values within the literature ranges in Table 4.5 are evaluated using our estimating technique, which takes experimental crossover frequencies into account. For single literature data in Table 4.5, values around (larger and smaller than) the particular reference value are evaluated. The goal is to determine property values that give a better fit between the theoretical crossover frequency and that which is experimentally measured.

Table 4.5 Hippocampal neuron and glial properties from literature.

	Cytoplasm dielectric constant $\varepsilon_c/\varepsilon_0$	Cytoplasm conductivity σ_c (S/m)	Membrane effective capacitance c_m (F/m^2)
Hippocampal Neuron	78 [33, 36]	0.4 - 1.0 [31, 33, 34]	0.002 – 0.013 [31-34]
Glial Cell	78[a]	0.1 [78, 79]	0.0106 [32]

[a] Assumed value.

As can be seen in equation (4.5), there are two sets of solutions to the quadratic equation (4.4) of ω^2, depending on the '+' and '-' signs. The DEP electric signals provided by the function generator have a maximum frequency of 30 MHz. To determine which solution is within our practically measurable frequency range, averaged property values from Table 4.5 for hippocampal neurons are fitted to select the reasonable theoretical crossover frequency (Fig. 4.14). Comparing the '+' sign solutions (circle) and the '-' sign solutions (triangle) in Fig. 4.14, crossover frequencies solved with '-' sign represent the measured values (stars). As a result, theoretical crossover frequencies are calculated with the '-' sign in the following discussions.

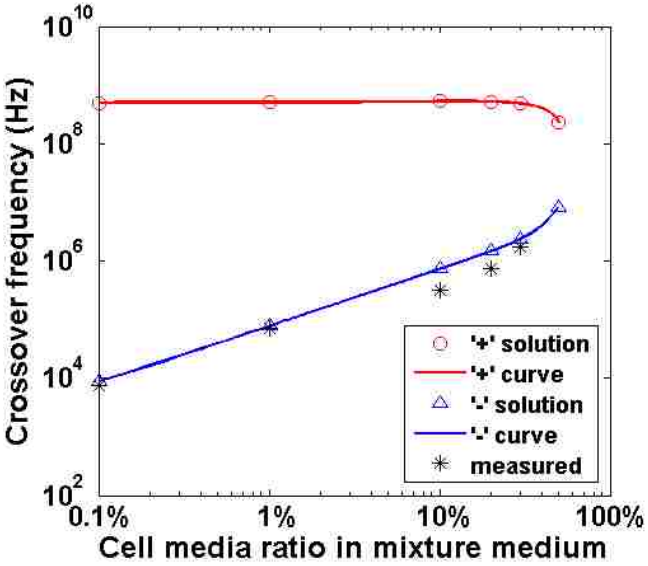

Figure 4.14 Comparison of theoretical crossover frequencies calculated with '+' sign (circle) and '-' sign (triangle) from equation (4.5). Triangle data points represent the measured values (stars). Property values of hippocampal neurons used in this calculation: $\varepsilon_c/\varepsilon_0$ *=78,* σ_c *=0.7 S/m,* c_m *=0.008 F/m*^{2}*, r=4* μ*m.*

4.6.3 Property Determination for Neurons and Glial Cells

Mouse hippocampal neuronal cytoplasm dielectric constant $\varepsilon_c/\varepsilon_0$, where ε_o is the dielectric permittivity of a vacuum, cytoplasm conductivity σ_c, and membrane effective capacitance c_m have been evaluated respectively, according to experimentally measured crossover frequencies in different suspension media (Table 4.3), using values obtained from the literature (values around a reference data, where available, or several different values, if a range has been reported). The dielectric permittivity of suspension medium ε_m is $80\varepsilon_o$; the averaged cell radius is measured as 4 μm for both hippocampal neurons and glial cells. Different suspension medium conductivity values σ_m are measured (see Table 4.2).

When one property value is being evaluated, the other two are fixed during the procedure. Optimal property values have been determined based on the fitted curves that are closest to the measured data. The theoretical crossover frequencies in 50% cell media also are calculated for each subfigure

in Fig. 4.15; however, it is not possible to measure the definite crossover range in 50% cell media because both pDEP and nDEP effects are very weak around crossover, and therefore the exact crossover frequency is very difficult to determine.

For hippocampal neuronal cytoplasm dielectric constant ($\varepsilon_c/\varepsilon_0$) evaluation, different selected property values do not affect the theoretical crossover frequencies much; as shown in Fig. 4.15(a), most of the fitted data and curves overlap on each other. However, we do find that smaller values give a slightly closer fit to the experimentally measured data (calculated data not shown). As a result, in contrast to the literature value of around 80, $\varepsilon_c/\varepsilon_0$ is believed to have a smaller value (e.g. 60) for hippocampal neurons.

Selected values within the literature range of cytoplasm conductivity σ_c have been fit to experimentally measured values in Fig. 4.15(b). As can be seen, greater conductivity values (0.75-0.95 S/m) have better theoretical fit in 20% and 30% cell media suspension mixture, but the fitted points in the lower cell media suspension mixture do not change substantially. These changes in crossover frequencies, therefore, may not be well represented, if only implementing medium with lower conductivity. Smaller cytoplasmic conductivity (0.45 S/m) makes the theoretical values disappear (complex number) in 50% cell media, as indicated by the data point in the lower right corner. Thus, the cytoplasm conductivity σ_c of hippocampal neurons is closer to the higher end (0.75-1.0 S/m) of the literature-value range.

For membrane effective capacitance c_m, greater property values provide a closer fit to the measured data (see Fig. 4.15(c)). Instead of literature-averaged 0.008 F/m^2, we believe the membrane effective capacitance c_m of hippocampal neurons is located at the higher end (0.01-0.012 F/m^2) of the literature range.

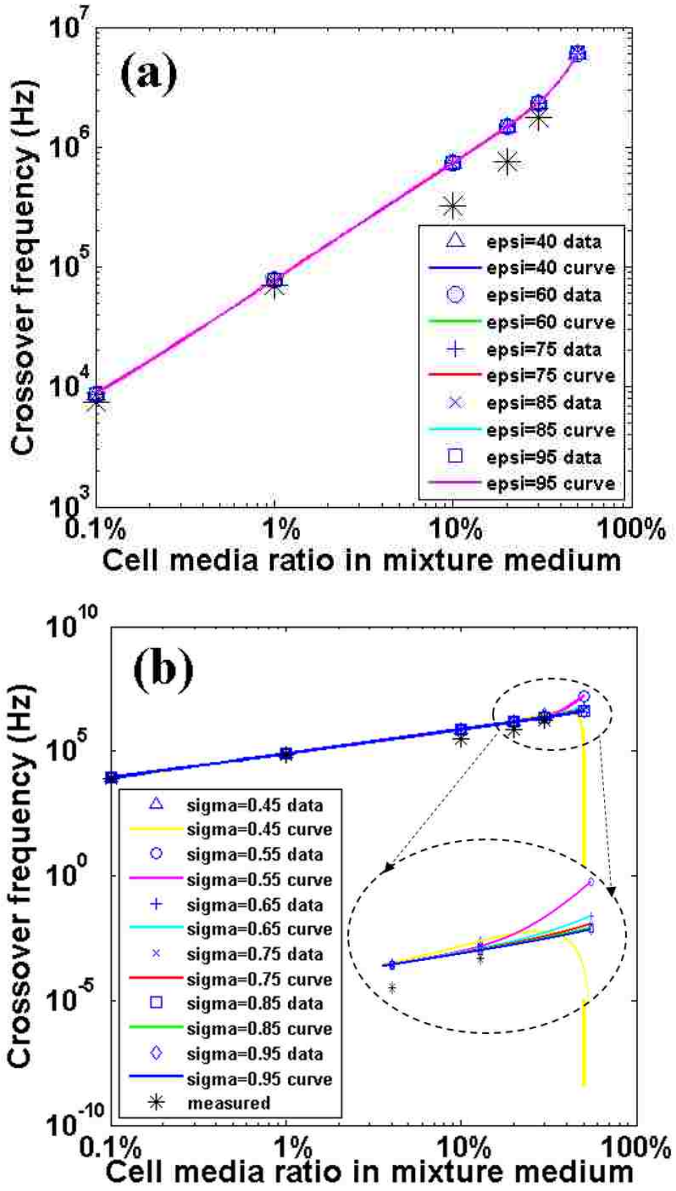
(a)
Crossover frequency (Hz)
Cell media ratio in mixture medium
epsi=40 data
epsi=40 curve
epsi=60 data
epsi=60 curve
epsi=75 data
epsi=75 curve
epsi=85 data
epsi=85 curve
epsi=95 data
epsi=95 curve
(b)
Crossover frequency (Hz)
Cell media ratio in mixture medium
sigma=0.45 data
sigma=0.45 curve
sigma=0.55 data
sigma=0.55 curve
sigma=0.65 data
sigma=0.65 curve
sigma=0.75 data
sigma=0.75 curve
sigma=0.85 data
sigma=0.85 curve
sigma=0.95 data
sigma=0.95 curve
measured

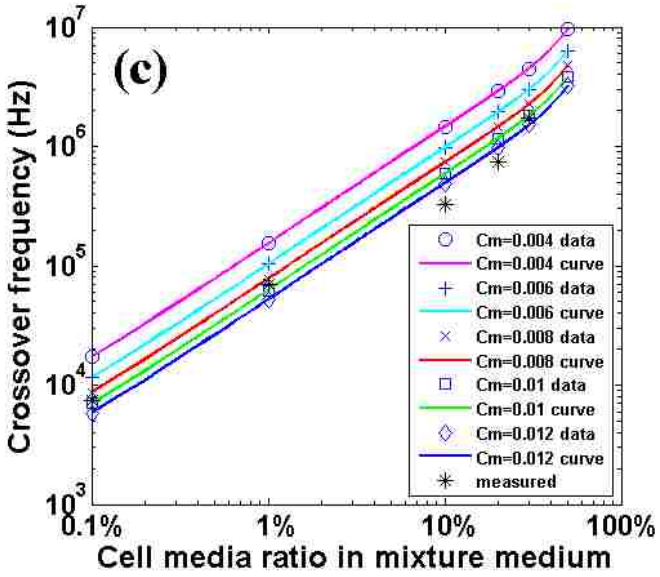

Figure 4.15 Dielectric property values for mouse hippocampal neurons based on values shown in Table 4.5 are evaluated, according to experimentally measured crossover frequencies. The theoretical data in 50% cell media are also calculated in each figure. One property is fit to the experimental values, whereas the other two values are fixed to the values described in each situation.

(a) Cytoplasm dielectric constant values $\varepsilon_c/\varepsilon_0$=40, 60, 75, 85 and 95 are fitted. Smaller values (40, 60) give slightly better fit. (σ_c=0.65 S/m, c_m=0.008 F/m^2).

(b) Cytoplasm conductivity values σ_c=0.45, 0.55, 0.65, 0.75, 0.85 and 0.95 S/m are fitted. Larger values (0.75-0.95) have closer fit. ($\varepsilon_c/\varepsilon_0$=78, c_m=0.008 F/m^2).

(c) Membrane effective capacitance values c_m =0.004, 0.006, 0.008, 0.01 and 0.012 F/m^2 are fitted. Larger values (0.01-0.012) provide closer fit to measured data. ($\varepsilon_c/\varepsilon_0$=78, σ_c=0.75 S/m).

With the same methodology applied for mouse hippocampal neurons above, the dielectric properties of glial cells derived from the literature have also been evaluated (Fig. 4.16).

From the evaluation of cytoplasm conductivity σ_c (see Fig. 4.16(a)), it is determined that smaller values (0.05-0.2 S/m) only give crossover frequencies in suspension medium with up to 10% cell media; but in 20% and 30% cell media solution, no crossovers are generated (complex numbers). These complex values are indicated by data points at the lower right corner because only the real part of complex numbers are plotted in MATLAB. A crossover is generated in 20% cell media solution if $\sigma_c = 0.3$ S/m, whereas greater values for σ_c (0.4, 0.5 S/m) also have crossovers in 30%

cell media solution. Experimentally, crossover frequencies are successfully measured in suspension medium with up to 20% cell media. However, in 30% cell media solution, the DEP effect is very weak at higher frequencies. Based on this, we conclude that the cytoplasm conductivity σ_c of glial cells is greater than literature-derived 0.1 S/m, and its value should be between 0.3 and 0.4 S/m, as demonstrated further in the following DEP spectra ($Re[K]$) simulation. Therefore, σ_c=0.3 S/m is applied for the evaluations of the other two properties.

As the cytoplasm dielectric constant ($\varepsilon_c/\varepsilon_0$) of glial cells is evaluated (Fig. 4.16(b)), we find that greater values (85: square, 95: diamond) produce unreasonable high crossover frequencies in 30% and 50% cell media solution, which cannot be experimentally confirmed. Although no crossover (complex number) is created in 30% and 50% cell media solution, smaller values (40: circle, 60: cross, and 75: diagonal cross) give crossovers that are very comparable to the four measured data points (see in Fig. 4.16(b)). It is also noticed that the theoretical values are slightly closer to measured data if smaller property values are used (data not shown here). Therefore, the cytoplasm dielectric constant of glial cells is believed to be less than assumed value of 78. In addition, with smaller dielectric constant, two very close possible crossovers can be generated in 30% cell media solution for glial cells, as demonstrated below in the following section.

For glial membrane effective capacitance c_m, the estimation results are similar to those of hippocampal neurons. Greater c_m values have closer fit to the experimentally measured data, and the complex numbers in 30% and 50% cell media solution are not considered. The literature data of 0.0106 F/m^2 is reasonable, as it is very close to our estimation range for c_m, which is 0.011-0.013 F/m^2.

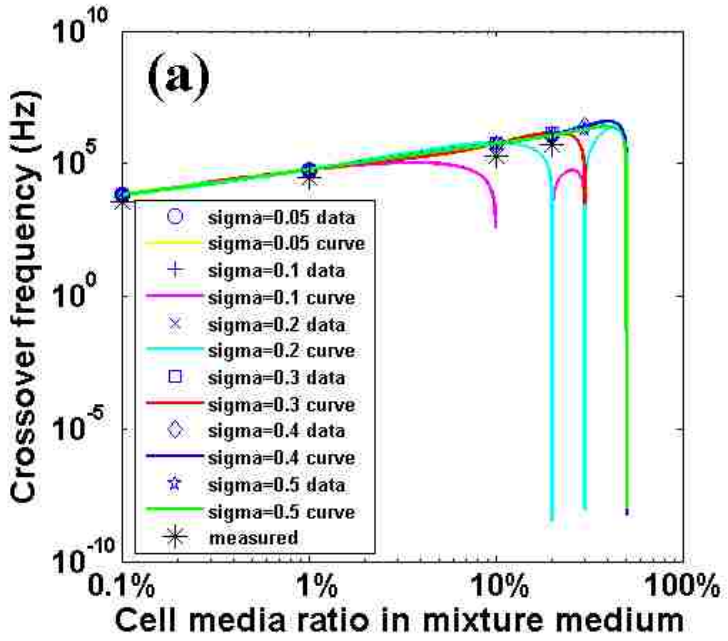
(a)
Crossover frequency (Hz)
10^10
10^5
10^0
10^-5
10^-10
0.1%
1%
10%
100%
Cell media ratio in mixture medium
sigma=0.05 data
sigma=0.05 curve
sigma=0.1 data
sigma=0.1 curve
sigma=0.2 data
sigma=0.2 curve
sigma=0.3 data
sigma=0.3 curve
sigma=0.4 data
sigma=0.4 curve
sigma=0.5 data
sigma=0.5 curve
measured

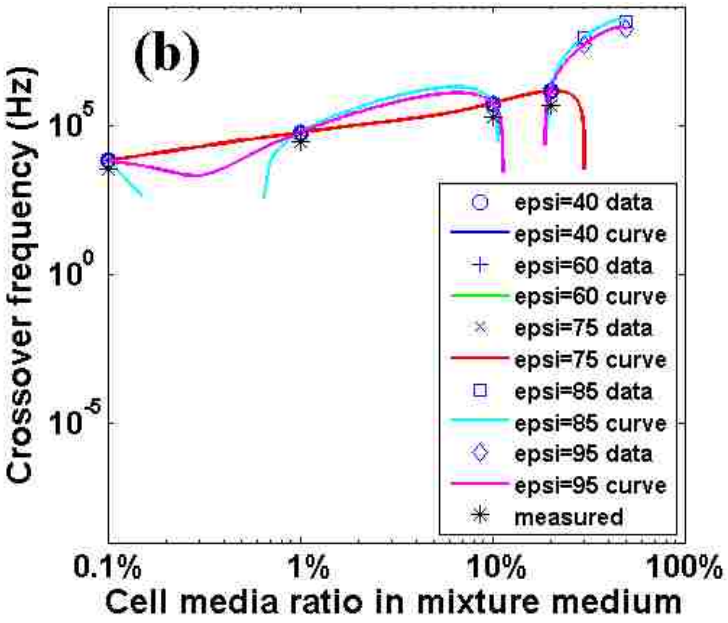
(b)
Crossover frequency (Hz)
10^5
10^0
10^-5
0.1%
1%
10%
100%
Cell media ratio in mixture medium
epsi=40 data
epsi=40 curve
epsi=60 data
epsi=60 curve
epsi=75 data
epsi=75 curve
epsi=85 data
epsi=85 curve
epsi=95 data
epsi=95 curve
measured

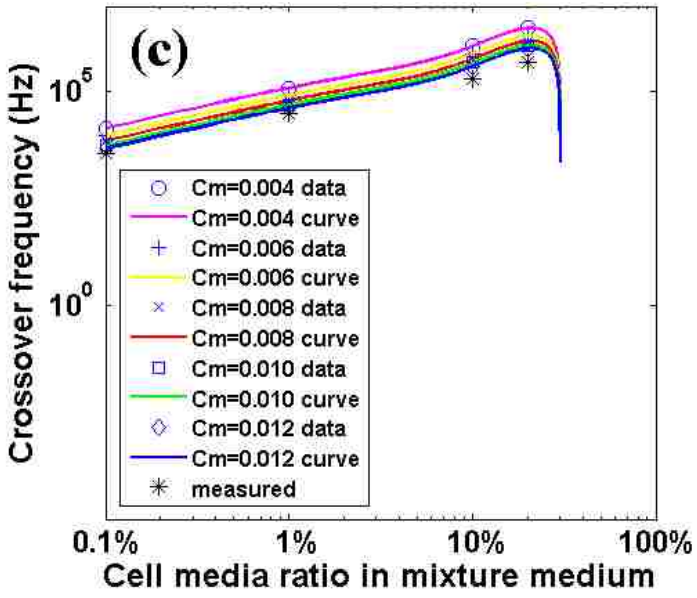

Figure 4.16 Dielectric property values for mouse hippocampal glial cells given in Table 4.5 are evaluated, according to experimentally measured crossover frequencies. One property is fit to the experimental values, whereas the other two values are fixed to the values described in each situation.

(a) Cytoplasm conductivity values σ_c=0.05, 0.1, 0.2, 0.3, 0.4 and 0.5 S/m are fitted. Only values $\sigma_c \geq 0.3$ will generate crossovers in 20% cell media solution. ($\varepsilon_c/\varepsilon_0$=78, c_m=0.0106 F/m^2).

(b) Cytoplasm dielectric constant values $\varepsilon_c/\varepsilon_0$=40, 60, 75, 85 and 95 are fitted. Smaller values have slightly closer fit. (σ_c=0.3 S/m, c_m=0.0106 F/m^2).

(c) Membrane effective capacitance values c_m =0.004, 0.006, 0.008, 0.01 and 0.012 F/m^2 are fitted. Larger values (0.01-0.012) give closer fit to measured data. ($\varepsilon_c/\varepsilon_0$=78, σ_c=0.3 S/m).

4.6.4 Discussion and Summary

In Fig. 4.15 and 4.16, most of the fitted data and curves are above the experimentally measured values. It is hypothesized that this might be caused by the cell deformation because of intense electric field near the electrode [92]. For instance, if cell radius of 5 μm instead of 4 μm is utilized in our equations, the fitted data and curves are much closer to the experimental values (see Fig. 4.17). Similar illustration can also be seen in Fig. 4.5. Furthermore, the measured cell radius is averaged from 20 cells; the actual sizes of the cells detected in experiments also could be larger

than this average [100, 101]. This consideration also eliminates the selection of some maximum property values (e.g. c_m=0.012 F/m^2) within literature ranges, as smaller values (e.g. c_m=0.01 F/m^2) already generate acceptable fit. With this consideration in mind, our results (Table 4.6 below) indicate that neurons have lower membrane effective capacitance than glial cells, similar characterization has been reported elsewhere [84].

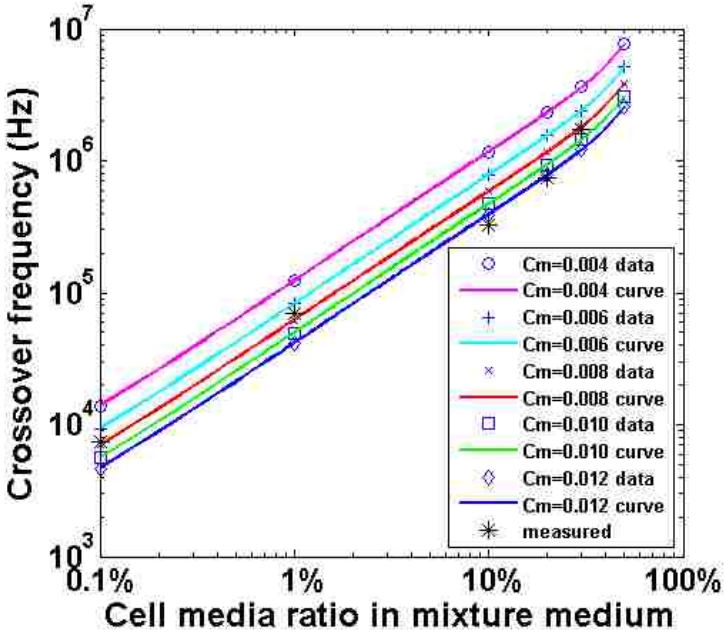

Figure 4.17 Recreated fitting curves for hippocampal neuronal c_m (Fig. 4.15(c)) with cell radius r of 5 μm.

The crossover of glial cells in 30% cell media solution could not be determined experimentally because the DEP effect is very weak at higher frequencies (>2 MHz), as mentioned before. Considering this observation, DEP spectra ($Re[K]$) of glial cells in 30% cell media solution are simulated with Maple (Maplesoft Inc.), using cytoplasm conductivity (σ_c) values from the determined range (0.3-0.4 S/m) above (see Fig. 4.18(a)). As shown, compared with other values, σ_c of 0.32 S/m (green) and 0.35 S/m (magenta) create the preferable curves at higher frequencies, because they are closer to the zero-value base line, and the resulted absolute values of $Re[K]$ are smaller, consequently so is the DEP effect. Although the magenta data line has a crossover point,

and the green data line does not, they both represent possible situations. Additionally, glial cells have nDEP effect at 2 MHz on the green and magenta data lines, confirming the experimental observations.

Furthermore, if smaller cytoplasm dielectric constant of glial cells than the assumed value is applied, two possible crossover frequencies are generated in certain compositions of suspension media, as can be seen in Fig. 4.18(b). In addition to the crossover within the measurable range (≤30 MHz), most of the lines have the second crossover points at around the frequency of 100 MHz. These second crossovers can be confirmed in MATLAB as the solution calculated with '+' sign in equation (4.5). Here, the DEP spectra curve in 30% cell media solution (magenta) has two CFs close to each other, which may occur in actual situations since the absolute value of $Re[K]$ also is very close to zero at higher frequency, leading to weak DEP effect. In addition, if specific signal generation equipment rather than the conventional function generator is used to measure the second crossover frequency, accurate determination of more cell dielectric properties could be possible [102].

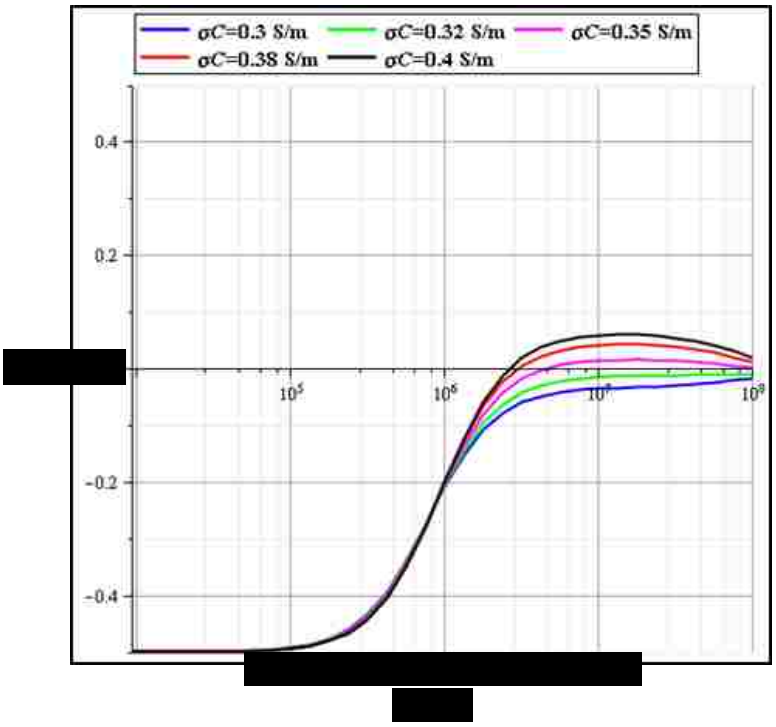

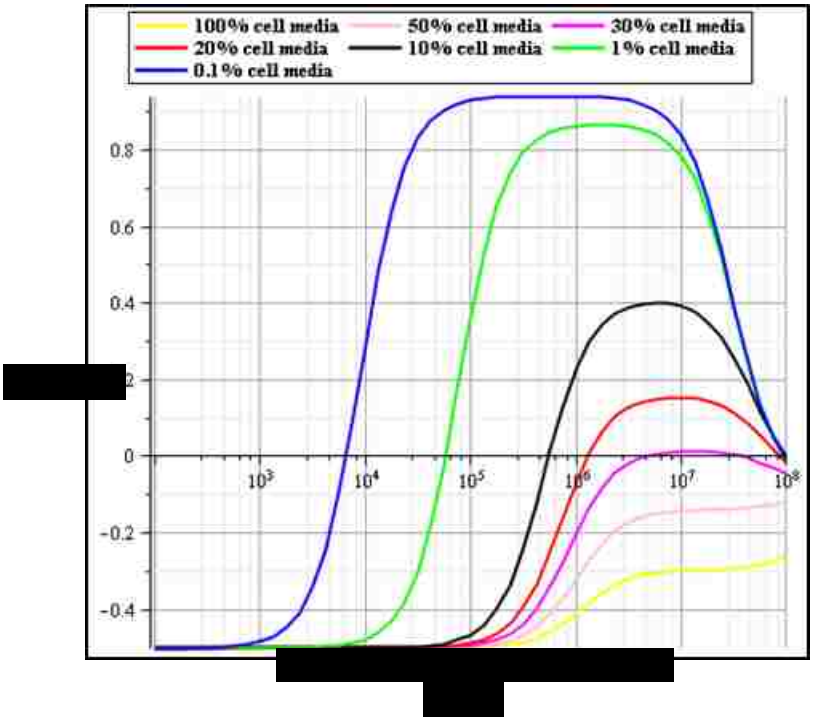

Figure 4.18 Maple simulation of DEP spectra for glial cells. (a) Different cytoplasm conductivity σ_c fit in 30% cell media solution. ($\varepsilon_c/\varepsilon_0$=78, c_m=0.01 F/m^2, r=4 μm). (b) In different suspension media. (σ_c=0.35 S/m, $\varepsilon_c/\varepsilon_0$=60, c_m=0.01 F/m^2, r=4 μm).

From Table 4.2, most of the conductivity of the suspension mixture is magnitudes higher than that of DEP buffers previously used because of the addition of cell culture media [80, 83, 96-98, 103], which compromises the validity of the low frequency approximation, as mentioned earlier. Hippocampal cell viability in different suspension medium has been verified in section 4.3 to ensure that cell are alive during the experimental crossover frequency measurements.

With these considerations in mind, we have summarized, in Table 4.6, the range of three dielectric and physical properties of mouse hippocampal neurons, as well as of glial cells, determined here.

Table 4.6 Dielectric properties of hippocampal neurons and glial cells determined in this work.

	Cytoplasm dielectric constant $\varepsilon_c/\varepsilon_0$	Cytoplasm conductivity σ_c (S/m)	Membrane effective capacitance c_m (F/m^2)
Hippocampal Neuron	≤60	0.75-0.95	0.01[a]
Glial Cell	≤60	0.35[a]	0.012[a]

[a] Parameter is determined to be close to this value.

In conclusion, the range of dielectric properties of mouse hippocampal neurons and glial cells, specifically cytoplasm permittivity, cytoplasm conductivity, and membrane effective capacitance, are determined from DEP crossover frequencies. Theoretical crossover frequencies are obtained directly from the governing equation of Clausius-Mossotti factor. The range of property values is determined by a fitting procedure, comparing theoretical and experimentally measured crossover data. Cell properties determined here provide valuable additional information to the current body of knowledge. While selected types of cells are experimentally verified here, this methodology can be applied to a wide variety of cells.

In this chapter, we have systematically developed a useful approach to separate and pattern primary mouse hippocampal neurons from non-neuronal glial cells, in a mixed cell suspension, with positive dielectrophoresis. DEP simulations are performed, based on hippocampal neuronal and glial dielectric and physical properties from measurement and literature. Simulations indicate particular frequencies where only neurons will be attracted to electrodes with pDEP. We experimentally verified the simulated crossover frequencies of hippocampal neurons and glial cells, DEP movement of hippocampal neurons and glial cells in targeted separation medium is analyzed. This neuronal separation technique, based on active pDEP trapping, has been applied to our DEP MEA to selectively recruit hippocampal neurons (from a neuron/glial mixed cell suspension) to the electrodes. The neuronal viability is verified through successful neuronal signal recording from anchored neurons, and fluorescent live/dead cell staining. In addition, based on theoretical and experimentally measured DEP crossover frequencies, the neuronal and glial dielectric and physical properties are refined, compared to the literature values.

Chapter 5: Supporting Electronics and LabView Control Interface

5.1 DEP Recruiting Interface

In order to facilitate the pDEP active neuronal recruiting process, a DEP recruiting interface printed circuit board (PCB) is designed, taking into account the packaging of our DEP MEA devices. The DEP Recruiting Interface PCB (2 inch by 3 inch) mainly provides two functions: a platform where the packaged DEP MEA device is anchored during the cell trapping process; and an electrical interface where sinusoidal AC electric signal and ground reference is connected to the MEA for the implementation of DEP.

The schematic and PCB design of the DEP Recruiting Interface is illustrated in Fig. 5.1. Fig. 5.2 demonstrates the PCB after the fabrication and assembling process and its application in cell trapping experiments. As can be seen, 16 electrode channels are connected to the AC electric signal port via two 8-channel DIP switches (C&K Components), which enable the separated control of "ON" and "OFF" of each channel, so that the DEP effect can be created on selected combinations of the electrodes. A ZIP IC Connection Socket (3M) is utilized to allow easy integration of the packaged DEP MEA device and the PCB interface. Four ground reference channels from the ZIP socket are connected directly to the ground signal port. Four through-holes are designed at the corners of the PCB for potential mechanical fixation during the experiments; however, sticky mounting tapes (3M) are applied in actual experiments, at each corner of the PCB, to stabilize it on the stage of a microscope. The PCB has two signal layers, with the AC electric signal on the front (1st) layer, and the ground signal on the back (2nd) layer. PCB circuit board was designed using PCB Artist software from Advanced Circuits (Aurora, CO).

In our previous neuron recruiting experiments, instead of using the ZIP socket, DEP MEA was directly inserted into the PCB for electric connections, as can be seen in Fig. 3.1(a). Therefore, one

bigger through-hole is also designed at the center of where the device is positioned, to enable the visualization of the neuronal trapping process on an inverted microscope. Furthermore, the 16 electrode channels were simultaneously connected (directly) to the AC signal port, without the DIP switches, as shown in Fig. 2.15(c).

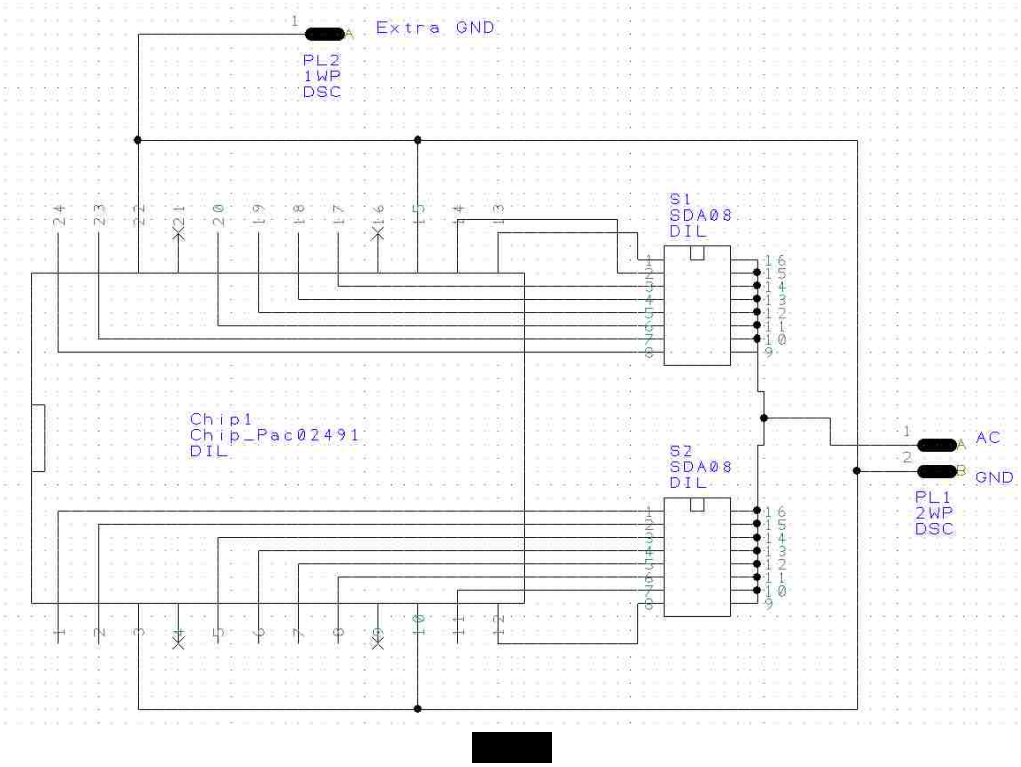

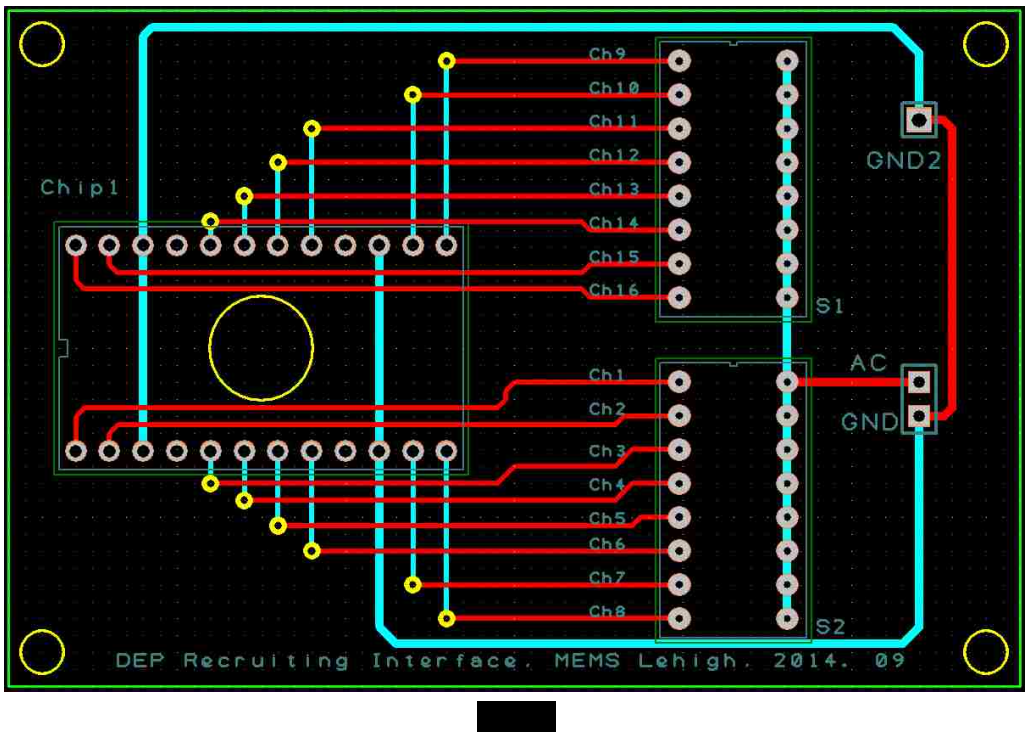

Figure 5.1 Schematic (a) and PCB (b) design of the DEP Recruiting Interface circuit board.

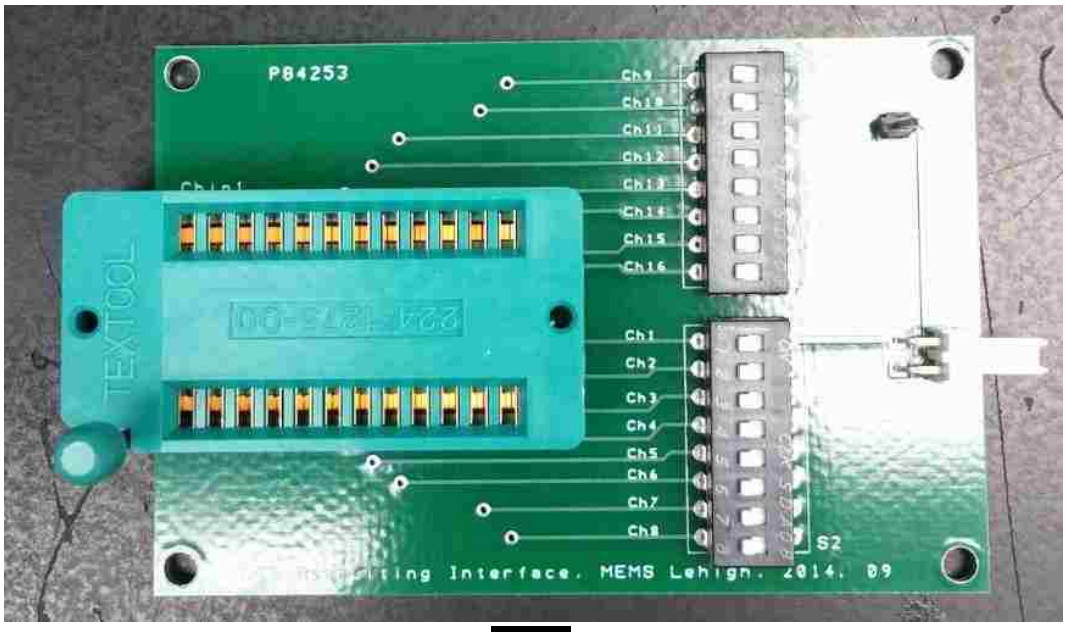

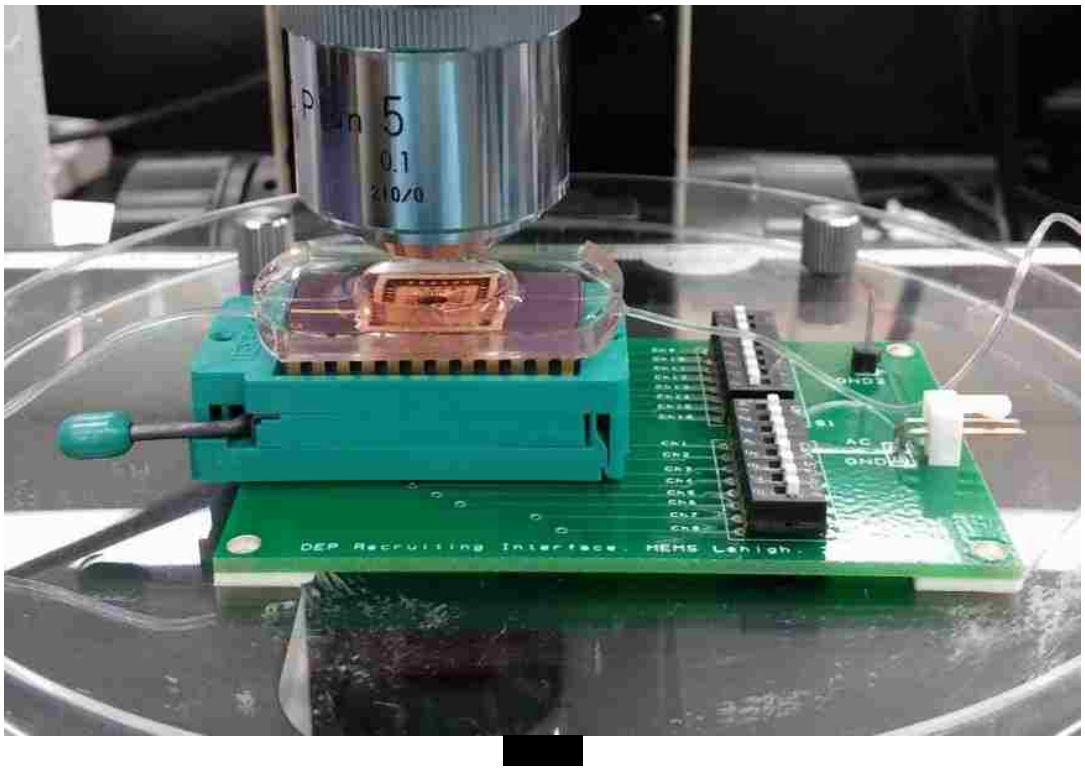

Figure 5.2 Assembled DEP Recruiting Interface PCB (a) and its application in cell trapping experiments on a microscope stage (b).

5.2 MEA Recording and Stimulation Interface

This main circuit system is a 4 inch by 6 inch PCB, where μV-level neuronal extracellular potential is filtered and amplified before it is recorded by a data acquisition system. With the capability of channel selection and switching between recording and stimulation, neuronal stimulation pulses are also fed through this PCB to specified electrode channel. Considering the packaging of our DEP MEA device, a ZIP IC Connection Socket (3M) (shown in the figure below) is also utilized in this PCB for convenient device fixation during neuronal measurements, and for the connection between the device and the PCB circuit system.

As described earlier in section 3.4, the amplitude of the neuronal extracellular potential is within the range of 100 μV to 200 μV [53-55]. The power spectrum of the neuronal action potential has been revealed to be primarily between 50-100 Hz and 2 KHz [55-57]; furthermore, the bursting

rate of neuronal action potential has been well established to be no more than 500 Hz to 1 KHz [104]. Based on this consideration of neuronal potential amplitude and power spectrum, a band-pass circuit based on precision low-noise amplifiers AD624 (Analog Devices, Inc.) and low-noise, high-speed operational amplifier LT1007 (Linear Technology), has been designed to filter and amplify the neuronal potential signals. The schematic design and simulated Bode-Plot of this band-pass signal filtration and amplification system is illustrated in Fig. 5.3.

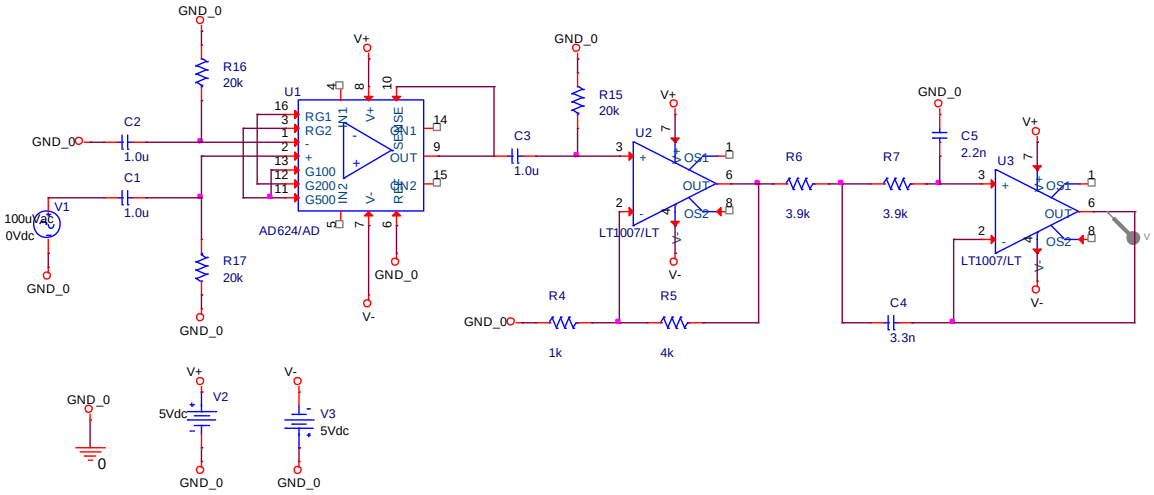

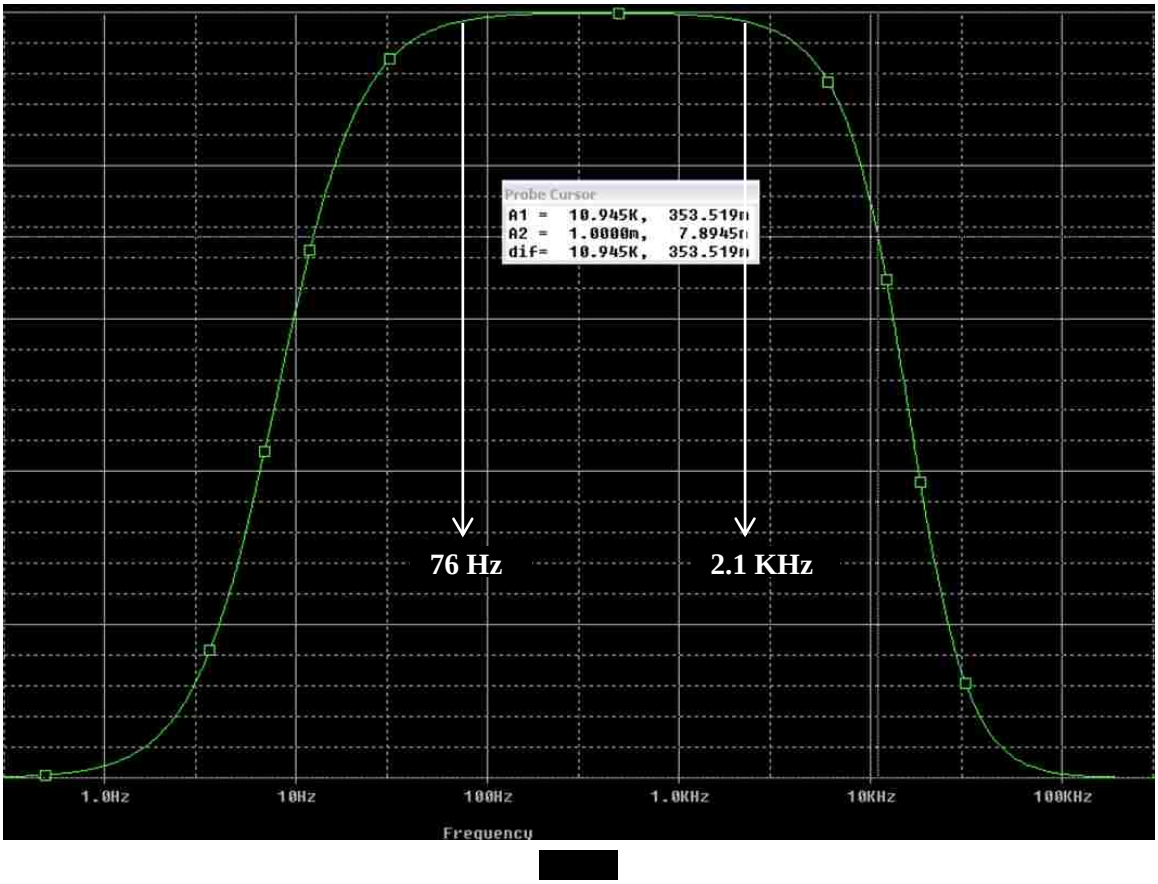

Figure 5.3 PSpice schematic design (a) and AC Sweep simulation Bode-Plot (b) of the extracellular neuronal potential processing (filtration + amplification) circuit.

As can be seen in Fig. 5.3(a), in the first stage of the circuit, the AD624 instrumentation amplifier is configured to have a gain of 1000, according to its datasheet; and differential input mode is configured to eliminate common-mode noise, such as the background noise from the cell media, and any DC offset or fluctuation. The second stage is a non-inverting positive gain block with amplification of 5, which also functions as a first-order high-pass filter with a cutoff frequency of 7.9 Hz. The last stage is a second-order Butterworth low-pass filter with a cutoff frequency of 16.9 KHz. The total gain of this signal-processing (ban-pass) circuit is 5000, and the combinational 3dB points are at 12.3 Hz and 10.9 KHz, respectively. Moreover, the band-pass circuit is designed to have 99% points at 76 Hz and 2.1 KHz, where the signal amplitude is 99% of its peak value in the band-pass Bode Plot, as indicated in Fig. 5.3(b). This 99% points design is based on the neuronal

potential power spectrum described above, to help filter the neuronal extracellular potential more precisely, while keeping the integrity of the essential frequency components of the signals. This three-stage signal processing circuit is designed based on the signal-processing module of previous MEA system [21].

Considering the original amplitude of the signals to be measured, the amplifier (both instrumentation amplifier AD624 and op-amp LT1007) and resistor noise has been carefully calculated within a designated bandwidth of 2.0 KHz, during circuit design, to ensure that the total noise voltage from each amplifier is less than 1.0 μV, compared to the 100 μV-level extracellular neuronal potential. The bandwidth, starting with the first 3dB point (12.3 Hz), is chosen to be 2.0 KHz because this is where the primary power spectrum of neuronal potentials located. One noise component from the resistors: thermal (Johnson-Nyquist) noise, and two noise components from the amplifiers: voltage and current noises, are considered here. The resistor thermal noise is calculated according to the following equation:

$$V_t = \sqrt{4K_B T R \Delta f} \tag{5.1}$$

where K_B is the Boltzmann constant (1.38 x 10-23 J/K), T is the absolute temperature (300 K), R is the resistor value, and Δf is the frequency bandwidth of interest. The amplifier voltage noise calculation is based on equation (5.2):

$$V_v = N_v \sqrt{\Delta f} \tag{5.2}$$

where voltage noise density versus frequency N_v is obtained from the amplifier's technical datasheet, which has a unit of $\mathrm{v}/\sqrt{\mathrm{Hz}}$, and Δf is the given bandwidth. Similarly, for the amplifier current noise, current noise density versus frequency N_i ($\mathrm{A}/\sqrt{\mathrm{Hz}}$) is extracted from the datasheet, and the noise is calculated according to:

$$V_i = N_i \sqrt{\Delta f} R \tag{5.3}$$

where Δf and R are the bandwidth and resistor value respectively, as described above. The total RMS noise for each amplifier is the combination of the three noise components:

$$V_n = \sqrt{{V_t}^2 + {V_v}^2 + {V_i}^2} \tag{5.4}$$

Based on the selected bandwidth, bias current-balancing and high-pass filtering resistors (20 KΩ) at the inputs of the first stage amplifier (AD624), and the high-pass filter resistor (20 KΩ) at the input of the second stage op-amp (LT1007) is carefully chosen, to ensure that the total noise from each amplifier is less than 1.0 μV.

Extracellular neuronal potentials, processed through the circuits above, are fed into the differential analog input of a data-acquisition (DAQ) card (NI USB-6211, National Instruments) for recording, which is in turn controlled by a LabView interface, as described in the following section. Analog stimulation pulses can be generated by the DAQ card, then transmitted to specific electrode channel of the MEA through two analog multiplexers CD4051 (Texas Instruments). Stimulation pulses are buffered through a LT1007 op-amp (voltage buffer configuration) before they enter specific electrode channel. Four-bit digital selection signals for the multiplexers are created by the DAQ card. The multiplexers also enable the selection of specified electrode channels to record from. The switching between stimulation and recording is realized through a low on-resistance (85 Ω), fast-action (100-200 ns) analog switch DG441 (Intersil Americas LLC). Channel ON/OFF control signal for the analog switch is also generated from the DAQ, which is programmed in the LabView interface. As discussed earlier in section 3.4, a switching time between stimulation and recording of less than 2 ms has proved to be suitable for detecting stimulated hippocampal neuronal signals while keeping stimulation artifact from being recorded [58]; therefore, the switching time is set to be 1 ms in the LabView system. The logic overview of the recording and stimulation system is illustrated in Fig. 5.4.

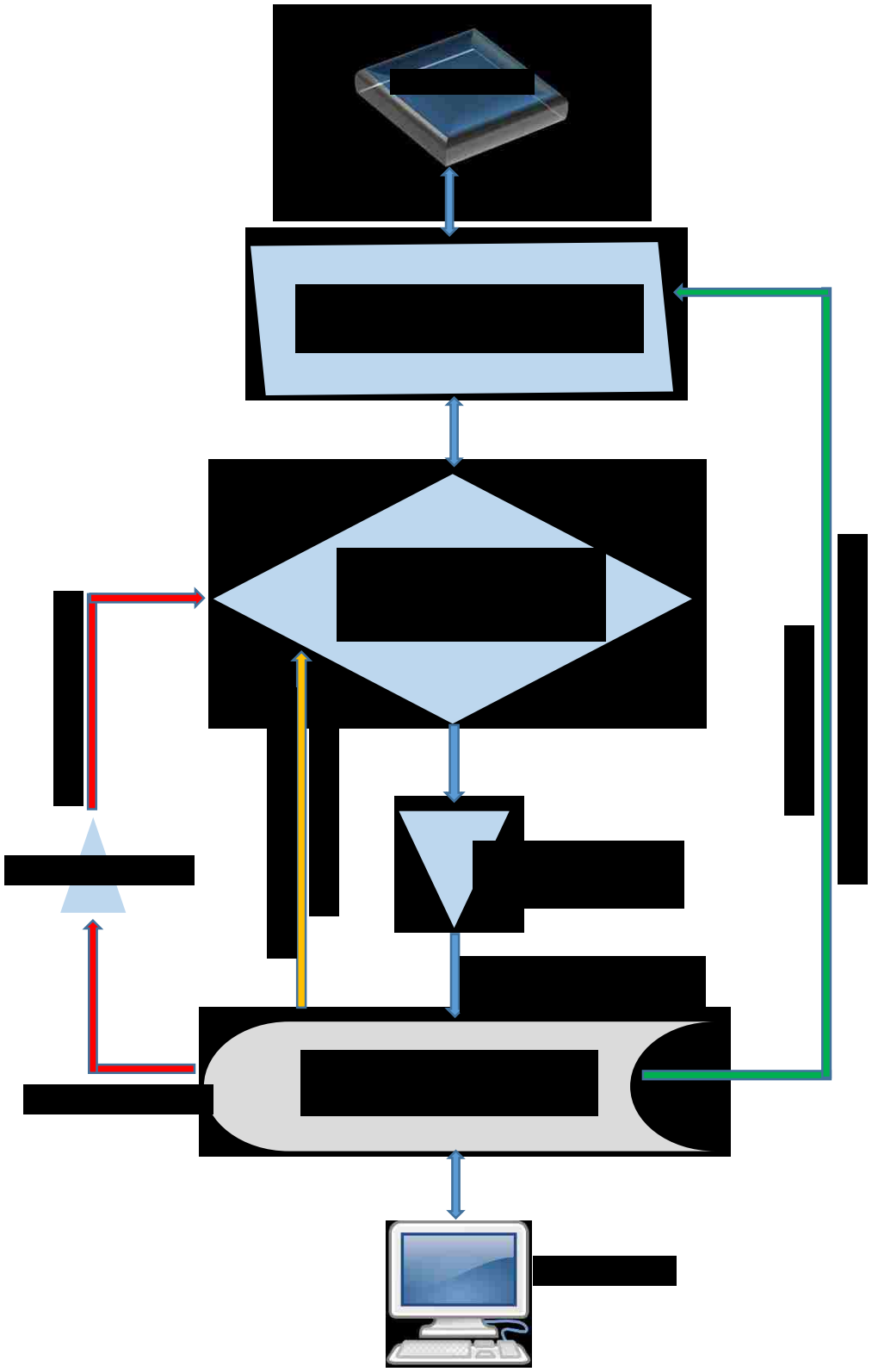

Figure 5.4 Recording and stimulation system diagram.

The DEP MEA Recording and Stimulation Interface PCB has been designed and fabricated (assembled) according to Fig. 5.5. The neuronal recording and stimulation experimental setup has been shown in Fig. 5.6, including the packaged DEP MEA, PCB interface and the DAQ card, which can also been seen in Fig. 3.13. Another consideration here is that because the frequency of 60 Hz is within the useful neuronal power spectrum, no notch filter is integrated to remove the 60 Hz noise from AC power supply; therefore, both the PCB and laptop in our experiments are powered by DC batteries. Two 9V DC batteries are integrated on the back side of the PCB in Fig. 5.5(b), which provide the ±5V power supply for the electronic components, through a voltage regulator. Even in this way, it was observed that noises from power adapters of nearby equipment, such as microscopes and computers, could cause disturbance in the signal, so an AC power-isolated environment is preferable for neuronal potential recording.

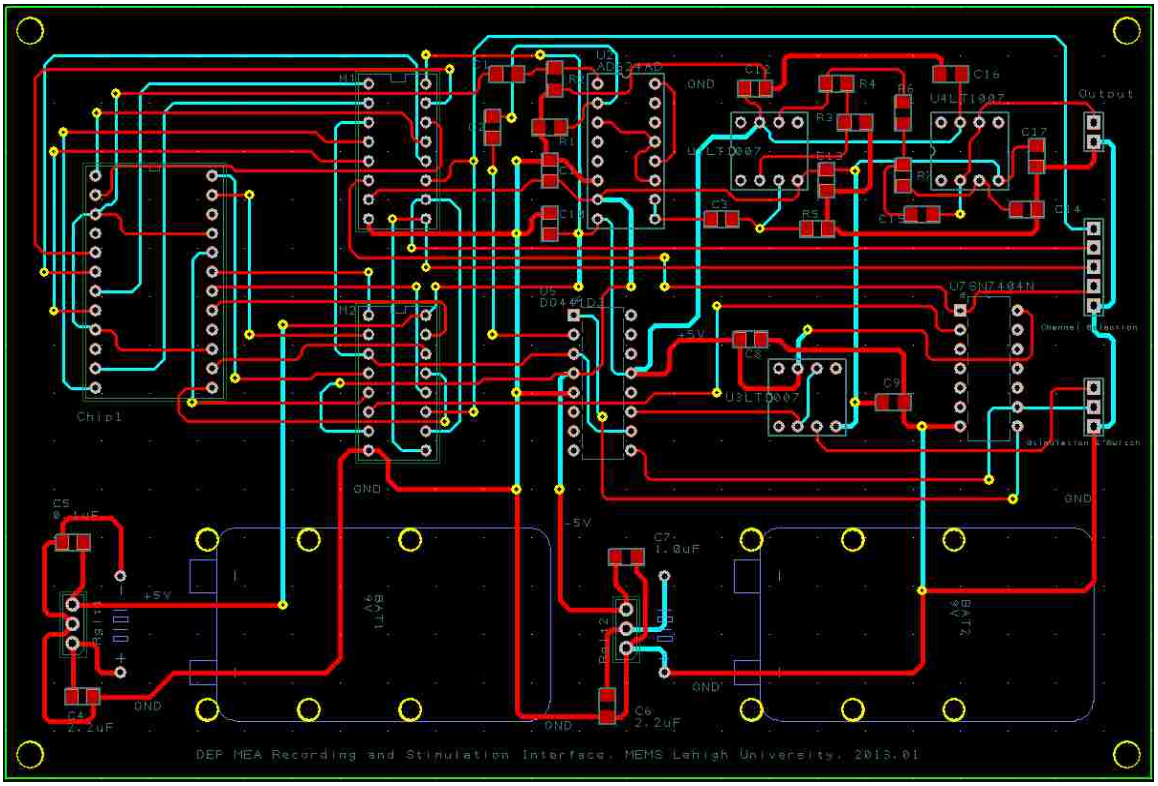

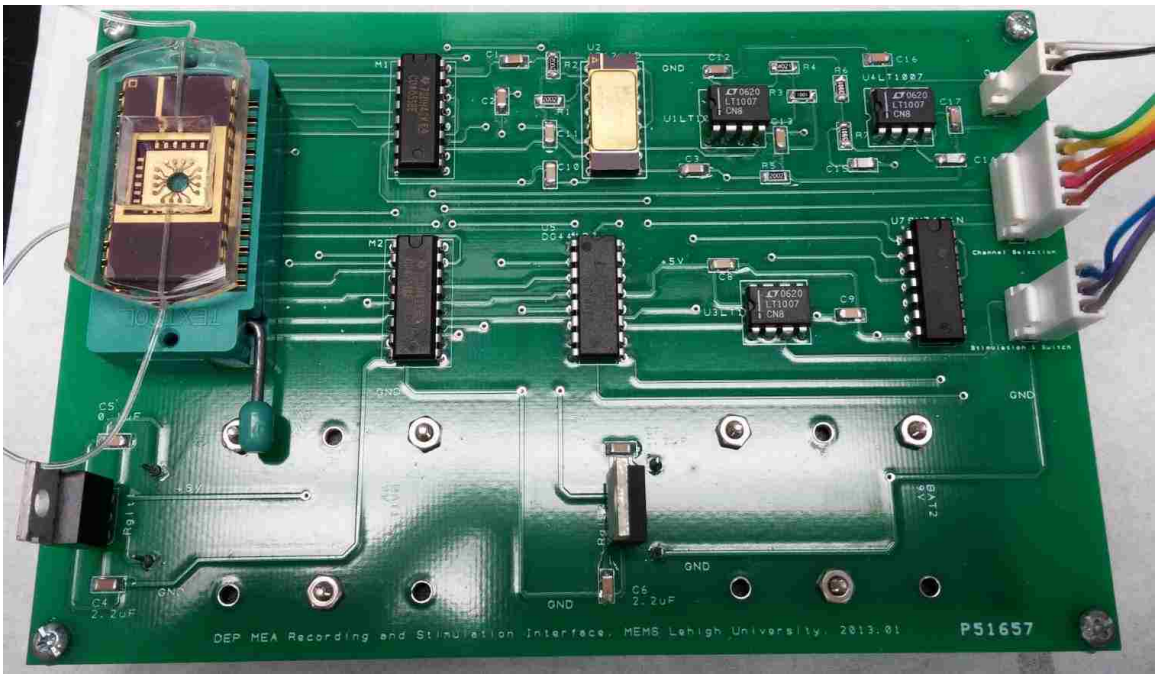

Figure 5.5 Designed (a) and assembled (b) DEP MEA Recording and Stimulation Interface PCB.

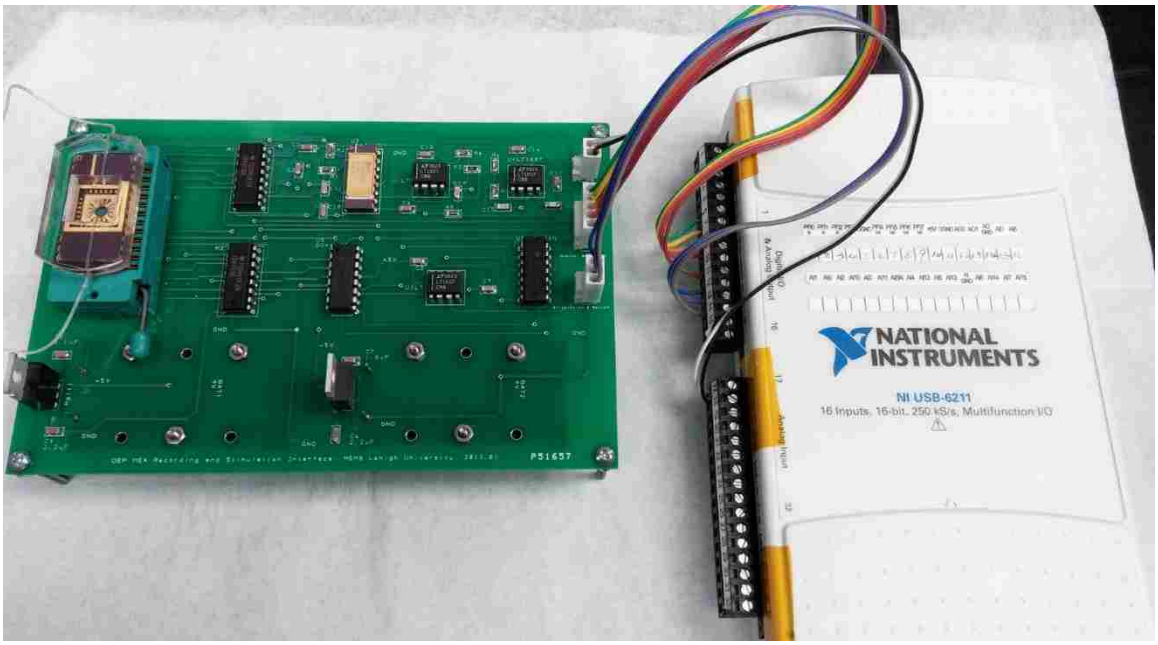

Figure 5.6 Neuronal recording and stimulation experimental setup, including a packaged DEP MEA, PCB interface and the NI DAQ card. The NI DAQ card is connected to a computer where LabView control panel is programmed.

5.3 LabView Control Interface

LabView control panel software is an important part of the experimental setup, which provides straightforward and instantaneous control and monitoring of the experimental electrical devices, such as function generator, DAQ card and oscilloscope, as well as the automation of data logging and signal display.

The first LabView control interface we programmed is for the implementation of DEP experiments. Instead of manually adjusting the function generator for the output of AC sinusoidal electric signals, a virtual instrument panel is created in LabView for the selection of waveform shape, frequency, amplitude and offset. By connecting with the LabView software, the output of the function generator can also be enabled on the virtual panel. The front panel of this control interface is displayed in Fig. 5.7.

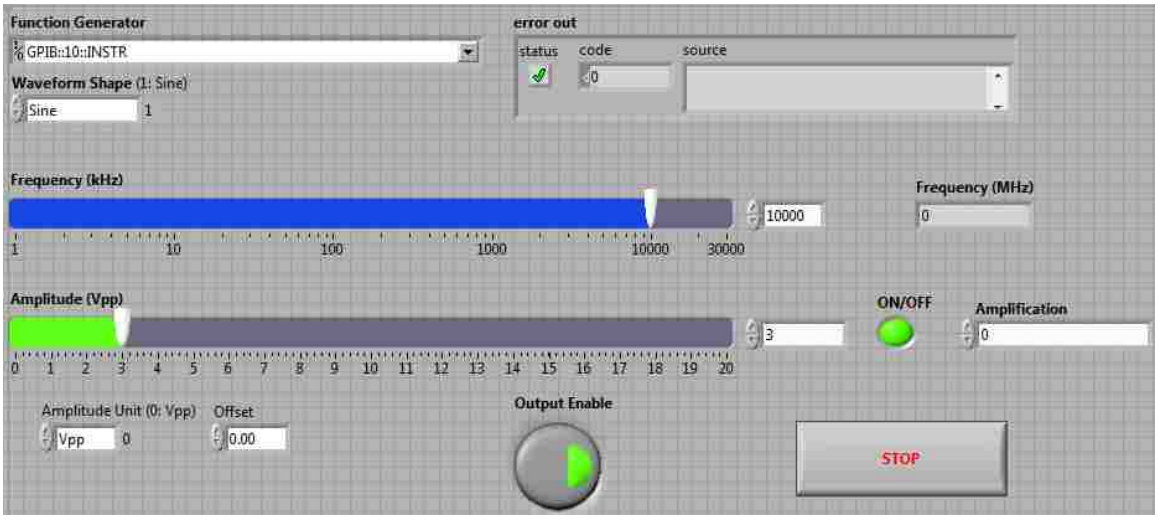

Figure 5.7 LabView front panel for the control of AC electric signals during DEP experiments.

For the preview and recording of neuronal potentials from a single channel, we created another control interface, where simultaneous signal display and recording is enabled. The front panel of this module is illustrated in Fig. 5.8. By selecting the channel number and document directory on the computer, neuronal potential data from particular electrode channel will be recorded to a

specified .txt file. The update period determines how long the potential data is recorded before being refreshed for a new cycle of recording; however, instantaneous neuronal signals are displayed continuously in the waveform window. Additionally, the sampling rate can be adjusted up to 40 KHz, with higher sampling rate capturing the original signal more accurately, which creates larger data files.

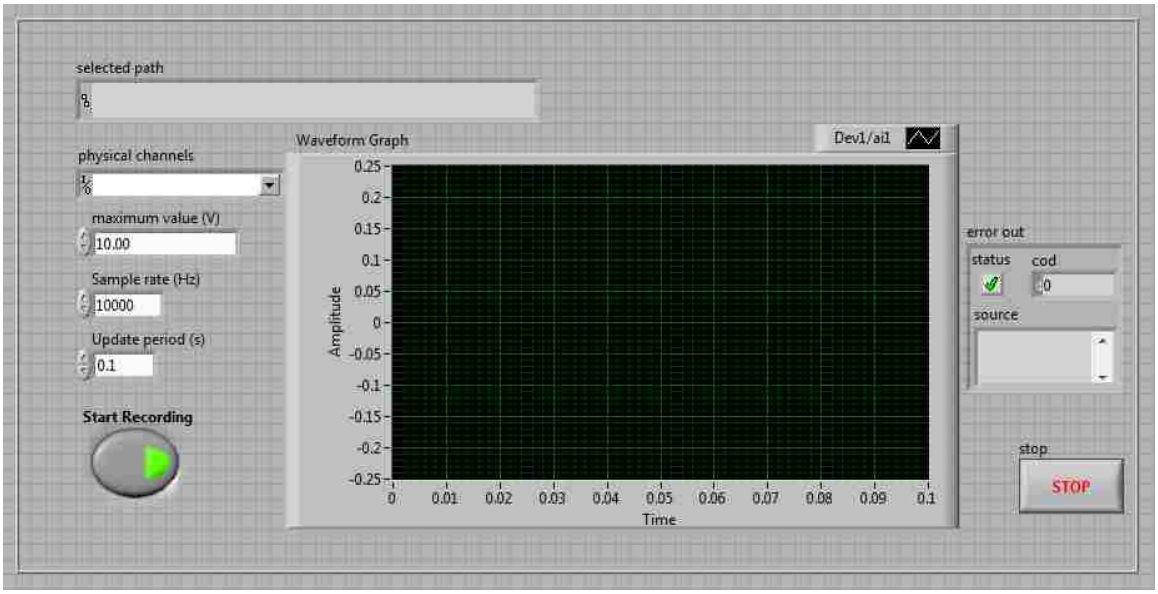

Figure 5.8 LabView front panel for the preview and recording of neuronal potentials from a single channel.

Finally, the most complicated stimulation + recording control interface has been created, which is designed for single channel only in the current system. The stimulation and recording channels (one for each) can be selected separately from 16 electrode channels. Four different types of stimulation pulses are available to choose from: monophasic positive, monophasic negative, biphasic positive + negative, and biphasic negative + positive. Several pulse parameters, including time offset, pulse duration, amplitude, time per cycle and pulse number, can be reset for various stimulation purposes. The stimulation progress and pulse shape are displayed at the lower half of the front panel (Fig. 5.9). After the implementation of stimulation, a waiting time of 1-2 ms is defined in the LabView program, before initiating the recording sequence. The recording function is similar to that in Fig.

5.8, with the evoked neuronal signal plotted at the upper half of the front panel, and a Boolean light indicating the progress of the recording process. The whole sequence is configured to be initiated and aborted by separate Boolean buttons.

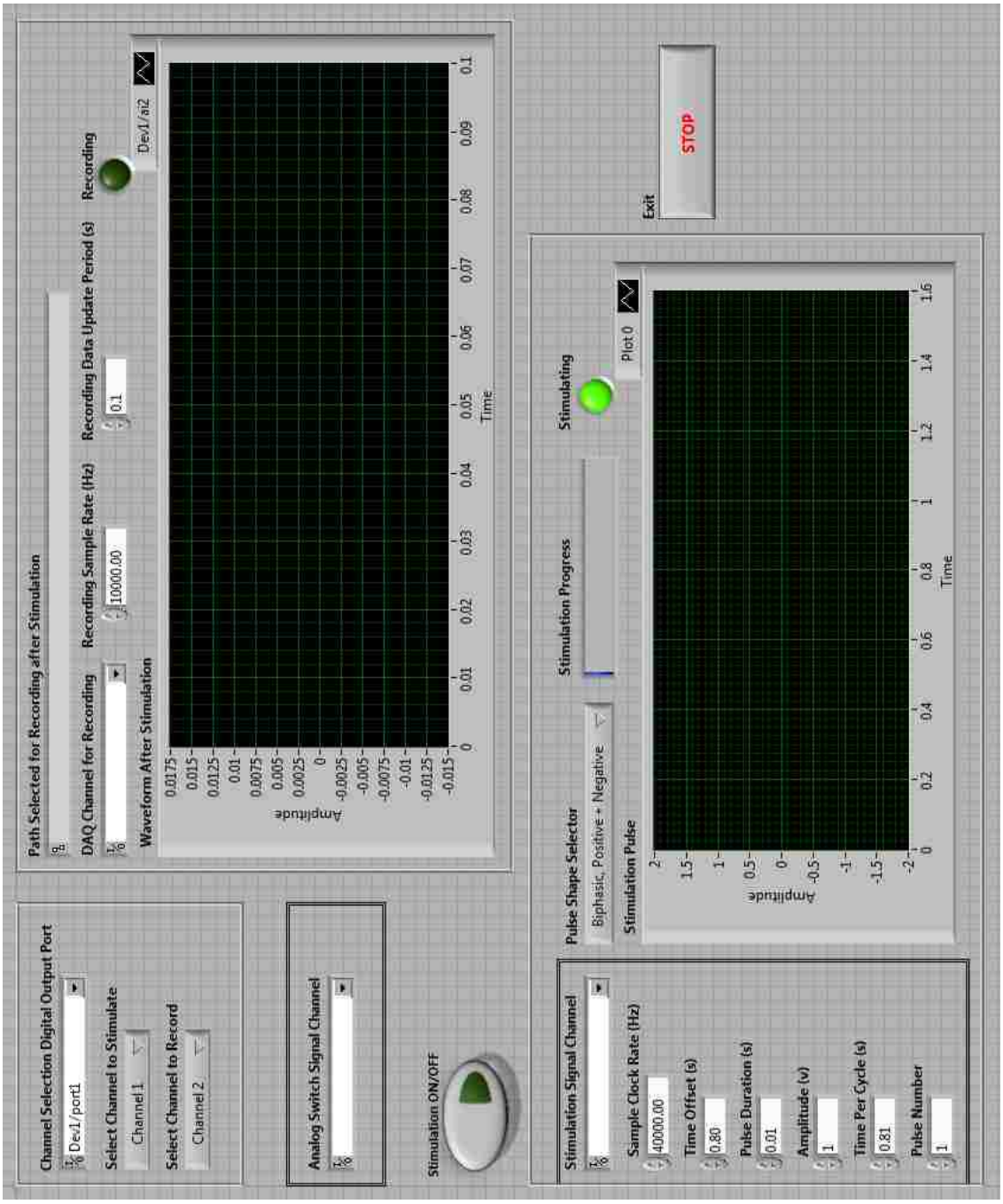

Figure 5.9 LabView front panel for the stimulation and subsequent recording from specified individual electrode channels.

Chapter 6: Conclusion and Future Work

A novel DEP MEA system has been designed and developed in this research to establish a platform to facilitate the study of the underlying mechanism of neural network activities. With this MEA system, embryonic mouse hippocampal neurons have been actively recruited to the electrodes by positive dielectrophoresis, and the growth of neuronal processes have been mechanically confined by predefined SU-8 microstructures to form patterned neuronal networks. With appropriate microstructure designs, hippocampal neurons have been attracted to the electrodes on the MEA with single-cell resolution. We investigated different pretreatment methods to improve the cytocompatibility of thin cured SU-8 layer on our DEP MEA devices, which enables our system to provide a suitable microenvironment for primary neuron culture, particularly for hippocampal neurons. Mouse hippocampal neurons have been successfully cultured on the DEP MEA, where the neuronal growth are confined by SU-8 microchambers and microtrenches so that precisely defined neuronal networks have been formed. With the well-patterned neuronal network, spontaneous and stimulated neuronal potentials are successfully recorded from specified neurons, through our signal-processing circuit and LabView control systems. Evoked neuronal spikes and their propagation are analyzed to reveal the neuronal signal transmission and the connections between neighboring neurons inside a functioning neuronal network. Furthermore, we investigated the viability of hippocampal neurons during and after the DEP process to ensure the health of neurons that are actively positioned on the MEA with pDEP.

In addition, we investigated the separation of mouse hippocampal neurons and glial cells using positive DEP. When dissociated from hippocampus tissue, the initial cell mixture contains both neurons and glial cells; however, only the neuronal sub populations are our research subject of interest because of their role in the process of thought and memory. After analyzing the neuronal and glial DEP movement in the targeted suspension medium, we successfully applied pDEP to

separate hippocampal neurons and glial cells based on their different dielectric and physical properties. The DEP crossover frequencies of neurons and glial cells in various suspension medium have been experimentally measured. By comparing these experimental values with our simulation results, we also suggested an approach to extract more accurate dielectric properties of neurons and glial cells than those previously available in literature. This technique is a valuable addition to the toolbox for making our DEP MEA system a more functional and versatile multi-electrode array.

At the same time, potential technique improvements and future research work can make such a BioMEMS system a more reliable and efficient platform for neural engineering research. During our system development, we found the DEP process compromised, in an unknown way, the neurons' ability to extend processes and fully grow out, although we have verified that neurons are live and electrically active after the DEP recruiting process. This makes the smooth transition between pDEP active recruiting and subsequent neuronal culturing and patterning challenging, as we have observed neurons still remained in spheres days after the DEP process. In our current experiments, hippocampal neurons have to be cultured directly on the MEA device, without DEP, to form a precisely patterned neuronal network, although we have demonstrated successful neuronal pDEP active trapping. Future investigations will be needed to optimize the primary neurons' ability to fully attach and grow after the DEP positioning, despite the fact that they can be verified live post DEP.

Another aspect that calls for potential improvements is the fabrication of SU-8 microstructures. In current device designs, different microtrench width (3 μm, 5 μm and 7 μm) are included. However, after the fabrication, except for the 7 μm trenches, photoresist (SU-8) residue can still be observed inside the 3 μm and 5 μm trenches, as can be seen in the SEM images of fabricated devices in Fig. 6.1. Some of the 5 μm trenches have residue inside, while most of the 3 μm trenches have residue left inside. Various fabrication parameters concerning the photolithography process, such as exposure does, development method and development time, have been tested; however, the

situation of SU-8 residue is not improved. This residue issue might be the reason why the growth of neurites cannot be well-guided in microtrenches with 5 μm or less width, as the residue could block the extension of neuronal processes. From literature research, although high aspect ratio SU-8 microstructures have been widely developed, most of the structures have simultaneous thicker and larger SU-8 features, compared to our feature structures (8 μm thick, 3 μm-5 μm wide). Therefore, we looked into another epoxy-based photoresist – KMPR (MicroChem Corp.), as an alternative structure material for our MEA devices.

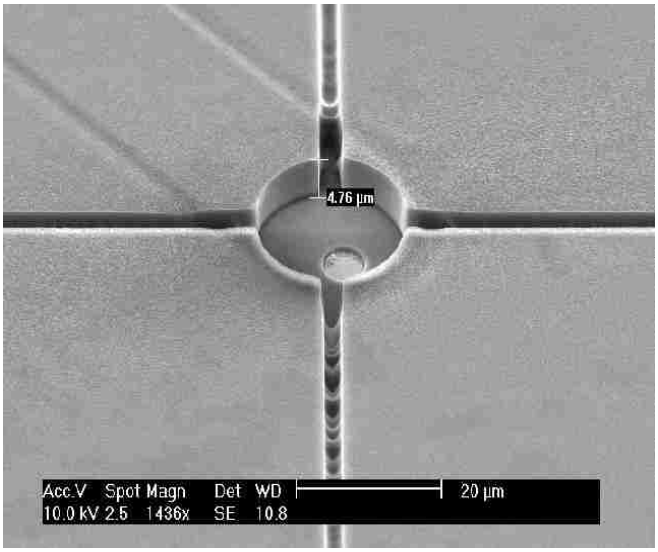

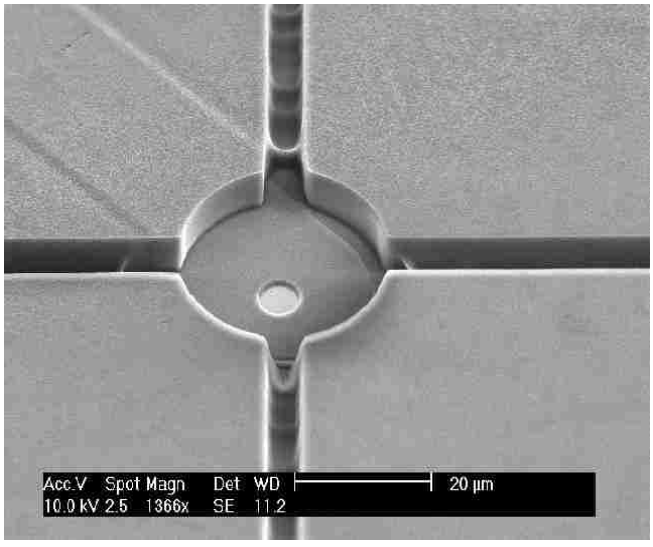

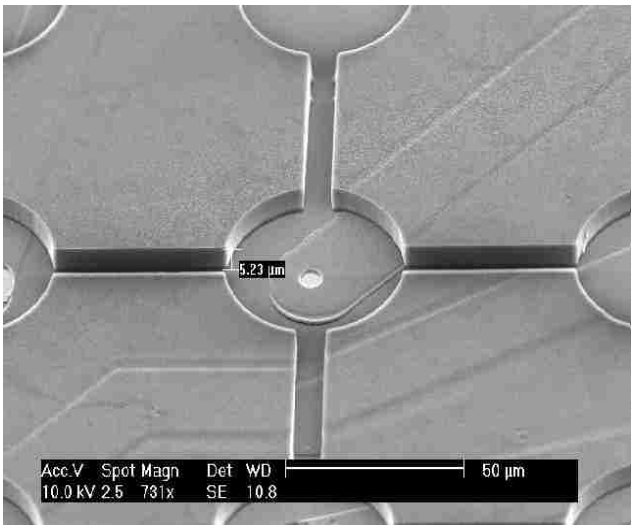

Figure 6.1 SEM micrographs of fabricated DEP MEA devices with (a) 3 µm, (b) 5 µm and (c) 7 µm microtrenches. SU-8 residue can still be observed in the 3 µm and 5 µm trenches, while 7 µm trenches are clear of residue.

Similar to SU-8, KMPR is also a negative photosensitive epoxy, which is mainly used for MEMS structure, Electrolytic Plating and DIRE applications, because of its excellent adhesion, chemical and plasma resistance. Compared to SU-8, KMPR has better internal stress situations, which makes simplified (time-efficient) fabrication process of KMPR. It also has superior resistance to fissuring and cracks, which were observed on current MEA devices fabricated with SU-8. Furthermore, KMPR has better moisture resistance, which may render it more suitable for cell culture and microfluidic applications. Although KMPR can be hard-baked for the purpose of creating permanent structure material; most of the time, it is used as sacrificial mask layers because it is formulated as much easier to strip after the photolithography process. Last but not least, 2 µm features, 10 µm coating KMPR have been shown to be realized in the material data sheet, with an i-line stepper on an unknown substrate.

Based on the thickness requirement (<10 µm), we chose KMPR 1005 to test-fabricate the microstructure layer of the DEP MEA devices. The detailed KMPR fabrication process, similar to SU-8, can be seen in Appendix II: DEP MEA Fabrication Process. Optical micrographs of the

fabricated structures are shown in Fig. 6.2. As can been seen, after repeated fabrication process test, clear microtrenches, without photoresist residue, can be consistently created with width down to 4 μm; trenches with 3 μm or less width may still have residue left inside.

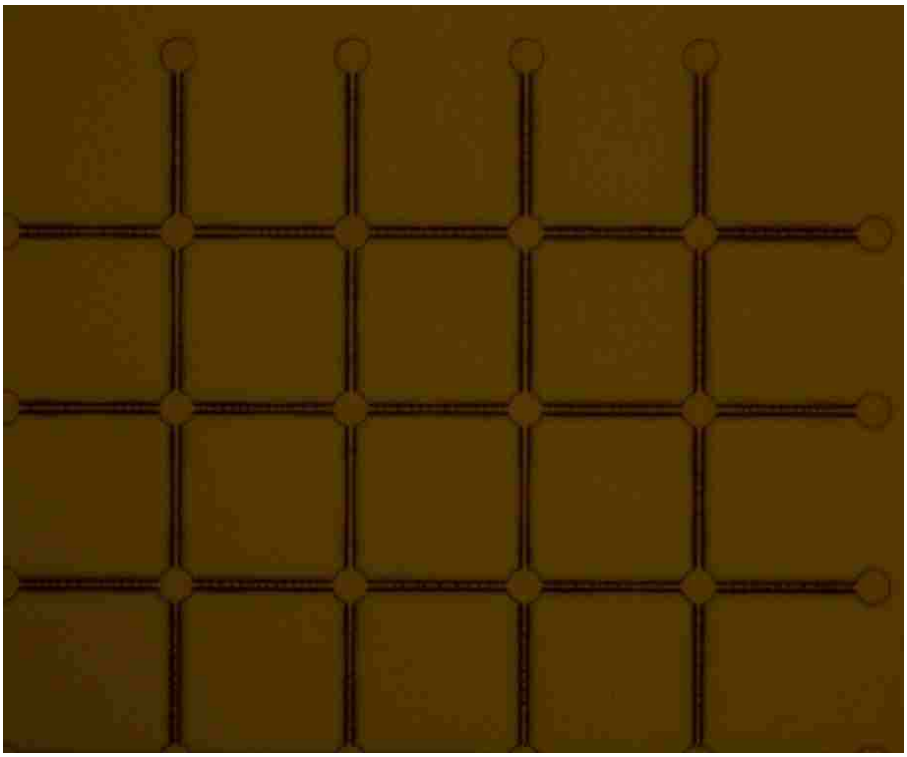

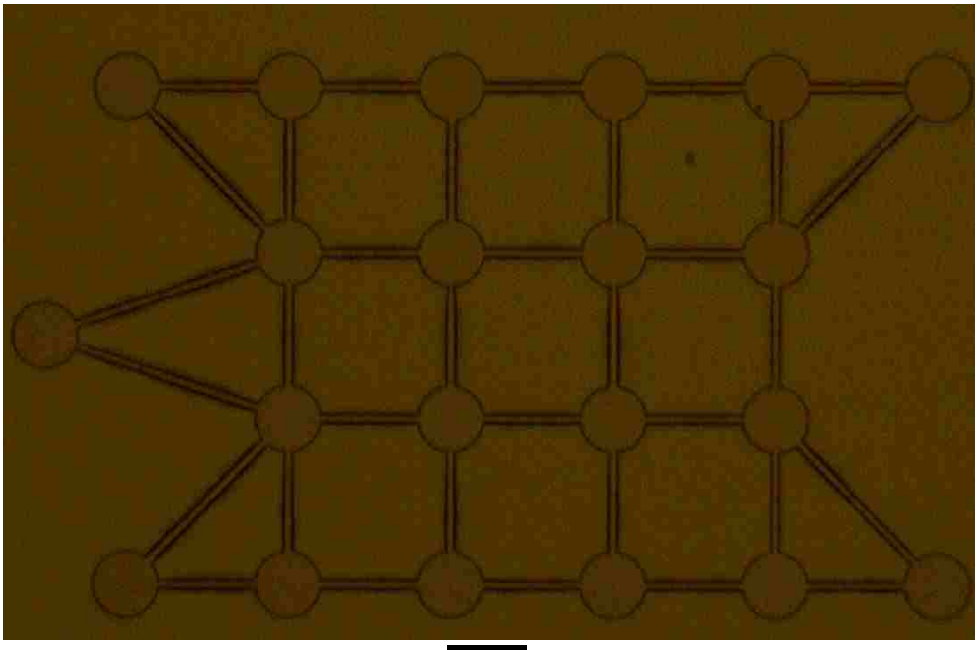

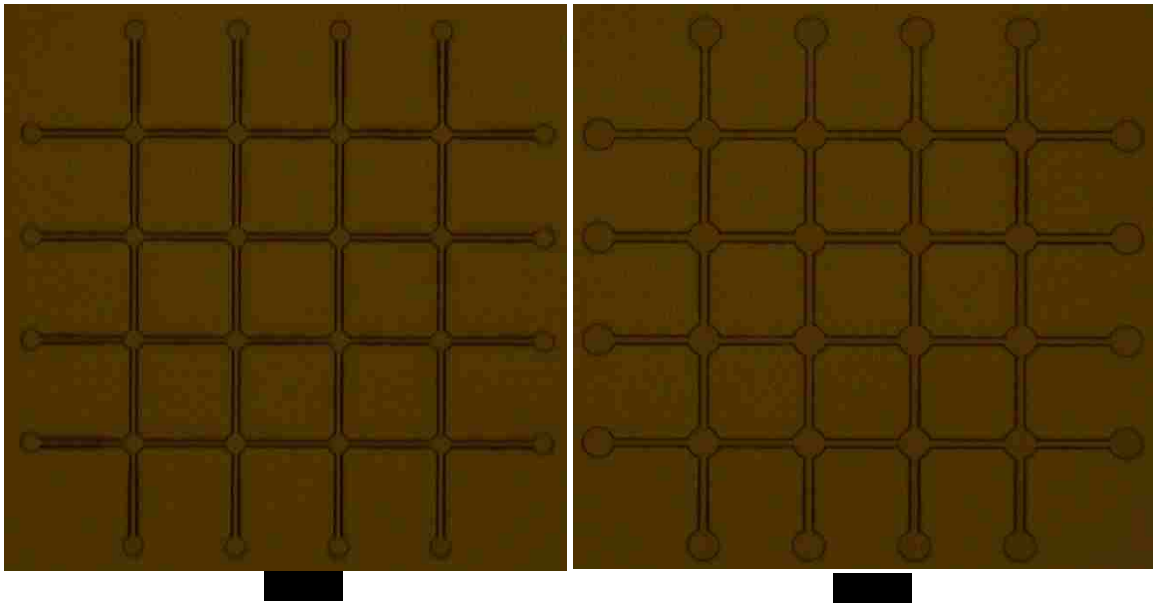

Figure 6.2 Optical micrographs of microstructure layers fabricated with KMPR. Photoresist residue can still be observed in 3 μm microtrenches (a), as indicated by dark-color cross bars inside the trenches. (b) 4 μm, (c) 5 μm and (d) 7 μm microtrenches are clear of residue.

Microstructures fabricated with KMPR have improved photoresist residue situations; however, the lithography process hasn't been optimized, as microstructures with 2 μm features are shown to be successfully fabricated in the data sheet, with 10 μm thick KMPR coating, which is even thicker than our application (8 μm). Considering a different photolithography aligner we used (h-line contact instead of i-line stepper), and possible different substrate (quartz glass versus silicon), future investigations will be needed to optimize the fabrication of the microstructure layer, which may allow the patterning of neuronal networks with better resolution.

Another potential technical improvement lies in the neuronal pDEP active recruiting process. Although much attention has been paid to the packaging of the DEP MEA devices to facilitate the neuron trapping, as described in section 2.4, we still found that rather than on the device surface, neurons were floating above the MEA because of the high viscosity of sucrose solution, which made the neuronal trapping process relatively time-consuming and inefficient, as neurons sometimes might have to be waited to settle on the device surface before they could be trapped by

pDEP to the electrodes. The main reason, we think, is that the height of the PDMS chamber on our MEA device is in mm rage, instead of μm range. This large space in the vertical direction compromises the ability to confine the neurons in desired surface plane for most effective DEP recruiting. Improved microfluidic device packaging (possibly involving glass slides) may allow high-throughput and more efficient neuronal active recruiting using this DEP MEA system.

In addition, with current electronic circuit system and LabView control interface, evoked neuronal potentials can be recorded immediately after the application of the stimulation pulses. However, the stimulation artifact and spontaneous neuronal potentials right before the stimulation are not designed to be recorded. On the other hand, it is sometimes beneficial, to also record the spontaneous neuronal potentials before the stimulus, as well as the stimulation artifact, so that the evoked neuronal potentials can be compared to the spontaneous signals prior to the stimulus, and the relationship between the stimulus trace and the evoked potentials can be visualized in a straightforward time scale. In order to realize this function, modifications will have to be made to the electronic circuit system, such as the analog switch control for signal recoding and stimulus pulse overshoot protection, as well as to the LabView control interface (the addition of a pre-stimulus recording module).

With all these potential future research work in mind, technical improvements, combined with thorough neuronal cell biology investigations, may one day allow more complicated geometrically-dependent studies of functioning neural networks, such as the precise mapping of *in vitro* neuronal networks based on the propagation of neuronal potentials, using a biosensor/bio-interface similar to our DEP MEA system.

Chapter 7: Protein Characterization and Manipulation with MEMS

During the last year of my Ph.D. research, I have been involved in a technical intern position at Bristol-Myers Squibb (BMS), Bloomsbury, NJ. BMS is a global biopharmaceutical company that discover, develop and deliver innovative medicines for patients. It manufactures prescription pharmaceuticals in several therapeutic areas such as cancer, HIV/AIDS, cardiovascular disease, diabetes, hepatitis, rheumatoid arthritis and psychiatric disorders.

The function of this internship is to engage in the biological downstream process development; particularly, protein (monoclonal antibody) purification process for drug substance production. I have held several independent research projects during this internship, including bench-scale protein purification chromatography experiments, high-throughput protein resin (adsorbent) screening using Tecan (Tecan Group Ltd.) liquid handler automation, and virus filtration/separation investigation.

While being trained on traditional pharmaceutical industry protein purification process, I have also actively explored the potential applications of MEMS/BioMEMS techniques towards the characterization, analysis, separation, and manipulation of biomolecules, such as proteins, DNA, and viruses, etc. In this chapter, I will summarize the principle idea of protein (antibody) purification in pharmaceutical industry. Based on this principle concept, different previously published studies, where MEMS/BioMEMS is utilized in the characterization and manipulation of biomolecules, such as proteins, will be described and discussed, to explore the potential application of MEMS in this particular field. Meanwhile, I will also discuss the feasibility of applying the techniques and system, which have been described above in this dissertation, into the field of protein biomedical sciences.

7.1 Principle of Industrial Protein Purification

In the biopharmaceutical industry, as the dominant therapeutic agents, hundreds of monoclonal antibodies (mAbs) are under development. These molecules (antibodies) are derived from a series of recovery and purification platform processes, before they are utilized in the production of drug substances. Typically, the first step in the antibody recovery process is to harvest the mammalian cell culture fluid (cell broth) from upstream process. This is generally accomplished, through the processes of centrifugation, flocculation/precipitation, tangential flow micro filtration, depth filtration and sterile filtration [105], to remove cells and cell debris. The harvested material is a filtered clarified bulk (CB), for downstream protein (antibody) purification process.

A typical downstream protein purification process flow is depicted in Fig. 7.1. Generally, mAbs are purified through multiple chromatography processes, which takes advantage of different physical and chemical properties between molecules for their separation.

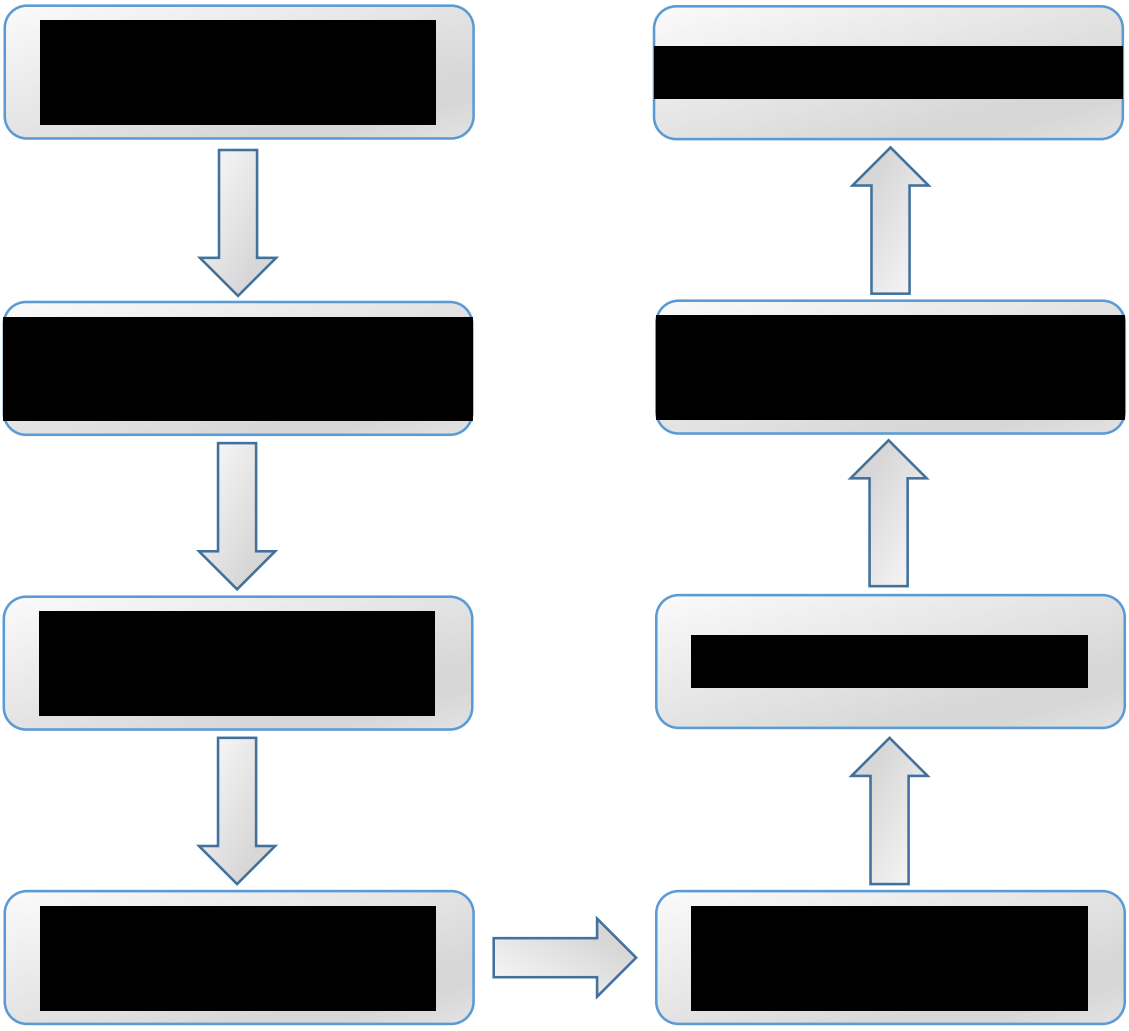

Figure 7.1 Typical platform process for monoclonal antibody downstream purification.

As shown in Fig. 7.1, the process flow starts with the cell broth clarified bulk (CB), which is prepared according to the process described above. The first and most important chromatography purification is a Protein A (ProA)-based affinity capture step, where ProA-based resins (stationary adsorbent) capture the target antibodies, and let impurities flow through. ProA chromatography clears most of the impurities, such as host cell proteins (HCP), DNA and viruses, and yields a relatively clean and pure product that only requires further removal of a small portion of impurities [106, 107]. This first purification directly decides the quality of the final drug substance. After the affinity capture, the target antibodies are eluted (separated from the resin) and collected. This

"capture-and-separate" process is known as a Bind-Elute mode (ProA) chromatography. The collection (eluent) is held in a low pH solution (pH: 3.4-3.5) for viral inactivation to inactivate endogenous/adventitious viruses; afterwards, the pH of the antibody solution is neutralized, for the flowing polishing chromatography steps, as described below.

One or two polishing chromatography processes are normally implemented to further clear impurities, according to drug substance quality requirements. In addition to HCP, DNA and viruses, these polishing steps also remove protein aggregates, unwanted product variant species and other minor contaminants [106]. These impurities, once inside the drug substance, are harmful to the patients' health. Polishing chromatography is usually cation exchange (CEX) and anion exchange (AEX) based, where electrostatic binding (to the resin) is integrated to attract either target mAbs or impurities. If the target antibodies are bonded, they are also eluted later based on the Bind-Elute chromatography mechanism; otherwise, if the impurities are bonded, target mAbs flow through the resin column and are collected, based on the Flow-Through mode chromatography mechanism.

In order to further remove viral contaminants, viral filtration is always performed after the previous chromatography purifications. Viral filtration is a size-based viral clearance step, where composite membranes with specific pore sizes are used to retain bigger viruses, and let smaller mAbs go through.

Finally, the purified mAb product, after all the platform processes described above, is concentrated using ultrafiltration, and diafiltered into the final formulation buffer. Both ultrafiltration and diafiltration are based on tangential flow filtration (TFF), where buffers flow through the membrane (filtrate), while proteins remained and collected through feedback (retentate).

7.2 MEMS Based Biomolecule Characterization, Analysis, Separation and Manipulation

Because of its μm and nm scale features and the advancement of microfabrication technologies, micro-electro-mechanical systems (MEMS) have been widely used in biomolecule sensing, diagnosis and analysis. Previously, fluorescence-based bio-sensing, analysis and separation has become the dominant technique. However, this method usually requires the labeling of fluorescent dyes to target molecules and specific equipment or arrays for fluorescent analysis. Integrating physical and chemical properties of different biomolecules with the mechanical structures of MEMS devices, a label-free protein sensing/detection technique has been enabled. By building a sensor array, such MEMS devices are even capable of high throughput protein screening, providing a potential replacement for conventional immunoassay techniques. In this section, some previously published research where MEMS biosensors have been successfully utilized in protein biomedical sciences will be described and discussed.

7.2.1 Stress-based MEMS Protein Sensor

In addition to being the dominant drug therapeutics, sometimes protein is also the disease-related clinical biomarkers that need to be detected [108]. For instance, cardiovascular-event-related proteins, such as disease-related C-reactive proteins (CRPs) have been detected based on the bending of microcantilevers [109]. Certain infection may cause higher CRP concentration in human serum, which raises the risk of heart attacks [110]. The structure of the MEMS CRP sensor microcantilever is shown in Fig. 7.2 [109], as well as the protein binding and sensing principle.

CMOS compatible silicon nitride is deposited on the silicon substrate for the cantilever, where Chromium (Cr) and gold (Au) layers are deposited as intermediate adhesion layer. A self-assembled molecule biolinker layer is coated to activate the binding of anti-CRP (antibody), for probing the antigen, CRP. When CRPs bind to anti-CRP, specific biomolecule interactions between them change the nanomechanical interactions within the biolinker layer, which leads to the bending of the microcantilever, as can be seen in Fig. 7.2(b) [109]. The bending of the cantilever is measured

by optical beam deflection through a position-sensitive detector (PSD). The fabricated "V" shaped CRP sensor and the experimental setup is shown in Fig. 7.3.

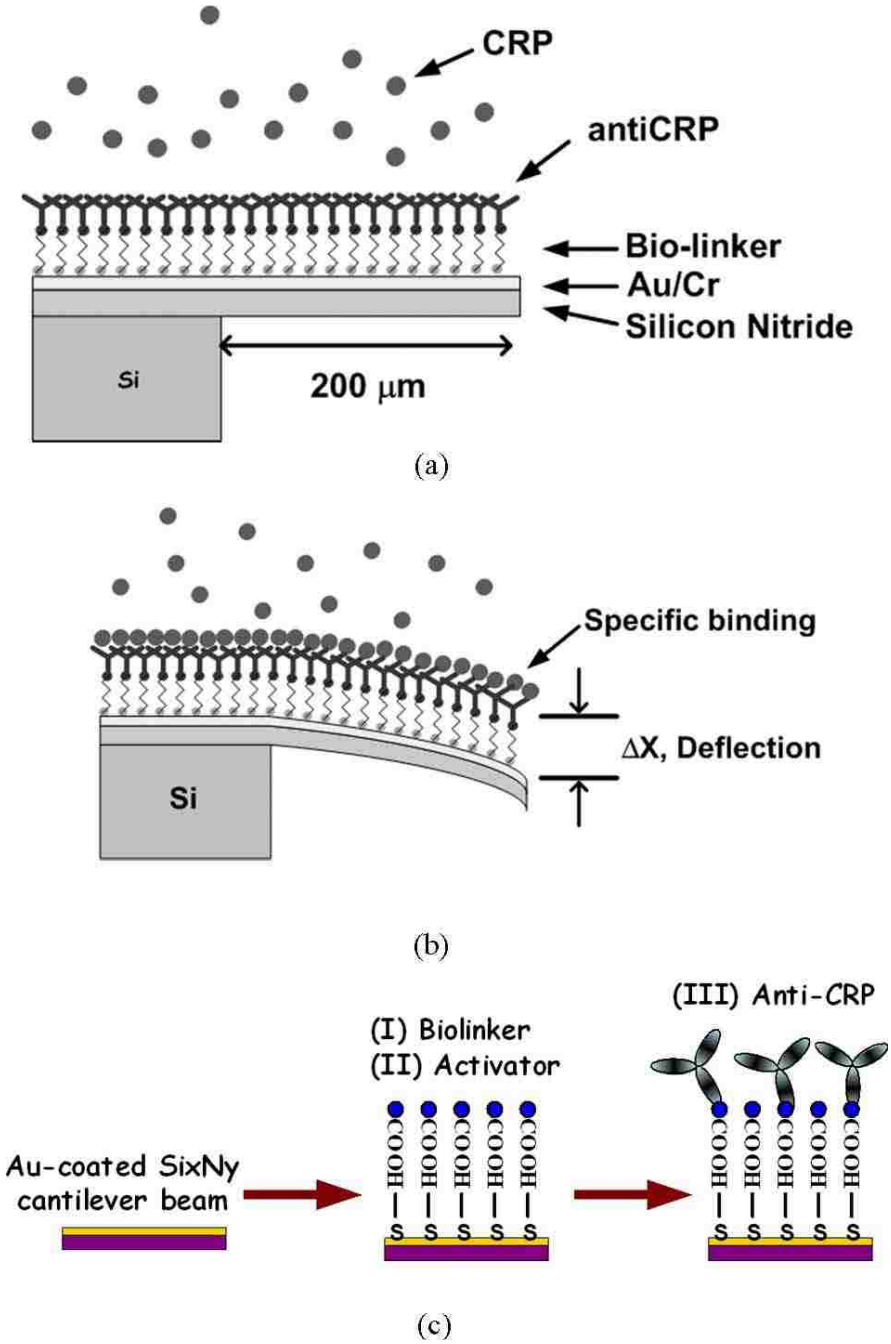

Figure 7.2 Structure of the CRP sensor and CRP sensing principle. (a) Before binding. (b) After binding. (c) Flow chart of attaching the antibody and different bio-layers to the cantilever surface [109].

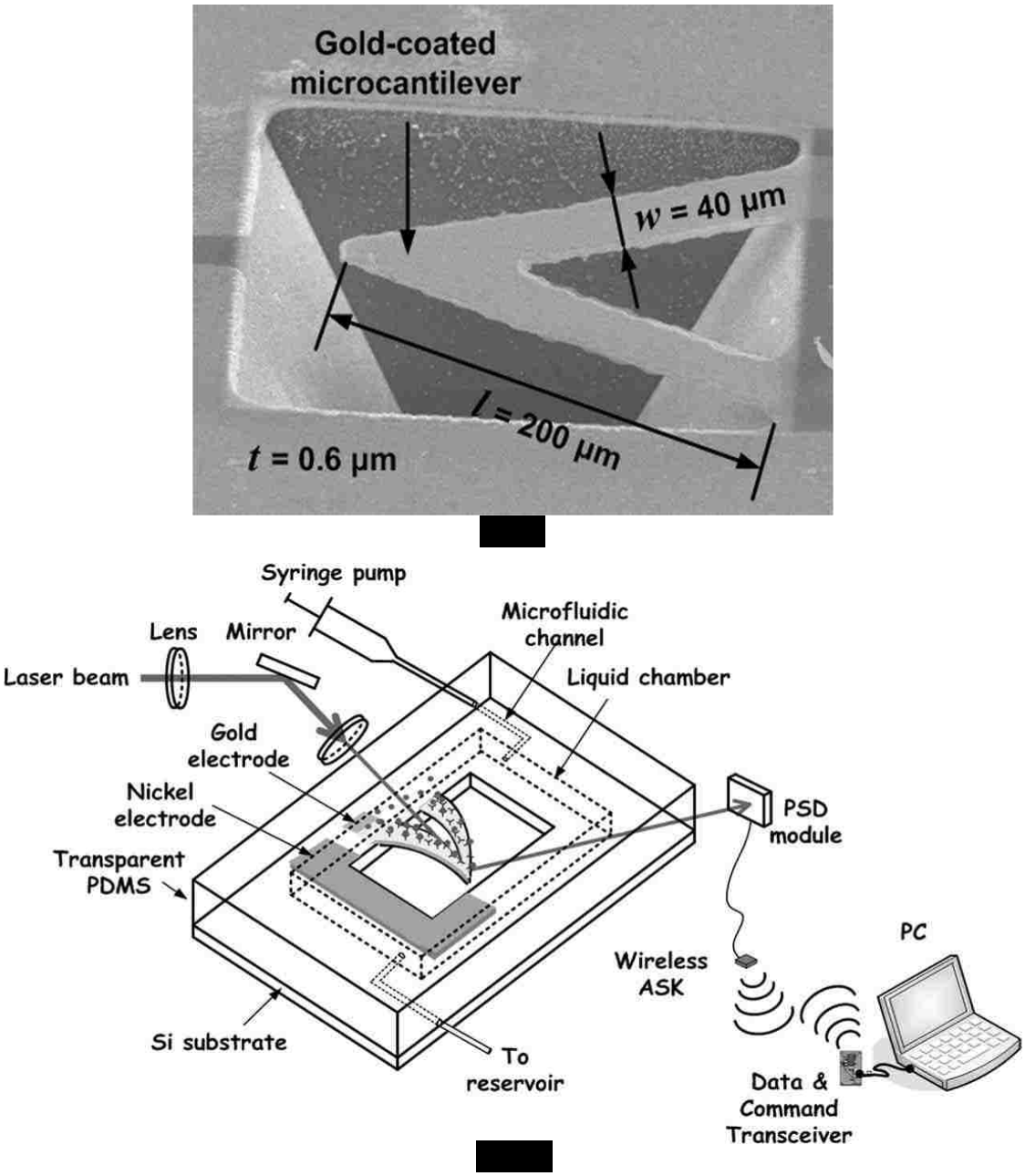

Figure 7.3 (a) SEM image of fabricated "V" shaped CRP sensor. (b) CRP detection experimental setup [109].

Another interesting aspect of this CRP sensor is that after the measurement, the CRPs can be physically removed from the cantilever for the sensor to be reused for successive experiments. Traditionally, bound proteins are separated from adsorbent surfaces by strong chemical acids or bases, similar to the elution process during Bind-Elute mode chromatography, where acidic buffers

are used to detach bound proteins from the adsorbent resins. But this chemical separation could also compromise the functionality and stability of the adsorbent anti-CRP layer, which prevents the sensor from multiple usages. In contrast, a low-frequency ac electric signal (0.2 Hz, 1V) is utilized here, to physically remove the CRPs from the cantilever. The electric signal is applied between the gold electrode connected to the cantilever and the nickel electrode around the cantilever, as can be seen in Fig. 7.3(b). Detailed mechanism of this electrical release can be found in [109]. Generally, the application of the electric field facilitates the cations and anions at the surface of the cantilever to move more freely in and out of the (anti-CRP)-CRP interface for binding relaxation. Then fluidic flow provides shear stress at the sensor surface to break those weak bonds, and the released CRPs are carried away with the flow. Compared to chemical elution, this electric separation method maintains the functionality of the anti-CRP layer for multiple cycles of detection. As we can see from this microcantilever protein sensor, the bind-release mechanism utilized here provides us a fresh perspective to look into the protein chromatography process, where alternative techniques can be exploited.

7.2.2 High Throughput Protein Screening Sensor Array

Another example I would like to mention here is also a surface stress-based protein sensor; however, a multi-dimensional arrayed sensor was built based on MEMS technology, for high throughput protein screening. Instead of measuring the optical deflection using a position-sensitive detector (PSD), as mentioned above, a silicon photodiode is integrated to enhance the surface-stress effect using nonlinear optical transmittance change by the Fabry-Perot interference [111, 112]. The device structure is illustrated in Fig. 7.4 [111], as well as the sensing principle in Fig. 7.5 [112].

This MEMS protein sensor consists of a suspended membrane film (Parylene-C) over a silicon photodiode with an air gap between. The Fabry-Perot cavity (air gap over a silicon oxide layer sitting above the photodiode) is changed because of the antigen-antibody interaction on the

membrane surface. When a single-wavelength laser light travels to the sensor, the transmitted light to the photodiode is dramatically changed based on Fabry-Perot interference [111], as well as the photocurrent, which can be read out as an electrical signal. The photocurrent signals are processed through integrated CMOS circuit, as can be seen in Fig. 7.4(a). By integrating MEMS sensor and CMOS circuit into a single chip, which eliminates complex external optical sensing components, an M x N sensor array can be built, for protein screening purposes. This also enables us with alternative techniques for biomolecule high throughput analysis applications.

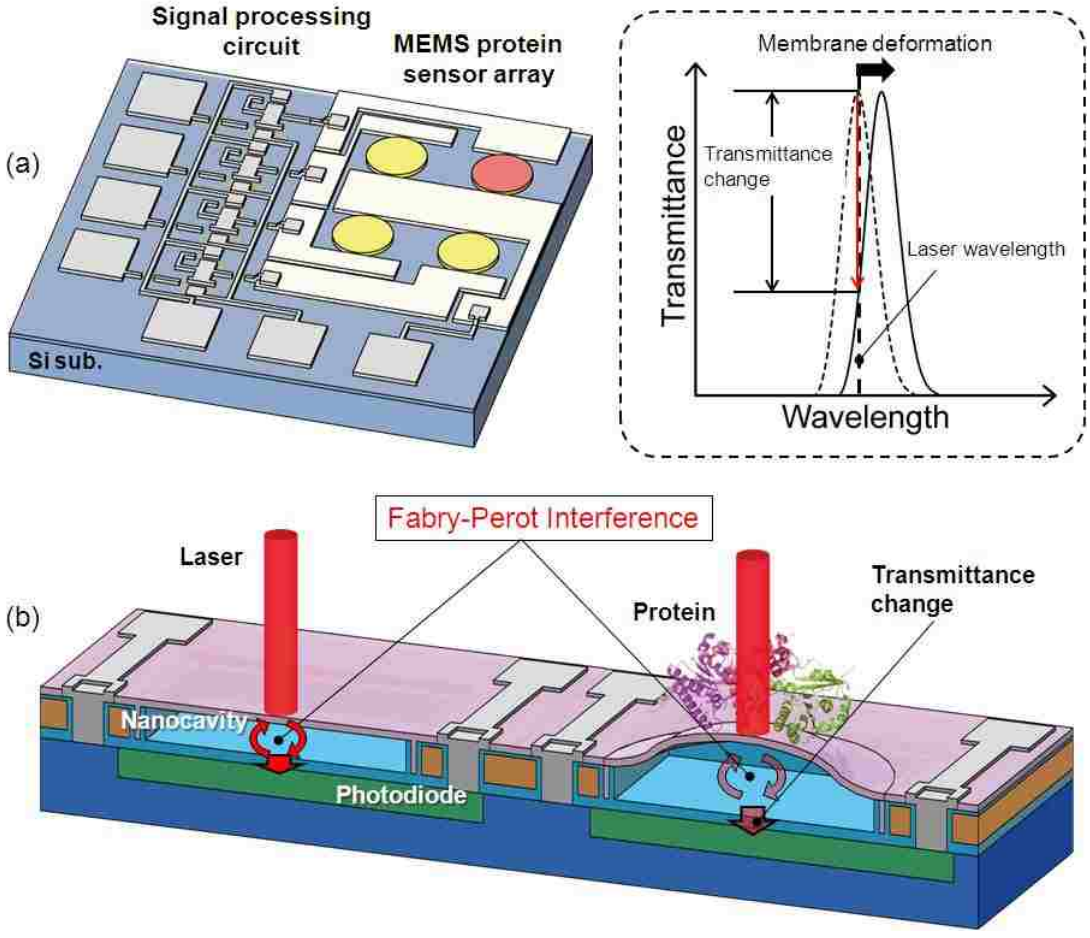

Figure 7.4 (a) Schematic of the MEMS Fabry-Perot interferometric protein sensor array, integrated with MOSFET signal processing circuit. (b) Schematic image of the Fabry-Perot interferometric protein sensor [111].

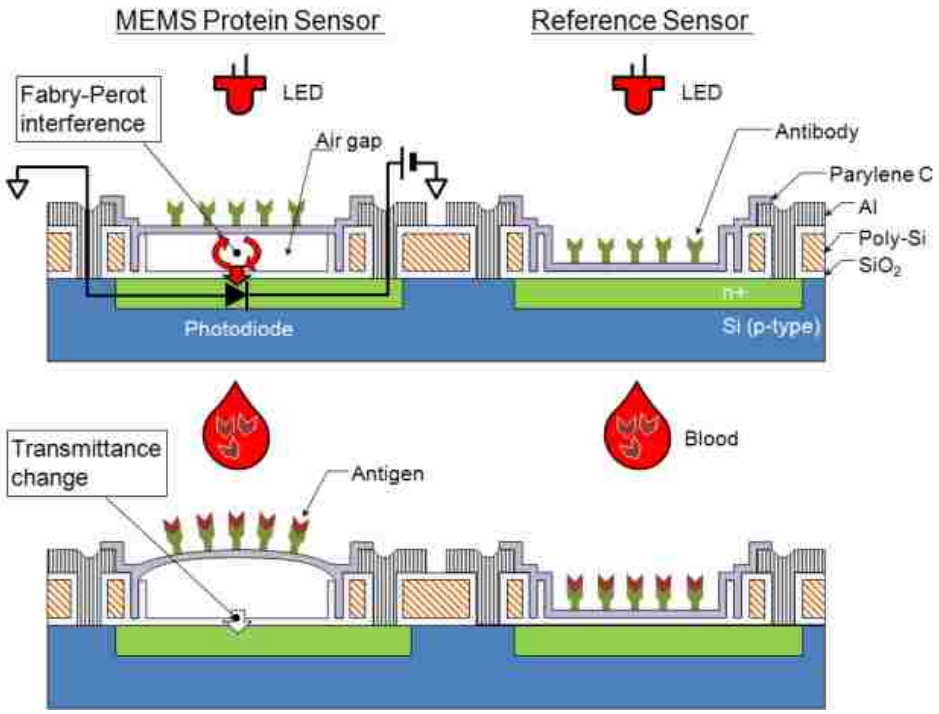

Figure 7.5 Sensing principle of a MEMS Fabry-Perot interferometric protein sensor. Photocurrent in the photodiode is changed with a deflection in the membrane by an antigen-antibody reaction [112].

7.2.3 MEMS based Protein Analysis Bioassay

Analytical department is an important functioning group in any biopharmaceutical companies. Protein samples from all stages of recovery and purification process should be analyzed for safety and drug product quality requirements. Conventional immunoassay technologies for life sciences, such as enzyme-linked immunosorbent assay (ELISA) and western blot are time consuming, and multiple manual steps are needed for the final assay analytical results. As a result, BioScale, Inc (Cambridge, MA) has developed a MEMS-based bioassay analysis system based on their acoustic membrane microparticle platform [113], as can be seen in Fig. 7.6. The system consists of eight identical MEMS sensors that can process eight samples simultaneously. A 96-well microtiter plate, which is commonly used for protein analytical purposes, can be processed sequentially analyzing 12 columns [113].

Figure 7.6 A MEMS based bioassay analysis system developed by BioScale, Inc (Cambridge, MA). Eight sensors function in parallel, corresponding to eight (8) rows of a 96-well (8 rows x 12 columns) microtiter plate, commonly used in life science analysis [113].

The operation and sensing principle of this bioassay analytical system is shown in Fig. 7.7. Samples are mixed with magnetic beads in the microtiter plate, where analyte (of interest) specific antibodies are coated on the magnetic beads, while another tagged antibody bind to the samples' analyte of interest. The mixture are flown over the anti-tag coated acoustic sensor membrane, where a magnet underneath captures the beads holding the analyte of interest. The magnetic field is then turned off, and only the biologically bound microparticles with the analyte remain on the sensor membrane.

Each of the acoustic sensor membrane is a piezoelectric vibrating component, whose resonant vibrating frequency changes with the binding of the microparticles, because of the mass loading. This resonant frequency is measured, as an indicator of the amount of analyte of interest, in the sample. After each cycle of measurement, the sensor can also be regenerated (detachment of microparticles) for reuse.

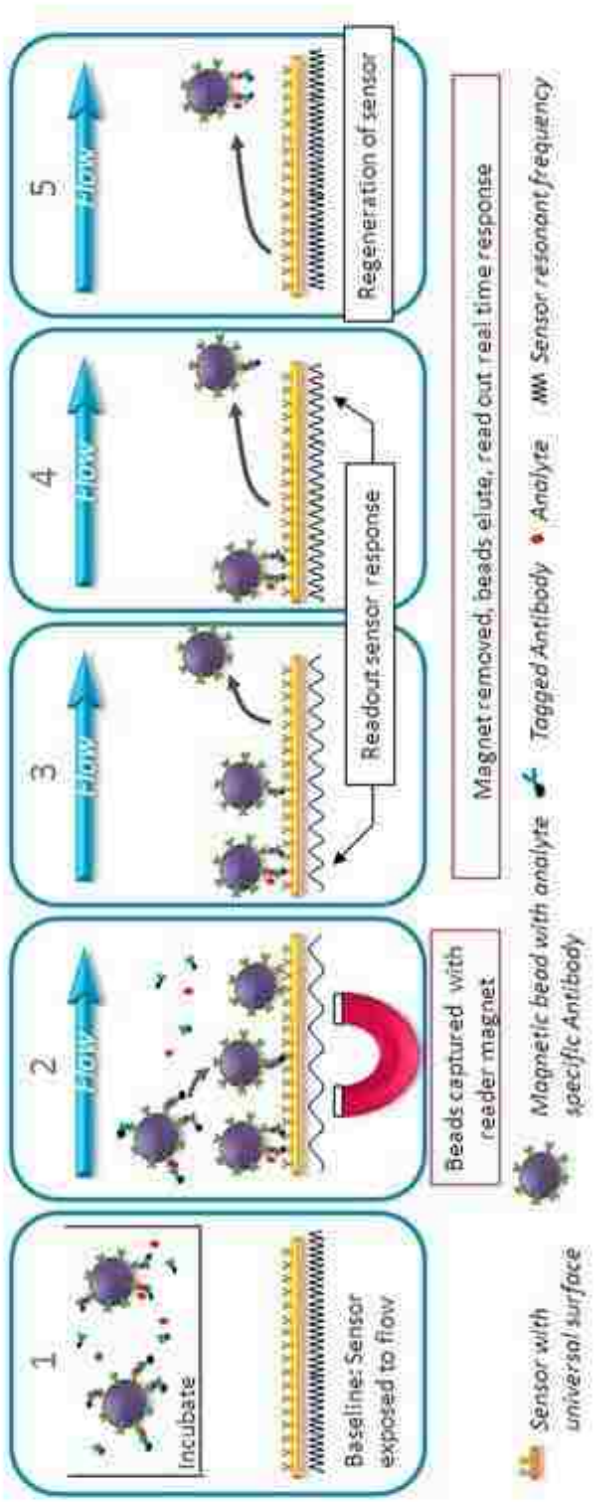

Figure 7.7 Sensing principle of the acoustic membrane MEMS bioassay analysis biosensor [113].

With this system, according to the company, multiple assays can be processed at the same time, while fewer basic steps are needed for lab personnel to run an assay. With great sensitivity and reproducibility, this MEMS based bioassay microsensor has the capability to measure low concentration of analyte that was not detectable before [113]. Here, MEMS technology once again, provides us with advanced alternative techniques for protein analytical applications.

7.3 Application of MEA Techniques in Protein Biomedical Sciences

As can be seen in the discussions above, MEMS technology has proven feasible and valuable for the characterization, analysis, separation and manipulation of biomolecules such as proteins. Particularly for MEMS multi-electrode array (MEA), as the system that has been described in this dissertation, we believe the technique also has potential applications in protein life sciences.

As mentioned previously, MEAs have been successfully utilized in cell/neuron patterning and biosensing. With appropriate surface chemical modifications, such as self-assembled protein-attractive monolayers, specific proteins can be captured and bind to the MEA for separation and purification purposes. Integrating microfluidics and the arrayed electrodes, high throughput screening is also achievable. On the other hand, advancing with the understanding of different electric properties of these biomolecules, interesting sensing mechanism can be explored based on the binding of proteins on the surface of MEA devices.

By fabricating nm-scale MEMS devices, it is also worth investigating the application of dielectrophoresis (DEP) for the characterization, separation and manipulation of various types of proteins. For instance, combining positive DEP capture and negative DEP repulsion, a Bind-Elute mechanism can be easily realized through the change of electric field frequency, without the need of strong acids or bases. Furthermore, as the cost of fabricating each MEMS MEA device is much lower than the adsorbent resins currently used in pharmaceutical industry, it could save millions of dollars every year for the company, by switching to alternative techniques based on MEMS.

With the help of wireless communication, portable, wearable, and even implantable personal medical and diagnostic equipment can be manufactured, bringing forward a new type of real-time health care system. With low-cost disposable diagnostic devices, more affordable medicines will come to people's normal lives.

Bibliography

[1] D. A. Stenger and T.M. McKenna, *Enabling Technologies for Cultured Neural Networks*, Dan Diego: Academic Press, Inc., 1994.

[2] M. Leow, J. Nobel, C. Harris, R. Diamond, and M. Weisinger, *Artificial Stimulation of the Temporal Lobe* [Online]. Available: http://www.macalester.edu/psychology/whathap/UBNRP/tle09/artificial_stim.html

[3] L. Berdondini, K. Imfeld, A. Maccione, M. Tedesco, S. Neukom, M. Koudelka-Hep, and S. Martinoia, Active pixel sensor array for high spatial-temporal resolution electrophysiological recordings from single cell to large scale neuronal networks. *Lab Chip* 9(18), 2644–2651, 2009.

[4] D. Eytan and S. Marom, Dynamics and effective topology underlying synchronization in networks of cortical neurons. *J. Neurosci.* 26(33), 8465–8476, 2006.

[5] L.R. Hochberg et al., Neuronal ensemble control of prosthetic devices by a human with tetraplegia. *Nature* 442, 164–171, 2006.

[6] M. Hutzler, A. Lambacher, B. Eversmann, M. Jenkner, R. Thewes, and P. Fromherz, High-resolution multitransistor array recording of electrical field potentials in cultured brain slices. *J. Neurophysiol.* 96(3), 1638–1645, 2006.

[7] D.J. Bakkum, U. Grey, M. Radivojevic, T.L. Russell, J. Muller, M. Fiscella, H. Takahashi, and A. Hierlemann, Tracking axonal action potential propagation on a high-density microelectrode array across hundreds of sites. *Nat. Commun.* 4, 2181, 2013.

[8] T.J. Blanche, M.A. Spacek, J.F. Hetke, and N.V. Swindale, Polytrodes: high-density silicon electrode arrays for large-scale multiunit recording. *J. Neurophysiol.* 93(5), 2987–3000, 2005.

[9] U. Frey, U. Egert, F. Heer, S. Hafizovic, and A. Hierlemann, Microelectronic system for high-resolution mapping of extracellular electric fields applied to brain slices. *Biosens. Bioelectron.* 24(7), 2191–2198, 2009.

[10] G. Gholmieh, W. Soussou, M. Han, A. Ahuja, M.C. Hsiao, D. Song, A.R. Tanguay Jr., and T.W. Berger, Custom-designed high-density conformal planar multielectrode arrays for brain slice electrophysiology. *J. Neurosci. Methods* 152(1-2), 116-129, 2009.

[11] F.O. Morin, Y. Takamura, and E. Tamiya, Investigating neuronal activity with planar microelectrode arrays: achievements and new perspectives. *J. Biosci. and Bioeng.* 100(2), 131-143, 2005.

[12] C.D. James, A.J.H. Spence, N.M. Dowell-Mesfin, R.J. Hussain, K.L. Smith, H.G. Craighead, M.S. Isaacson, W. Shain, and J.N. Turner, Extracellular recordings from patterned neuronal networks using planar multielectrode arrays. *IEEE Trans. Biomed. Eng.* 51(9), 1640-1648, 2004.

[13] J.L. Tan, W. Liu, C.M. Nelson, S. Raghavan, and C.S. Chen, Simple approach to micropattern cells on common culture substrates by tuning substrate wettability. *Tissue Eng.* 10(5-6), 865-872, 2004.

[14] G. Jing, S.F. Perry, and S. Tatic-Lucic, Precise cell patterning using cytophobic self-assembled monolayer deposited on top of semi-transparent gold. *Biomed. Microdevices* 12(5), 935-948, 2010.

[15] J. Erickson, A. Tooker, Y.C. Tai, and J. Pine, Caged neuron MEA: a system for long-term investigation of cultured neural network connectivity. *J. Neurosci. Methods* 175(1), 1-16, 2008.

[16] G. Zeck and P. Fromherz, Noninvasive neuroelectronic interfacing with synaptically connected snail neurons immobilized on a semiconductor chip. *Proc. Natl. Acad. Sci. U. S. A.* 98(18), 10457-10462, 2001.

[17] J.T. Robinson, M. Jorgolli, A.K. Shalek, M.H. Yoon, R.S. Gertner, and H. Park, Vertical nanowire electrode arrays as a scalable platform for intracellular interfacing to neuronal circuits. *Nature Nanotech.* 7(3), 180-184, 2012.

[18] C. Xie, L. Hanson, W. Xie, Z. Lin, B. Cui, and Y. Cui, Noninvasive neuron pinning with nanopillar arrays. *Nano Lett.* 10(10), 4020-4024, 2010.

[19] M.E. Spira and A. Hai, Multi-electrode array technologies for neuroscience and cardiology. *Nature Nanotech.* 8, 83-94, 2013.

[20] F.T. Jaber, F.H. Labeed, and M.P. Hughes, Action potential recording from dielectrophoretically positioned neurons inside micro-wells of a planar microelectrode array. *J. Neurosci. Methods* 182(2), 225-235, 2009.

[21] G. Jing, A Multi-electrode Array (MEA) System for Patterned Neural Networks, Ph.D. Dissertation, Lehigh University, Bethlehem, 2009, pp. 167-178.

[22] W. Tonomura, R. Kitazawa, T. Ueyama, H. Okamura, and S. Konishi, Electrophysiological biosensor with microchannel array for sensing of signals from single cells. Proc. *IEEE Conf. Sensors*, Daegu, Korea (2006) 140-143. DOI: 10.1109/ICSENS.2007.355738

[23] H. Zhang and K.K. Liu, Optical tweezers for single cells. *J. R. Soc. Interface* 5(24), 671-690, 2008.

[24] T. Heida, P. Vulto, W.L.C. Rutten, and E. Marani, Viability of dielectrophoretically trapped neural cortical cells in culture. *J. Neurosci. Methods* 110, 37-44, 2001.

[25] H.A. Pohl, *Dielectrophoresis: The behavior of neutral matter in nonuniform electric fields*, Cambridge University Press, New York, 1978.

[26] J. Wosik, D. Padmaraj, C. Darne, and W. Zagozdozon-Wosik, Dielectrophoresis of Biological Cells and Single-walled Carbon Nanotubes. Univ. of Houston, Houston, TX, *Institute for Space Systems Operation – Y2006 Annual Report*, 2006.

[27] R. Pethig, Dielectric Properties of Biological Materials: Biophysical and Medical Applications. *IEEE Trans. Electr. Insul.*, EI-19, 453-474, 1984.

[28] T.B. Jones, Electromechanics of Particles, New York: Cambridge University Press, 1995.

[29] H.A. Pohl and J.S. Crane, Dielectrophoresis of Cells. *Biophysical J.*, 11, 711-727, 1971.

[30] C.P. Jeng, C.T. Huang, and H.Y. Shih, Hydrodynamic separation of cells utilizing insulator-based dielectrophoresis. *Microsystem Technologies* 16(7), 1097-1104, 2010.

[31] R.A. Chitwood, A. Hubbard, and D.B. Jaffe, Passive electronic properties of rat hippocampal CA3 interneurons. *J. Physiol.* 515(3), 743-756, 1999.

[32] L.J. Gentet, G.J. Stuart, and J.D. Clements, Direct measurement of specific membrane capacitance in neurons. *Biophys. J.* 79(1), 314-320, 2000.

[33] T. Heida, W.L.C. Rutten, and E. Marani, Dielectrophoretic trapping of dissociated fetal cortical rat neurons. *IEEE Trans. Biomed. Eng.* 48(8), 921-930, 2001.

[34] G. Major, A.U. Larkman, P. Jonas, B. Sakmann, and J.J. Jack, Detailed passive cable models of whole-cell recorded CA3 pyramidal neurons in rat hippocampal slices. *J. Neurosci.* 14(8), 4613-4638, 1994.

[35] C.G. Malmberg and A.A. Maryott, Dielectric constants of aqueous solutions of dextrose and sucrose. *J. Res. Natl. Bur. Stand.* 45(4), 299-303, 1950.

[36] Z. Yu, G. Xiang, L. Pan, L. Huang, Z. Yu, W. Xing, and J. Cheng, Negative dielectrophoretic force assisted construction of ordered neuronal networks on cell positioning bioelectronic chips. *Biomed. Microdevices* 6(4), 311-324, 2004.

[37] T. Zhou and S. Tatic-Lucic, On application of positive dielectrophoresis and microstructure confinement on multielectrode array with sensory applications. *In Proc. IEEE Sensors Conf.*, Taipei, Taiwan, 2012.

[38] J. Lu, C.A. Barrios, A.R. Dickson, J.L. Nourse, A.P. Lee, and L.A. Flanagan, Advancing practical usage of microtechnology: a study of the functional consequences of dielectrophoresis on neural stem cells. *Integr. Biol.*, 4, 1223-1236, 2012.

[39] C. Huang, C. Liu, J. Loo, T. Stakenborg, and L. Lagae, Single cell viability observation in cell dielectrophoretic trapping on a microchip. *Appl. Phys. Lett.*, 104, 013703, 2014.

[40] R. Pethig, Review article-dielectrophoresis: status of the theory, technology, and applications. *Biomicrofluidics*, 4, 022811, 2010.

[41] M.D. Vahey and J. Voldman, High-throughput cell and particle characterization using isodielectric separation. *Anal. Chem.*, 81(7), 2446-2455, 2009.

[42] T. Heida, J.B. Wagenaar, W.L.C. Rutten, and E. Marani, Investigating membrane breakdown of neuronal cells exposed to nonuniform electric fields by finite-element modeling and experiments. *IEEE Trans. Biomed. Eng.*, 49(10), 1195-1203, 2002.

[43] U. Zimmermann and G.A. Neil, *Electromanupulation of Cells*, CRC Press. Florida, 1996.

[44] T. Zhou, S.F. Perry, Y. Ming, S. Petryna, V. Fluck, and S. Tatic-Lucic, Separation and assisted patterning of hippocampal neurons from glial cells using positive dielectrophoresis. *Biomed. Microdevices*, 17(3), 9965, 2015.

[45] A. LaLonde, M.F. Romero-Creel, and B.H. Lapizco-Encinas, Assessment of cell viability after manipulation with insulator-based dielectrophoresis. *Electrophoresis*, 35, 1-6, 2014.

[46] G. Buzsaki, C.A. Anastassiou, and C. Koch, The origin of extracellular fields and currents – EEG, ECoG, LFP and spikes. *Nat. Rev. Neurosci.*, 13, 407-420, 2012.

[47] L. Pan, S. Alagapan, E. Franca, G.J. Brewer, and B.C. Wheeler, Propagation of action potential activity in a predefined microtunnel neural network. *J. Neural Eng.* 8(4), 046031, 2011.

[48] A.M. Taylor, M. Blurton-Jones, S.W. Rhee, D.H. Cribbs, C.W. Cotman, and N.L. Jeon, A microfluidic culture platform for CNS axonal injury, regeneration and transport. *Nat. Methods* 2(8), 599-605, 2005.

[49] V.N. Vernekar, D.K. Cullen, N. Fogleman, Y. Choi, A.J. Garcia, M.G. Allen, G.J. Brewer, and M.C. LaPlaca, SU-8 2000 rendered cytocompatible for neuronal bioMEMS applications. *J. Biomed. Mater. Res.* 89(1), 138-151, 2009.

[50] S.L. Tao, K.C. Popat, J.J. Norman, and T.A. Desai, Surface modification of SU-8 for enhanced biofunctionality and nonfouling properties. *Langmuir* 24(6), 2631-2636, 2008.

[51] G. Liu, Y. Tian, and Y. Kan, Microfabrication of high-aspect-ratio microstructures using SU8 photoresist. *Microsyst. Technol.* 11(4-5), 343-346, 2005.

[52] G. Jing, Y. Wang, T. Zhou, S.F. Perry, M.T. Grimes, and S. Tatic-Lucic, Cell patterning using molecular vapor deposition of self-assembled monolayers and lift-off technique. *Acta Biomater.* 7(3), 1094-1103, 2011.

[53] M. Grattarola and S. Martinoia, Modeling the neuron-microtransducer junction: from extracellular to patch recording. *IEEE Trans. Biomed. Eng.* 40(1), 35-41, 1993.

[54] J. Pine, Recording action potentials from cultured neurons with extracellular microcircuit electrodes. *J. Neurosci. Methods* 2(1), 19-31, 1980.

[55] S. Prasad, X. Zhang, M. Yang, Y. Ni, V. Parpura, C.S. Ozkan, and M. Ozkan, Separation of individual neurons using dielectrophoretic alternative current fields. *J. Neurosci. Methods* 135(1-2), 79-88, 2004.

[56] B.H. Brown, Frequency analysis used for interpretation of human nerve action potentials obtained from surface electrodes. *Med. and Biol. Eng.* 6(5), 493-502, 1968.

[57] T. Ogura, T. Kubo, Y. Okuda, K. Lee, Y. Kira, S. Aramaki, and F. Nakanishi, Power spectrum analysis of compound muscle action potential in carpal tunnel syndrome patients. *J. Orthop. Surg.* 10(1), 67-71, 2002.

[58] Y. Jimbo, N. Kasai, K. Torimitsu, T. Tateno, and H.P.C. Robinson, A system for MEA-based multisite stimulation. *IEEE Trans. Biomed. Eng.* 50(2), 241-248, 2003.

[59] D.A. Wagenaar, J. Pine, and S.M. Potter, Effective parameters for stimulation of dissociated cultures using multi-electrode arrays. *J. Neurosci. Methods* 138(1-2), 27-37, 2004.

[60] M. Merz and P. Fromherz, Silicon chip interfaced with a geometrically defined net of snail neurons. *Adv. Funct. Mater.* 15(5), 739-744, 2005.

[61] L. Berdondini et al. A microelectrode array (MEA) integrated with clustering structures for investigating in vitro neurodynamics in confined interconnected sub-populations of neurons. *Sens. Actuators B Chem.* 114(1), 530-541, 2006.

[62] M.A.P. Idiart and L.F. Abbott, Propagation of excitation in neural network models. *Network* 4, 285-294, 1993.

[63] R. Miles, R.D. Traub, and R.K. Wong, Spread of synchronous firing in longitudinal slices from the CA3 region of the hippocampus. *J. Neurophysiol.* 60(4), 1481-1496, 1988.

[64] W.A. Bonner, H.R. Huleft, R.G. Sweet, and L.A. Herzenberg, Fluorescence activated cell sorting. *Rev. Sci. Instrum.* 43(3), 404-409, 1972.

[65] A. Suzuki, Y.W. Zheng, R. Kondo, M. Kusakabe, Y. Takada, K. Fukao, K. Nakauchi, and H. Taniguchi, Flow-cytometric separation and enrichment of hepatic progenitor cells in the developing mouse liver. *Hepatology* 32(6), 1230-1239, 2000.

[66] S.H. Yuan et al. Cell-surface marker signatures for the isolation of neural stem cells, glia and neurons derived from human pluripotent stem cells. *PLoS One* 6(3), e17540, 2011.

[67] S. Miltenyi, W. Muller, W. Weichel, and A. Radbruch, High gradient magnetic cell separation with MACS. *Cytometry* 11(2), 231-238, 1990.

[68] M. Zobrowski and J.J. Chalmers, Magnetic cell sorting, *Methods Mol. Biol.* 295, 291-300, 2005.

[69] Y. Nagata, K. Mokishiba, and Y. Tsukada, Neuronal cell body enriched glial cell enriched fractions from young and adult rat brains: preparation and morphological and biochemical properties. *J. Neurochem.* 22, 493-503, 1974.

[70] V. Gupta, I. Jafferji, M. Garza, V.O. Melnikova, D.K. Hasegawa, R. Pethig, and D.W. Davis, ApoStream, a new dielectrophoretic device for antibody independent isolation and recovery of viable cancer cells from blood. *Biomicrofluidics* 6, 024133, 2012.

[71] C.T. Ho et al. Liver-cell patterning lab chip: mimicking the morphology of liver lobule tissue. *Lab Chip* 13, 3578-3587, 2013.

[72] M. Li, W.H. Li, J. Zhang, G. Alici, and W. Wen, A review of microfabrication techniques and dielectrophoretic microdevices for particle manipulation and separation. *J. Phys. D: Appl. Phys.* 47, 063001, 2014.

[73] J.L. Prieto, J. Lu, J.L. Nourse, L.A. Flanagan, and A.P. Lee, Frequency discretization in dielectrophoretic assisted cell sorting arrays to isolate neural cells. *Lab Chip* 12(12), 2182-2189, 2012.

[74] X. Zhao, A. Ahram, R.F. Berman, J.P. Muizelaar, and B.G. Lyeth, Early loss of astrocytes after experimental traumatic brain injury. *Glia* 44(2), 140-152, 2003.

[75] F. Jabr. *Know Your Neurons: What Is the Ratio of Gila to Neurons in the Brain.* (Scientific American Blogs, 2012), http://blogs.scientificamerican.com/brainwaves/2012/06/13/know-your-neurons-what-is-the-ratio-of-glia-to-neurons-in-the-brain/ (Assessed 29 October 2014)

[76] M.S. Grady, J.S. Charleston, D. Maris, B.M. Witgen, and J. Lifshitz, Neuronal and glial cell number in the hippocampus after experimental traumatic brain injury: analysis by stereological estimation. *J. Neurotrauma* 20(10), 929-941, 2003.

[77] L. Korbo, Glial cell loss in the hippocampus of alcoholics. *Alcohol. Clin. Exp. Res.* 23(1), 164-168, 1999.

[78] Y.C. Okada, J. Huang, M.E. Rice, D. Tranchina, and C. Nicholson, Origin of the apparent tissue conductivity in the molecular and granular layers of the in vitro turtle cerebellum and the interpretation of current source-density analysis. *J. Neurophysiol.* 72(2), 742-753, 1994.

[79] M. Peters, J. Stinstra, I. Leveles, Modeling and Imaging of Bioelectrical Activity Principles and Applications, in *Bioelectric Engineering*, ed. By B. He (Springer, New York, 2005), pp. 281-319.

[80] M.D. Vahey and J. Voldman, An equilibrium method for continuous-flow cell soring using dielectrophoresis. *Anal. Chem.* 80, 3135-3143, 2008.

[81] Z. Gagnon, S. Senapati, J. Gordon, and H.C. Chang, Dielectrophoretic detection and quantification of hybridized DNA molecules on nano-genetic particles. *Electrophoresis* 29, 4808-4812, 2008.

[82] K. Goslin, H. Asmussen, and G. Banker, Culturing Nerve Cells, 2nd edn, in *Cellular and Molecular Neuroscience*, ed. By G. Banker, K. Goslin (The MIT Press, Cambridge, 1998), pp. 339-370.

[83] L.A. Flanagan, J. Lu, L. Wang, S.A. Marchenko, N.L. Jeon, A.P. Lee, and E.S. Monuki, Unique dielectric properties distinguish stem cells and their differentiated progeny. *Stem Cells* 26(3), 656-665, 2008.

[84] F.H. Labeed, J. Lu, H.J. Mulhall, S.A. Marchenko, K.F. Hoettges, L.C. Estrada, A.P. Lee, M.P. Hughes, and L.A. Flanagan, Biophysical characteristics reveal neural stem cell differentiation potential. *PLoS ONE* 6(9), e25458, 2011.

[85] J.L. Nourse, J.L. Prieto, A.R. Dickson, J. Lu, M.M. Pathak, F. Tombola, M. Demetriou, A.P. Lee, and L.A. Flanagan, Membrane biophysics define neuron and astrocyte progenitors in the neural lineage. *Stem Cells* 32(3), 706-716, 2013.

[86] G.J. Brewer, J.R. Torricelli, E.K. Evege, and P.J. Price, Optimized survival of hippocampal neurons in B27-supplemented neurobasal, a new serum-free medium combination. *J. Neurosci. Res.* 35(5), 567-576 (1993)

[87] B. Gao and L. Ziskind-Conhaim, Development of ionic currents underlying changes in action potential waveforms in rat spinal motoneurons. *J. Neurophysiol.* 80, 3047-3061, 1998.

[88] G. Pilwat and U. Zimmermann, Determination of intracellular conductivity from electrical breakdown measurements. *Biochimica et Biophysica Acta*, 820, 305-314, 1985.

[89] R. Pethig, A. Menachery, S. Pells, and P.D. Sousa, Dielectrophoresis: A review of applications for stem cell research. *J. Biomed. Biotechnol.* 182581, 2010.

[90] Z.R. Gagnon, Cellular dielectrophoresis: applications to the characterization, manipulation, separation and patterning of cells. *Electrophoresis*, 32, 2466-2487, 2011.

[91] H. Morgan, T. Sun, D. Holmes, S. Gawad, and N.G. Green, Single cell dielectric spectroscopy. *J. Phys. D: Appl. Phys.* 40, 61-70, 2007.

[92] T.L. Mahaworasilpa, H.G.L. Coster, and E.P. George, Forces on biological cells due to applied alternating (AC) electric fields. I. Dielectrophoresis. *Biochimica et Biophysica Acta*, 1193, 118-126, 1994.

[93] P. Gascoyne, R. Pethig, J. Satayavivad, F.F. Becker, and M. Ruchirawat, Dielectrophoretic detection of changes in erythrocyte membranes following malarial infection. *Biochimica et Biophysica Acta*, 1323, 240-252, 1997.

[94] D.M. Vykoukal, P.R. Gascoyne, and J. Vykoukal, Dielectric characterization of complete mononuclear and polymorphonuclear blood cell subpopulations for label-free discrimination. *Integr. Biol.(Camb.)* 1(7), 477-484, 2009.

[95] Z. Gagnon, J. Gordon, S. Sengupta, and H-C. Chang, Bovine red blood cell starvation age discrimination through a glutaraldehyde-amplified dielectrophoretic approach with buffer selection and membrane cross-linking. *Electrophoresis*, 29, 2272-2279, 2008.

[96] P.R.C. Gascoyne, S. Shim, J. Noshari, F.F. Becker, and K. Stemke-Hale, Correlations between the dielectric properties and exterior morphology of cells revealed by dielectrophoretic field-flow fractionation. *Electrophoresis*, 34, 1042-1050, 2013.

[97] U. Lei, P-H. Sun, and R. Pethig, Refinement of the theory for extracting cell dielectric properties from dielectrophoresis and electrorotation experiments. *Biomicrofluidics*, 5(4), 044109, 2011.

[98] Y. Huang, X.B. Wang, F.F. Becker, and P.R.C. Gascoyne, Membrane changes associated with the temperature-sensitive P85gag-mos-dependent transformation of rat kidney cells as determined by dielectrophoresis and electrorotation. *Biochimica et Biophysica Acta*, 1282, 76-84, 1996.

[99] Y. Huang, X.B. Wang, F.F. Becker, and P.R. Gascoyne, Introducing dielectrophoresis as a new force field for field-flow fractionation. *Biophysical Journal*, 73(2), 1118-1129, 1997.

[100] M.P. Maher, H. Dvorak-Carbone, J. Pine, J.A. Wright, and Y.C. Tai, Microstructures for studies of cultured neural networks. *Med. Biol. Eng. Comp.* 37(1), 110-118, 1999.

[101] L.M. Levy, O. Warr, and D. Attwell, Stoichiometry of the glial glutamate transporter GLT-1 expressed inducibly in a Chinese hamster ovary cell line selected for low endogenous Na+-dependent glutamate uptake. *J. Neurosci.* 18(23), 9620-9628, 1998.

[102] C. Chung, M. Waterfall, S. Pells, A. Menachery, S. Smith, and R. Pethig, Dielectrophoretic characterisation of mammalian cells above 100 MHz. *J. Electr. Bioimp.* 2, 64-71, 2011.

[103] M.B. Sano, E.A. Henslee, E. Schmelz, and R.V. Davalos, Contactless dielectrophoretic spectroscopy: examination of the dielectric properties of cells found in blood. *Electrophoresis*, 32(22), 3164-3171, 2011.

[104] *Neuronal Action Potential* (Online), 2012, Available: http://www.physiologyweb.com/lecture_notes/neuronal_action_potential/neuronal_action_potential.html (accessed 07.30.14)

[105] A. Mehta, M.L. Tse, J. Fogle, A. Len, R. Shrestha, N. Fontes, B. Lebreton, B. Wolk, R.V. Reis, Purifying therapeutic monoclonal antibodies, *CEP Magazine, Society for Biological Engineering, SBE Special Section, Bioprocessing*, S14-S20, May 2008.

[106] H.F. Liu, J. Ma, C. Winter, and R. Bayer, Recovery and purification process development for monoclonal antibody production. *MAbs* 2(5), 480-499, 2010.

[107] S. Hober, K. Nord, and M. Linhult, Protein A chromatography for antibody purification. *J. Chromatography B* 848(1), 40-47, 2007.

[108] G. Wu, R.H. Datar, K.M. Hansen, T. Thundat, R.J. Cote, and A. Majumdar, Bioassay of prostate-specific antigen (PSA) using microcantilevers. *Nat. Biotechnol*. 19, 856–860, 2001.

[109] C.-H. Chen et al. A wireless bio-MEMS sensor for C-Reactive Protein detection based on nanomachanics. *IEEE Trans. Biomed. Eng.* 56(2), 462-470, 2009.

[110] G.J. Blake, N. Rifai, J.E. Buring, and P.M. Ridker, Blood pressure, c-reactive protein, and risk of future cardiovascular events. *Circulation* 108, 2993–2999, 2003.

[111] K.Takahashi, R. Ozawa, H. Oyama, M. Futagawa, F. Dasai, M. Ishida, and K. Sawada, A CMOS-MEMS-based label-free protein sensor for high-sensitive and compact system.

Proceedings of IEEE International Electron Devices Meeting (IEDM), 24.6.1-24.6.4, Dec. 2012.

[112] H. Oyama, K. Takahashi, N. Misawa, K. Okumura, M. Ishida, and K. Sawada, A MEMS-based Fabry-Perot protein sensor with reference sensor. *Proceedings of the 14th International Meeting on Chemical Sensors*, 352-355, 2012.

[113] J. Williamson, MEMS based sensors enable protein analysis system. MEMS Investor Journal, 2010. Available: http://bioscale.com/wp-content/uploads/2014/04/mems_investor_journal_-_6-23-10.pdf (accessed 11.26.15)

Appendix I: Layout

Mask Design

The dimensions of all features that were varied are listed in Table A.1 for design revision 1, and Table A.2 for design revision 2.

Table A.1 Design parameters for all DEP MEA device dies (revision 1).

Die label	Oxide via diameter (μm)	Array (mxn)	Pathway length[1] (μm)	Chamber diameter (μm)	Trench width (μm)	Bonding pad size[2] (μm)	Count
PDEP MEA6 4x4_100_50umChamber7	6	4x4	100	50	7	600	3
PDEP MEA6 4x4_100_30umChamber5	6	4x4	100	30	5	600	3
PDEP MEA6 4x4_100_20umChamber2	6	4x4	100	20	2	600	2
PDEP MEA8 4x4_100_50umChamber7	8	4x4	100	50	7	600	3
PDEP MEA8 4x4_100_30umChamber5	8	4x4	100	30	5	600	3
PDEP MEA8 4x4_100_20umChamber2	8	4x4	100	20	2	600	2
PDEP MEA10 4x4_100_50umChamber7	10	4x4	100	50	7	600	2
PDEP MEA10 4x4_100_30umChamber5	10	4x4	100	30	5	600	2
PDEP MEA8 4x4_200_50umChamber7	8	4x4	200	50	7	600	3
PDEP MEA8 4x4_200_60umChamber10	8	4x4	200	60	10	600	2

[1] Distance between neighboring electrodes
[2] Wire bonding pad square length

Table A.2 Design parameters for all DEP MEA device dies (revision 2).

Die label	Oxide via diameter (μm)	Array (mxn) or electrodes number[1]	Pathway length[2] (μm)	Chamber diameter (μm)	Trench width (μm)	Count
LEHIGH MEMS DEP_MEA_6_4x4_100_20_3	6	4x4	100	20	3	2
LEHIGH MEMS DEP_MEA_6_4x4_100_20_5	6	4x4	100	20	5	2
LEHIGH MEMS DEP_MEA_6_4x4_100_30_3	6	4x4	100	30	3	2
LEHIGH MEMS DEP_MEA_6_4x4_100_30_5	6	4x4	100	30	5	2
LEHIGH MEMS DEP_MEA_6_4x4_100_30_7	6	4x4	100	30	7	2
LEHIGH MEMS DEP_MEA_6_4x4_100_50_5	6	4x4	100	50	5	2
LEHIGH MEMS DEP_MEA_6_4x4_100_50_7	6	4x4	100	50	7	2
LEHIGH MEMS DEP_MEA_6_4x4_150_30_5	6	4x4	150	30	5	2
LEHIGH MEMS DEP_MEA_6_4x4_150_50_7	6	4x4	150	50	7	2
LEHIGH MEMS DEP_MEA_6_4x4_200_30_5	6	4x4	200	30	5	2
LEHIGH MEMS DEP_MEA_6_4x4_200_50_7	6	4x4	200	50	7	2
LEHIGH MEMS PDEP MEA 5x4_100_50chamber5	6	5x4	100	50	5	6
LEHIGH MEMS PDEP MEA21 100_40chamber4	6	21	100	40	4	7
LEHIGH MEMS PDEP MEA21_100_30umChamber5	6	21	100	30	5	5
LEHIGH MEMS PDEP MEA22_100_20umChamber3	6	22	100	20	3	6
LEHIGH MEMS PDEP MEA23_99_20umChamber5	6	23	99	20	5	4

[1] Total number of electrodes when the electrode are not a mxn array

[2] Distance between neighboring electrodes

Mask Layout

Snapshots of four-inch masks are shown below in Fig. A.1 (Metal), Fig. A.2 (Passivation), and Fig. A.3 (Trench) for design revision 1. In design revision 1, DEP MEA devices are arranged in half of the wafer, while the other half is designated for MEA test devices, which we used for preliminary cell trapping and patterning experiments. Details of these MEA test devices are described in Appendix VII: Preliminary pDEP Cell Trapping Experiments and Microstructure Cell Patterning Study.

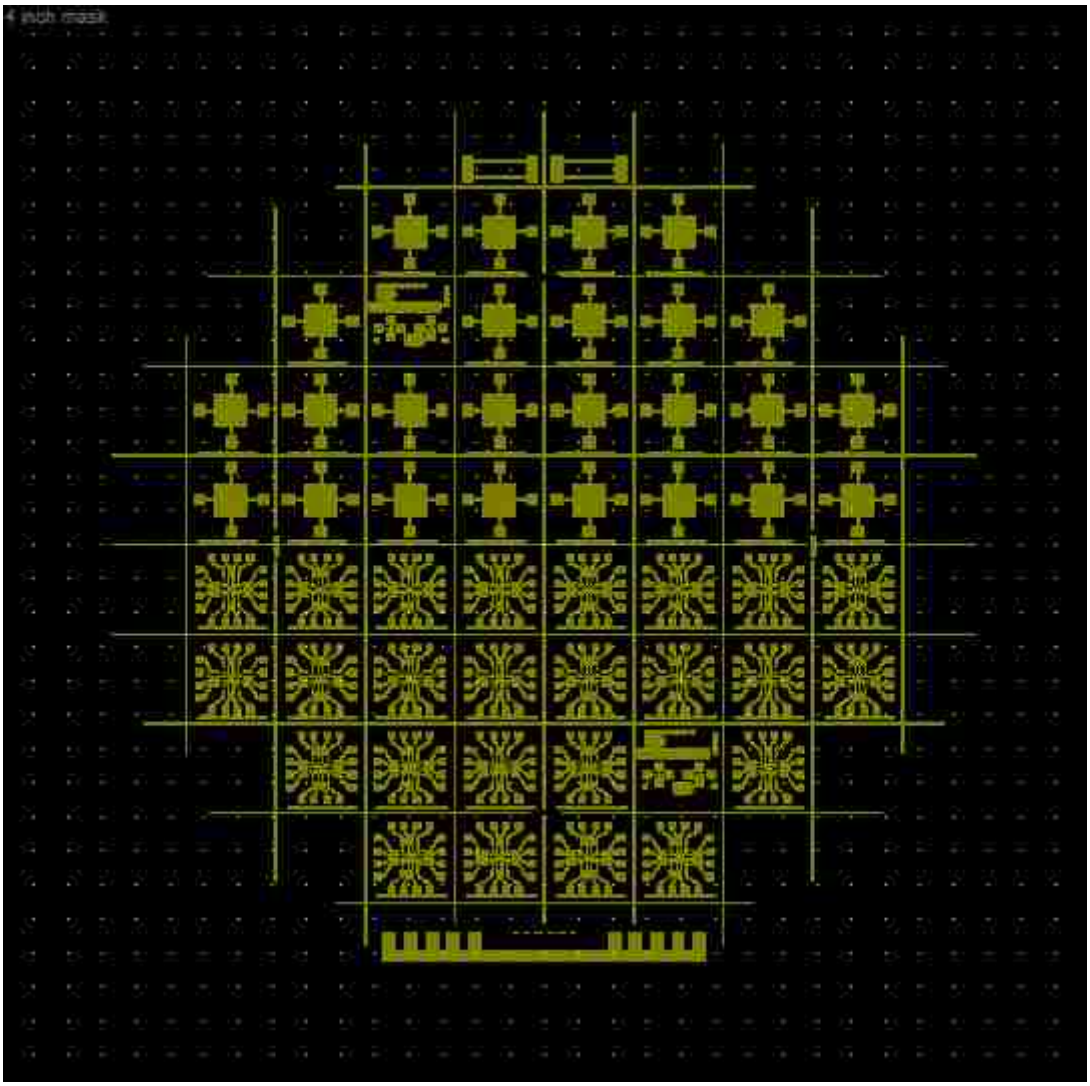

Figure A.1 Metal mask (revision 1) layout for three-inch wafers (four-inch quartz AR chrome mask). Wafer flat alignment mark is at the bottom.

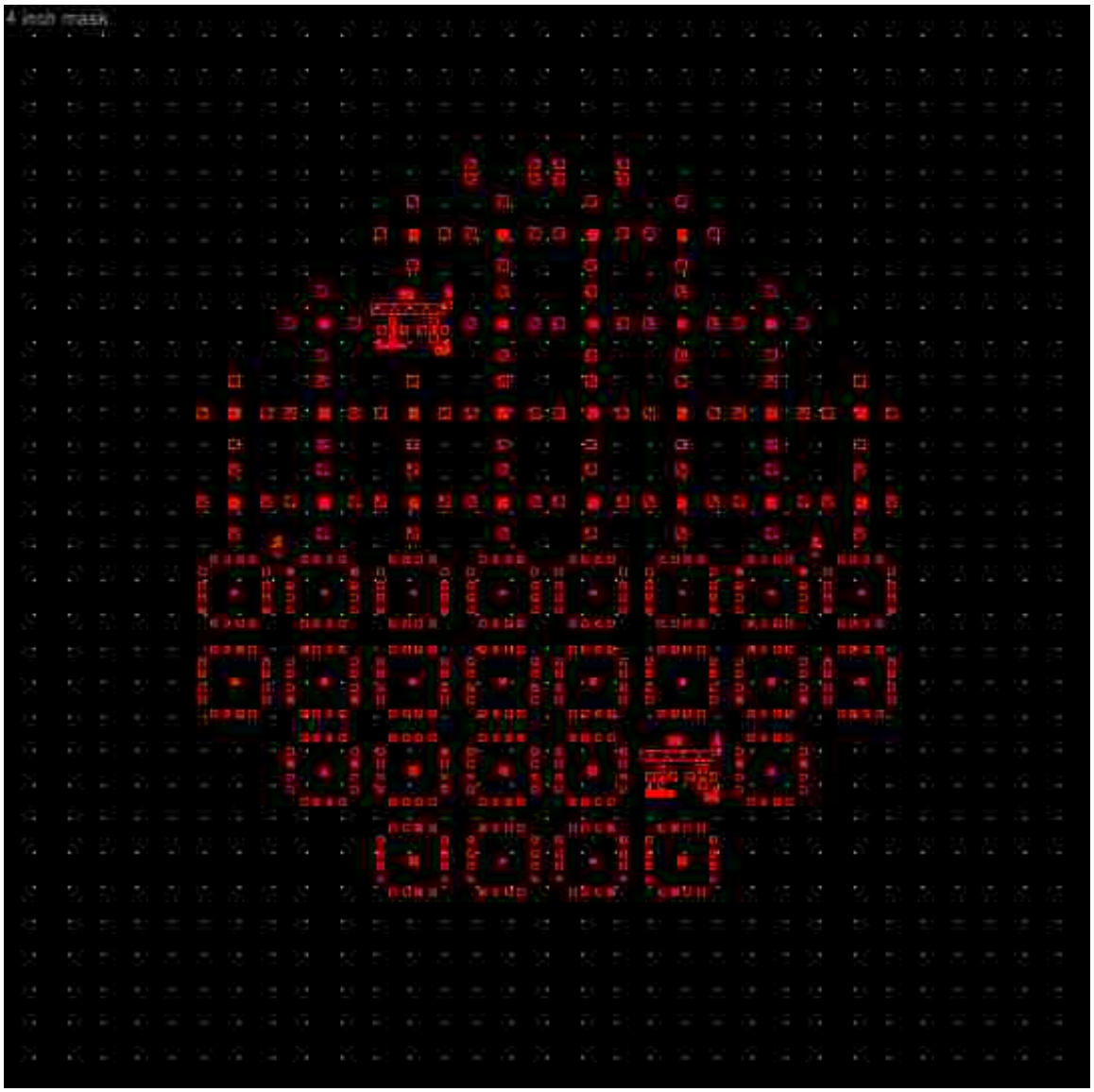

Figure A.2 Passivation mask (revision 1) layout for three-inch wafers (four-inch quartz AR chrome mask).

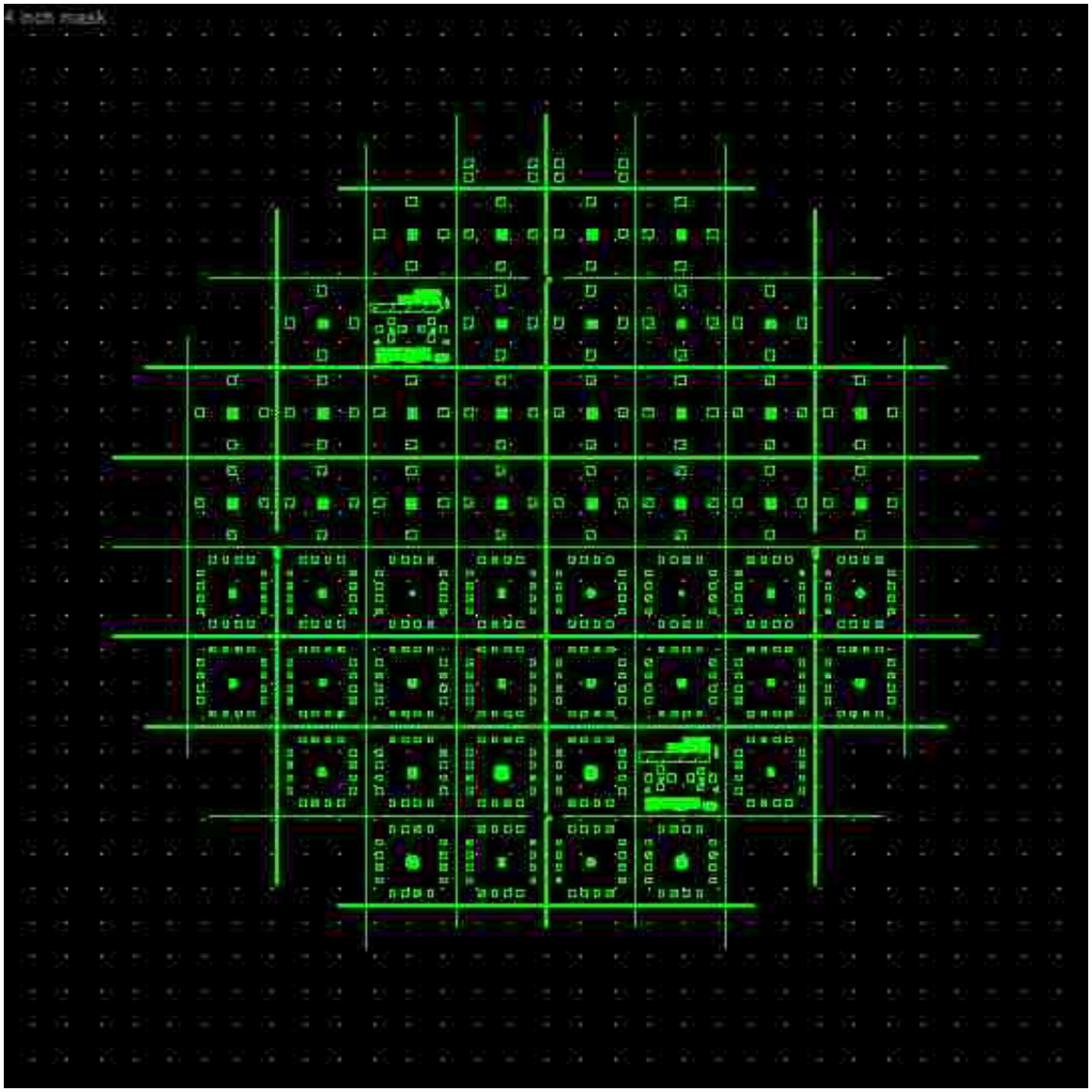

Figure A.3 Trench mask (revision 1) layout for three-inch wafers (four-inch quartz AR chrome mask).

A typical DEP MEA device layout for revision 1 is shown in Fig. A.4, where metal layer is dark yellow, passivation layer is red, and trench layer (SU-8) is green. Each device measures 8 mm by 8 mm.

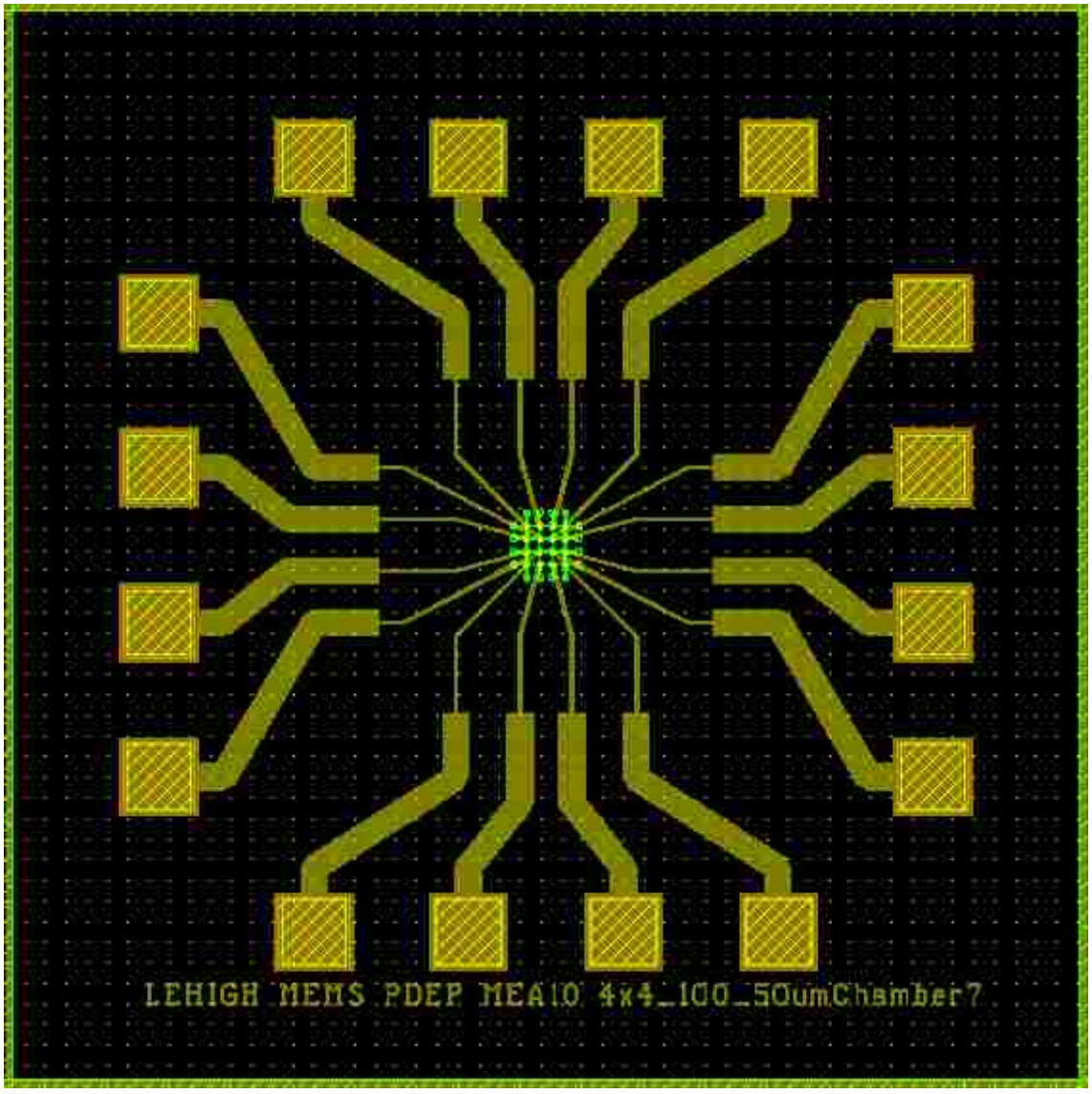

Figure A.4 Typical device die layout (revision 1) showing metal layer in dark yellow, passivation layer in red, and trench layer in green.

For design revision 2, the three layer four-inch masks are shown in Fig. A.5 (Metal), Fig. A.6 (Passivation), and Fig. A.7 (Trench).

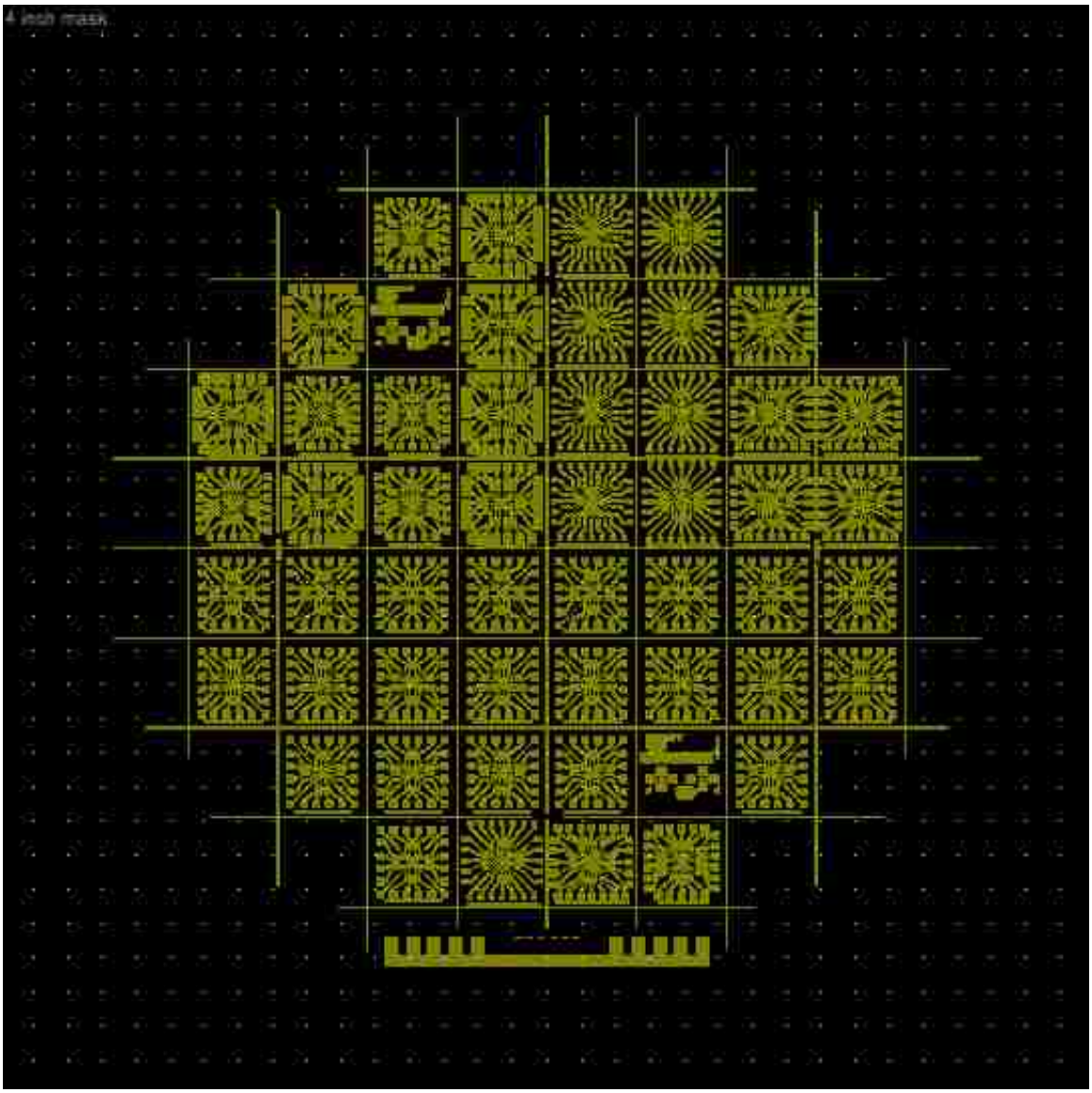

Figure A.5 Metal mask (revision 2) layout for three-inch wafers (four-inch quartz AR chrome mask). Wafer flat alignment mark is at the bottom.

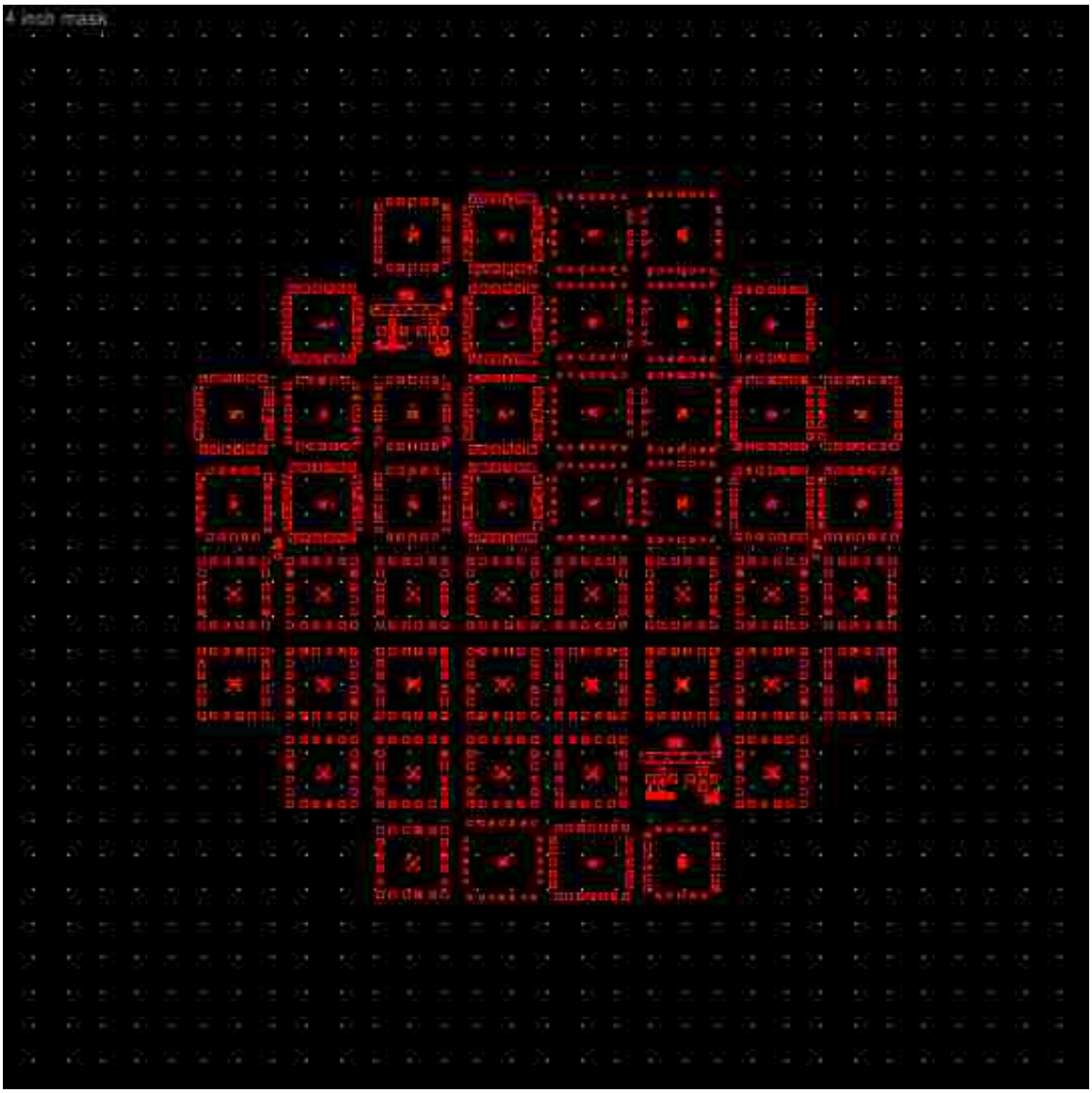

Figure A.6 Passivation mask (revision 2) layout for three-inch wafers (four-inch quartz AR chrome mask).

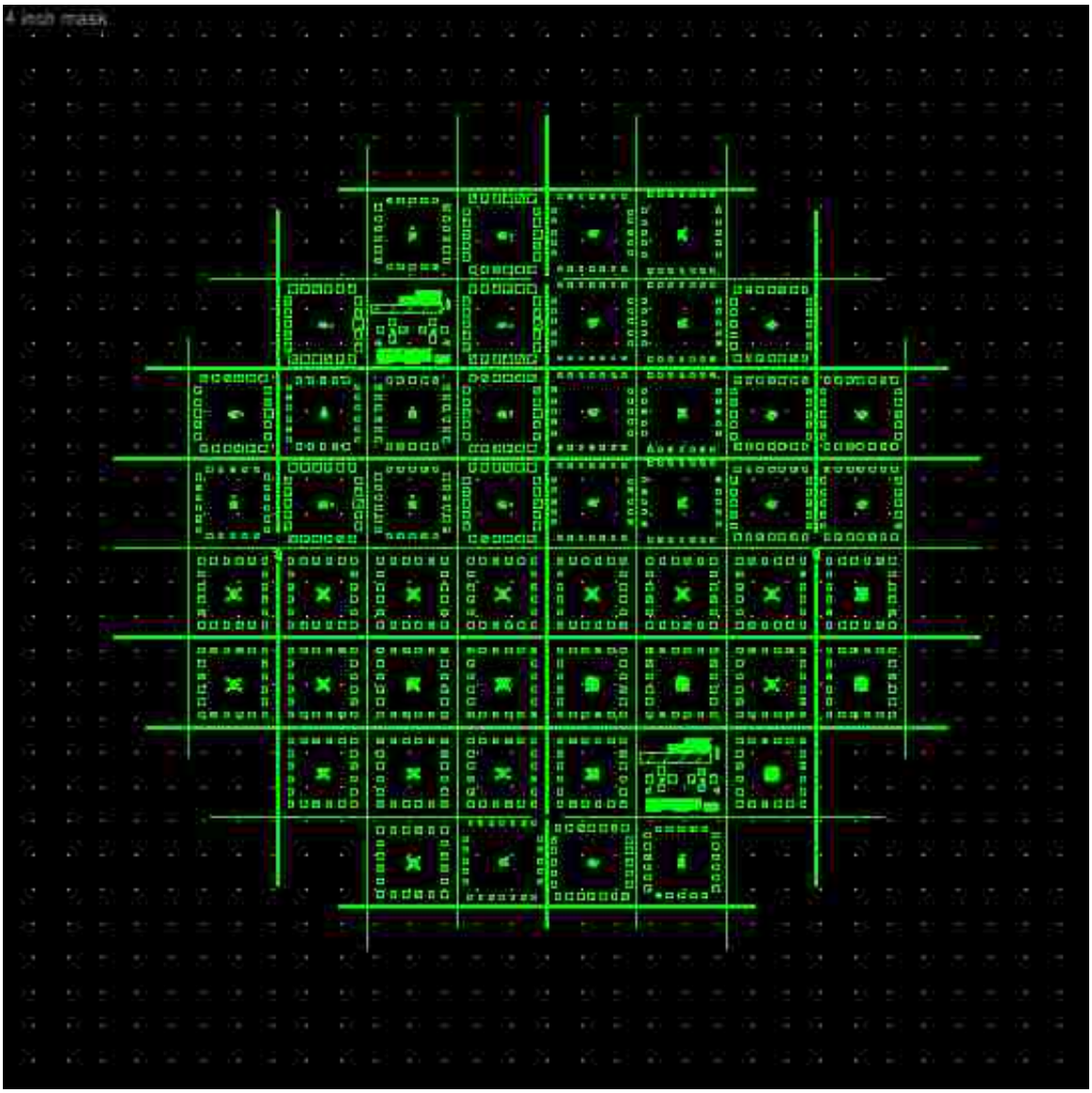

Figure A.7 Trench mask (revision 2) layout for three-inch wafers (four-inch quartz AR chrome mask).

A typical DEP MEA device layout for revision 2 is shown in Fig. A.8, where metal layer is dark yellow, passivation layer is red, and trench layer (SU-8) is green. Each device also measures 8 mm by 8 mm.

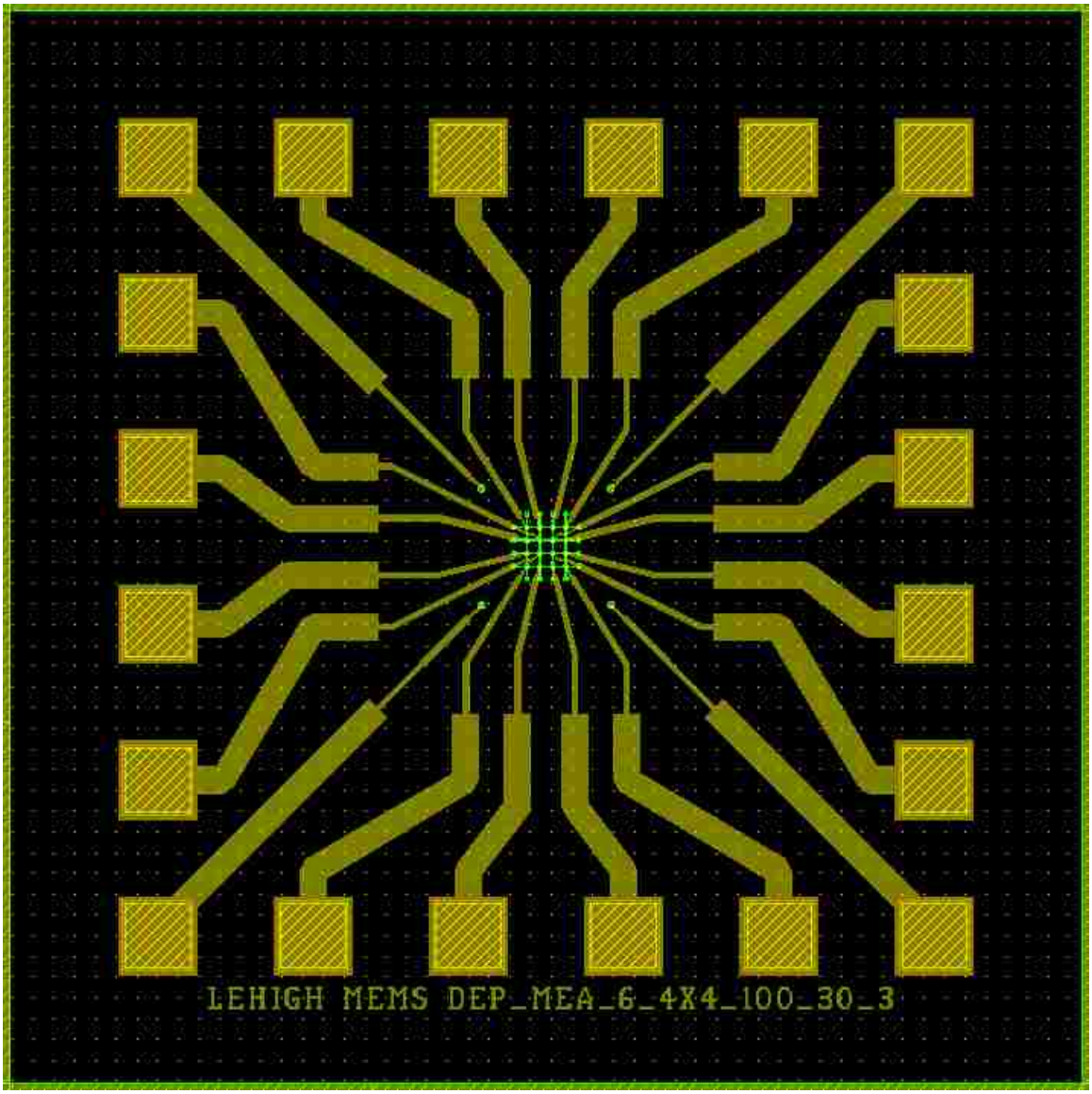

Figure A.8 Typical device die layout (revision 2) showing metal layer in dark yellow, passivation layer in red, and trench layer in green. Extra four reference electrodes are visible.

Two test dies (Fig. A.9) were included in the upper left and lower right of the wafer. Different resolution test structures for each layer, such as lines, trenches and microchambers; bulk metal resistivity test bars; replication of alignment marks; and misalignment check Vernier scales were designed in the test dies.

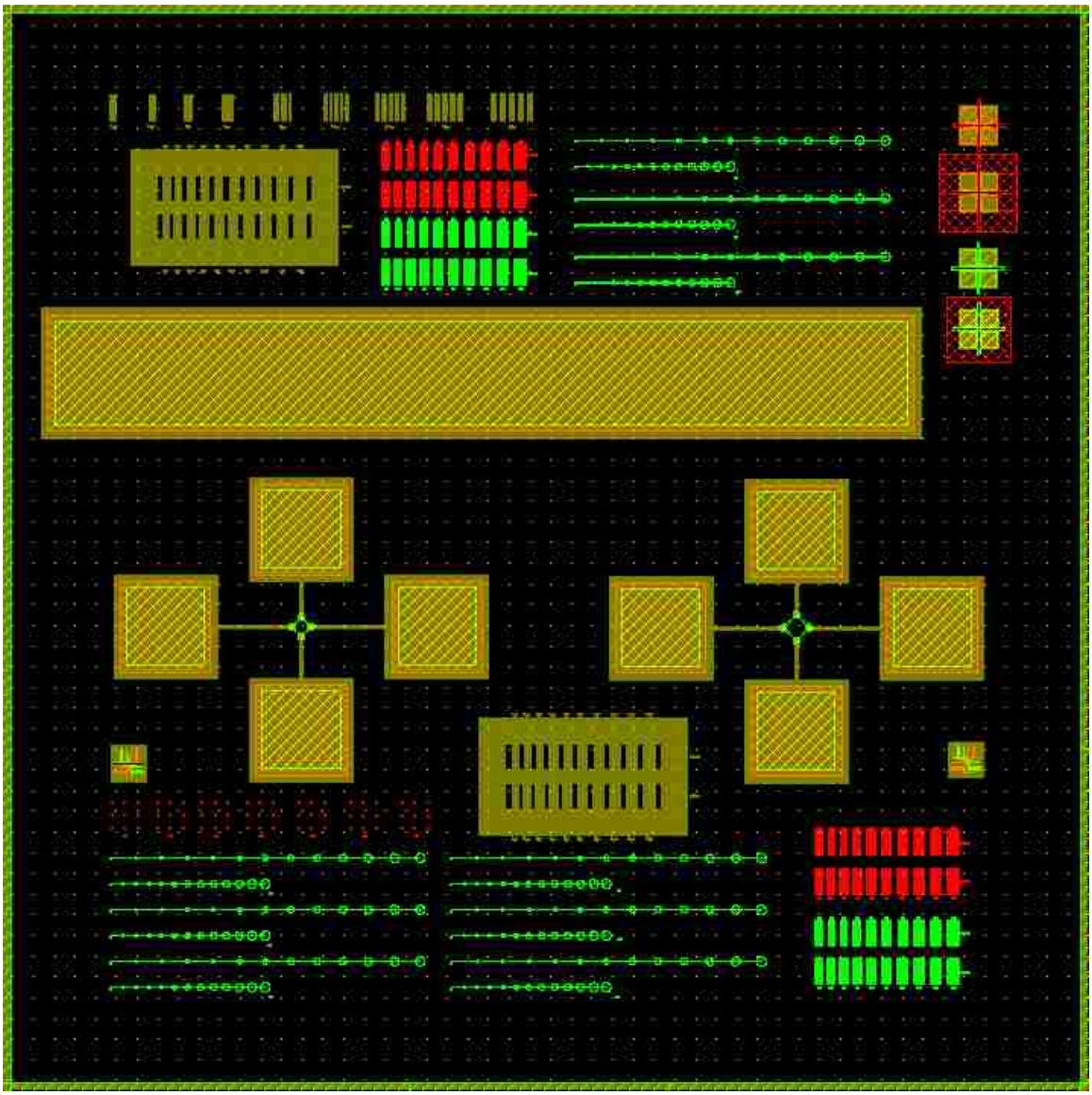

Figure A.9 Two test dies were included in the wafer for resolution (metal layer: dark yellow, passivation layer: red, trench layer: green), metal bulk resistivity ("big" metal bar), and misalignment check (lower left & right).

Appendix II: DEP MEA Fabrication Process

Starting Materials

1. 3-inch quartz glass wafers, two types:
    a. One primary flat 22mm+/-2mm, 500μm+/-25μm thick, polished both sides, rounded edges.
    b. Two flats, 1st flat 22mm+/-2mm, 2nd flat 11.18mm+/-1.52mm, 2nd flat 90° from 1st, 500μm+/-25μm thick, polished both sides, rounded edges.
2. 3-inch soda-lime glass wafers
    a. One primary flat 22mm+/-2mm, 550μm+/-50μm thick, polished both sides.
3. Mark wafer identification before process (Optional)
    a. Possible tools: diamond scribe or stainless steel scalpel.
    b. Good for identification of wafers during following fabrication process.

Glass Wafer Cleaning

1. 5-10% ammonium hydroxide NH_4OH (29%). 2L glass beaker if clean multiple wafers at one time with process boat; small plastic beaker if dip one wafer at a time.
2. Rinse with DI water for five times, blow dry.
3. Place cleaned wafers in one wafer carrier (only for cleaned wafers).
4. Dump ammonium hydroxide and rinse with fresh water.
5. Inspection under microscope, no dust or residue should be seen, unless there was some sticky dust on the wafer originally (sometimes even eye visible).

Metal Layer Photoresist Patterning (Metal Mask)

1. Warm up the hotplate to 110 °C
    a. Use aluminum blast-proof to stabilize temperature on hotplate surface.
    b. Monitor the temperature with spot-check thermometer.
2. Dehydration
    a. Place wafers to be processed in PP blue process carrier.
    b. 120 °C in convection oven for 20 min.
    c. Use Teflon (white) wafer cassette. (Teflon is suggested, but pp (blue) is ok for 120 °C, though it will become soft after 20 min.)
3. Vapor prime
    a. Process immediately after dehydration bake.
    b. 10 min in priming box with HMDS : XYlene in 1:1 ratio in the glass dish, approximately 12 drops of each, total.
    c. Use same wafer cassette.
    d. Start the UV light source of the aligner. (20 min warm-up) (N_2 valve first and then “power” button under the table)

e. Start power of the aligner. ("power" button on front panel)

4. Spin-coat negative tone lift-off photoresist
    a. AZ nLOF 2070 lift-off photoresist target thickness ~ 5 μm.
    b. 5000 RPM, 60 sec, low acceleration setting: 0.
5. Softbake
    a. Verify temperature with spot-check thermometer (110 ^{o}C+/-2 ^{o}C).
    b. Hot plate 110 ^{o}C for 60 seconds.
    c. Let cool 5 min. (rehydrate is not necessary)
6. Mask exposure
    a. Warm-up UV lamp by performing two to three 10 sec. exposure with no wafer.
    b. Turn on the pump for the aligner.
    c. Load PDEP MEA METAL mask.
    Shiny (glass) side against metal holder/ dark (chrome) side facing you
    Position mask with primary flat alignment mark on the right
    Place mask as close to the center as possible, press "vacuum" of the aligner.
    d. Carefully adjust height setting and record height setting.
    (2.00 for soda lime test wafers, 1.60 for quartz device wafers)
    e. Align wafer's flat to the primary flat alignment on the mask. (Only use the objective on the right)
    f. Press HP (high performance) and Vacuum Chunk. (Better resolution)
    g. Expose each quartz device wafer for 4.0 sec. @25 mW/cm^2. (or 100mJ/cm^2)
    For soda lime test wafers, 5*1.5sec=7.5sec. @25 mW/cm^2. (or 125*1.5mJ/cm^2)
7. Post exposure bake (PEB)
    a. Hotplate 110 ^{o}C for 60 seconds for each wafer.
8. Develop
    a. AZ 300MIF developer full strength. (600mL plastic beaker)
    b. Submerge for 2 min and agitate with gentle swirling motion.
    For soda lime test wafers, 1.5 min development.
9. Rinse and dry
    a. Rinse in DI water for 5 times.
    b. Blow dry with nitrogen
10. Microscope inspection
    a. Resolution test structures 2μm trenches should turn out, 2070 bridges on the second row may be peeled off from 5μm. 1μm structure on alignment marks should turn out.
    b. If failure, strip in Shipley 1165 or AZ 400T stripper (two bath, PTFE cassette), and repeat photoresist patterning.
    c. Actual thickness of photoresist is around 5.1 μm, measured with profilometer.

Oxygen Plasma Cleaning before Metal Deposition (Optional)

1. Clean possible photoresist residue after MIF 300 development.
2. 30-60 sec, 300 mtorr (actually ~380 on the front panel), 300 Watts, 50 sccm O_2.

Metal Deposition and Lift-Off

1. E-beam metal deposition total thickness of 340 nm.

   20 nm Titanium or 200 Å, as metal adhesion layer.

   300 nm Gold or 3000 Å, supposed to be 300nm, as the metal electrode layer.

   20 nm Chrome or 200 Å, as a sacrificial metal layer for better SU-8 adhesion in the following process.

   NOTE: To have better AU deposition quality (reduce pinholes), first 500 Å deposition speed can be controlled as 'slow'.

2. Lift-off
   a. AZ 400T or Shipley 1165. (Two 80 ^{o}C hot bathes, 1.5 to 3 hours, depending on the actually lift-off speed.)
   b. Rinse in DI water for 5 times.
   c. Do not let wafers dry and rinse thoroughly with IPA squeeze bottle.

PECVD Oxide Deposition

1. Plasma Enhanced Chemical Vapor Deposition (PECVD) silicon oxide deposition total thickness of 1μm at COT clean room.
2. Detailed procedure of PECVD at COT clean room is trained by technician.

Photoresist Patterning for PECVD Oxide Etch Mask (Passivation Mask)

- **AZ 9260**

1. Dehydration
   a. Place wafers to be processed in PP blue process carrier.
   b. 120 ^{o}C in convection oven for 20 min.
   c. Use Teflon (white) wafer cassette. (Teflon is suggested, but pp (blue) is ok for 120 ^{o}C, though it will become soft after 20 min.)
2. Vapor prime
   a. Process immediately after dehydration bake.
   b. 10 min in priming box with HMDS : XYlene in 1:1 ratio in the glass dish, approximately 12 drops of each, total.
   c. Use same wafer cassette.
   d. Start the UV light source of the aligner. (20 min warm-up) (N_2 valve first and then "power" button under the table)
   e. Start power of the aligner. ("power" button on front panel)
3. Spin-coat positive tone photoresist
   a. AZ 9260 (520CPS) positive photoresist target thickness ~ 6 μm.

b. 5500 RPM, 60 sec, low acceleration setting: 20.
c. Edge bead removal using Kimwipes (with Acetone) at 1000 RPM, set time = 0, keep pressing to start the spinner.

4. Softbake
   a. Convection Oven 95 °C for 15 min.
      Place wafer cassette upright so that wafers are lying flat during bake.
   b. Let cool and rehydrate at room temperature for 15 min.
5. Mask exposure
   a. Warm-up UV lamp by performing two to three 10 sec. exposure with no wafer.
   b. Turn on the pump for the aligner.
   c. Load PDEP MEA PASSIVATION mask.
      Shiny (glass) side against metal holder/ dark (chrome) side facing you
      Position mask with PASSIVATION text on top (i.e. away from you when mask is loaded)
      Place mask as close to the center as possible, press "vacuum" of the aligner.
   d. Carefully adjust height setting and record height setting.
      (200 for soda lime test wafers, 160 for quartz device wafers)
   e. Align to the corresponding mask alignment mark on wafer.
   f. Press HP (high performance) and Vacuum Chunk. (Better Resolution)
   g. Expose each quartz device wafer for 6.8 sec. @25 mW/cm^2. (or 170mJ/cm^2)
      For soda lime test wafers, also 6.8 sec exposure @25 mW/cm^2. (or 170mJ/cm^2)

      No post-exposure bake, but 5 min post exposure delay.
6. Develop
   a. AZ 400K Developer and DI water solution 1:4 mix. (2000ml glass beaker)
      Make sure DI water is not that warm. (Development at ~25 ºC)
   b. Submerge for 3 min and agitate with gentle swirling motion. (Teflon wafer cassette for multiple wafers at a time)
      For soda lime test wafers, also 3 min development.
7. Rinse and dry
   a. Rinse in DI water for 5 times.
   b. Blow dry with nitrogen
8. Microscope inspection
   a. Resolution test structures:
      2 μm lines and trenches should turn out;
      1 μm trenches should turn out;
      1 μm lines will possibly turn out.
   b. If failure, strip in AZ 400T stripper (two bath, 15 min each, PTFE cassette), and repeat photoresist patterning.
   c. Actual thickness of photoresist is around 6 μm under profilometer. (5.93-6.06 μm)
9. Hard bake

a. 95 °C in convection oven for 5 min, place wafer cassette upright.
   Take wafer out, let cool down a couple of min.
   Repeat the hard bake steps above 3 times. (Total 15 min hard bake)
   120 °C convection oven for 30 min, photoresist will melt.

   (AZ 9260 might start to melt from 110 °C)

10. Oxygen plasma cleaning before oxide etch if there is photoresist residue left
    a. 300 W RF power, 50 sccm O_2, 300 mTorr pressure (~370 mTorr displayed).
    b. 1-2 min.
    c. Microscope inspection: all pads should be clear of red photoresist residue, showing bare oxide layer color.

RIE Etch of PECVD Oxide

1. Pattern AZ 9260 photoresist as mask layer, followed by hard bake and oxygen plasma cleaning 1 min. (thickness of photoresist decreases from 6.0 μm to about 5.6 μm)
2. RIE plasma etching of PECVD oxide for 30-40 min at SFC cleanroom.
   CF_4: 30 on flow meter, 30*5*0.475(gas factor) =71.25sccm;
   O_2: 2.9 on flow meter, 2.9*1*1(gas factor) =2.9 sccm;
   RF power: 300 W;
   Pressure: 300 mTorr, ~360 displayed.
   Rotate the wafer after 15 min of etching to get evenly etched wafer surface.
3. Oxide layer should be etched completely (already over etched), almost no undercut. Step height measured now is approximately 4.7-4.8 μm with photoresist on.
4. Etch selectivity: 1 μm: 1.58 μm= 0.63: 1, oxide layer step height measured after stripping photoresist: 1.0-1.1 μm, etch complete.

PECVD Silicon Oxide RIE Etching at COT Cleanroom

Machine: TECHNICS MICRO-RIE SERIES 8000

Pump and gas (O_2 & CF_4) need to be open before running. (Switches are in another room, email the technician one day before work)

Pressure at rest: pump down to 50mTorr (0.05Torr).

Operation Setps:

1. Sol'N OFF, Vent ON, reaction chamber should open fast, load wafer, and fix edge with silicon pieces on the table.
2. Close chamber, Vent OFF, Sol'N ON, wait until pressure down to ~50mTorr.
3. Turn on Gas1 (O_2), set flow rate until chamber pressure reaches 125mTorr, turn off Gas1, and wait for pressure to reach 50mTorr.

4. Turn on Gas2 (CF_4), set flow rate until chamber pressure reaches 250mTorr, turn off Gas2, and wait for pressure to reach 50mTorr.
5. Turn on Gas1 and Gas2, pressure displayed should be ~280mTorr. Turn on power after the timer is set and when you are ready to etch. Power displayed is 10-20 Watts, actually is 80/90-100 Watts.
6. Chamber pressure will drop slightly at the end of etching. When etching is complete, turn off power, Gas1 and Gas2, wait until pressure is ~50mTorr.
7. Sol'N OFF, Vent ON. Take wafer out when the chamber is open.
8. Load another wafer if continuing…
9. Or, close chamber, Vent OFF, Sol'N ON, let machine pumping.

PECVD Silicon Oxide RIE Etch Rate Test

Table A.3 Silicon oxide thickness measurement with ellipsometer before and after test RIE runs.

Before etch	Ellipsometer at 70° laser angle: (Å)		Ellipsometer at 70° laser angle: (Å)
Sample 1:	2777	Sample 2:	217
	5609		3084
	8440		5880
	11272		**8712**

After 1 min etch	Ellipsometer at 70° laser angle: (Å)	Ellipsometer at 60° laser angle: (Å)		Ellipsometer at 70° laser angle: (Å)	Ellipsometer at 60° laser angle: (Å)
Sample 1:	1695	2006	Sample 2:	1867	2190
	4527	4698		4698	4882
	7359	**7390**		**7530**	**7573**
	10190	10081		10362	10265

So tested PECVD oxide etch rate: ~1100 Å /min (18.33 Å /sec), or 110 nm/min (1.83 nm/sec).

Concerning the oxide thickness on wafer is approximately 0.9 μm (9000 Å /900 nm), estimated etching time (etching complete guaranteed) is ~8.5 min. PECVD oxide (silicon substrate) sample did etch complete after 8.5 min.

However, different for wafers, after 20 min continuous etching, colorful oxide layer still can be observed on metal pads, after another 10 min etch (total 30 min etching), pads are clear, and etch is complete. Actual etching time maybe between 28 min and 25 min. There is still photoresist left on the chip after 30 min of etching.

Possible reason for longer than expected etch time: photoresist residual on pads.

Photoresist Stripping

Strip the photoresist mask for PECVD oxide etch.

1. AZ 9260 strip in AZ 400T stripper for 30 min at 80 ^{o}C (two bath, PTFE cassette).
2. Rinse in DI water five times.
3. Blow dry with Nitrogen.

SU-8 Trench Layer Patterning (Trench Mask)

Fresh SU-8 should be prepared in small bottle on the bench at least two days earlier to let it warm up slowly and outgas.

1. Rinse wafers with DI water five times before this process to clean wafer surface.
2. Warm two hotplates: one hotplate to 100 °C, one hotplate to 70 °C.
3. Dehydration
    a. Place wafers to be processed in PP blue process carrier.
    b. 120 ^{o}C in convection oven for 20 min.
    c. Use Teflon (white) wafer cassette. (Teflon is suggested, but pp (blue) is ok for 120 ^{o}C, though it will become soft after 20 min.)
4. Spin-coat negative tone photosensitive epoxy
    a. SU-8 3010 target thickness 5 to 6 μm coverage.
    5000 RPM, 60 sec, low acceleration setting, acceleration = 0
    b. Edge bead removal using Kimwipes (with Acetone) at 1000 RPM, set time = 0, keep pressing to start the spinner.
    c. After spin-coating, SU-8 surface should be rather smooth.
    d. Actual photoresist thickness measured to be around 8.4 μm.
    e. Cover wafer with a glass petri dish and let it sit on bench top overnight to relax, and reduce internal stress.

    <u>After spin-coating, SU-8 surface should be rather smooth.</u>
5. Softbake
    a. Verify temperature with spot-check thermometer (+/- 2 ℃)
    b. Place wafer on 4-inch diameter, 2mm thick aluminum block
    c. Hot-plate 70 ℃ for 10 mins, remove wafer and let cool 4 min.
    d. Put wafer back on the hotplate for another 5-7 min.
    e. Let cool 4 min.

    <u>After Softbake, SU-8 surface should be generally smooth.</u>
    <u>During Softbake, bubble-like bumps may appear on SU-8 surface because of photoresist outgasing, high bake temperature (95 ℃), and/or high humidity. So the only baking temperature chosen is 65 ℃. That's also the reason for fresh SU-8 to outgas for 2 days before processing and overnight relax after spin-coating.</u>

6. Mask Exposure
    a. Warm up UV lamp by performing two 10 sec. exposures with no wafer
    b. Load PDEP MEA TRENCH mask
       Shiny side against metal holder / dark side facing you
       Position mask with TRENCH text on top (i.e. away from you when mask is loaded)
    c. Carefully adjust height setting and record height setting
       (200 for soda lime test wafers, 160 for quartz device wafers)
    d. Align to the corresponding mask alignment mark on wafer
    e. Press HP (high performance) and Vacuum Chunk to ensure straight sidewalls.
    f. Using dedicated UV filter for SU8,
       expose each wafer for 20.00 sec @ 25 mW/cm^2. (or 500mJ/cm^2)
7. Post Exposure Bake
    a. Place wafer on 4-inch diameter, 2 mm thick aluminum block.
    b. Hot-plate 70 ℃ for 60 seconds.
    c. Hot-plate 100 ℃ for 60 seconds.
    d. Hot-plate 70 ℃ for 60 seconds.
    e. Let cool 4 min
8. Develop
    a. SU-8 Developer full strength.
       Typically, use 200 ml in 2000 ml beaker
    b. Submerge for 60 seconds and gently swirl.
9. Dry
    a. Gently blow dry with nitrogen pointed at the center of the wafer.
    b. DO NOT rinse in DI water.
10. Rinse & spin
    a. Place wafer on spin-coater.
    b. Using small pipette cover wafer with a puddle of fresh SU-8 developer, and wait 10 seconds.
    c. Spin at 1500 RPM for 60 seconds to dry.
11. Inspection (optical microscope)
    a. 2 μm trenches seem to have residue left, all the other trenches should look clear if there's Cr layer underneath. But 5 μm and 7 μm trenches still seem to have residue if there's only oxide layer underneath. Microchambers should be clear with possible transparent residue on the edges.
    b. If failure, SU-8 can be slowly stripped with oxygen plasma RIE as long as it has not been hard baked.

Clean & Harden

1. 4 min oxygen plasma descum in RIE
   50 sccm oxygen, 300W power, 300 mTorr pressure
   SU-8 etched during this 4 min is 1.1-1.2 μm.

2. Hardbake 120 ℃ dehydration convection oven for 20 minutes.

Pad Etch

(This process should be performed after SU-8 patterning because SU-8 has poor adhesion on gold)

Chromium Etchant is acidic and produces toxic fumes. Be careful. Check the MSDS.

1. Place a small amount of Transene Chomium Etchant 1020 **(prefer used etchant to fresh etchant)** in a glass petri dish. **(Etching is very fast!)**
2. Prepare a second dish or beaker with DI water.
3. Place the wafer (with SU-8 mask) in the Cr etchant and wait 10 seconds.
    a. The pads will change from silver color to gold color. (Cannot be seen in etchant)
    b. Remove the wafer and transfer immediately to the water bath
    c. Do not over etch or the metal pads will start to peel off. **(Cr etchant will migrate through pin holes in the gold layer)**
    d. Cr etchant could also penetrate through pinholes in the oxide layer.
4. Rinse carefully in DI water 5 times.
5. Blow dry gently with nitrogen.
6. Inspect wafers under microscope to see if all the pads and open vias have been cleared. If not, put the wafer back into Cr etchant for another **5** seconds. **(Estimated total etch time: 15-20sec)**
7. If the undercut in PECVD oxide layer and SU-8 layer is properly controlled during previous processes, the undercut (over etch) in Cr layer should also be very small and acceptable.

Protection Layer & Wafer Dicing

1. Dehydration
    a. 120 ℃ in convection oven for 20 min.
    b. Use Teflon wafer cassette.
2. Vapor prime
    a. Process immediately after dehydration bake.
    b. 10 min. in priming box with HDMS : Xylene in 1:1 ratio in the glass dish.
    c. Use approximately 12 drops of each, total.
    d. Start the UV light source for the aligner (20 min warm-up).
3. Spin-coat positive tone photoresist as protective layer
    a. AZ 9260 target thickness 6 μm coverage,
    5500 RPM, 60 sec, low acceleration setting, acceleration = 20.
4. Softbake
    a. Convection oven 95 ℃ for 15 min.
    b. Let cool and rehydrate for 15 min.
5. Flood Exposure

a. Warm up UV lamp by performing two 10 sec. exposures with no wafer.
b. Flood expose each wafer three times for 5 seconds at 25 mW/cm^2 with a 60 second wait between exposures.
Note: nitrogen bubbles will form in resist if exposure dose is too high

6. Wafer Dicing
    a. Follow instructions from SFC cleanroom technician for dicing the wafer and use 8.000 mm for X-axis and Y-axis index. **(Or send wafers out for commercial dicing service)**
7. Remove resist
    a. Develop for 6-10 minutes in AZ 400K 1:4 mix with DI water with plastic tape on.
        i. Carefully handle wafer during rinsing, it can easily break into die pieces.
        ii. Load a blank wafer directly underneath the diced device wafer (in the same slot in the cassette) to provide mechanical support.
8. Rinse carefully in DI water 5 times.
9. Blow dry gently with nitrogen. (Be careful of the separated dies)
10. Remove residue.
    There may be photoresist residue on die surface,
    a. Prepare two petri dishes: one with acetone and one with IPA.
    Soak wafer/die in acetone for 5-10 minutes to dissolve remaining resist.
    b. Transfer wafer/die to IPA without letting any acetone dry on wafer (it leaves a residue that is hard to remove).
    c. Soak wafer/die in IPA for 5-10 minute.
11. Rinse carefully in DI water.
    Blow dry gently with nitrogen.

Appendix III: DEP MEA Device Packaging Process

As has been briefly described in section 2.4, Side-Brazed Dual In-Line Ceramic Package DIP (Spectrum Semiconductor Materials, Inc. CSB02491) was used for the device packaging process. A three-mm-diameter hole was first drilled at the center, using a diamond tip, at SFC mechanical shop of Lehigh University (Fig. 2.15(b)). After the DEP MEA chip is attached, with PDMS pad underneath, to the DIP package, wire bonding is performed to connect the metal pads on the MEA chip and headers on the ceramic package. A wedge bonder (Tempress Model 1100 with CoorsTek 2G30-2030 bonding wedge) and gold bonding wire (American Fine Wire Corp. 0.001 inch diameter, 99.99% gold with trace beryllium) was used for the wire bonding. The bonding diagram for first generation of DEP MEA devices is shown in Fig. A.10.

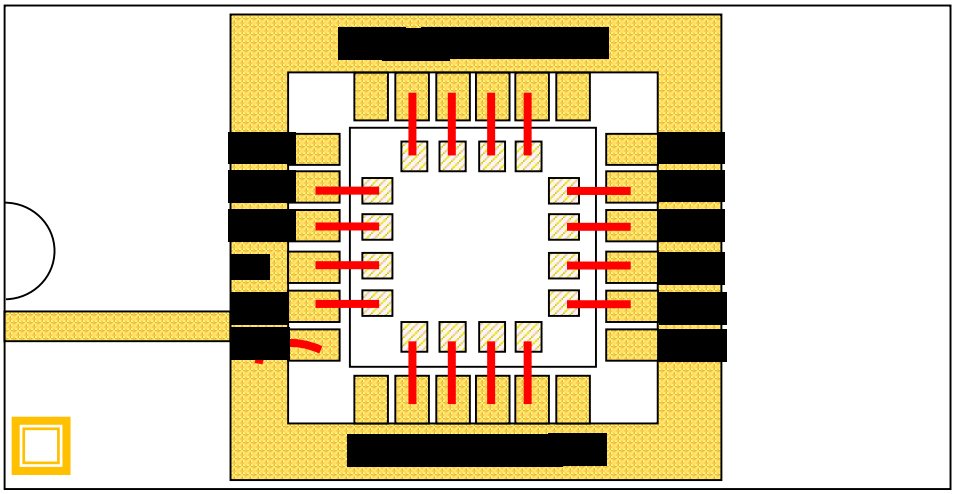

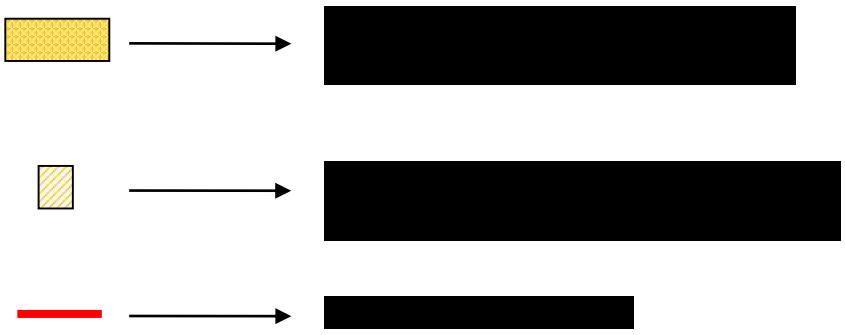

Figure A.10 Wire bonding diagram for 1st generation of DEP MEA chips in a 24-pin DIP package. In addition to the 16 pad-to-header connections, header #3 on the DIP package is specifically bonded to the metal skirt, which functions as the reference electrode, exposed to cell culture media.

For the first generation of DEP MEA chips, 16 wire bonding pads are connected to 16 electrodes respectively, but no reference electrode/pad was designed; therefore, gold "skirt" on the ceramic package was utilized as the reference electrode of the MEA, and it was specifically bonded to one of the headers (header #3) on the package, as shown in Fig. A.10, above. 16 gold pads on the DEP MEA chip, representing 16 electrodes, were bonded to 16 headers of the ceramic package, respectively.

After wire bonding, the devices were encapsulated carefully, with Dow-Corning Sylgard 184 (silicon elastomer PDMS). A disposable 5 mL syringe was filled with liquid PDMS, and used with a blunt needle to encapsulate each device. Special care was taken to apply the encapsulation material only to the outer edges of the chip, covering the wirebonds while leaving the central area open. Because liquid PDMS is self-leveling, small amount was dispensed and baked (65 ℃, 20 min) to cure for repeated dispense-cure-dispense cycles.

A five-mm-thick PDMS mold was pre-cured inside a polystyrene petri dish lid (Corning 430165 35mm), with microfluidic Tygon microbore tubing (Cole-Parmer) embedded (Fig. 2.15(b)). A square cutout (chamber) was made at the center of the PDMS mold, and attached on the DIP package with uncured PDMS to form a neuronal culture chamber. This PDMS mold covers the top

and bottom metal skirts of the DIP package, but leaves the left and right metal skirts open, exposed to neuron culture media later, as the reference electrode.

For second generation of DEP MEA chips (section 2.3.2), four reference electrodes/pads were designed; therefore, the corresponding wire bonding pads of the chip were bonded to four metal headers of the DIP package (3, 9, 15 and 21), respectively. The wire bonding diagram for second generation of devices is shown in Fig. A.11.

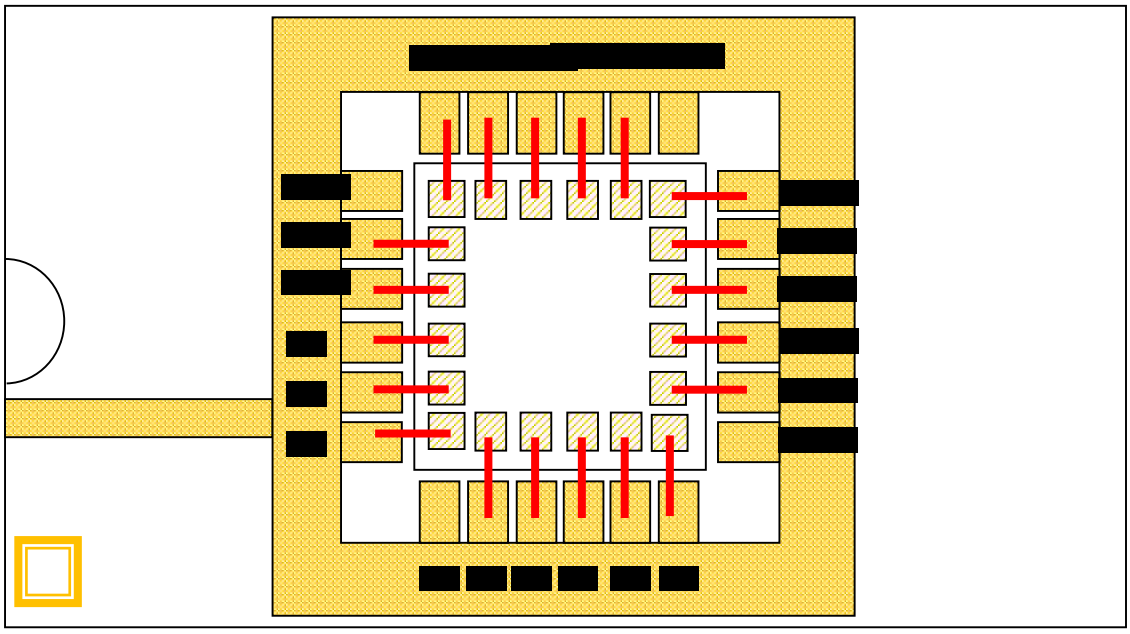

Figure A.11 Wire bonding diagram for 2nd generation of DEP MEA chips in a 24-pin DIP package. In addition to the 16 pad-to-header connections, four headers (#3, #9, #15, and #21) on the DIP package are bonded to the reference pads.

The metal skirts are wholly covered by the PDMS chamber mold, while glued onto the DIP package with uncured PDMS, for the second generation of devices. Finally, a commercially available ITO (Indium tin oxide)-coated cover slide (Sigma-Aldrich Co. LLC.), was used to cover the PDMS chamber during the active neuronal recruiting process. The ITO slides are connected to the ground signal by gluing them to wires or probe tips with silver-filled conductive epoxy paste.

Appendix IV: Mouse Hippocampal Neuron Dissociation and Culture Protocol

Primary mouse/rat hippocampus tissues are purchased from BrainBits, LLC. (Springfield, IL), and more information about the neuron culturing protocol can be found on the website:

https://store-4bc41.mybigcommerce.com/primary-neuronal-cell-culture-protocol-from-hibernate-tissue/

Generally, the process of culturing hippocampal neurons is to dissociate singular hippocampal neurons from hippocampus tissue through chemical (Hibernate medium with papain solution) and physical (triturating) methods, then seed the singular neurons onto different culture surfaces, as shown in Fig. A.12.

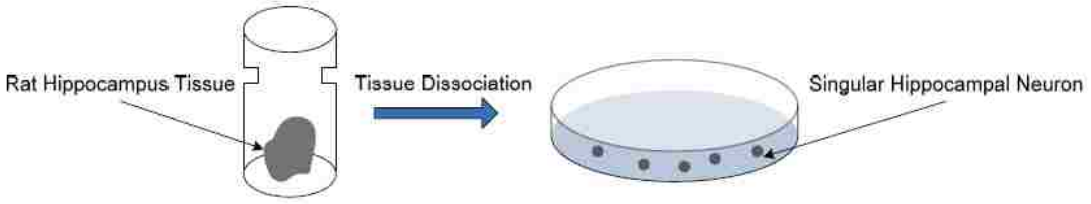

Figure A.12 Schematic diagram of culturing hippocampal neurons from rat hippocampus tissue.

Preparation

(1) Turn on the water bath and set at 30 ºC.
(2) Take out ① Hibernate E – Ca without B27 medium, ② NbActiv4/NbActiv1 neuron culture media, ③ Papain powder (Worthington Biochemical, NJ, PAPL, LS003119), and ④ B27/Neurobasal + 0.5 mM glutamine + 25 μM glutamate (12 mL media provided by BrainBits in a 15ml tube) from refrigerator.
(3) Put toolbox into hood with U.V. light on, including 2-3 15 mL Falcon centrifuge tubes.
(4) Make sure all the necessary material and tools are available. (This can be done days earlier)

Making papain solution:

(1) Get 5 ml ① into a 15 mL Falcon tube.
(2) Prepare 10 mg ③ with an electric balance and weighing paper—0.010 g.

(3) Mix the 10 mg powder into 5mL ① (2 mg/ml), vortex for approximately 10 minutes (well mixed until most solids are dissolved) and get the papain solution.

Filtering the papain solution:

(1) Pour the papain solution into a petri dish.
(2) Suck the solution with a syringe + syringe filter, leave the bubbles remained on the bottom of the petri dish.
(3) Inject the solution into a new sterilized 15 mL Falcon tube, now the solution should be approximately 4.5 mL. (Papain solution ready)

Dissociating hippocampus tissues:

(1) Flip the sample tube containing hippocampus tissues several times and dump all the tissues and B27/Hibernate medium into a petri dish. (Make sure all the tissues are dumped out)
(2) Obtain the hippocampus tissues with a sterilized 9-inch Pasteur pipette (Fisher Scientific, 13-678-20C) and transfer the tissues to the papain solution prepared above.
(Avoid breaking up the tissues and suck as little medium as possible)
(3) Put the 15 mL Falcon tube into a 50 mL Falcon tube with approximately 20 mL sterilized DI water inside, as shown in Fig. A.13.

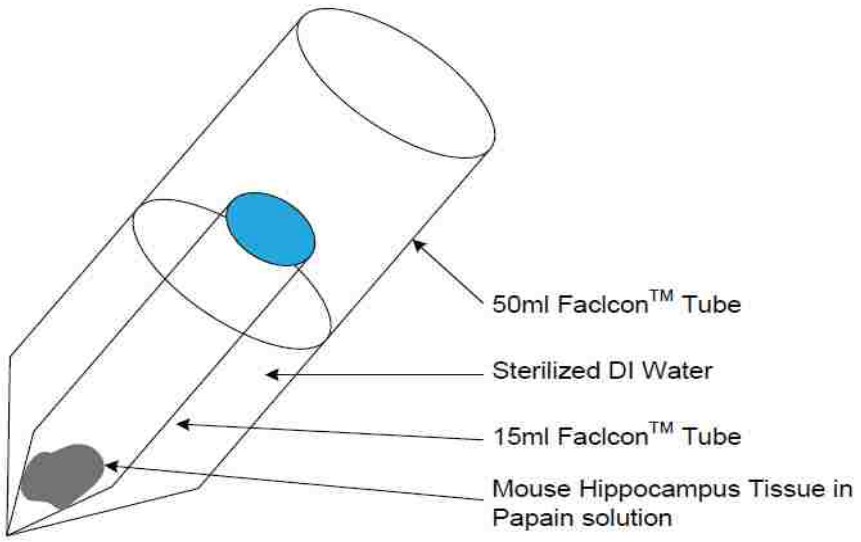

Figure A.13 Schematic diagram of dissociating hippocampus tissues in Hibernate medium with papain. To avoid contamination from the water in a water bath, a small tube (15 mL) with the brain tissue was placed inside a bigger tube (50 mL) with sterilized DI water inside.

(4) Make sure the water temperature is stabilized at 30 ^{o}C, put the 50 mL Falcon tube into the water bath for 30 minutes (use glass beaker as a holder).
(5) Take out the tube from the water bath, usually the hippocampus tissues are now at the bottom of the tube. Obtain the hippocampus tissue from the tube with another sterilized 9-inch Pasteur pipette, and dispense it back into the petri dish with 2 mL B27/Hibernate medium in step (1).
(6) Use 1 mL plastic pipette tip (P1000) to triturating until most of the tissue pieces are dispersed. Be careful not to create bubbles.
(7) Transfer all the medium (with 1 mL pipette) with triturated tissues into a new sterilized 15 mL Falcon tube.
(8) Let undispersed pieces settle down by gravity for 1 minute, and transfer the supernatant into a new sterilized 15 mL tube.
(This step can be skipped if all the tissue pieces have been dispersed or some tissue pieces have been lost during the previous processes)
(9) Centrifuge at 200 g for 1 minute and discard the supernatant. Now the hippocampal neuron cell pellet should be at the bottom of the tube.

Counting cells:

(1) Add 1 ml ④ (provided by BrainBits with hippocampus tissues) to resuspend the neuron cell pellet.
(2) Counting neuron cell density using a hemocytometer. (10 μL cell solution + 90 μL trypan blue, C=X*10^5/mL)

Seeding cells:

(1) Add 3 mL ② NbActiv4/NbActiv1 into cell culture petri dishes or 1 mL ② into packaged DEP MEA devices, and seed hippocampal neurons according to desired density. For hippocampal neurons,
    a. The normal volume seeding density is 1.0 x 10^5/ mL.
    b. The normal area seeding density is 1.6 x 10^4/ cm^2.
(2) Incubator condition set: 37 ^{o}C, 5% CO_2.

Primary Astroglial Culture

(1) The tissue dissociation process for glial cell culture is the same as for neurons. After centrifugation, the astroglial cell pellet is resuspended in 1 mL glial cell culture media NbASTRO.
(2) The glial cells are also seeded on different culture substrates, such as petri dishes and poly-d-lysine (PDL) coated cover slides, according to desired seeding density. Glial cells are normally cultured at 7.5 x 10^4/cm^2.
(3) Incubator condition set: 37 ^{o}C, 5% CO_2. Glial cells will be 80-90% confluent after 10-14 days, and ready to harvest/pass.

Appendix V: Immunocytochemistry (ICC) Neuron/Glial Staining Protocol

General overview of ICC cell/tissue staining procedure (direct/indirect)

1. ***Fixation:*** *In order to maintain the integrity of the cells (keep expression of cells), the cells' proteins must be chemically cross-linked in a formaldehyde, ethanol or methanol solution.*
2. ***Permeabilization:*** *In order to poke holes in the membrane of cells to allow antibody (Ab) to penetrate into cell body. Solutions such as light detergent are usually used. This step is not needed if the binding protein is on the surface of the cell.*
3. ***Blocking:*** *In order to decrease non-specific binding of Ab (increase signal-to-noise ratio), blocking is performed through the treatment of a high protein solution. The species of the second Ab must be known in order to determine the appropriate blocking agent.*
4. ***Ab incubation****: incubation of cell sample with direct or indirect staining Abs.*

   Direct ICC → Rinse → Visualize

   Indirect →Rinse →Second Antibody →Rinse →Visualize
5. ***Notice****: Special care should be taken while changing media between various steps, to avoid neurons being blown away.*

Detailed neuron/glial ICC staining protocol

1. Add 3.7% formaldehyde (dilute from 37% stock with PBS) or 4% paraformaldehyde (also diluted with PBS), to completely cover the chip/slide sample that will be stained for the glial fibrillary acidic protein (GFAP) and/or neuronal β-tubulin. Let sample soak in solution for 20 minutes -1 hour.

   GFAP is expressed in glial cells, whereas β-tubulin is expressed in neurons. Make sure the paraformaldehyde and formaldehyde is disposed of in the formaldehyde waste container next to the sink (brown bottle).

2. Rinse samples in PBS (phosphate buffer saline) twice for five minutes each time. Note the PBS doesn't need to be sterile.

3. Pipette 0.1% Triton X-100 so the chip/slide sample is completely covered for 15 minutes. Note that the Triton (light detergent) can be reused (centrifuge tube in the refrigerator for used Triton X-100).
    a. This step is for permeabilization.

4. Rinse samples in PBS twice for five minutes each time.

5. Add 10% Normal Goat Serum (NGS) so the chip/slide sample is completely covered for 15 minutes. Note that the NGS can be reused (centrifuge tube in the refrigerator for used NGS).
    a. This step is for blocking.
    b. NGS was changed to 0.01% Triton X-100 in 1% bovine serum albumin (BSA) in most of the later ICC procedure.

6. Rinse samples in PBS twice for five minutes each time.

7. Add α-GFAP to the glial staining sample (1:500 dilution with 10% NGS) and α-β tubulin to the neuron staining sample (1:1000 dilution with 10% NGS) and incubate overnight at 4°C (refrigerator). α-GFAP and α-β tubulin can both be added for simultaneous glial and neuron staining.
    a. 10% NGS was replaced with 0.001% Trition-X100 in 1% BSA for most of the later ICC experiments.

    If the small circular glass cover slide sample is used in the experiments, the antibody solution (50 μL) can be pipetted onto a piece of parafilm in a petri dish, and the slide can be placed over the antibody solution (cells facing down immersed in liquid), with a damped paper towel attached in the dish lid. (Ab incubation can also be performed at 37˚C for 1 hour or room temperature for 4 hours, depending on the temperature).

8. After Ab incubation, rinse samples in PBS twice for five minutes each time.

9. At this point, if using direct primary fluorescent α-β tubulin and/or α-GFAP Abs, the sample is ready to be visualized. View under a fluorescent microscope (green filter for neurons, red filter for glial cells) with some PBS covering the chip/slide sample.

10. If using indirect Ab staining, such as the situation described as follows, after the α-GFAP (primary Ab) staining sample has been rinsed in PBS, add Goat α-Rabbit 2˚ Alexa 488 (GAR-488) at a 1:50 dilution with PBS. As described above (step 7), if the α-GFAP staining sample is a coverslide in the experiment, the secondary antibody solution can be added onto a parafilm piece in a petri dish, and the sample slide can be placed over the antibody solution (cells facing down immersed in liquid), with a damped paper towel attached in the dish lid.
    a. Because Goat α-Rabbit 2˚ Alexa 488 (GAR-488) is used as the secondary Ab, whose species is goat, 10% Normal Goat Serum (NGS) is used as the blocking agent, which is from the same species.

11. Incubate the secondary Ab for 30 minutes at 37ºC. (unsterile incubator)

12. Rinse samples in PBS twice for five minutes each time.

13. Visualize sample under a fluorescent microscope (green filter for neurons, red filter for glial cells), with some PBS covering the chip/slide sample.

Note: In most of the later experiments, primary antibodies, including Alexa Fluor-labeled, monoclonal neuronal class III β-Tubulin (TUJ1) (Covance; 1:500, in PBS containing 0.01% Triton X-100 and 1% BSA) and mouse monoclonal, Cy3-labeled, anti-glial fibrillary acidic protein antibody (GFAP-Cy3, 1:500, in PBS containing 0.01% Triton X-100 and 1% BSA; Sigma-Aldrich), were used for direct neuron and glial ICC, respectively.

DAPI nuclei staining for individual cell recognition

If individual cells (neuron or glial) need to be identified, DAPI (4',6-diamidino-2-phenylindole) staining will be performed, which binds strongly to DNA.

1. DAPI (4',6-diamidino-2-phenylindole) diluted at (1:1000) 2 mg/ml concentration with PBS or DI water.

2. Sample immersed in DAPI solution for 2 min.

3. Rinse sample with PBS twice (5 min each).

4. Cover sample with PBS and visualize under a fluorescent microscope (blue filter).

Appendix VI: Live/Dead Cell Staining Protocol

1. Make up the stain solution.

The live stain is Calcein AM and the stock concentration of the vial is 4 mM. The working concentration is 2 μM or a 1:2000 dilution of the stock (for every 2 mL of stain solution, add in 1 μL of the stock). The dead stain is Ethidium homodimer, the stock is 2 mM and the working concentration is 1 μM (again a 1:2000 dilution).

2. Remove cell culture media from the sample. Rinse gently with PBS one time.

3. Pipette stain solution to cover the sample. Cover with a box or put in a drawer for 15 minutes (room temp).

4. Remove stain solution and replace with fresh cell culture media.

5. View under epifluorescence and capture images. (Each stain excites at a different wavelength Calcein AM emits green light and Ethidium Homodimer emits red)

Appendix VII: Preliminary pDEP Cell Trapping Experiments and Microstructure Cell Patterning Study

Before the DEP MEA device design, in order to explore the active recruitment of cells to electrodes with positive DEP, and to investigate the efficacy of cell patterning with microstructures, we have designed and fabricated a specialized multi-electrode array test device. The material structure and fabrication process of this test device is the same as the DEP MEA chips. The fabricated MEA test device is shown in Fig. A.14, it has one "big" square electrode and individual electrode sites and arrays are defined by 64 silicon oxide open vias, as well as SU-8 microchambers at the central area (black circle). Four metal pads at the edge connected to the square electrode are for DEP electric signal connection, as two of them are shown in Fig. A.14.

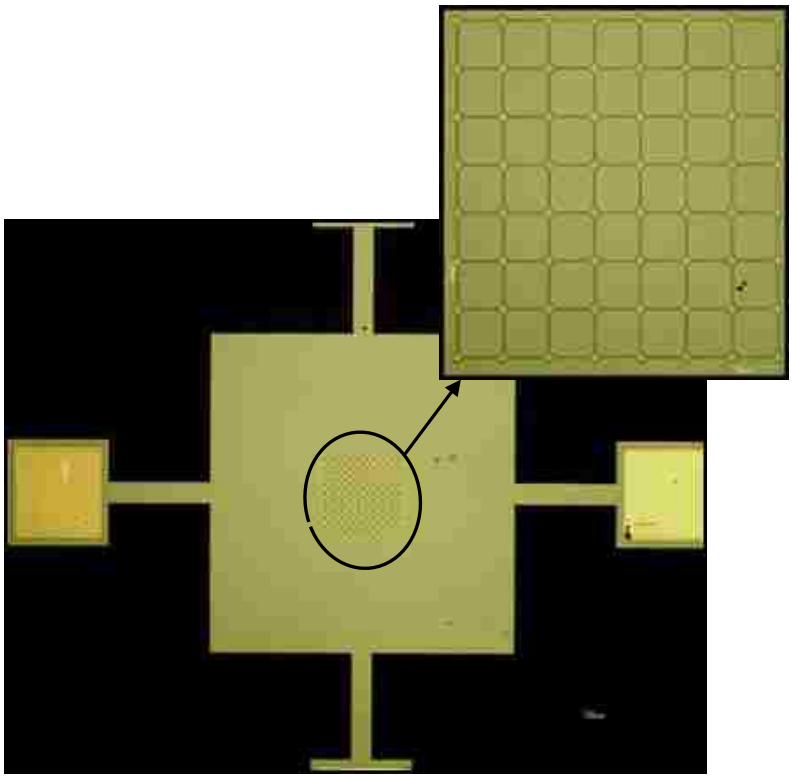

Figure A.14 Optical view of fabricated MEA test device and a close-up view of the central 8 x 8 = 64 electrode array area. Each electrode site is defined by a silicon oxide open via and a SU-8 microchamber on top of it. Four metal pads at the edge, connected to the square electrode, are for the application of DEP electric signals through probe tips. (Scale bar is 100 μm)

This simplified MEA test device, compared to the DEP MEA, has essentially the same single-electrode structure, and field distribution when electric potential is applied to the square electrode. It can be easily utilized for pDEP cell recruiting experiments on a probe station, without device packaging process. The experimental setup, similar to Fig. 4.3 (a), is shown in Fig. A.15, where two metal pads on the test chip are connected through probe tips to 10 Vpp AC sinusoidal wave, and two probe tips for electric ground are immersed in the trapping solution. The test chip is attached to the bottom of a 35 mm petri dish, which is stabilized on the probe station with a vacuum pump.

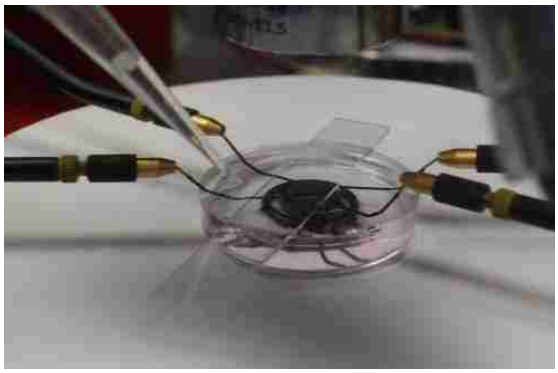

Figure A.15 pDEP cell trapping experiment setup with a MEA test device on the probe station. The glass cover slide sitting above the petri dish is utilized to stabilize the liquid media during experiments.

In this preliminary cell trapping experiments, the DEP trapping solution that we utilized consisted of 10% sucrose (w/v in deionized water):cell media at 9:1 ratio. Based on DEP spectra Maple simulation for different type of cells, 2 MHz AC electric signal was chosen to obtain the maximum pDEP effect. Mouse fibroblast cells (NIH3T3) and mouse hypothalamic neurons (GT1-7), both are immortalized cell lines, were used in the cell trapping experiments, and the final pDEP cell trapping results are shown in Fig. A.16.

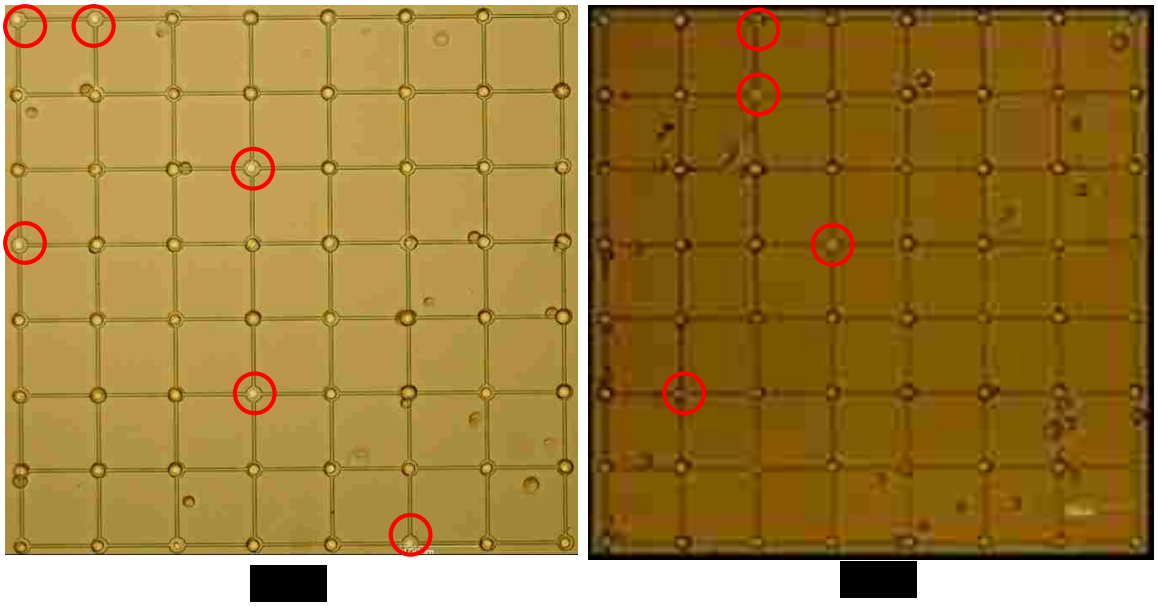

Figure A.16 NIH3T3 (a) and GT1-7 (b) pDEP cell trapping results on MEA test devices. Red circles indicate unoccupied electrode sites. Scale bar is 100 μm.

Cells were pipetted into the petri dish, and settled down on the test device surface before they were trapped onto the electrode sites. For NIH3T3 cell trapping, as can be seen in Fig. A.16(a), 58 out of the 64 electrode sites have been occupied, among which 48 electrode sites were occupied by single cell only, resulting in a 90.6% occupancy ratio and a 75% single-cell trapping ratio. Similar result was also achieved with GT1-7 cells (Fig. A.16(b)), where 60 out of 64 electrode sites have been occupied by GT1-7 neurons, among which 53 electrode sites were occupied by single cell only, resulting in a 93.7% occupancy ratio and a 82.8% single-cell trapping ratio. In addition to verifying precise active recruiting of cells with pDEP, this result is also significant for our ultimate goal of having a one-to-one neuron-to-electrode correspondence in MEAs and neuronal signal recording with reliable cell origin.

In order to find the optimal SU-8 microstructure design for single-cell patterning, GT1-7 neurons were cultured on MEA test devices with microchambers and microtrenches, but without implementing active trapping. The intention was to investigate the relation between different microchamber diameters and cell occupancy ratio (Fig. A.17). Neurons anchored in microchambers

were counted after cell plating. The neurites anchored inside and crossover (extended out of) microtrenches were also counted after one day of culturing (DIV.1), as shown in Fig. A.18. It can be seen that chambers with 30 μm diameter are the best option for GT1-7 single-cell occupancy, and trenches with 7 μm width are the best for guiding GT1-7 neurites and not allowing cell bodies to anchor inside. It is observed in our experiments later, that different kinds of cells/neurons have different preferences for optimal microstructure designs.

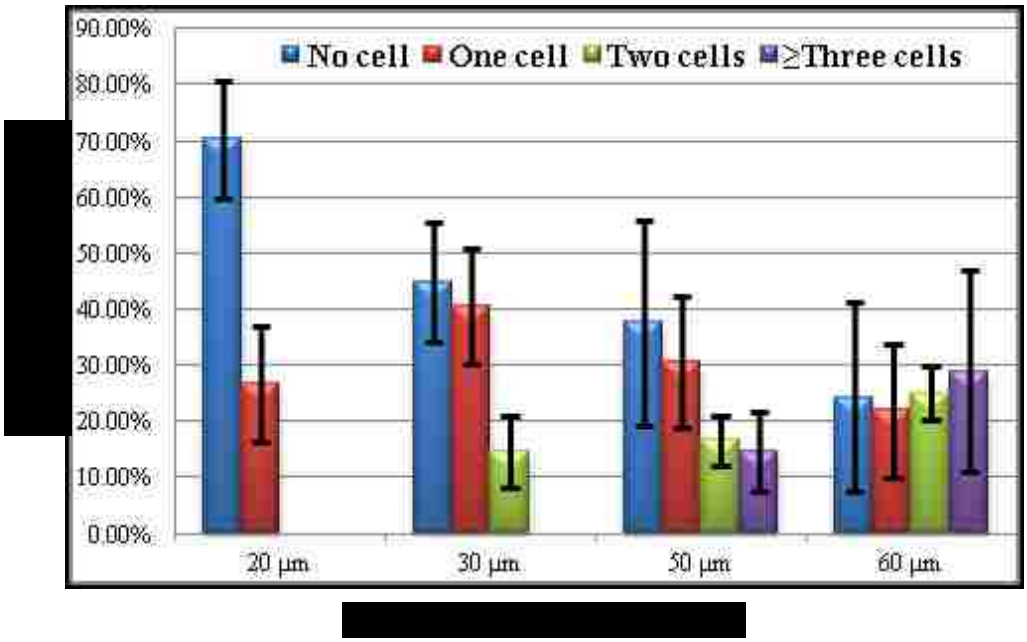

Figure A.17 Cell occupancy vs. microchamber diameter for GT1-7 cells.

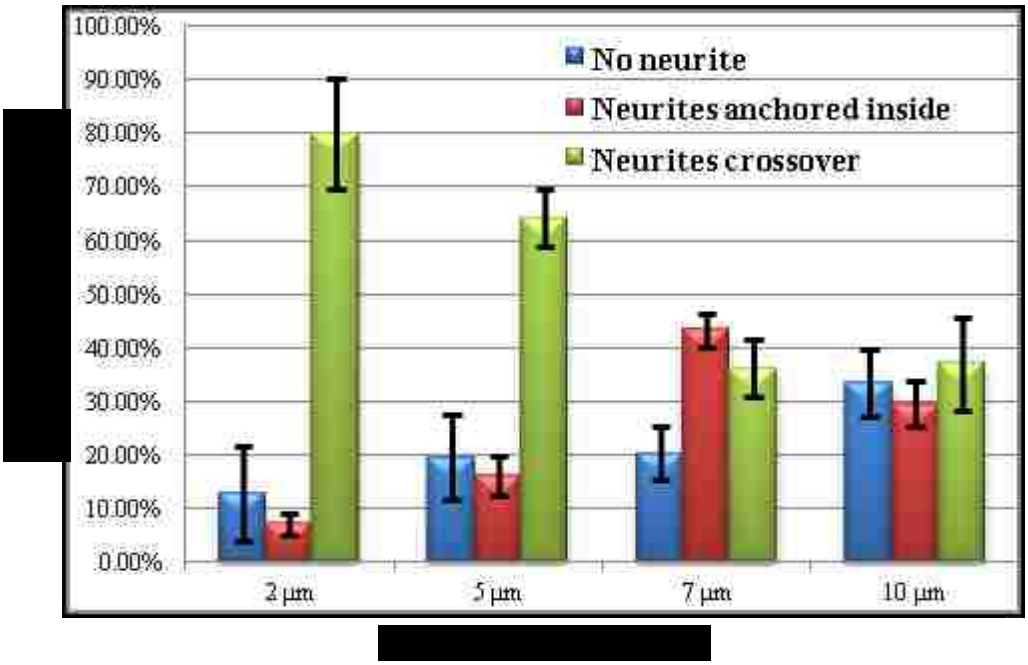

Figure A.18 Neurite anchoring ratio vs. microtrench width for GT1-7 cells.

Publications

Journals

Gaoshan Jing, Yu Wang, Tianyi Zhou, Susan F. Perry, Michael T. Grimes, Svetlana Tatic-Lucic, "Cell patterning using molecular vapor deposition of self-assembled monolayers and lift-off technique" *Acta Biomaterialia*, Vol. 7, Issue 3, pp. 1094-1103, 2011. doi: 10.1016/j.actbio.2010.09.040

Tianyi Zhou, Susan F. Perry, Yevgeny Berdichevsky, Susanne Petryna, Vicki Fluck, Svetlana Tatic-Lucic, "Multi-electrode array capable of supporting precisely patterned hippocampal neuronal networks" *Biomedical Microdevices*, 17(1):2, 2015. doi:10.1007/s10544-014-9907-8

Tianyi Zhou, Susan F. Perry, Yixuan Ming, Susanne Petryna, Vicki Fluck, Svetlana Tatic-Lucic, "Separation and assisted patterning of hippocampal neurons from glial cells using positive dielectrophoresis" *Biomedical Microdevices*, 17(3):62, 2015. doi:10.1007/s10544-015-9965-6

Tianyi Zhou, Susan F. Perry, Svetlana Tatic-Lucic, "Estimation of physical properties of neurons and glial cells using dielectrophoresis crossover frequency" *Journal of Biological Physics*, submitted.

Conferences

Tianyi Zhou, Svetlana Tatic-Lucic, "On Application of Positive Dielectrophoresis and Microstructure Confinement on Multielectrode Array with Sensory Applications" *In Proc. IEEE Sensors Conf.*, Taipei, Taiwan, 28-31 Oct. 2012. doi: 10.1109/ICSENS.2012.6411487

Tianyi Zhou, Susan F. Perry, Svetlana Tatic-Lucic, "On Combining the Dielectrophoresis and Microdevices: Investigation of Hippocampal Neuronal Viability after Implementing Dielectrophoretic Positioning on Multi-electrode Arrays" *BIODEVICES 2015, Proceedings of the International Conference on Biomedical Electronics and Devices*, Lisbon, Portugal, 12-15 January, 2015, pp 71-77. doi: 10.5220/0005180200710077

Svetlana Tatic-Lucic, Gaoshan Jing, Tianyi Zhou, "A System for Extracellular Recording from Patterned Neuronal Networks with Sensing Applications" *NSF Workshop on Micro, Nano, BioSystems*, Arlington, VA, 2012.

Vita

Tianyi Zhou was born in 1987 in Yangzhou, China to Mr Zhi Zhou and Ms. Houjun Lan. He received his B.S. degree in Measurement & Control Technologies and Instrumentation from Huazhong University of Science and Technology, Wuhan, China in 2009. In 2012, he received his M.S. degree in Electrical Engineering from Lehigh University and will receive his Ph.D. in Electrical Engineering in May 2016 under the supervision of Prof. Svetlana Tatic- Lucic. He joined Prof. Tatic-Lucic's group in 2009 to pursue his graduate research in Micro-electro-mechanical Systems (MEMS), biosensors, MEMS for biomedical applications. While at Lehigh University, Mr. Zhou is a P.C. Rossin College Doctoral Fellow, the recipient of the Sherman Fairchild Fellowship from 2011 to 2014, as well as the recipient of the Doctoral Travel Grant for Global Opportunities (DTG-GO) from the Office of International Affairs. During his last year of Ph.D. research, Mr. Zhou spent five months working as a technical intern at Bristol-Myers Squibb, Bloomsbury, NJ, a global pharmaceutical company, exploring the application of MEMS in protein purification processes.